2021

Nanoparticle sensors and lubricants for degenerative articular cartilage

BOSTON UNIVERSITY

COLLEGE OF ENGINEERING

Dissertation

NANOPARTICLE SENSORS AND LUBRICANTS FOR

DEGENERATIVE ARTICULAR CARTILAGE

by

TAYLOR BURGESS LAWSON

B.S., Oregon State University, 2014
M.S., Boston University, 2018

Submitted in partial fulfillment of the

requirements for the degree of

Doctor of Philosophy

2021

Approved by

First Reader   _____

Mark W. Grinstaff, Ph.D.
Distinguished Professor of Translational Research
Professor of Chemistry
Professor of Biomedical Engineering
Professor of Materials Science and Engineering
Professor of Medicine

Second Reader   _____

Brian D. Snyder, M.D./Ph.D.
Professor of Orthopedic Surgery
Harvard Medical School

Research Professor of Biomedical Engineering
Boston University, College of Engineering

Third Reader   _____

Michael Albro, Ph.D.
Assistant Professor of Mechanical Engineering
Assistant Professor of Materials Science and Engineering
Assistant Professor of Biomedical Engineering

Fourth Reader   _____

Katherine Yanhang Zhang, Ph.D.
Professor of Mechanical Engineering
Professor of Biomedical Engineering
Professor of Materials Science and Engineering

DEDICATION

This dissertation is dedicated to Boston and all the people who have shaped my time in this city that has become home.

To Laurel, especially: Thank you for being my best friend, for your unwavering dedication and sacrifices, for enduring the ups and downs of this whole process, for listening to countless practice presentations, and for being willing to continue this journey with me.

To my family: Thank you for always sounding so effortlessly enthusiastic when listening to my research and being but a phone call away.

To the family I have acquired, the Kazanjians: Thank you for your support and countless family dinners.

To my friends, particularly John and Allie: Thank you for being cheerleaders when I needed it and constant sources of comedic relief.

ACKNOWLEDGMENTS

This dissertation along with my development as a graduate student and a professional would not be possible without several individuals.

Firstly, I acknowledge and thank my two advisors, Mark Grinstaff and Brian Snyder for all of their support, direction and instruction throughout my PhD process. Especially Mark Grinstaff, who apart from nurturing my growth as a scientist, has provided me with great life advice. I would also like to thank my committee members, Michael Albro and Katherine Zhang for providing feedback and ensuring that I am laudable of a PhD degree. Particularly Michael Albro for teaching me valuable experimental techniques.

Secondly, I want to acknowledge and thank the entire Grinstaff group. Particularly 'Team Cartilage', Katherine Hohl, Anisha Joenathan, and Christian Demoya, who have helped me complete experiments that led to the creation of this dissertation. Furthermore, I want to thank Janne Mäkelä and Brad Nelson, who apart from becoming close friends, taught me most of what I know about cartilage mechanics and imaging.

Finally, I would like to express my gratitude for my colleagues at the Center for Advanced Orthopaedic Studies at Harvard Medical School.

NANOPARTICLE SENSORS AND LUBRICANTS FOR

DEGENERATIVE ARTICULAR CARTILAGE

TAYLOR BURGESS LAWSON

Boston University College of Engineering, 2021

Major Professor: Mark W. Grinstaff, Distinguished Professor of Translational Research,
Professor of Chemistry, Professor of Biomedical Engineering,
Professor of Materials Science and Engineering, Professor of Medicine

ABSTRACT

Articular cartilage is a highly organized, anisotropic tissue lining the ends of bones within synovial joints. Composed primarily of water, collagens, proteoglycans and chondrocytes which synergistically give rise to the tissue's mechanical and tribological properties. Fluid pressurization and resistance to fluid flow within the porous extracellular matrix of cartilage, coupled with the low hydraulic permeability of the tissue endow the tissue with a viscoelastic response to loading and aid to reduce the coefficient of friction between articulating surfaces, with the pressurized fluid supporting 95% of applied loads. Experiencing millions of articulations throughout an average lifetime, articular cartilage possesses distinct biotribological properties. These require effective lubrication, mediated by the synergistic interaction between fluid and boundary lubricants, to provide a low coefficient of friction and prevent wear at the cartilage surface.

Osteoarthritis is the progressive deterioration of articular cartilage and synovial joint structure and function, leading to softer and wear prone tissue on account of altered biochemical composition of the extracellular matrix. Plain radiography remains the most accessible tool and the current standard of care to visualize musculoskeletal diseases and

injuries (*e.g.*, osteoarthritis), but cannot directly visualize soft tissues or cartilage, and diagnoses are based solely on boney changes, which occur in the later stages of the disease. Coupled with no way to quantitatively assess tissue health prior to irreversible deterioration, there remains no cure for osteoarthritis. Integral to OA pathology are concomitant changes in the biochemical composition of synovial fluid that result in deterioration of rheological properties, contributing to increased cartilage wear.

To address both the lack of quantitative diagnosis methods and lack of chondroprotective therapies, this dissertation presents a dual faceted approach to quantitatively image articular cartilage health, coupled with lubrication strategies to improve cartilage lubrication, and preserve cartilage tissue. This dissertation describes the synthesis of tantalum oxide nanoparticles of varying surface charges for use as contrast agents for rapid, minimally invasive, non-destructive, and quantitative contrast-enhanced computed tomography to assess both the biochemical content and biomechanical integrity of articular cartilage. *Ex vivo c*ontrast enhanced computed tomography attenuation using the nanoparticle contrast agent reveals correlations between attenuation and the mechanical and biochemical properties of the tissue.

The lubrication strategy described within this dissertation involves introducing a rolling ball element between two surfaces to reduce friction. In this strategy, either single, globular macromolecules or nanoparticles are employed as ball bearings between articulating surfaces to reduce friction when asperities on the surfaces are in direct contact. Rheological characterization and construction of classical Stribeck curves using the lubricant formulations reveal that introducing the rolling element reduces the coefficient

of friction during boundary lubrication, while leaving the rheological properties of the base fluid intact. *Ex vivo* cartilage mechanical testing involving shear deformation under varying speeds and loads reveal improved biotribological performance compared to pure synovial fluid or saline.

TABLE OF CONTENTS

LIST OF TABLES

LIST OF FIGURES

LIST OF ABBREVIATIONS

ACLT .... Anterior Cruciate Ligament Transection

AFM .... Atomic Force Microscopy

BLOKS .... Boston Leeds Osteoarthritis Knee Score

BSF .... Bovine Synovial Fluid

CAP .... Chondrocyte Affinity Peptide

CECT .... Contrast Enhanced Computed Tomography

COF .... Coefficient of Friction

CT .... Computed Tomography

dGEMRIC .... delayed Gadolinium-Enhanced MRI of Cartilage

DLS .... Dynamic Light Scattering

DMMB .... 1,9-Dimethylmethylene Blue

E .... Equilibrium Modulus

ECM .... Extracellular Matrix

FTIR .... Fourier Transform Infrared

GAG .... Glycosaminoglycan

HA .... Hyaluronic Acid

hBMSCs .... Human Bone Marrow Derived Mesenchymal Stem Cells

HPG .... Hyperbranched Polyglycerols

IA .... Intra-Articular

IFLS .... Interstitial Fluid Load Support

MASIs .... Matrix Associated Stem Cell Implants

GLOSSARY

Biomimetic lubricant

A macromolecule or synthetic material that reduces friction or prevents wear in a biological system.

Boundary lubrication

Lubrication mode characterized by a low speed and a high load, where asperities on opposing articulating surfaces are in direct contact, separated by a single molecular layer of lubricant.

Coefficient of friction

A dimensionless number that represents the ratio of the force and normal force between two surfaces sliding over one another. Depends on the nature of the material and surface roughness. Values less than 0.1 are considered lubricious materials.

Contrast Enhanced CT

Use of imaging agents to afford a temporary enhancement of contrast between tissues of similar compositions for use in a computed tomography scan.

Donnan equilibrium theory

Equilibrium of charged particles near a semi-permeable membrane, often failing to distribute evenly across the two sides of the membrane. The fixed negative charge of articular cartilage causes an imbalance of ions between external solution and interstitium, leading to a swelling pressure inside the cartilage.

Equilibrium compressive modulus	Measure of the stiffness of a material, which quantifies the relationship between stress (force per unit area) and strain (proportional deformation)
Hersey number	A dimensionless lubrication parameter that is the product of viscosity and rotational speed over-load.
Hydrodynamic lubrication	Lubrication mode marked by low loads and high speeds, with articulating surfaces fully separated by a fluid film.
Interstitial fluid load support	Proportion of load supported by the fluid phase of a biphasic material. Upon loading, the fluid film becomes pressurized with the solid phase, bearing the load.
Intraarticular	Within or administered into a joint cavity.
k-edge	Increase in the attenuation coefficient of photons occurring when the incoming x-ray beam is just above the binding energy of the K shell electron of those atoms interacting with the x-ray beam.
Mixed mode lubrication	Transitional region between boundary and full hydrodynamic lubrication, where some areas between articulating surfaces exist in boundary lubrication whereas others are fully separated by a fluid film and exist in hydrodynamic lubrication.

Nanolubricant	Colloidal suspension of nanoparticles within a base fluid.
Nanoparticle	An ultrafine particle of matter between 1 and 500nm displaying unique material characteristic.
Strain	Amount of deformation of a material per unit length in the direction of applied forces, relative to original length
Stribeck curve	Depicts the non-linear function of friction as a function of the contact load, lubricant viscosity and velocity.
Tribology	The study of friction, lubrication and wear
Tribosupplementation	Intra-articular injection of a lubricating substance with the goal of preserving cartilage and re-establishing boundary or hydrodynamic lubrication.
Viscosupplementation	Intra-articular injection of a hyaluronic acid solution to improve synovial fluid elasticity and viscosity, to reduce pain and improve ambulation.
Wear	Damaging, gradual removal, or deformation of materials in contact. Causes may be mechanical or chemical.
Weight percent (weight basis)	Concentration that is determined from mass (g) per total mass (g)

Zwitterionic   Possessing both a formal positive and negative charge

PART I: QUANTITATIVE IMAGING OF ARTICULAR CARTILAGE

CHAPTER ONE. Nanotechnology and Osteoarthritis: Clinical landscape and opportunities for advanced diagnostics

1.1 Abstract

Osteoarthritis (OA) is a disease of the entire joint, often triggered by cartilage injury, mediated by a cascade of inflammatory pathways involving a complex interplay among metabolic, genetic, and enzymatic factors that alter the biochemical composition, microstructure and biomechanical performance. Clinically, OA is characterized by degradation of the articular cartilage, thickening of the subchondral bone, inflammation of the synovium, and degeneration of ligaments that in aggregate reduce joint function and diminish quality of life. OA is the most prevalent joint disease, affecting 140 million people worldwide; these numbers are only expected to increase, concomitant with societal and financial burden of care. This review encompasses the applications of nanotechnology to the diagnosis and treatment of osteoarthritis. Specifically, the focus is on OA treatment options and advancements in nanotechnology for the diagnosis of OA and imaging of articular cartilage, beginning with a concise evaluation of the clinical landscape of OA, along with current diagnosis and treatments, followed by an assessment of nanoparticle contrast agents for minimally invasive detection, diagnosis, and monitoring of OA via MRI, CT, and photoacoustic imaging techniques. We conclude by identifying opportunities for nanomedicine advances, and prospects for imaging and diagnostics.

1.2 Introduction

Nanotechnology is the design, manipulation, and control of materials and phenomena at atomic, molecular, and macromolecular scales. Physical, rheological, and mechanical properties as well as biological responses of materials depend on their size. At very small dimensions – *i.e.,* nano-scale, 10^9 meters – materials exhibit novel properties including fluorescence, enhanced magnetism, augmented load capacity, and improved cell internalization, often the consequence of confined electronic structure and increased surface area. Nano is not new; early examples of nanomaterials date back centuries to craftsmen who created stained glass windows and wine glasses using silicate (Egyptian Blue), as well as gold and silver nanoparticles (Lycurgus cup).[1,2] Nanotechnology is part of our daily lives, from Apple's "iPod Nano" to protective sunscreens. In medicine, clinically approved nano-technologies include: 1) liposome encapsulated amphotericin B (AmBisome®), doxorubicin (Doxil®), and irinotecan (Onivyde®) for treating fungal infections, ovarian cancer, and pancreatic cancer, respectively; 2) iron nanoparticles (Ferumoxytol®) for treating of iron deficiency anemia; 3) albumin coated paclitaxel nanoparticles (Abraxane®) for treating metastatic breast cancer and non-small-cell lung cancer; 4) nanocrystals of Aprepitant® as an antiemetic; 5) dendritic polymers (Adherus®) as a tissue sealant. Currently, there is no FDA approved technology for the diagnosis or treatment of osteoarthritis (OA). However, opportunities abound, and results from pre-clinical studies, described below, warrant continued efforts and translation to the clinic. Herein, we review applications for nanotechnology within the context of evaluating and diagnosing OA (**Figure 1.1**).

1.3 Osteoarthritis

OA is a chronic, synovial joint arthrosis afflicting 140 million people worldwide. Associated treatments cost $125 billion annually.[3] OA is progressive; changes in joint structure and function appear relatively late in the disease process, but account for long-term morbidity and disability experienced by OA patients. OA affects all synovial joint structures, including the synovium, joint capsule, cartilage, and bone. Biochemical,[4] mechanical ,[5] metabolic ,[6,7] and genetic[8] factors are etiologically related to OA. While the etiology is multi-factorial, OA is typically induced by acute or chronic mechanical injury to hyaline cartilage - the smooth, hydrated tissue that lines articular joint surfaces (**Figure 1.2**) - as a consequence of trauma, joint instability, ligamentous deficiency, skeletal malalignment, obesity or anatomic deformity. Mechanical overloading results in glycosaminoglycans (GAG) loss,[9] collagen disorganization,[10] fibrillation,[11] tissue swelling,[12] and surface wear[13] and incites an inflammatory response mediated by a cascade of cytokines. Elevated cytokines in OA synovial fluid (*e.g.*, IL-1β, TNF-α)[14] induce enzyme-mediated (*e.g.*, metalloproteinases and ADAMTS) cartilage degeneration.[15] Additionally, in OA, the synovial fluid's capacity for both fluid and boundary lubrication decreases due to a reduction in hyaluronic acid Mw and lubricin degradation.[16] In advanced OA, synovial fluid contains minimal hyaluronic acid and lubricin, further contributing to poor lubricity and higher coefficient of friction (similar to saline). [16]

Histopathologically, OA is characterized by the simultaneous presence of cartilage matrix degradation and repair including chondrocyte death, replication, and regeneration. At a cellular level, cartilage is catabolized by increased levels of cathepsins B and D,

metalloproteinases, and IL-1 which result in increased water content, depleted proteoglycans, collagen, and altered binding of proteoglycans to hyaluronic acid in the synovial fluid. As OA progresses, there is an increased production of matrix-degrading enzymes and pro-inflammatory cytokines, which damage cartilage further. Loss of GAG, an early hallmark of OA, results in increased tissue porosity thus increasing hydraulic permeability, and increasing the flux of water through the porous network, with more of the internal load support to the solid collagen network. Repetitive damage to the collagen network further decreases tensile stiffness with subsequent loss of tissue.

OA is diagnosed based on clinical symptoms (*e.g.*, pain, swelling, impaired function) and confirmed using imaging (*e.g.*, plane radiographs, computed tomography (CT), magnetic resonance imaging (MRI)). Unfortunately, imaging is biased toward visualizing late-stage OA pathoanatomy (i.e., cartilage volume loss, bone marrow edema, subchondral bone thickening, cyst formation and marginal osteophyte formation).[17] The ability of hyaline cartilage for self-repair is limited, and irreversible breakdown occurs long before clinical symptoms and radiographic signs are evident. OA diagnosed at a late stage, after micro- and macroscopic changes in tissue structure have transpired, worsens the prognosis and limits treatment options.

OA is incurable and difficult to treat. To ameliorate OA requires a comprehensive approach: 1) correct mechanical factors that contribute to acute or chronic injury of chondrocytes and wear of hyaline cartilage; 2) abrogate the inflammatory cascade and neutralize catabolic enzymes that degrade hyaline cartilage; 3) reconstitute degraded cartilage tissue properties by augmenting constituent tissue elements or replacing end-

stage chondral lesions

1.4 Osteoarthritis Diagnosis

The inability to identify cartilage damage early, when chondroprotective or chondroregenerative strategies will be most effective, presents a clinical obstacle. Magnetic resonance imaging (MRI) and computed tomography (CT) are widely used to visualize musculoskeletal pathology. MRI possesses several advantages, including absence of ionizing radiation and capacity to examine the entire joint. Using semi-automated segmentation algorithms to create 3D surface representations of articular cartilage, MRI measures the thickness, volume and surface topography of articular cartilage.[18-20] Semiquantitative scales such as the Whole Organ MRI Score (WORMS)[21] and the Boston-Leeds Osteoarthritis Knee Score (BLOKS)[22] are used to score multiple features in affected joints. Several MRI-based techniques (T1 mapping, T2 mapping, T1ρ, Na^+ mapping and dGEMRIC) provide images that reflect the GAG and collagen content of articular cartilage.[23] Predicated on Donnan equilibrium theory, delayed Gadolinium-enhanced MRI of cartilage (dGEMRIC) uses gadopentetic acid (Gd^{2-}) as a mobile anionic probe that partitions throughout the cartilage ECM in inverse proportion to the fixed negative charge density conferred by GAG.[24 - 27] Since T1 relaxation time varies inversely with the concentration of Gd^{2-} diffused throughout the cartilage matrix, mapped T1 relaxation time directly indicates the spatial distribution and concentration of GAG distributed throughout the tissue, allowing differentiation between healthy and OA cartilage based on chemical composition.[28-30]

CT provides affordable, fast, high-resolution images of bone, but since cartilage

does not attenuate x-rays well, standard CT does not readily measure thickness, volume, or surface topography of articular cartilage *in vivo*. Intra-articular injection of an iodinated contrast agent facilitates visualization of articular surfaces. Computed arthrotomography has been used for decades to image articular surfaces comprising the hip, shoulder, knee, elbow and foot.[31] CT arthrography is particularly useful for defining intra-articular pathoanatomy, providing rapid image acquisition, 2D-tomographic and 3D image reconstruction capability, excellent contrast resolution and segmentation of cartilage from bone, without the need for specialized sequences.[32,33] Similar to dGEMRIC, contrast-enhanced computed tomography (CECT), uses an anionic, iodinated contrast agent (Ioxaglate) that partitions throughout the tissue in inverse relation to local cartilage GAG content. To enhance CT based quantitative assessment of anionic tissue GAG composition, Grinstaff and Snyder developed cationic contrast agents that partition directly into the tissue in accordance to Donnan equilibrium so as to maintain electroneutrality.[33-38]

Nanoparticles of iron, gold, bismuth, or tantalum of less than 100 nm in diameter are of significant interest as medical imaging contrast agents.[33,39–41] Advances in the synthesis of nanoparticles are yielding various types of nanoparticles for qualitative and quantitative medical applications. Utilizations of these for cartilage imaging is still rare.[42-44] Articular cartilage permeability is low, possesses a fixed negative charge, and pore size is typically less than 10 nm hindering nanoparticle diffusion. [45,46]

1.4.1 Magnetic Resonance Imaging (MRI)

MRI contrast agents contain paramagnetic or superparamagnetic metal ions that alter intrinsic T1 or T2 relaxation times of nearby water molecules in the tissue where they

accumulate. [46] Superparamagnetic iron oxide nanoparticles (SPIONs) are extensively employed as MRI contrast agents, owing to their unique physical, chemical, magnetic and biocompatibility properties. SPIO agents, regulatory approved for clinical use, include ferumoxides (Feridex in the USA, Endorem in Europe) with a particle size of 120 to 180 nm, and ferucarbotran (Resovist®) with a particle size of about 60 nm.[47] Labens et al. report the first use of SPIONs as intra-articular MRI contrast agent for studying cartilage barrier function in a large animal model. [48] Injection of 12 nm SPIONs in matrix depleted and pristine porcine metacarpophalangeal joints followed by 1.5 T MRI pre- and post-imaging reveals an increased MRI signal in the matrix depleted porcine joints, indicating the MRI signal reflects the permeability caused by OA. Other uses for SPIONS in relation to OA are covered in a later section within this review. Yarmola et al. describe a SPION based technology (termed magnetic capture) for the determination of an OA biomarker in small volumes of synovial fluid in vitro and from a rat model of knee OA.[49] Magnetic capture capitalizes on the translational force experienced by SPIONs in a high-gradient magnetic field to collect the magnetized material. A targeting molecule, in this case anti-CTXII to target the c-terminus telopeptide of type II collagen, is conjugated to the polymeric particles containing SPIONs within the core.[49] The functionalized particles, after mixing with bovine synovial fluid and exposure to a magnetic field, aggregate on the magnetic probe. Intra-articular injection of the anti-CTXII particles in a rat stifle joint followed by collection with a magnetic probe reveals detectable levels of c-terminus telopeptide of type II collagen in the 25 µL collected synovial fluid.[49]

1.4.2 Contrast-enhanced computed tomography (CECT)

Cationic contrast agents accumulate in cartilage tissue to a greater extent than neutral or anionic agents, due to favorable electrostatic interactions between the cationic contrast agent and the anionic GAGs.[35,50] Freedman et al. report 5-10 nm in diameter tantalum oxide (Ta_2O_5) nanoparticles with neutral phosphonate, cationic ammonium, or anionic carboxylate ligands as potential CECT agents. The cationic Ta_2O_5 NP readily diffuse into *ex vivo* bovine cartilage and human index finger cartilage compared to neutral and anionic NPs. After IA administration in an *in vivo* mouse stifle joint, the cationic NPs penetrate the entire depth of the cartilage and enable imaging of cartilage tissue. [51]

The concurrent loss of anionic GAGs and decrease in steric hindrance (due to increasing tissue porosity) induce contradictory effects on the diffusion of cationic contrast agents, reducing the diagnostic accuracy of CECT. Furthermore, demarcation of the synovial fluid-cartilage interface for measuring the thickness, volume and surface topography of contrast enhanced cartilage becomes more difficult as clear distinction of the tissue boundary diminishes with diffusion time. To overcome these shortcomings, Töyräs et al. describe the combined, simultaneous use of two or three cartilage permeable and impermeable contrast agents.[52,53] Bismuth oxide nanoparticles, being too large to diffuse into cartilage, accumulate at the cartilage surface and provide a high contrast signal,[52,54] while tissue-permeable agents (anionic, neutral, and cationic small molecule iodine, neutral gadolinium) diffuse within cartilage and provide an attenuation reflective of GAG content or porosity.[52-55] CT's capability to separate X-ray photon energy spectra allows the interrogation of multiple contrast agents (**Figure 1.3**).

1.4.3 Photoacoustic imaging (PA)

Photoacoustic imaging (PA) integrates advantages of ultrasound with deep tissue penetration and optical imaging with high spatial resolution. Briefly, light energy absorbed by tissues causes a thermoelastic expansion generating ultrasound waves that are detected by a transducer. Optical absorption contrast images are obtained at penetration depths of only a few centimeters due to light scattering.

PA is particularly suited for imaging of peripheral joints such as fingers, hands, elbows, shoulders, knees, and ankles and thus of interest for diagnosing arthritis.[56,57] Ishihara et al. show that PA estimates the biomechanical and viscoelastic properties of tissue-engineered cartilage cultured from rabbit chondrocytes.[58] Sun et al. report detection of osteoarthritis in an *in vivo* finger joint using three-dimensional quantitative photoacoustic tomography.[59] Distal interphalangeal joints of female subjects, scanned *in vivo*, reveal differences in the absorption coefficients between healthy and osteoarthritic subjects. A homemade multispectral photoacoustic ultrasound computed tomography system, described by Liu et al., visually reconstructs the human finger joint systems including the skins, the blood vessels, the tendon, and the bone simultaneously.[60]

PA contrast agents absorb the energy of an optical laser and convert it to thermal energy.[61-63] Gold nanostructures ,[64,65] carbon nanotubes,[66] graphene-based nanomaterials among others are used for contrast enhancement.[67] However examples of PA nano contrast agents for OA diagnosis are rare. Chen et al. describe an intra-articular injection of cationic charged melanin nanoparticles (MNPs) coated with poly-L-lysine (PLL) in a live mouse model.[68] PLL–MNPs exhibit roughly a two-fold stronger PA signal in a normal joint (with

high GAG content) than an OA joint (with low GAG content) and importantly the PA signal intensity strongly correlates with sample GAG content (R^2=0.83).

1.5 Nanoparticles for Labeling and Targeting Chondrocytes and Stem Cells

Nanoparticle-based labeling of chondrocytes and mesenchymal stem cells increases target specificity and enables non-invasive, long term tracking of cells once administered *in vivo* through fluorescence, MRI, or CT based imaging.[69] Today, quantum dots, superparamagnetic iron oxide, and gold NPs are such tracers or labels. Mesenchymal stem cells (MSCs) are multipotent cells with potential to differentiate into various tissue types, including bone and cartilage. Quantum dots offer one solution to tracking MSCs, since they are resistant to chemical and metabolic degradation, possess long term photostability, and a narrow band emission coupled with broadband excitation.[69] Furthermore, when conjugated with an anti-mortalin antibody, quantum dots, provide a stable fluorescent signal of MSCs which were seeded in a 3D scaffold up to 26 weeks post-transplantation into an osteochondral defect.[70] This provides a better understanding of the healing process after MSC implantation. NPs afford an alternate way to track MSCs. MSCs when loaded with 20 nm, 40 nm, and 60 nm citrate-stabilized and poly-L-lysine coated gold NPs, are viable, and function normally. These NPs enable long-term tracking of MSC differentiation and migration which can elucidate the MSCs role in tissue repair (**Figure 1.4**).[71]

Superparamagnetic iron oxide nanoparticles (SPIONs) are also tracers for MSCs. Tracking transplanted stem cells longitudinally in time and space enables non-invasive monitoring of cell delivery, bio-distribution, migration, survival, and tissue integration.[72,73] To enhance target cell uptake of SPIONs to detectable levels for MRI applications, cationic

compounds such as poly-L-lysine, protamine sulfate, lipofectamine, and polyethylenimine are used to produce cationic SPION complexes that electrostatically attach to the anionic cell membranes.[74-76] In an *ex vivo* model of human osteochondral fragments, possessing a central cartilage defect, human bone marrow MSCs labelled with SPIONs accumulate in the defect target region as followed by a T2-weighted MRI.[77] To minimize dose-dependent toxic effects on MSCs by the uptake of SPIONs, Markides et al. use the commercially available Nanomag, a 250-nm SPION to enhance the intracellular activity of standard cell-penetrating peptides, to track autologous mesenchymal stromal cells in an ovine osteochondral defect model.[78] Van Buul et al. employ ferumoxides complexed to protamine sulfate to label human bone marrow-derived mesenchymal stem cells (hBMSCs).[79] Using T_2 or T_2* MRI sequences, SPION-labeled cells appear as a hypo-intensity after injected in an OA joint model, do not impair hBMSC secretion profiles, and enable accurate visualization by MRI using a porcine knee model.[79] Polyethylenimine (PEI)-wrapped SPION–labeled bone marrow–derived mesenchymal stem cells , reported by Chen et al., enable stem cell identification in repaired articular cartilage in a minipig model.[74] To improve uptake efficiency, Pang et al. describe surface neutral ganglioside GD2 modified SPIONs, as neutral ganglioside GD2 is highly expressed on the surface of MSCs.[80]

Magnetic NPs are also used to track chondrocytes in order to monitor growth, differentiation, and regeneration in osteochondral defect repair. Labeling human derived MSCs and chondroprogenitor cells with SPIONs does not hinder cell viability, MSC marker expression, or chondrocyte differentiation.[72-74] Similarly, the SPION-labeling process does not adversely affect the phenotype or viability of chondrocytes or the

production of major cartilage matrix constituents *in vitro* or *in vivo*.[73, 80-82] Ferumoxytol-labeled matrix-associated stem cell implants (MASIs) show significant T2 shortening (22.2±3.2 ms vs 27.9±1.8 ms; $P < .001$) and no difference in cartilage repair outcomes compared with unlabeled control MASIs ($P > .05$) in a porcine model, as described by Theruvath et al.[83] 2 weeks after implantation, ferumoxytol-labeled apoptotic MASIs show a loss of iron signal and higher T2 relaxation times compared with ferumoxytol-labeled viable MASIs (26.6±4.9 ms vs 20.8±5.3 ms; $P = .001$).[83] Standard MRI shows incomplete cartilage defect repair of apoptotic MASIs at 24 weeks. Signal loss at 2 weeks correlates with incomplete cartilage repair, diagnosed at histopathologic examination at 12-24 weeks.[83] Chen et al. describe an ultrasmall superparamagnetic iron oxide (USPIO)-labeled cellulose nanocrystal/silk fibroin-blended hydrogel system for noninvasive visualization and semiquantitative analysis of hydrogel degradation and cartilage regeneration *in vitro* and in rabbit cartilage regeneration *in vivo*.[84] The USPIO-labeled hydrogel system allows for *in vivo* MRI detection of hydrogel absorption and neo-tissue replacement, confirmed via conventional Hematoxylin-eosin and Prussian blue staining.[84]

Zare et al. report a novel scaffold-free complex microtissue of chondrogenic and osteogenic cell sheets using magnetically labelled dental pulp stem cells.[85] A magnetic force organizes the dental pulp stem cells, which have internalized Fe_3O_4 magnetic nanoparticles, to form a multilayered osteochondral complex after being seeded onto a graphene oxide sheet.[85] Following implantation into nude mice, the stem cells differentiate into chondrocytes and osteoblasts.[85] Su et al. further explore this strategy using iron-oxide based magnetic nanoparticles to both label and track chondrocytes and homogenously

incorporate chondrocytes onto biphasic scaffolds. Results indicate chondrocytes successfully incorporate the magnetic nanoparticles, reaching roughly 95% incorporation when the concentration of magnetic nanoparticles is greater than 250 µg/mL.[86] Further, labeled chondrocytes, when seeded into the biphasic scaffold under a one Tesla magnetic field for 60 minutes, migrate and distribute more evenly between both layers, compared to the untreated group (*i.e.*, no magnetic field).[86]

1.6 Conclusions and perspectives

Nanotechnology offers significant potential to enhance current OA management through new diagnostic capabilities. As discussed above a number of new technologies and materials are in pre-clinical development to address this multifactorial disease. With regards to the diagnostic front, nanoparticle contrast agents for use in MRI, CT, and PA afford additional qualitative and quantitative information on cartilage structure and lesions as well as GAG content and its spatial distribution within cartilage – a known biomarker for early OA.

Although the application of nanotechnology in orthopaedics is still in its infancy, several new research opportunities exists to include 1) MRI and CT contrast agents that provide quantitative assessment of a tissue component other than GAG; 2) functional MRI or CT agents that provide information on the biochemical or metabolic state of the tissue; 3) nanotracers for specific cells types; and 4) theranostics, which act simultaneously as a diagnostic agent and a therapy.

1.7 References

(1)   Murr, L. E. & Murr, L. E. Serendipitous Nanotechnology in Antiquity. in *Handbook of Materials Structures, Properties, Processing and Performance* 703–717 (Springer International Publishing, 2015). doi:10.1007/978-3-319-01815-7_44.

(2)   Nanotechnology is ancient history | Nanotechnology world | The Guardian. https://www.theguardian.com/nanotechnology-world/nanotechnology-is-ancient-history.

(3)   NIS Database Documentation. https://hcup-us.ahrq.gov/db/nation/nis/nisdbdocumentation.jsp.

(4)   Martel-Pelletier, J., Battista, J. di & Lajeunesse, D. Biochemical Factors in Joint Articular Tissue Degradation in Osteoarthritis. in *Osteoarthritis* 156–187 (Springer Berlin Heidelberg, 1999). doi:10.1007/978-3-642-60026-5_9.

(5)   Guilak, F. Biomechanical factors in osteoarthritis. *Best Practice and Research: Clinical Rheumatology* **25**, 815–823 (2011).

(6)   Garnero, P. *et al.* Cross sectional evaluation of biochemical markers of bone, cartilage, and synovial tissue metabolism in patients with knee osteoarthritis: Relations with disease activity and joint damage. *Annals of the Rheumatic Diseases* **60**, 619–626 (2001).

(7)   Petersson, I. F., Boegård, T., Svensson, B., Heinegård, D. & Saxne, T. Changes in cartilage and bone metabolism identified by serum markers in early osteoarthritis of the knee joint. *British Journal of Rheumatology* **37**, 46–50 (1998).

(8)   Aigner, T. *et al.* Large-scale gene expression profiling reveals major pathogenetic pathways of cartilage degeneration in osteoarthritis. *Arthritis and Rheumatism* **54**, 3533–3544 (2006).

(9)   DiMicco, M. A. *et al.* Mechanisms and Kinetics of Glycosaminoglycan Release Following In Vitro Cartilage Injury. *Arthritis and Rheumatism* **50**, 840–848 (2004).

(10)   Clements, K. M., Hollander, A. P., Sharif, M. & Adams, M. A. Cyclic loading can denature type II collagen in articular cartilage. *Connective Tissue Research* **45**, 174–180 (2004).

(11)   Workman, J., Thambyah, A. & Broom, N. The influence of early degenerative changes on the vulnerability of articular cartilage to impact-induced injury. *Clinical Biomechanics* **43**, 40–49 (2017).

(12)   Steinmeyer, J., Knue, S., Raiss, R. X. & Pelzer, I. Effects of intermittently applied cyclic loading on proteoglycan metabolism and swelling behaviour of articular cartilage explants. *Osteoarthritis and Cartilage* **7**, 155–164 (1999).

(13)   Oungoulian, S. R. *et al.* Articular cartilage wear characterization with a particle sizing and counting analyzer. *Journal of Biomechanical Engineering* **135**, 024501 (2013).

(14)   McNulty, A. L., Rothfusz, N. E., Leddy, H. A. & Guilak, F. Synovial fluid concentrations and relative potency of interleukin-1 alpha and beta in cartilage and meniscus degradation. *Journal of Orthopaedic Research* **31**, 1039–1045 (2013).

(15)   van den Berg, W. B., van de Loo, F. A. J., Zwarts, W. A. & Otterness, I. G. Effects of murine recombinant interleukin 1 on intact homologous articular cartilage: A quantitative and autoradiographic study. *Annals of the Rheumatic Diseases* **47**, 855–863 (1988).

(16)   Hills, B. A. & Monds, M. K. Deficiency of lubricating surfactant lining the articular surfaces of replaced hips and knees. *British journal of rheumatology* **37**, 143–7 (1998).

(17)   Hayashi, D., Roemer, F. W. & Guermazi, A. Imaging for osteoarthritis. *Annals of Physical and Rehabilitation Medicine* **59**, 161–169 (2016).

(18)   Kauffmann, C., Gravel, P., Godbout, B., al. Et & Kauffmann C Godbout B, et al., G. P. Computer-aided method for quantification of cartilage thickness and volume changes using MRI: validation study using a synthetic model. *IEEE Trans Biomed Eng.* **50**, 978–988 (2003).

(19)   Solloway, S., Hutchinson, C. E., Waterton, J. C. & Taylor, C. J. The use of active shape models for making thickness measurements of articular cartilage from MR images. *Magnetic Resonance in Medicine* **37**, 943–952 (1997).

(20)   Eckstein Reiser M, Englmeier KH, Putz R., F. In vivo morphometry and functional analysis of human articular cartilage with quantitative magnetic resonance imagin - from image to data, from data to theory. *Anat Embryol.* **203**, 147–173 (2001).

(21)   Peterfy C Janzen D, et al., van D. C., Peterfy, C., van Dijke, C., Janzen, D. & al. Et. Quantification of articular cartilage in the knee with pulsed saturation transfer subtraction and fat-supressed MR imaging: optimization and validation. . *Radiology* **193**, 485–491 (1994).

(22)   Hunter D Grainger G, et al., G. D., Hunter, D., Gale, D. & Grainger, G. The reliability of a new scoring system for knee osteoarthritis MRI and the validity of bone marrow lesion assessment: BLOKS (Boston Leeds Osteoarthritis Knee Score). *Ann Rheum Dis* **67**, 206–211 (2008).

(23)   Strickland, C. D. & Kijowski, R. Morphologic imaging of articular cartilage. *Magnetic Resonance Imaging Clinics of North America* **19**, 229–248 (2011).

(24)   Ling, W., Regatte, R. R., Navon, G. & Jerschow, A. Assessment of glycosaminoglycan concentration in vivo by chemical exchange-dependent saturation transfer. *Proceedings of the National Academy of Sciences of the U S A* **105**, 2266–2270 (2008).

(25)   Wheaton, A. J., Dodge, G. R., Elliott, D. M., Nicoll, S. B. & Reddy, R. Quantification of cartilage biomechanical and biochemical properties via T1ρ magnetic resonance imaging. *Magnetic Resonance in Medicine* **54**, 1087–1093 (2005).

(26)   Wheaton, A. J. *et al.* Proteoglycan loss in human knee cartilage: Quantitation with sodium MR imaging - Feasibility study. *Radiology* **231**, 900–905 (2004).

(27)   Bashir, A., Gray, M. L., Hartke, J. & Burstein, D. Nondestructive imaging of human cartilage glycosaminoglycan concentration by MRI. *Magnetic Resonance in Medicine* **41**, 857–865 (1999).

(28)   Tiderius, C. J., Jessel, R., Kim, Y. J. & Burstein, D. Hip dGEMRIC in asymptomatic volunteers and patients with early osteoarthritis: The influence of timing after contrast injection. *Magnetic Resonance in Medicine* **57**, 803–805 (2007).

(29)   Gray, M. L., Burstein, D., Kim, Y.-J. & Maroudas, A. Magnetic resonance imaging of cartilage glycosaminoglycan: Basic principles, imaging technique, and clinical applications. *Journal of Orthopaedic Research* **26**, 281–291 (2008).

(30)   Bashir, A., Gray, M. L. & Burstein, D. Gd-DTPA2− as a measure of cartilage degradation. *Magnetic Resonance in Medicine* **36**, 665–673 (1996).

(31)   Buckwalter, K. A. CT Arthrography. *Clinical Sports Medicine* **25**, 899–915 (2006).

(32)   Palmer, A. W., Guldberg, R. E. & Levenston, M. E. Analysis of cartilage matrix fixed charge density and three-dimensional morphology via contrast-enhanced microcomputed tomography. *Proceedings of the National Academy of Sciences of the United States of America* **103**, 19255–19260 (2006).

(33)   Lusic, H. & Grinstaff, M. W. X-ray-Computed Tomography Contrast Agents. *Chemical Reviews* **113**, 1641–1666 (2013).

(34)   Lakin, B. A. *et al.* Contrast-enhanced CT using a cationic contrast agent enables non-destructive assessment of the biochemical and biomechanical properties of mouse tibial plateau cartilage. *Journal of Orthopaedic Research* **34**, 1130–1138 (2016).

(35).   Lakin, B. A. *et al.* Cationic agent contrast-enhanced computed tomography imaging of cartilage correlates with the compressive modulus and coefficient of friction. *Osteoarthritis and Cartilage* **21**, 60–68 (2013).

(36)   Lakin, B. A. *et al.* Contrast-enhanced CT facilitates rapid, non-destructive assessment of cartilage and bone properties of the human metacarpal. *Osteoarthritis and Cartilage* **23**, 2158–2166 (2015).

(37)   Stewart, R. C. *et al.* Contrast-enhanced CT with a high-affinity cationic contrast agent for imaging ex vivo bovine, intact ex vivo rabbit, and in vivo rabbit cartilage. *Radiology* **266**, 141–150 (2013).

(38)   Lee, N., Choi, S. H. & Hyeon, T. Nano-Sized CT Contrast Agents. *Advanced Materials* **25**, 2641–2660 (2013).

(39)   Ashton, J. R., West, J. L. & Badea, C. T. In vivo small animal micro-CT using nanoparticle contrast agents. *Frontiers in Pharmacology* **6**, 256 (2015).

(40)   Xi, D. *et al.* Gold nanoparticles as computerized tomography (CT) contrast agents. *RSC Advances* **2**, 12515–12524 (2012).

(41)   Attia, M. F., Wallyn, J., Anton, N. & Vandamme, T. F. Inorganic nanoparticles for X-ray computed tomography imaging. *Critical Reviews in Therapeutic Drug Carrier Systems* **35**, 391–432 (2018).

(42)   Shreffler, J. W., Pullan, J. E., Dailey, K. M., Mallik, S. & Brooks, A. E. Overcoming Hurdles in Nanoparticle Clinical Translation: The Influence of Experimental Design and Surface Modification. *International journal of molecular sciences* **20**, (2019).

(43)   Fitzgerald, P. F. *et al.* Proposed computed tomography contrast agent using carboxybetaine zwitterionic tantalum oxide nanoparticles imaging, biological, and physicochemical performance. *Investigative Radiology* **51**, 786–796 (2016).

(44)   Majda, D. *et al.* New approach for determining cartilage pore size distribution: NaCl-thermoporometry. *Microporous and Mesoporous Materials* **241**, 238–245 (2017).

(45)   Mow, V. C., Ratcliffe, A. & Poole, A. R. Cartilage and diarthrodial joints as paradigms for hierarchical materials and structures. *Biomaterials* **13**, (1992).

(46)   Ibrahim, M. A. & Dublin, A. B. *Magnetic Resonance Imaging (MRI), Gadolinium. StatPearls* (StatPearls Publishing, 2018).

(47)   Raghava Reddy, K. *et al.* Functionalized magnetic nanoparticles/biopolymer hybrids: Synthesis methods, properties and biomedical applications. in *Methods in Microbiology* **46**, 227–254 (2019).

(48)   Labens, R., Daniel, C., Hall, S., Xia, X. R. & Schwarz, T. Effect of intra-articular administration of superparamagnetic iron oxide nanoparticles (SPIONs) for MRI assessment of the cartilage barrier in a large animal model. *PLoS ONE* **12**, (2017).

(49)   Yarmola, E. G., Shah, Y., Arnold, D. P., Dobson, J. & Allen, K. D. Magnetic Capture of a Molecular Biomarker from Synovial Fluid in a Rat Model of Knee Osteoarthritis. *Annals of Biomedical Engineering* **44**, 1159–1169 (2016).

(50)   Bansal, P. N., Stewart, R. C., Entezari, V., Snyder, B. D. & Grinstaff, M. W. Contrast agent electrostatic attraction rather than repulsion to glycosaminoglycans affords a greater contrast uptake ratio and improved quantitative CT imaging in cartilage. *Osteoarthritis and Cartilage* **19**, 970–976 (2011).

(51)   Freedman, J. D., Lusic, H., Snyder, B. D. & Grinstaff, M. W. Tantalum oxide nanoparticles for the imaging of articular cartilage using X-ray computed tomography: Visualization of ex vivo/in vivo murine tibia and ex vivo human index finger cartilage. *Angewandte Chemie - International Edition* **53**, 8406–8410 (2014).

(52)   Saukko, A. E. A. *et al.* Dual Contrast CT Method Enables Diagnostics of Cartilage Injuries and Degeneration Using a Single CT Image. *Annals of Biomedical Engineering* **45**, 2857–2866 (2017).

(53)   Honkanen, M. K. M. *et al.* Triple Contrast CT Method Enables Simultaneous Evaluation of Articular Cartilage Composition and Segmentation. *Annals of Biomedical Engineering* **48**, 556–567 (2020).

(54)   Myller, K. A. H. *et al.* In Vivo Contrast-Enhanced Cone Beam CT Provides Quantitative Information on Articular Cartilage and Subchondral Bone. *Annals of Biomedical Engineering* **45**, 811–818 (2017).

(55)   Bhattarai, A. *et al.* Dual contrast in computed tomography allows earlier characterization of articular cartilage over single contrast. *Journal of Orthopaedic Research* **38**, 2230–2238 (2020).

(56)   Zhu, Y. *et al.* Light emitting diodes based photoacoustic imaging and potential clinical applications. *Scientific Reports* **8**, 1–12 (2018).

(57)   Jo, J. *et al.* A Functional Study of Human Inflammatory Arthritis Using Photoacoustic Imaging. *Scientific Reports* **7**, (2017).

(58)   Ishihara, M. *et al.* Usefulness of photoacoustic measurements for evaluation of biomechanical properties of tissue-engineered cartilage. in *Tissue Engineering* **11**, 1234–1243 (2005).

(59)   Sun, Y., Sobel, E. S. & Jiang, H. First assessment of three-dimensional quantitative photoacoustic tomography for in vivo detection of osteoarthritis in the finger joints. *Medical Physics* **38**, 4009–4017 (2011).

(60)   Liu, Y., Wang, Y. & Yuan, Z. Dual-Modality Imaging of the Human Finger Joint Systems by Using Combined Multispectral Photoacoustic Computed Tomography and Ultrasound Computed Tomography. *Biomed Research International* **2016** (2016).

(61)   Jiang, Y. & Pu, K. Advanced Photoacoustic Imaging Applications of Near-Infrared Absorbing Organic Nanoparticles. *Small* **13**, 1700710 (2017).

(62)   Weber, J., Beard, P. C. & Bohndiek, S. E. Contrast agents for molecular photoacoustic imaging. *Nature Methods* **13**, 639–650 (2016).

(63)   Fu, Q., Zhu, R., Song, J., Yang, H. & Chen, X. Photoacoustic Imaging: Contrast Agents and Their Biomedical Applications. *Advanced Materials* **31**, 1805875 (2018).

(64)   Li, W. & Chen, X. Gold nanoparticles for photoacoustic imaging. *Nanomedicine* **10**, 299–320 (2015).

(65)   Bogdanov, A. A. *et al.* Synthesis and Testing of Modular Dual-Modality Nanoparticles for Magnetic Resonance and Multispectral Photoacoustic Imaging. *Bioconjugate Chemistry* **27**, 383–390 (2016).

(66)   Avouris, P., Freitag, M. & Perebeinos, V. Carbon-nanotube photonics and optoelectronics. *Nature Photonics* **2**, 341–350 (2008).

(67)   Lin, J., Chen, X. & Huang, P. Graphene-based nanomaterials for bioimaging. *Advanced Drug Delivery Reviews* **105**, 242–254 (2016).

(68)   Chen, L. *et al.* Cationic poly-l-lysine-encapsulated melanin nanoparticles as efficient photoacoustic agents targeting to glycosaminoglycans for the early diagnosis of articular cartilage degeneration in osteoarthritis. *Nanoscale* **10**, 13471–13484 (2018).

(69)   Muller-Borer, B. J., Collins, M. C., Gunst, P. R., Cascio, W. E. & Kypson, A. P. Quantum dot labeling of mesenchymal stem cells. *Journal of Nanobiotechnology* **5**, 9 (2007).

(70)   Yoshioka, T. *et al.* Fate of bone marrow mesenchymal stem cells following the allogeneic transplantation of cartilaginous aggregates into osteochondral defects of rabbits. *Journal of Tissue Engineering and Regenerative Medicine* **5**, 437–443 (2011).

(71)   Ngen, E. J. & Artemov, D. Advances in monitoring cell-based therapies with magnetic resonance imaging: Future perspectives. *International Journal of Molecular Sciences* **18**, (2017).

(72)   Wimpenny, I., Markides, H. & el Haj, A. J. Orthopaedic applications of nanoparticle-based stem cell therapies. *Stem Cell Research and Therapy* **3**, 13 (2012).

(73)   Jasmin *et al.* Labeling stem cells with superparamagnetic iron oxide nanoparticles: Analysis of the labeling efficacy by microscopy and magnetic resonance imaging. *Methods in Molecular Biology* **906**, 239–252 (2012).

(74) Chen, J. *et al.* In Vivo MRI Tracking of Polyethylenimine-Wrapped Superparamagnetic Iron Oxide Nanoparticle-Labeled BMSCs for Cartilage Repair: A Minipig Model. *Cartilage* **4**, 75–82 (2013).

(75)   Li, L. *et al.* Superparamagnetic iron oxide nanoparticles as MRI contrast agents for non-invasive stem cell labeling and tracking. *Theranostics* **3**, 595–615 (2013).

(76)   Feng, Y. *et al.* In vitro targeted magnetic delivery and tracking of superparamagnetic iron oxide particles labeled stem cells for articular cartilage defect repair. *Journal of Huazhong University of Science and Technology - Medical Science* **31**, 204–209 (2011).

(77)   Markides, H. *et al.* Ex vivo MRI cell tracking of autologous mesenchymal stromal cells in an ovine osteochondral defect model. *Stem Cell Research and Therapy* **10**, 25 (2019).

(78)   van Buul, G. M. *et al.* Clinically translatable cell tracking and quantification by MRI in cartilage repair using superparamagnetic iron oxides. *PLoS ONE* **6**, (2011).

(79)   Pang, P. *et al.* An MRI-Visible Non-Viral Vector Bearing GD2 Single Chain Antibody for Targeted Gene Delivery to Human Bone Marrow Mesenchymal Stem Cells. *PLoS ONE* **8**, e76612 (2013).

(80)   Chen, J. *et al.* In vivo tracking of superparamagnetic iron oxide nanoparticle labeled chondrocytes in large animal model. *Annals of biomedical engineering* **40**, 2568–2578 (2012).

(81)   Farrell, E. *et al.* Cell labelling with superparamagnetic iron oxide has no effect on chondrocyte behaviour. *Osteoarthritis and Cartilage* **17**, 961–967 (2009).

(82)   Ramaswamy, S. *et al.* Magnetic resonance imaging of chondrocytes labeled with superparamagnetic iron oxide nanoparticles in tissue-engineered cartilage. *Tissue Engineering - Part A* **15**, 3899–3910 (2009).

(83)   Theruvath, A. J. *et al.* Tracking stem cell implants in cartilage defects of minipigs by using ferumoxytol-enhanced MRI. *Radiology* **292**, 129–137 (2019).

(84)   Chen, Z. *et al.* Non-invasive monitoring of in vivo hydrogel degradation and cartilage regeneration by multiparametric MR imaging. *Theranostics* **8**, 1146–1158 (2018).

(85)   Zare, S. *et al.* MRI-Tracking of Dental Pulp Stem Cells In Vitro and In Vivo Using Dextran-Coated Superparamagnetic Iron Oxide Nanoparticles. *Journal of Clinical Medicine* **8**, 1418 (2019).

(86)   Su, J.-Y., Chen, S.-H., Chen, Y.-P. & Chen, W.-C. Evaluation of Magnetic Nanoparticle-Labeled Chondrocytes Cultivated on a Type II Collagen–Chitosan/Poly(Lactic-co-Glycolic) Acid Biphasic Scaffold. *International Journal of Molecular Sciences* **18**, 87 (2017).
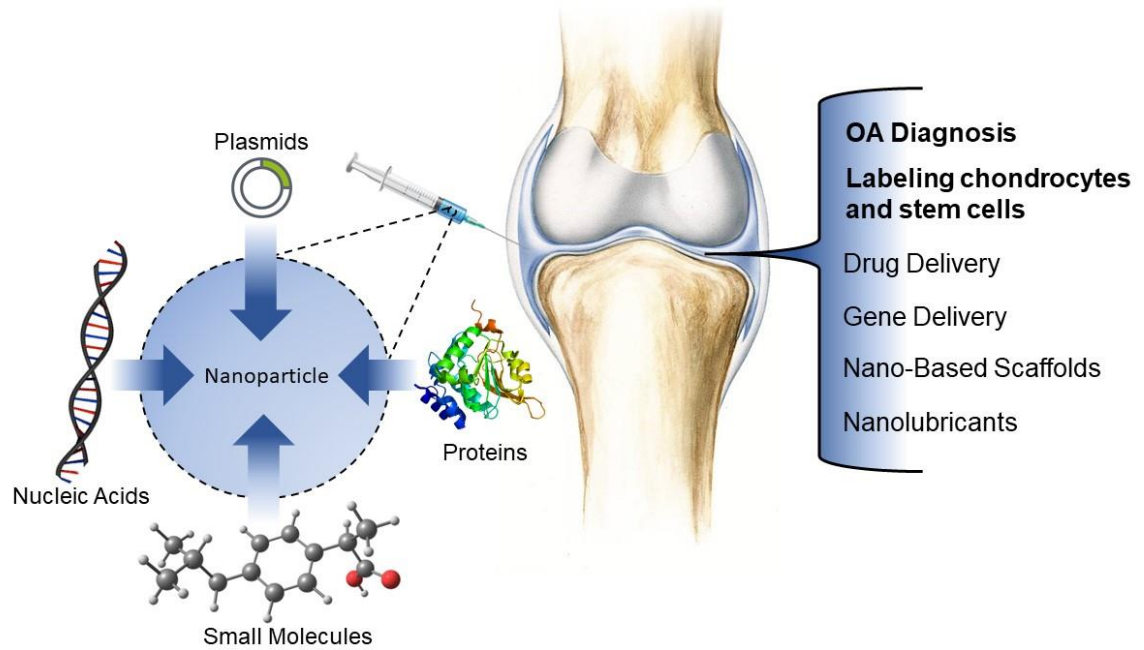
Figure 1.1. Facets of nanotechnology investigated for a multitude of applications for osteoarthritis, from drug delivery to diagnosis
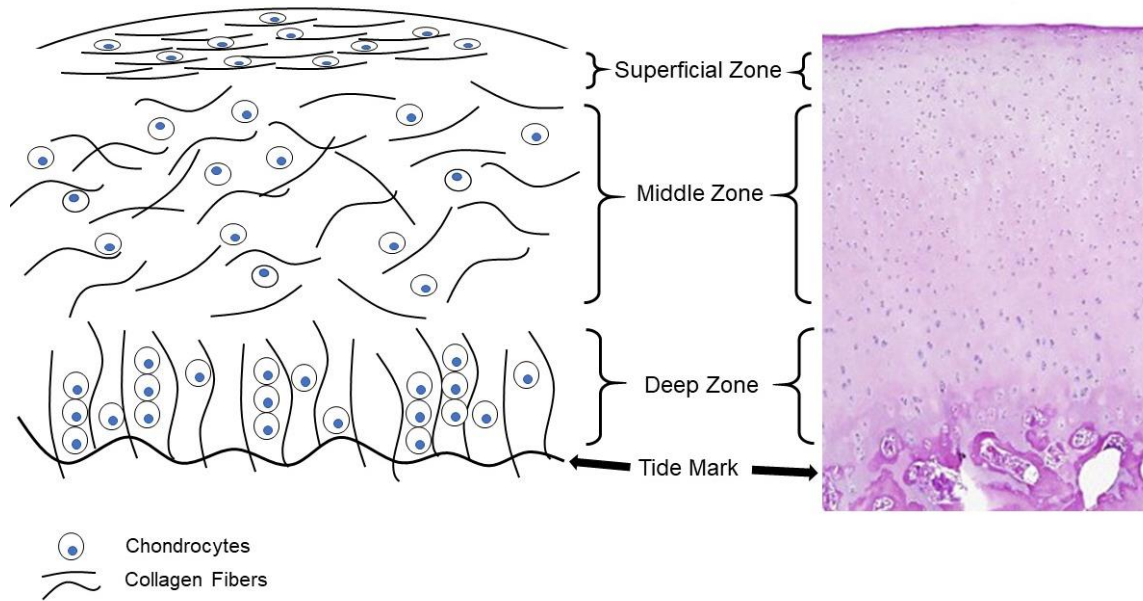
Figure 1.2. Schematic of zonal differentiation within articular and a representative histological slice. Histological slice reprinted with permission.
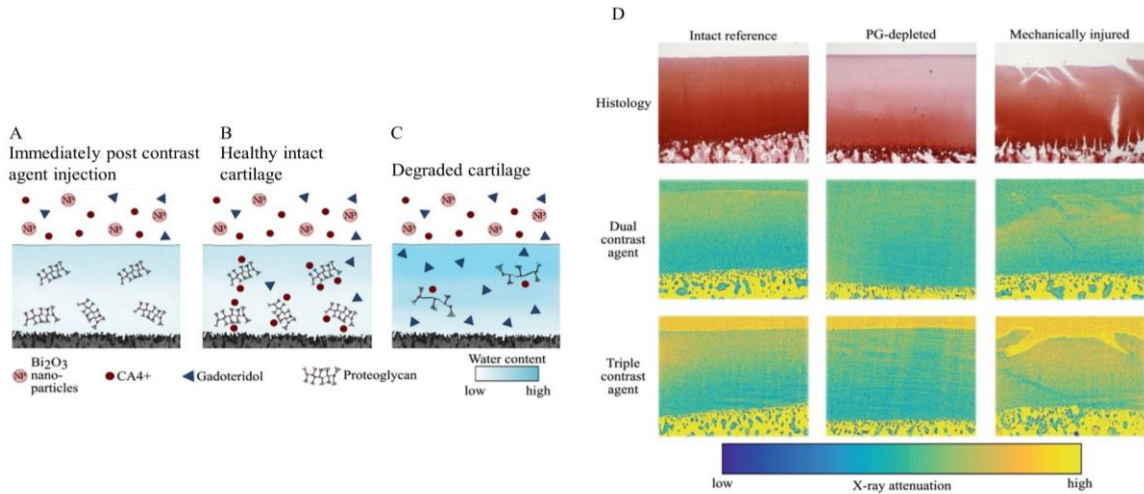
Figure 1.3. A – C) Basic mechanism for simultaneous use of three cartilage permeable/impermeable contrast agents. **A**) Cartilage bathed in contrast agents immediately post contrast agent injection. **B**) Healthy cartilage contrast agent uptake, CA4+ is proportional to the fixed charge density conferred by proteoglycans (PGs) and uptake is high in healthy cartilage but low in **C**) degraded cartilage. In degenerated cartilage the tissue water content increases and steric hindrance decreases allowing more contrast agent molecules (both CA4+ and gadoteridol) to penetrate the tissue. Bismuth nanoparticles (average diameter of 194 nm) are too large to be able to diffuse into either, thus maintaining the contrast at the articulating surface at all diffusion time points.[32] **D**) histology and synchron micro computed tomography (microCT) slices of cartilage. Articulating surface and cracks are better visualized with the triple contrast agent owing to better contrast induced by bismuth nanoparticles that, due to their size, are too large to diffuse into cartilage.
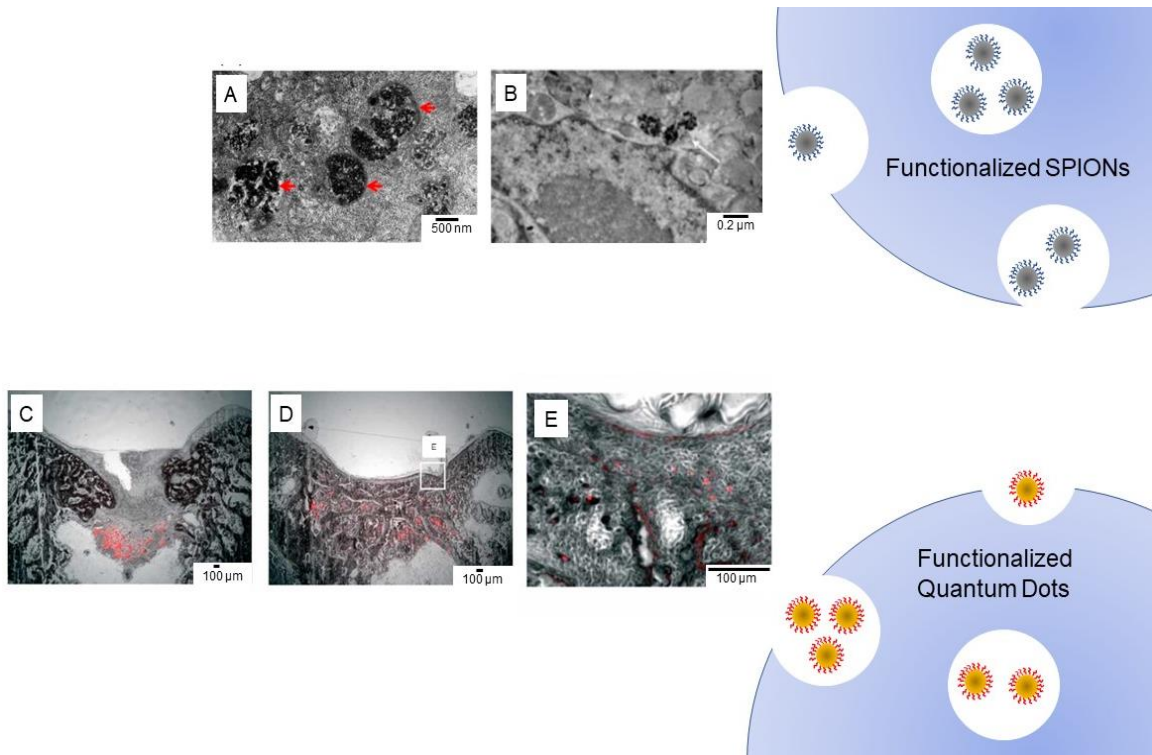
Figure 1.4. TEM images representing cellular internalization of SPIONs and quantum dots for labeling and tracking chondrocytes. **A**) Cellular uptake and subcellular localization of magnetic nanoparticles in chondrocytes treated with 250 µg/mL magnetic nanoparticles, arrows indicate the locations of magnetic particles in the cells.[114] **B**) Superparamagnetic iron oxide nanoparticle (SPION)- labeled human bone marrow MSCs. Arrows indicate SPIONs in cytoplasm.[104] (**C-E**) Mesenchymal stem cells (MSCs) labelled via internalizing quantum dots in reparative tissues, followed by the allogeneic transplantation of three-dimensional cartilaginous aggregates into osteochondral defects of rabbits. (C) At 4 weeks, (D) at 8 weeks, (E) higher magnification of framed area in D.[71] All figures reprinted with permission.

CHAPTER TWO: Tantalum Oxide Nanoparticles for Quantitative Contrast Enhanced Computed Tomography Assessment of Biochemical Composition and Biomechanics of Ex Vivo Human Cartilage

2.1 Abstract

Nanoparticle based contrast agents, when used in concert with imaging modalities such as computed tomography (CT), enhance visualization of tissues and boundary interfaces. However, determination of the physiological state of the tissue via quantitative assessment of biochemical or biomechanical properties remains elusive. We report the synthesis and characterization of tantalum oxide (Ta_2O_5) nanoparticle (NP) contrast agents for rapid, non-destructive, and quantitative contrast-enhanced computed tomography (CECT) to assess both the glycosaminoglycan (GAG) content and biomechanical integrity of human metacarpal phalangeal joint (MCPJ) articular cartilage. Ta_2O_5 NPs of 3-7 nm in diameter, coated with either poly(ethylene) glycol (neutral) or ammonium (cationic) ligands, readily diffuse into both healthy and osteoarthritic MCPJ cartilage. CECT attenuation for the cationic and neutral NPs correlates with GAG content ($R^2 = 0.8975$, p<0.05 and 0.7054, respectively) and the equilibrium modulus ($R^2 = 0.8285$, p<0.05 and 0.9312, p<0.05, respectively). The results highlight the importance of surface charge and size in the design of NP agents for targeting and imaging articular cartilage. Further, nanoparticle CECT offers visualization of both cartilage and bone, unlike plain radiography, the standard for imaging bone in musculoskeletal diseases, and, as first demonstrated herein, the ability to provide real time quantitative assessment of tissue health and disease.

2.2 Introduction

Plain radiography remains the most accessible tool and the current standard of care to visualize musculoskeletal diseases and injuries. This is especially true for the diagnosis of osteoarthritis (OA). OA, a degenerative disease affecting synovial joint structure and function, afflicts 80% of people over the age of 65 worldwide.[1] While X-ray plain radiographs are accessible and inexpensive, they cannot directly visualize soft tissues or cartilage, and diagnoses are based solely on boney changes such as joint space narrowing, osteophytes, sclerosis, joint incongruity and malalignment,[2,3] which occur in the later stages of the disease.

Of the imaging modalities for soft tissue, contrast-enhanced computed tomography (CECT) is of particular interest as it has the potential to provide real time quantitative assessment of soft tissues, *e.g.,* cartilage, using a readily accessible and cost-effective technique. Additionally, CT imaging, over MRI, affords the ability to assess bony changes. Subchondral bone sclerosis is commonly associated with articular cartilage degradation and plays an integral role in the initiation, as well as progression of OA. Anionic iodinated contrast agents are the mainstay in CECT, however nanoparticular agents offer a number of potential advantages. Due to their composition, small diameter, high surface area and confined electronic structure, nanoparticles (NPs) possess distinctive properties apart from individual atoms, small molecules, or bulk materials.[4] To date, NPs are being investigated for use as biosensors,[5,6] reagents for diagnostic assays,[7,8] as both gene and drug delivery vehicles,[9–11] and as imaging contrast media for MRI, fluorescence, PET and X-Ray.[12,13] Specifically, those NPs containing gold,[14,15] bismuth,[16] and tantalum[17,18] are used as X-ray

contrast agents for contrast enhanced computed tomography (CECT) of lymph nodes,[17] vasculature,[18–23] and cartilage.[24–26] Tantalum is an ideal NP material for CT imaging as it possesses a higher k-edge (67.4 keV) than conventional iodinated contrast agents and as such, absorbs a larger amount of X-rays produced at clinical scanning voltages (80-140 keV),[27] as well as lessens beam hardening artifacts. However quantitative biochemical or biomechanical assessment of tissue using nanoparticles and contrast enhanced CT imaging (be it cartilage or any other tissue) is lacking as prior studies involved only visualization of the tissue.

Our objective is to develop a contrast agent that enables both qualitative visualization of the tissue and quantitative assessment of physiological state or tissue function. Herein we synthesize cationic and neutral tantalum oxide nanoparticles (Ta_2O_5 NPs) for use in CECT and determine the effectiveness to distinguish both biochemical changes and alterations in tissue mechanical integrity associated with early-stage OA, along with the assessment of bony changes. OA disease pathology simultaneously involves changes in articular cartilage and the subchondral bone network, therefore tangential investigation of changes in the bone and cartilage is required to most accurately diagnose disease state. With a mindset towards translation in conjunction with the complexities of imaging both cartilage and bone in early disease, we selected *ex vivo* human, cadaveric metacarpal phalangeal joints (MCPJs) as our model. OA commonly occurs in human fingers,[28] and is associated with overuse from activities such as typing and texting, as well as with injury and age.[29] MCPJs contain intact, hemispherical, nearly axisymmetric cartilage surfaces that are ideal for high-resolution imaging, biochemical evaluation, and

mechanical testing. Additionally, the underlying subchondral bone provides a suitable size for high resolution imaging. We hypothesize that tetra-ammonium functionalized cationic Ta_2O_5 NPs (NP1) will accumulate in direct proportion to the tissue glycosaminoglycan (GAG) content, an established biomarker of early OA, via electrostatic interactions with negatively charged GAGs. The resulting X-ray attenuation of the cationic NPs will positively correlate with GAG content and tissue stiffness while the CT signal obtained with neutral NPs (NP2) will be inversely correlated and of a smaller magnitude in attenuation change, while strongly correlating with tissue stiffness as it reflects the porosity of the tissue.

2.3 Methods

2.3.1 Preparation and Characterization of Ta₂O₅ Nanoparticles

We prepared core-shell tantalum oxide (Ta_2O_5) NPs possessing cationic or neutral silane ligands surrounding the radiopaque Ta_2O_5 core (**Figure 2.1**). Building off of the publications from Hyeon,[17] Kulkami,[18] and others,[22] we performed the controlled hydrolysis of tantalum (V) ethoxide, $Ta(OEt)_5$, in the presence of isobutryric acid to form the Ta_2O_5 NPs. NP diameter was altered by varying the molar ratio of isobutryric acid to tantalum oxide. After the Ta_2O_5 NP solution stirred for 16 hours, we added a solution of n-propanol, 2- [methoxy(polyethyleneoxy)6-9propyl]trimethoxysilane and N-trimethoxysilylpropyl-N,N,N-trimethylammonium chloride (1:1, mass ratio) to the reaction mixture and refluxed for an additional 2 hours in air to prepare the cationic NP1. Alternatively, we added a solution of n-propanol, 2- [methoxy(polyethyleneoxy)6-9propyl]trimethoxysilane to synthesize the neutral NP2. After the reaction mixture cooled

to room temperature, we neutralized the pH of the reaction mixture, and purified the NPs by dialysis (see SI for complete synthetic details). We subsequently lyophilized the sample to obtain the NPs as a white powder.

2.3.2 Specimen Preparation

The 2nd and 3rd MCPJ were dissected from 12 human cadaver hands (10 donors, no reported hand pathology, 70% male, mean age: 68 yrs, purchased from Medcure, Inc, Portland, OR). For each joint, all surrounding soft tissue was removed and the joint disarticulated. Surfaces were rinsed in a 400mOsm saline solution including GIBCO Anti-Anti stock solution (Invitrogen, Grand Island, NY), 5mM of EDTA (Sigma, St. Louis, MO), and benzamidine HCl (Sigma B6506, St. Louis, MO) to prevent cartilage degradation. In order to facilitate manipulation in mechanical testing and imaging, the metacarpal diaphysis was embedded in polymethylmethacrylate (PMMA) bone cement.

2.3.3 Nanoparticle Diffusion Kinetics

2nd and 3rd MCPJs from 6 cadaveric hands were disarticulated, all the surrounding soft tissue removed, submerged in saline to remove excess synovial fluid, and separated into two groups (n = 5). The MCPJ surfaces were immersed in 1 mL of either NP1 or NP2 (80 mg NP/mL 400 mOsm, ionic strength of synovial fluid, pH 7.4) at room temperature. Samples were removed from their respective NP solution, gently blotted to remove excess contrast agent and individually positioned in an airtight holder. Samples were serially imaged after being immersed for: 0, 30, 60, 120, 240, 480, 720, 1440, 2880 minutes. Sequential transaxial µCT images of both the cartilage and subchondral bone were acquired

at an isotropic voxel resolution of 36 um, 70-kVp tube voltage, 113-uAmp current, and 300-ms integration time. Scans were converted to DICOM format using proprietary software from Scano Medical AG followed by import for post processing analysis into Analyze^{TM} (AnalyzeDirect, Overland Park, KS). and articular cartilage volumetric maps were created using a semi-automatic threshold-based algorithm, which were manually reviewed and adjusted if necessary. The attenuation values for all transaxial μCT slices were combined, averaged, and normalized by the 0-min time point attenuation.

2.3.4 Mechanical Testing

Initial μCT baseline scans of all MCPJs were conducted to measure mean cartilage thickness at the apex of the hemispherical cartilage surface. The samples were scanned at an isotropic voxel resolution of 36 um, 70-kVp, 113-uAmp, 300 ms integration time (μCT40, Scanco Medical AG). μCT data was converted into DICOM format and imported into Analyze for post-processing analysis as previously described. The mean cartilage thickness at the apex was determined by a custom code (MATLAB version). The equilibrium modulus (E) of each sample was evaluated using a standard indentation procedure. Each MCPJ was potted in PMMA and clamped into a mechanical testing apparatus (Enduratec3230, BOSE, Eden Prairie, MN). The MCPJ apex (a locally flat surface) was aligned perpendicular to a 1-mm diameter, flat-ended, stainless steel indenter tip. Samples were submerged in 400-mOsm saline followed by a 2N pre-load. Each sample was compressed using a 4-step stress relaxation protocol consisting of four 5% strain steps with a displacement rate of 0.005 mm/s followed by a 300s relaxation period. A linear regression line was fit to the resulting equilibrium stress-strain data to compute the

equilibrium compressive modulus.

2.3.5 CECT Imaging and Analyses

Following mechanical testing, MCPJ samples were immersed in 2mL of 80 mg NP/mL for 24 hrs at room temperature. Prior to imaging, samples were gently blotted dry and imaged in air as previously described. Cartilage surfaces were segmented from the subchondral bone using the same software and threshold-based algorithm as previously mentioned. The mean CECT attenuation was obtained by averaging the X-ray attenuation over all transaxial μCT slices containing cartilage tissue. Effects from biological variations alongside trace residual contrast agents was negated by normalizing CECT attenuation values by baseline CT attenuation. The subchondral trabecular network was assessed from the μCT baseline scan and bone was segmented using a fixed threshold of 500 mgHA/cm3. Structural model index (SMI), bone volume fraction (%BV/TV), trabecular number (Tb.N, 1/mm), trabecular thickness (Tb.Th/mm), trabecular spacing (Tb.Sp,mm), and connectivity density (1/mm3) are reported.

2.3.6 Determination of Cartilage Glycosaminoglycan Content

Samples were equilibrated overnight in saline (40mL, room temperature), to remove residual NPs. The cartilage surface was removed, and GAG content was assessed using the standard 1,9-dimethylmethylene blue (DMMB) colorimetric assay.[9]

2.3.7 Cytotoxicity

NIH3T3 murine fibroblast cells were maintained in Dulbecco's Modified Eagle Media, with 10% fetal bovine serum and 1% penicillin/streptomycin. Cells were

maintained in a humidified atmosphere at 37 °C and 5% CO2. Sub-confluent cells were harvested and seeded on 96 well plates at 3,000 cells/well for use in in vitro cytotoxicity studies. After 24-hours, the cells were treated with nanoparticles suspended in nanopure water, starting at 120 mg/mL and serially diluted by 1/3 until a final concentration of 0.002 mg/mL. After a 24-hour exposure, cell viability was tested using a colorimetric MTS [3-(4,5-dimethylthiazol-2-yl)-5-(3- carboxymethoxyphenyl)-2-(4-sulfophenyl)-2H-tetrazolium] cell proliferation assay (Sigma, St. Louis, MO) and absorbance read at 490 nm on a Biotek Synergy HT Plate Reader (Winooski, VT). Cell viability in each well was calculated as the percentage of the positive control absorbance.

2.3.8 Statistical Analysis

Univariate linear regression analysis (GraphPad) was applied to examine relationships between E, CECT attenuations, and GAG content. The coefficient of determination (R^2) was used to assess the strength of correlations, and significance was defined as two-tailed t-test, P-value <0.05.

2.4 Results

2.4.1 NP Characterization

FTIR and 1 H NMR showed the characteristic peaks and confirmed the silane coating on the particle (**Figure 2.2**). As shown in Table 2.1, the hydrodynamic size of the NP1s and NP2s are 5.6 ± 1.2 and 4.4 ± 1.3, respectively, by dynamic light scattering (DLS). NP1 possess an overall positive charge of 13.22 ± 2.44 mV as measured using Brookhaven Instruments ZetaPALS Zeta Potential Analyzer, while NP2 exhibits a charge closer to

neutrality (0.10 ± 0.13 mV). TEM images of both NP formulations reveal a diameter of 3.78 ± 0.8, for the cationic NP1, and 3.45 ± 1.2, for the neutral NP2 (measure 200+ nps from the image), and in agreement with the DLS data.

2.4.2 Cytotoxicity

The nanoparticle concentration response curves for both NP1 and NP2 were fit with a dose response curve in order to obtain an IC50 value. IC50 value for the NP1 is 24.29 mg/mL. IC50 for the NP2 is 20.07 mg/mL (**Figure 2.3**).

2.4.3 Diffusion Kinetics

The diffusion kinetics of the Ta_2O_5 NPs into MCPJ cartilage were measured as a function of time and of both the entirety of the cartilage (**Figure 2.4** and **2.5**) and by cartilage layer (surface, middle and deep) (**Figure 2.6**). We chose a concentration of 40 mg NP/mL based on a prior study[24] and that this concentration afforded sufficient attenuation for cartilage imaging and we balanced the osmolality to 400 mOsm; the ionic strength of synovial fluid. The diffusion kinetics for NP1 and NP2 were fit with an exponential function for the average of the entire depth of the MCPJ cartilage (**Figure 2.4** and **2.5**, respectively) and for each cartilage layer (**Figure 2.6**). Both NP formulations disseminate throughout all layers of the articular cartilage, increasing attenuation of the tissue and allowing clear visualization of the cartilage and delineation between the cartilage and subchondral bone. Figure 2.4 and 2.5 establish the diffusion kinetics of both NP1 and NP2, respectively, for average of all the cartilage layers ($Y = 0.9618 + (0.1453 - 0.9618)e^{0.002094X}$ and $Y = 0.940 + (0.002532 - 0.940)e^{0.002532X}$ for NP1 and NP2, respectively). Outerbridge

score of tissue used for diffusion study ranged from II – IV.

NP1 fully diffuses throughout all three cartilage layers (surface, middle, deep) after 24 hours, providing the highest attenuation values in the surface zone (**Figure 2.6**). NP2 fully diffuses throughout the surface layer but continues to accumulate in the middle and deep zones after 48 hours (**Figure 2.6**).

2.4.4 Visualization of MCPJ cartilage using CECT with NPs

Color maps generated from NP1 and NP2 enhanced CT scans reflect GAG distribution within the three layers of articular cartilage, and the thickness and gross morphology can be easily visualized. The cartilage appears vague and without distinction of layers without contrast agent (**Figure 2.7**).

2.4.5 Relationship between CECT Attenuation with NP1, GAG Content and Equilibrium Modulus

The cationic NP1 enhanced CT attenuation significantly and positively correlates with GAG content, with coefficients of variation greater than or equal to 0.89 ($p < 0.05$) (**Figure 2.8**). As shown in Figure 2.8, a positive correlation exists between equilibrium compressive modulus and attenuation with NP1 ($R^2 \geq 0.82$, $p < 0.05$). The strong, positive correlation between cationic NPs and GAG content and tissue stiffness indicate the electrostatic attraction between the two.

2.4.6 Relationship between CECT Attenuation with NP2, GAG Content and Equilibrium

Modulus

The neutral NP2 enhanced CT attenuation was negatively and significantly correlated with the equilibrium modulus, with coefficients of variation greater than or equal to 0.93 (p<0.05) (**Figure 2.8**). Following the same trend, attenuation values were linearly and inversely correlated with the cartilage GAG content, accounting for 70% of the variation in cartilage GAG concentration (p<0.05) (**Figure 2.8**).

2.4.7 Relationships between Cartilage and the Subchondral Trabecular Network

The correlations between both cartilage and nanoparticle enhanced attenuation and the subchondral trabecular network are presented in **Figure 2.9** for both NP formulations. Trabecular structural indices examined included trabecular number (Tb.N), trabecular spacing (Tb.sp), trabecular thickness (Tb.Th), bone volume/total volume (BV/TV), and SMI. Strong positive correlations were observed between equilibrium modulus and trabecular number ($R^2 = 0.9264$, p<0.05) for NP2 enhanced CT attenuation (**Figure 2.10**). Additionally, a strong negative correlation was noted between NP2 enhanced attenuation and trabecular number (R2 = 0.9782, p<0.05) (**Figure 2.10**). There were no significant correlations noted between NP1 and trabecular structural indices.

2.5 Discussion

Osteoarthritis is a disease of the whole joint afflicting 80% of people over the age of 65.[30,31] Integral to OA pathology is the loss of cartilage function and structure, as cartilage serves as a smooth, lubricated surface for articulation and transmit loads to underlying subchondral bone. The biomechanical behavior of articular cartilage is best

described as a biphasic medium, its unique properties a result of the poroelastic collagen fibril network, which provides structure and tensile strength, complemented by the GAG matrix of anionic polysaccharides covalently attached to a proteoglycan backbone. The solid phase consists of the 3D poroelastic collagen network, while the fluid phase consists primarily of water, up to 80% of cartilage wet weight.[32,33] GAGs maintain the hydrated state of articular cartilage by conferring a fixed negative charge by way of their heavily carboxylated and sulfated side chains.[32,33] The pressurization of fluid within the solid collagen matrix in conjunction with the frictional resistance to water flow through the cartilage forms the mechanisms by which articular cartilage derives its ability to withstand significant load, frequently upwards of multiple times bodyweight.[33–36] Upon loading, water becomes pressurized within the pores of cartilage. It will slowly efflux out of the tissue, but is faced with significant frictional drag forces, this interstitial fluid pressure allows cartilage to support large loads, up to 20MPa on a repeated basis, without wearing away.[35,36] The ability of cartilage to withstand physiologic loads and shear forces depends on both the composition and structural integrity of the extracellular matrix. During early-stage OA the composition and structural integrity of the extracellular matrix is perturb via a decrease in GAG content coupled with collagen degradation.[33] Together these perturbations lead to an increase in cartilage permeability and a decrease in tissue stiffness. Higher permeability of the tissue causes rapid exudation of interstitial fluid upon tissue loading resulting in the solid collagen matrix bearing more of the load and leaving cartilage vulnerable to further mechanical damage and propagating a positive feedback loop of pathological changes. This feedback cycle of cartilage degradation continues throughout

disease progression, exacerbated by other factors such as the increased production of inflammatory cytokines and matrix metalloproteinases. As such, loss of GAGs (i.e., the anionic polysaccharides) is an early sign of disease[1] and an established biomarker.[37,38]

In conjunction with biochemical and biomechanical changes in the cartilage, OA disease pathology encompasses changes in the subchondral bone and trabecular network morphometry. Techniques to assess both cartilage and bone simultaneously are of significant interest to gather comprehensive information regarding disease state. Herein, the use of the human metacarpal enables the study of the relationship between cartilage and bone properties, specifically using contrast-enhanced CT. OA commonly occurs in human fingers,[28] and specifically the metacarpal phalangeal joint (MCPJ) (the knuckle) presents an intact, hemispherical, nearly axisymmetric cartilage surfaces that is ideal for high-resolution imaging, biochemical evaluation, and mechanical testing. Using MCPJs obviates damaging the bone and cartilage through sample extraction methods such as coring, while providing an ideal geometry for testing and imaging. Additionally, use of MCPJs alleviates the need to artificially degrade cartilage to create an OA model for study and naturally provides a range of cartilage health as the extent of OA increases in each MCPJ along the hand (with the pointer finger having highest degree and OA prevalence decreasing towards the last finger).[39,40]

The two nanoparticle formulations described herein, cationic NP1 and neutral NP2, diffuse throughout the entirety of MCPJ cartilage. Macroscopically, articular cartilage is divided into three layers – surface, middle and deep. Upon analyzing these different layers for diffusion kinetics of both NP1 and NP2, results indicate that NP1 fully diffused

throughout all layers (**Figure 2.6**). On the other hand, results clearly indicate that NP2 had not fully diffused through the middle and deep layers (**Figure 2.6**). Despite not having diffused throughout the entirety of all cartilage layers, the NP2 still provide significant correlations between both CT attenuation and GAG content and CT attenuation and equilibrium modulus. This suggests that if allowed to diffuse longer those correlations may improve even further in strength, and that if there is a significant correlation with GAG and E before the NP2 has reached full diffusion equilibrium, that a full 24 hours may not be needed to achieve significant correlations. This is important from a clinical perspective as a 1 – 2-hour incubation time would be more appropriate. Further studies are warranted to examine if significant correlations can be achieved with GAG and E using a short diffusion time.

The results presented in **Figure 2.8** show strong significant correlations between both NP1 and NP2 enhanced CT attenuation and GAG content. The neutral NP2 enhanced CT attenuation accounts for 70% of the variation in GAG content, while the positively charged NP1 enhanced CT attenuation accounts for 89% of the variation in GAG content and is a stronger correlation. Similarly, strong significant correlations between both NP formulations and equilibrium modulus are present. The neutral NP2 enhanced CT attenuation accounts for 98% of the variation in equilibrium modulus and the positively charged NP enhanced CT attenuation accounts for 83% of the variation in equilibrium modulus. The positively charged Ta_2O_5 NP2 more closely reflect the local fixed charge density of the cartilage as a whole – i.e., GAG, due to the favorable electrostatic interactions between the cationic NPs and the anionic GAGs. Additionally, in healthy

cartilage with simultaneously high GAG content and high tissue stiffness, the electrostatic attraction between the positively charged NP1 and negatively charged GAGs resulted in higher overall tissue uptake of the NP1 compared to NP2. The positively charged NP1 exhibit a 1.33-fold greater CT attenuation dynamic range (linear attenuation ranging from 2453 to 3636.71) compared to the neutral NP2s (linear attenuation ranging from 1154 to 2044) (**Figure 2.11**).

In contrast**,** the neutral NPs have no electrostatic interaction with the ECM and diffuse into the tissue in direct reflection of the structural integrity and stiffness of the ECM, an indirect reflection of GAG content. The structural integrity of the solid collagen network of cartilage, presents a key component of cartilage mechanical function and tissue health, with the solid collagen matrix giving rise to the compressive and tensile strength of the tissue. Coupled with a high GAG content, a high equilibrium modulus is an indicator of healthier tissue, where healthy human cartilage typically has GAG content in the range of 5-10% wet weight and an equilibrium modulus of 0.5-1 MPa.[33,41] The porosity of cartilage arises as a result of the interaction between GAGs, collagen fibrils and interstitial fluid.[33,42] The solid collagen matrix alone has pore sizes ranging from 50 to 200 nm, and is densely packed with aggrecan molecules, with anywhere from 4.5 to 15 nm between GAG side chains.[42] This results in an overall pore size of $6 - 11$nm for the ECM.[42] The concurrent loss of anionic GAGs and decrease in steric hindrance (due to increasing tissue porosity) during OA pathogenesis, decreases the fixed charge density of the tissue and results in more porous, softer tissue, thereby allowing for a higher partitioning of the neutral NP2 within diseased tissue. However, due to low tissue porosity and permeability in healthy

cartilage, the neutral NP2 was largely excluded from healthy cartilage, resulting in a slightly weaker correlation between NP2 enhanced attenuation and GAG content compared to the cationic NP1.

Our depth wise analysis of the diffusion kinetics of NP1 and NP2 indicate the diffusion of both contrast agents is non-uniform throughout the three layers cartilage. For the cationic NP1, the time constant increases from surface to deep zones, with the deep zone failing to reach equilibrium In contrast, the neutral NP2, fails to reach equilibrium at 48 hours in any of the zones of cartilage, so far as to present a linear diffusion curve in the deep zone. Degraded articular cartilage possesses higher tissue porosity due to a degradation of the solid collagen network, increasing tissue permeability and in turn facilitating diffusion. Concurrent with degradation of the solid collagen matrix, the GAG content decreases with cartilage degradation, lowering the fixed negative charge density, which we surmise slows the diffusion of the cationic NP1 but aids to increase the passive diffusion of NP1. These simultaneous, but opposite effects make the interpretation of diffusion kinetic results complicated. How exactly NP1 and NP2 diffusion relates to variation in the depth wise organization of the cartilage constituents requires further experimentation in combination with finite element modeling.

Contrast enhanced CT (CECT) allows for analysis of both cartilage and bone. OA causes concurrent changes in cartilage and subchondral bone; an ideal model would allow characterization of both. With the MCPJ model, NP2 contrast enhanced CT attenuation negatively correlates between trabecular morphological indices, specifically trabecular number, and both CECT attenuation and equilibrium modulus (**Figure 2.10**). Increased

CECT attenuation with NP2 signifies decreasing trabecular number. This result is corroborated by the positive correlation between trabecular number and equilibrium modulus, where a higher equilibrium modulus *(e.g.,* healthier tissue) significantly correlates with a larger trabecular number. Trabecular number, a component of the bone volume fraction, along with trabecular thickness and trabecular spacing, is one morphometric to measure boney changes in the subchondral trabecular network, of which deterioration is indicated during OA pathogenesis.[43,44] These correlations described between decreases in the trabecular morphological indices with OA disease progression, are corroborated by results from studies using early-stage osteoarthritic mice[45] and rats,[46] concomitant with studies of beginning-stage OA in humans.[47] Correlations were not all significant, although trends were noted between attenuation and both bone mineral density and bone structural model index (a measure of the shape of the trabeculae) (**Figure 2.9**). Cartilage degeneration with age is a natural occurrence resulting from accumulation of advanced glycation end products and senescent chondrocytes. One short coming of this study is that there was not a truly normal, healthy population, with all donors being above 55 years of age and naturally having some degree of cartilage degradation. Additionally, the MCPJ is not a heavy load bearing joint, and therefore changes in trabecular morphometrics may be diffuse compared to those changes in load bearing joints such as the knee and hip. CECT using tantalum oxide nanoparticles enables simultaneous evaluation of both cartilage biochemical and mechanical healthy in addition to bone properties of the human metacarpal.

Plain radiography remains the most accessible tool and the current standard of care

to diagnose OA. While it is accessible and inexpensive, it cannot directly visualize soft tissues or cartilage, and diagnoses are based solely on boney changes such as joint space narrowing, osteophytes, sclerosis, joint incongruity and malalignment,[48,49] which typically occur in the later stages of the disease. Other imaging modalities include MRI, which is able to visualize soft tissues and cartilage directly. Specifically, gadolinium enhanced MRI (dGEMRIC) which uses gadopentetate as a mobile anionic probe to measure cartilage composition and structure.[49–51] Yet this is not a perfect scenario, dGEMRIC is hindered by nephrotoxicity concerns associated with the IV injection, specifically for elderly and diabetic patients.[52,53] Additionally, deeper joints such as the hip cannot be imaged with standard coils and require high field strength magnets and specialized coils.[54] MRI is also costly, and research has shown non-unanimous results between studies.[55] Detecting early changes in the biochemical composition of cartilage is key in order to implement therapeutics at a point when the cartilage may be salvaged to prolong the lifespan of the joint or joints in question. Therefore, minimally invasive techniques, specifically targeted contrast agents, that quantitatively assess changes in cartilage are of great interest, as cartilage thickness, morphology and GAG content correlate with tissue health and disease state. As such CT is a key imaging modality for musculoskeletal diseases and injuries and when combined with contrast agents offers the potential to both visualize and quantify tissue composition and properties.

Advances in the synthesis of nanoparticles are yielding various types of nanoparticles for medical imaging. Although up to now, their use as has been restricted to non-quantitative imaging of soft tissues.[56–58] With regards to detection and treatment

monitoring, nanotechnology offers significant potential through new diagnostic capabilities. Herein we demonstrate the use of Ta_2O_5 NPs for CECT imaging and quantitative assessment of cartilage biochemical and mechanical health, as well as a 3D spatial determination of cartilage and bone. Ta_2O_5 NPs, regardless of charge, offer an alternative to dGEMRIC MRI and iodinated contrast agents for measuring articular cartilage functional properties non-invasively. Contrast agents for CT imaging are of immediate interest for use in diagnosing subtle changes correlated with early-stage osteoarthritis. Early intervention via detection is key to prolonging the lifespan of existing cartilage and preventing further degradation and irreversible damage of the tissue.

2.6 References

1.   Zhang, Y. & Jordan, J. M. Epidemiology of Osteoarthritis. *Clinics in Geriatric Medicine* **26**, (2010).

2.   Amin, S. *et al.* The relationship between cartilage loss on magnetic resonance imaging and radiographic progression in men and women with knee osteoarthritis. *Arthritis and Rheumatism* **52**, 3152–3159 (2005).

3.   Braun, H. J. & Gold, G. E. Diagnosis of osteoarthritis: Imaging. *Bone* **51**, 278–288 (2012).

4.   Roduner, E. Size matters: Why nanomaterials are different. *Chemical Society Reviews* **35**, 583–592 (2006).

5.   Farka, Z., Juřík, T., Kovář, D., Trnková, L. & Skládal, P. Nanoparticle-Based Immunochemical Biosensors and Assays: Recent Advances and Challenges. *Chemical Reviews* **117,** 9973–10042 (2017).

6.   Holzinger, M., Goff, A. le & Cosnier, S. Nanomaterials for biosensing applications: A review. *Frontiers in Chemistry* **2**, 63 (2014).

7.   Larguinho, M. & Baptista, P. v. Gold and silver nanoparticles for clinical diagnostics - From genomics to proteomics. *Journal of Proteomics* **75**, 2811–2823 (2012).

8.   Azzazy, H. M. E. & Mansour, M. M. H. In vitro diagnostic prospects of nanoparticles. *Clinica Chimica Acta* **403**, 1–8 (2009).

9.   Lawson, T. B., Mäkelä, J. T. A., Klein, T., Snyder, B. D. & Grinstaff, M. W. Nanotechnology and Osteoarthritis. Part 2: Opportunities for advanced devices and therapeutics. *Journal of Orthopaedic Research* **39,** 473-484(2021).

10.   Patra, J. K. *et al.* Nano based drug delivery systems: Recent developments and future prospects. *Journal of Nanobiotechnology* **16**, (2018).

11.   Mitchell, M. J. *et al.* Engineering precision nanoparticles for drug delivery. *Nature Reviews Drug Discovery* 1–24 (2020)

12.   Lawson, T. B., Mäkelä, J. T. A., Klein, T., Snyder, B. D. & Grinstaff, M. W. Nanotechnology and Osteoarthritis. Part 1: Clinical Landscape and Opportunities for Advanced Diagnostics. *Journal of Orthopaedic Research* **39**, 465-472 (2021).

13.   Han, X., Xu, K., Taratula, O. & Farsad, K. Applications of nanoparticles in biomedical imaging. *Nanoscale* **11**, 799–819 (2019).

14.   Cole, L. E., Ross, R. D., Tilley, J. M., Vargo-Gogola, T. & Roeder, R. K. Gold nanoparticles as contrast agents in X-ray imaging and computed tomography. *Nanomedicine* **10**, 321–341 (2015).

15.   Kim, D., Park, S., Jae, H. L., Yong, Y. J. & Jon, S. Antibiofouling polymer-coated gold nanoparticles as a contrast agent for in vivo X-ray computed tomography imaging. *Journal of the American Chemical Society* **129**, 7661–7665 (2007).

16.   Wei, B. *et al.* Facile Synthesis of Uniform-Sized Bismuth Nanoparticles for CT Visualization of Gastrointestinal Tract in Vivo. *ACS Applied Materials and Interfaces* **8**, 12720–12726 (2016).

17.   Oh, M. H. *et al.* Large-scale synthesis of bioinert tantalum oxide nanoparticles for X-ray computed tomography imaging and bimodal image-guided sentinel lymph node mapping. *Journal of the American Chemical Society* **133**, 5508–5515 (2011).

18.   Bonitatibus, P. J., Torres, A. S., Goddard, G. D., Fitzgerald, P. F. & Kulkarni, A. M. Synthesis, characterization, and computed tomography imaging of a tantalum oxide nanoparticle imaging agent. *Chemical Communications* **46**, 8956–8958 (2010).

19.   Rabin, O., Perez, J. M., Grimm, J., Wojtkiewicz, G. & Weissleder, R. An X-ray computed tomography imaging agent based on long-circulating bismuth sulphide nanoparticles. *Nature Materials* **5**, 118–122 (2006).

20.   Au, J. T. *et al.* Gold Nanoparticles Provide Bright Long-Lasting Vascular Contrast for CT Imaging. *American Journal of Roentgenology* **200**, 1347–1351 (2013).

21. Torres, A. S. *et al.* Biological performance of a size-fractionated core-shell tantalum oxide nanoparticle X-ray contrast agent. *Investigative Radiology* **47**, 578–587 (2012).

22. Bonitatibus, P. J. *et al.* Preclinical assessment of a zwitterionic tantalum oxide nanoparticle X-ray contrast agent. *ACS Nano* **6**, 6650–6658 (2012).

23. Xiao, Q. *et al.* Radiopaque fluorescence transparent TaOx decorated upconversion nanophosphors for in vivo CT/MR/UCL trimodal imaging. *Biomaterials* **33**, 7530–7539 (2012).

24. Freedman, J. D., Lusic, H., Snyder, B. D. & Grinstaff, M. W. Tantalum oxide nanoparticles for the imaging of articular cartilage using X-ray computed tomography: Visualization of ex vivo/in vivo murine tibia and ex vivo human index finger cartilage. *Angewandte Chemie - International Edition* **53**, 8406–8410 (2014).

25. Honkanen, M. K. M. *et al.* Triple Contrast CT Method Enables Simultaneous Evaluation of Articular Cartilage Composition and Segmentation. *Annals of Biomedical Engineering* **48**, 556–567 (2020).

26. Saukko, A. E. A. *et al.* Dual Contrast CT Method Enables Diagnostics of Cartilage Injuries and Degeneration Using a Single CT Image. *Annals of Biomedical Engineering* **45**, 2857–2866 (2017).

27. Cormode, D. P., Naha, P. C. & Fayad, Z. A. Nanoparticle contrast agents for computed tomography: A focus on micelles. *Contrast Media and Molecular Imaging* **9**, 37–52 (2014).

28. Kalichman, L. & Hernández-Molina, G. Hand osteoarthritis: An epidemiological perspective. *Seminars in Arthritis and Rheumatism* **39**, 465–476 (2010).

29. Williams, F. M. K. & Spector, T. D. Osteoarthritis. *Medicine* **34**, 364–368 (2006).

30. Aigner, T. & McKenna, L. Molecular pathology and pathobiology of osteoarthritic cartilage. *Cellular and Molecular Life Sciences* **59**, 5–18 (2002).

31. Chen, D. *et al.* Osteoarthritis: Toward a comprehensive understanding of pathological mechanism. *Bone Research* **5**, 16044 (2017).

32. Setton, L. A., Elliott, D. M. & Mow, V. C. Altered mechanics of cartilage with osteoarthritis: Human osteoarthritis and an experimental model of joint degeneration. *Osteoarthritis and Cartilage* **7**, 2–14 (1999).

33. Sophia Fox, A. J., Bedi, A. & Rodeo, S. A. The basic science of articular cartilage: Structure, composition, and function. *Sports Health* **1**, 461–468 (2009).

34. Mankin, H. J. Biochemical and metabolic aspects of osteoarthritis. *Orthopedic Clinics of North America* **2**, 19–31 (1971).

35. Park, S., Krishnan, R., Nicoll, S. B. & Ateshian, G. A. Cartilage interstitial fluid load support in unconfined compression. *Journal of Biomechanics* **36**, 1785–1796 (2003).

36. Ateshian, G. A. The Role of Interstitial Fluid Pressurization in Articular Cartilage Lubrication. **42**, 1163-1176 (2009)

37. Wei, L. *et al.* Comparison of differential biomarkers of osteoarthritis with and without posttraumatic injury in the Hartley guinea pig model. *Journal of Orthopaedic Research* **28**, 900–906 (2010).

38. Mazor, M., Best, T. M., Cesaro, A., Lespessailles, E. & Toumi, H. Osteoarthritis biomarker responses and cartilage adaptation to exercise: A review of animal and human models. *Scandinavian Journal of Medicine and Science in Sports* **29**, 1072–1082 (2019).

39. Egger, P. *et al.* Patterns of joint involvement in osteoarthritis of the hand: The Chingford study. *Journal of Rheumatology* **22**, 1509–1513 (1995).

40. Chaisson, C. E. *et al.* Radiographic hand osteoarthritis: incidence, patterns, and influence of pre-existing disease in a population-based sample. *The Journal of rheumatology* **24**, 1337–43 (1997).

41. M, H., S, T. & Anatomy, L. F. Anatomy, Biochemistry and Physiology of articular cartilage. *Investigative Radiology* **35**, 573–580 (2000).

42. Mow, V. C., Holmes, M. H. & Michael Lai, W. Fluid transport and mechanical properties of articular cartilage: A review. *Journal of Biomechanics* **17**, 377–394 (1984).

43. Botter, S. M. *et al.* Quantification of subchondral bone changes in a murine osteoarthritis model using micro-CT. *Biorheology* **43**, 379–388 (2006).

44. Li, G. *et al.* Subchondral bone in osteoarthritis: insight into risk factors and microstructural changes. *Arthritis research and therapy* **15**, 223 (2013).

45. Botter, S. M. *et al.* Osteoarthritis induction leads to early and temporal subchondral plate porosity in the tibial plateau of mice: An in vivo microfocal computed tomography study. *Arthritis and Rheumatism* **63**, 2690–2699 (2011).

46. Hayami, T. *et al.* Characterization of articular cartilage and subchondral bone changes in the rat anterior cruciate ligament transection and meniscectomized models of osteoarthritis. *Bone* **38**, 234–243 (2006).

47. Chang, G. *et al.* 7T MRI detects deterioration in subchondral bone microarchitecture in subjects with mild knee osteoarthritis as compared with healthy controls. *Journal of Magnetic Resonance Imaging* **41**, 1311–1317 (2015).

48. Wick, M. C., Kastlunger, M. & Weiss, R. J. Clinical Imaging Assessments of Knee Osteoarthritis in the Elderly: A Mini-Review. *Gerontology* **60** (2014)

49. Peterfy, C. & Kothari, M. Imaging Osteoarthritis: Magnetic Resonance Imaging Versus X-ray. *Current rheumatology reports* **8**, 18-21 (2006).

50. Tiderius, C. J., Olsson, L. E., Leander, P., Ekberg, O. & Dahlberg, L. Delayed gadolinium-enhanced MRI of cartilage (dGEMRIC) in early knee osteoarthritis. *Magnetic Resonance in Medicine* **49**, 488–492 (2003).

51. Williams, A., Sharma, L., McKenzie, C. A., Prasad, P. v. & Burstein, D. Delayed gadolinium-enhanced magnetic resonance imaging of cartilage in knee osteoarthritis: Findings at different radiographic stages of disease and relationship to malalignment. *Arthritis & Rheumatism* **52**, 3528–3535 (2005).

52. Grobner, T. Gadolinium - A specific trigger for the development of nephrogenic fibrosing dermopathy and nephrogenic systemic fibrosis? *Nephrology Dialysis Transplantation* **21**, 1104–1108 (2006).

53. Bhave, G., Lewis, J. B. & Chang, S. S. Association of Gadolinium Based Magnetic Resonance Imaging Contrast Agents and Nephrogenic Systemic Fibrosis. *Journal of Urology* **180**, 830–835 (2008).

54. Potter, H. G. & Schachar, J. High resolution noncontrast MRI of the hip. *Journal of Magnetic Resonance Imaging* **31**, 268–278 (2010).

55. Roemer, F. W., Eckstein, F., Hayashi, D. & Guermazi, A. The role of imaging in osteoarthritis. *Best Practice and Research: Clinical Rheumatology* **28**, 31–60 (2014).

56. Attia, M. F., Wallyn, J., Anton, N. & Vandamme, T. F. Inorganic nanoparticles for X-ray computed tomography imaging. *Critical Reviews in Therapeutic Drug Carrier Systems* **35**, 391–432 (2018).

57. Shreffler, J. W., Pullan, J. E., Dailey, K. M., Mallik, S. & Brooks, A. E. Overcoming Hurdles in Nanoparticle Clinical Translation: The Influence of Experimental Design and Surface Modification. *International journal of molecular sciences* **20**, (2019).

58. Fitzgerald, P. F. *et al.* Proposed computed tomography contrast agent using carboxybetaine zwitterionic tantalum oxide nanoparticles imaging, biological, and physicochemical performance. *Investigative Radiology* **51**, 786–796 (2016).

Table 2.1. Nanoparticle diameter measured via DLS and TEM

Nanoparticle Type	Diameter by DLS (nm)	Diameter by TEM (nm)	Zeta Potential in D.I. H_2O (mV)
Cationic (NP1)	5.6 $\pm$ 1.2	3.78 $\pm$ 0.8	13.22 $\pm$ 2.44
Neutral (NP2)	4.4 $\pm$ 1.3	3.45 $\pm$ 1.2	0.10 $\pm$ 0.13
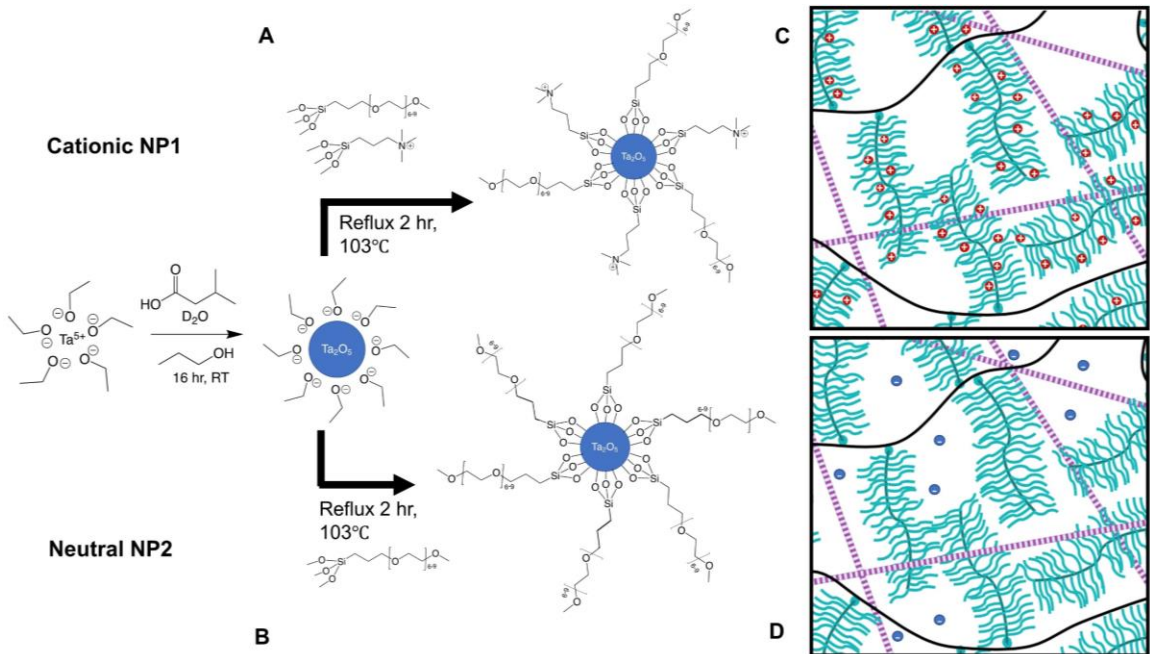
Figure 2.1. Synthesis schematic of both cationic (**A**) and neutral (**B**) nanoparticle synthesis. **C**) Cartoon representation of cationic charged nanoparticles attracted to the negatively charged GAGs within cartilage. **D**) Cartoon representation of the neutral nanoparticles within the pores of the ECM of cartilage.
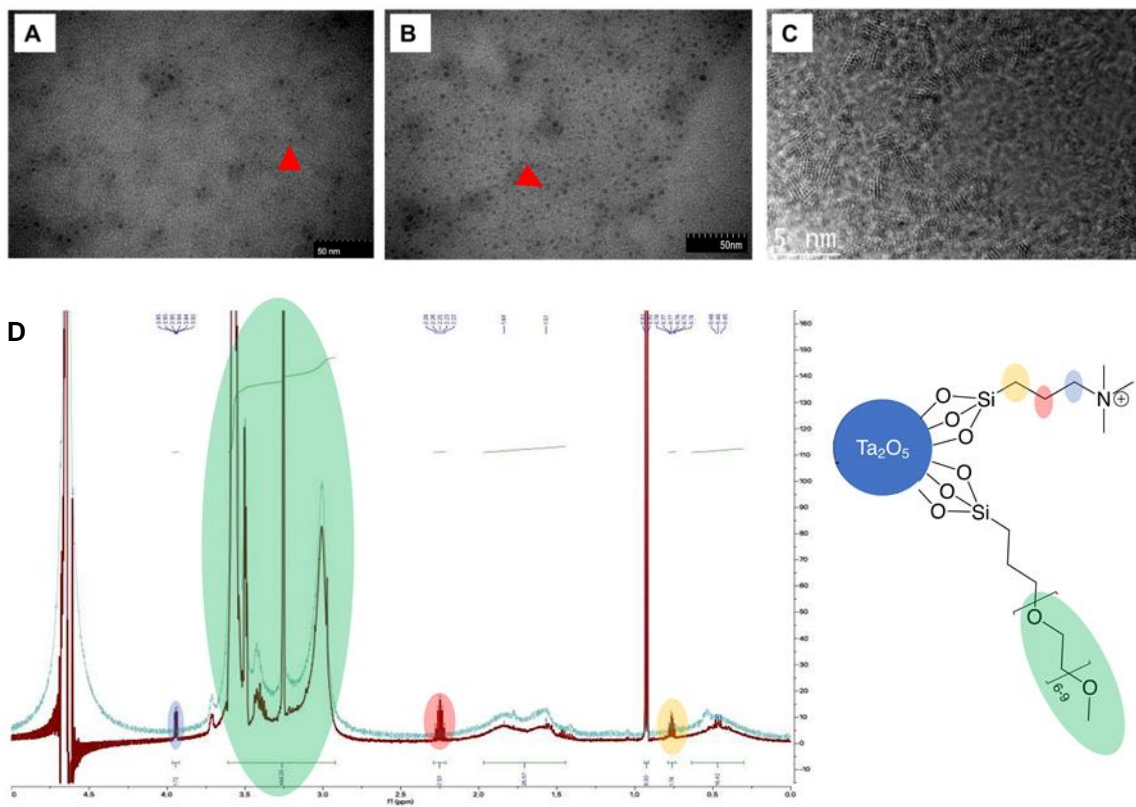
Figure 2.2. TEM images of synthesized nanoparticles. A) TEM of positively charged particles NP1, B) TEM of neutral nanoparticles NP2, C) higher magnification TEM of positively charged particles where bonds between chemical groups are visualized. D) H1 NMR of cationic NP1 (red) and neutral NP2 (blue).
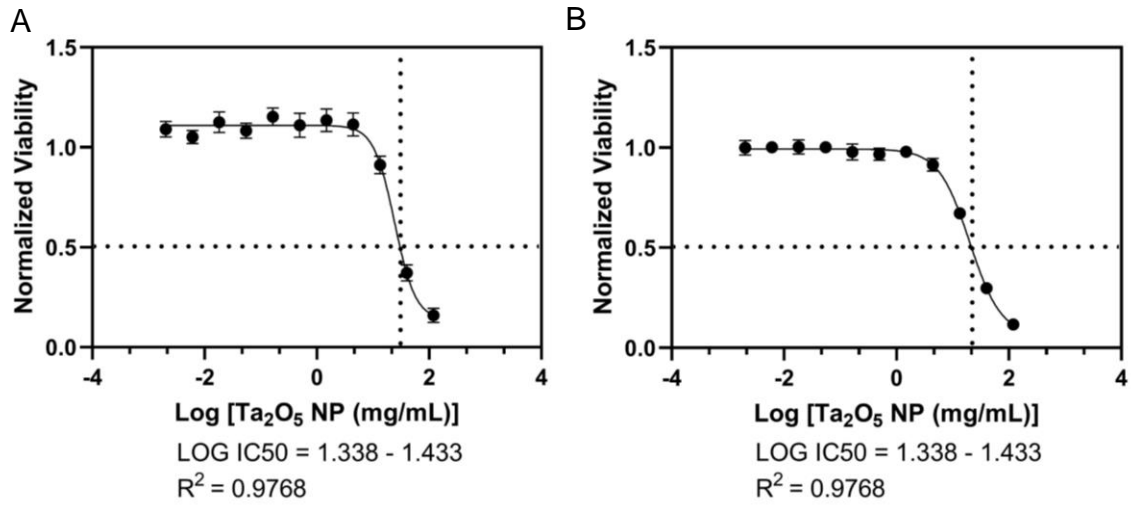
Figure 2.3. IC50 for tantalum oxide nanoparticles **A**) cationic NP1 and **B**) neutral NP2 particles. Determined by measuring cell viability of NIH 3T3 fibroblasts after 24 hours of exposure to varying concentrations, ranging from 120 mg/mL to 0.002 mg/mL of particles.
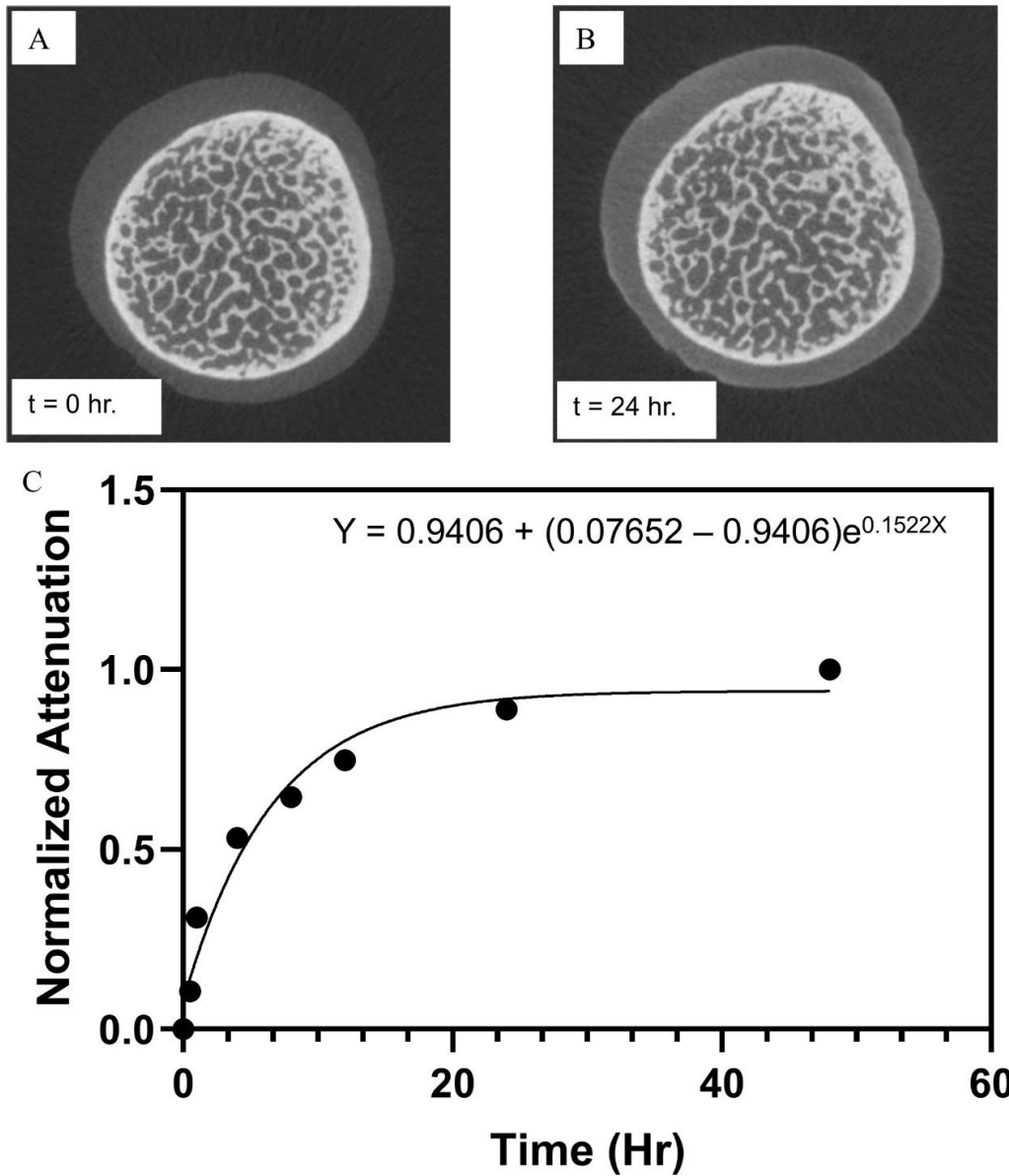
Figure 2.4. Representative, single CT slices at **A**) T = 0 hours and **B**) T = 24 hours. C) Diffusion kinetics of cationic NP1 into the cartilage of three MCPJs. Data are plotted as the normalized CECT attenuation. By fitting the data for each sample with an exponential decay equation, tau values can be calculated for each sample. Mean tau value 477.7 min. N = 3 replicates, exponential decay analysis, R2 = 0.943.
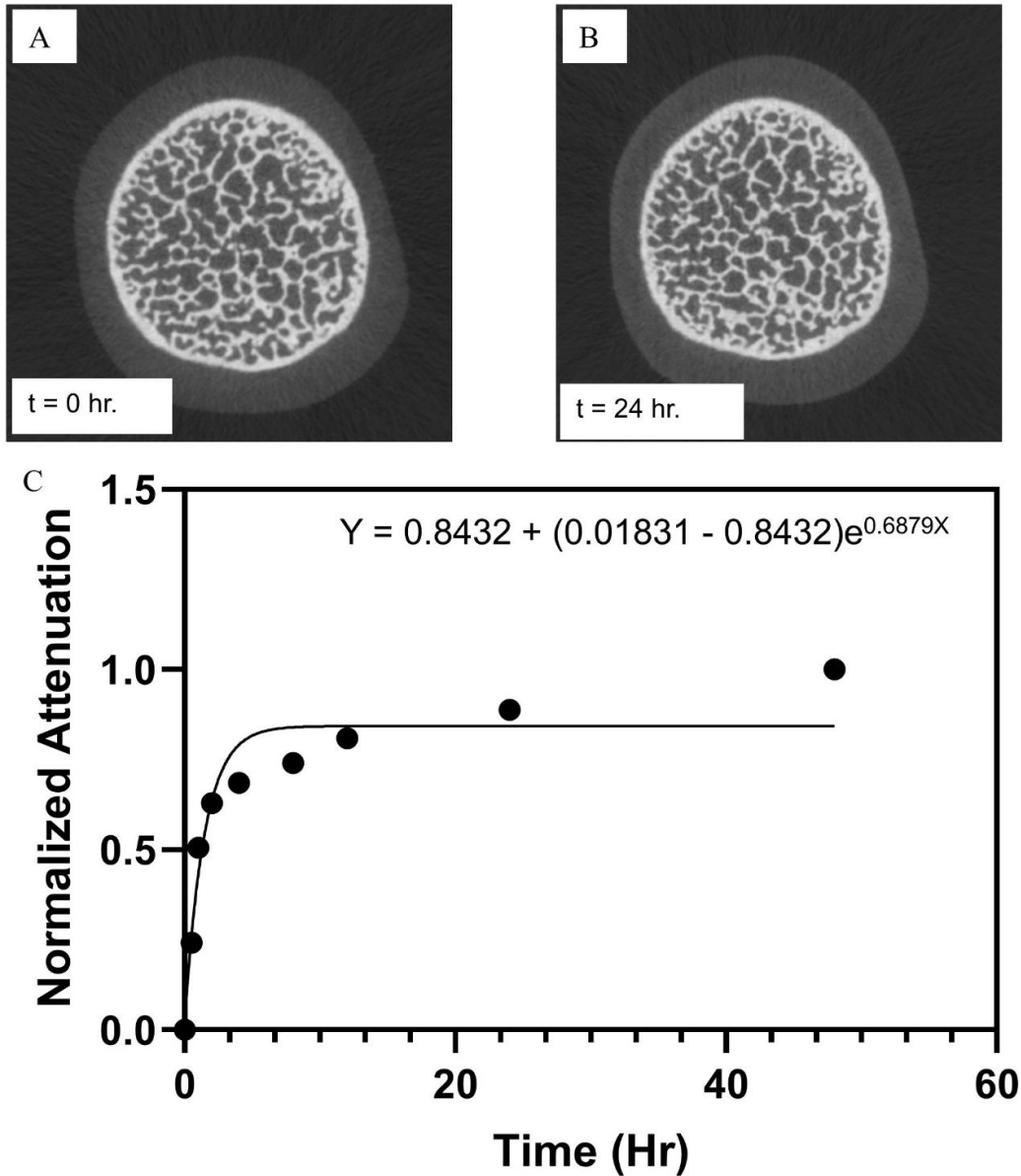
Figure 2.5. Representative, single CT slices at **A**) T = 0 hours and **B**) T = 24 hours. C) Diffusion kinetics of cationic NP1 into the cartilage of three MCPJs. Data are plotted as the normalized CECT attenuation. By fitting the data for each sample with an exponential decay equation, tau values can be calculated for each sample. Mean tau value 395.0 min. N = 3 replicates, exponential decay analysis, $R^2 = 0.9645$**.**
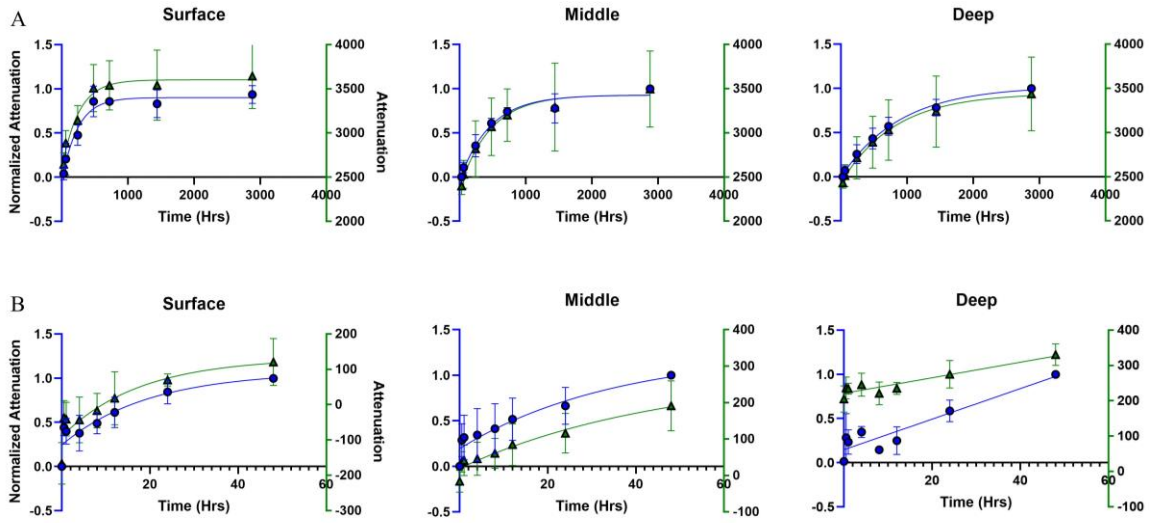
Figure 2.6. A) Diffusion kinetics of cationic NP1 through the surface, middle and deep zones of articular cartilage. N = 3 replicates, exponential decay analysis. **B**) Diffusion kinetics of neutral NP2 through the surface, middle and deep zones of articular cartilage. N = 3 replicates, exponential decay analysis.
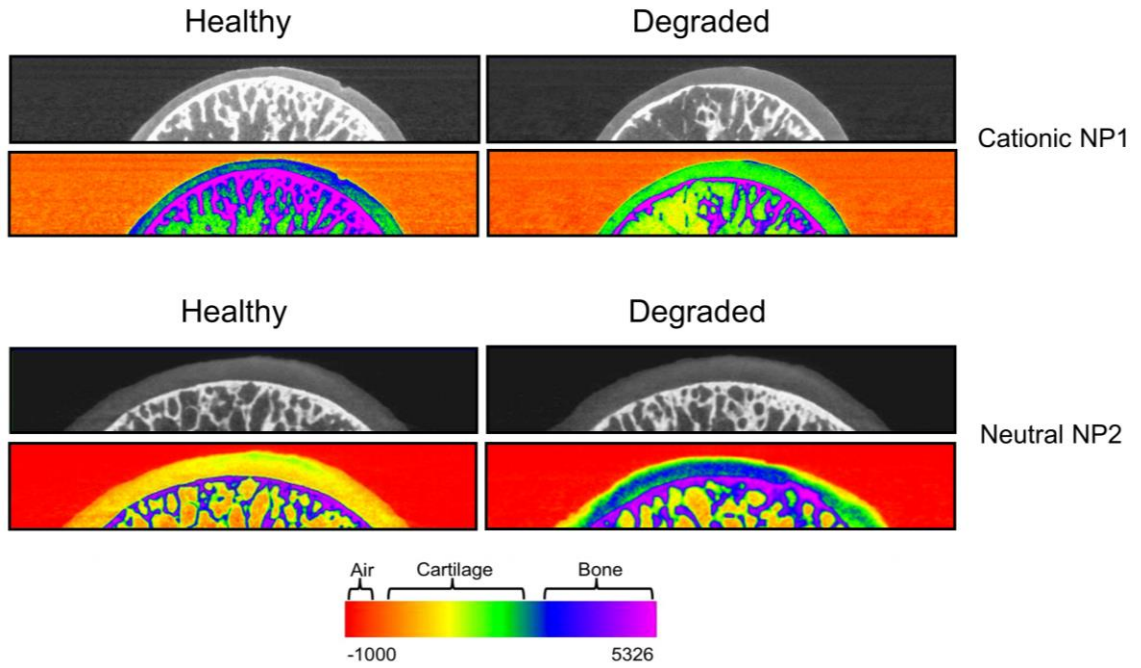
Figure 2.7. Representative color maps and corresponding contrast enhanced CT slice of coronal slices of MCPJs using cationic NP1 or neutral NP2 for healthy and naturally osteoarthritic samples.
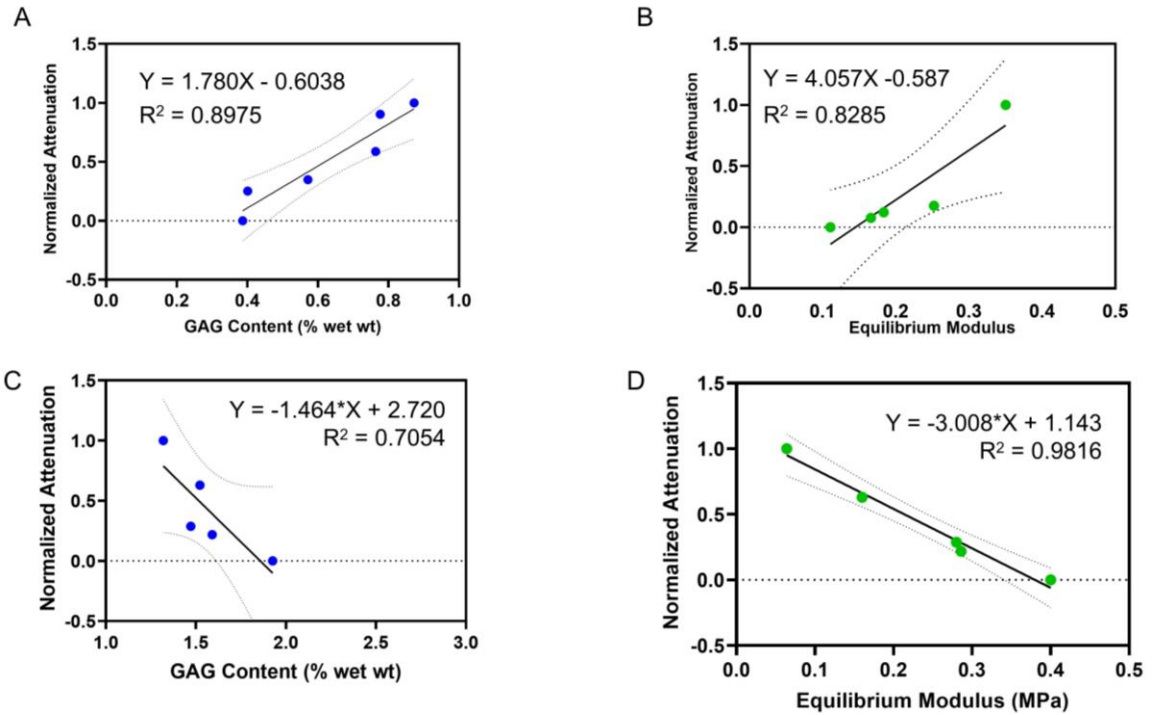
Figure 2.8. Correlation between X-ray attenuation (**A**) and equilibrium modulus (**B**) for NP1. Correlations were statistically significant at $P = 0.0041$ and $P = 0.0318$, respectively. N = 3 replicates, linear regression analysis, dashed lines indicate 95% confidence bands of best fit line. Correlation between X-ray attenuation (**C**) and equilibrium modulus (**D**) for NP2. Correlations were statistically significant at $P = 0.00750$ and $P = 0.0011$, respectively. N = 3 replicates, linear regression analysis, dashed lines indicate 95% confidence bands of best fit line.
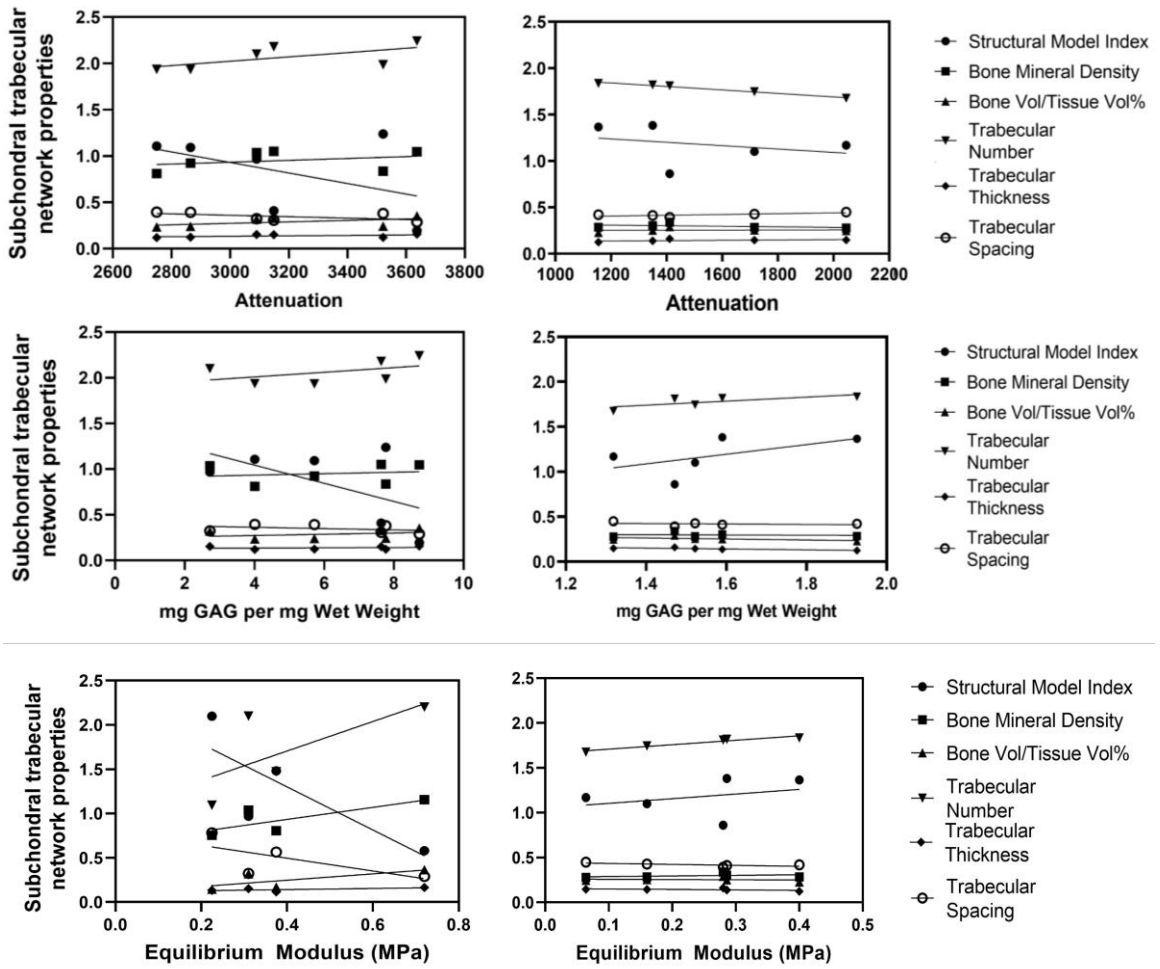
Figure 2.9. Subchondral bone indices vs CECT attenuation, GAG content and equilibrium modulus.
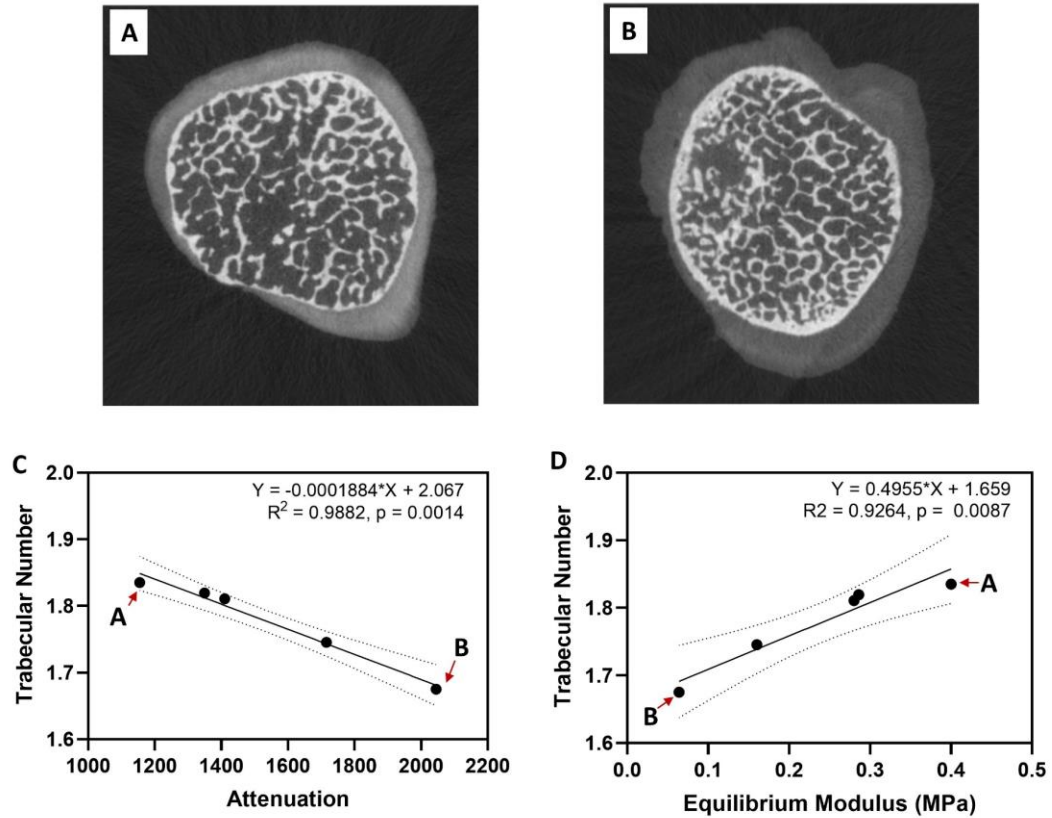
Figure 2.10. Representative coronal μCT slices of MCPJs reflecting the Trabecular number vs Attenuation relationship for a sample with A) late-stage OA and B) early-stage OA. C) Significant negative correlation between subchondral trabecular number and contrast enhanced attenuation. D) Significant positive correlation between Trabecular number vs Equilibrium modulus. Linear regression analysis, dashed lines indicate 95% confidence bands of best fit line.
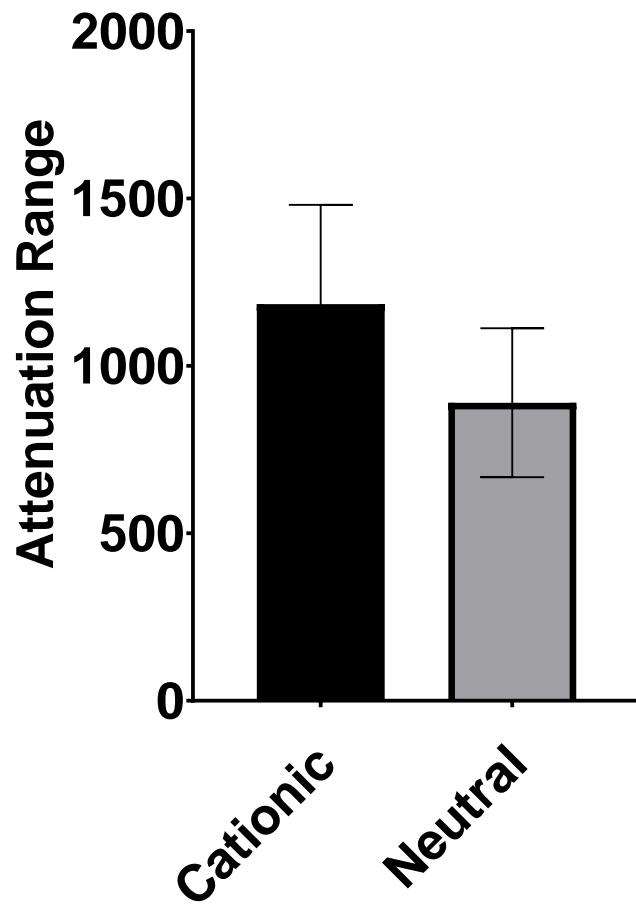
Figure 2.11. Attenuation ranges for NP1 and NP2.

CHAPTER THREE: Nanotechnology and Osteoarthritis: Opportunities for

Advanced Devices and Therapeutics

3.1 Abstract

Osteoarthritis (OA) is a multifactorial disease of the entire joint which afflicts 140 million individuals worldwide regardless of economic or social status. Current clinical treatments for OA primarily center on reducing pain and increasing mobility, and there are limited therapeutic interventions to restore degraded cartilage or slow disease pathogenesis. This review focuses first on current surgical and non-surgical treatments for OA and then summarizes recent advancements in nanotechnology-based treatments. We review nano delivery systems for small molecule drugs, nucleic acids, and proteins followed by nano-based scaffolds for neocartilage formation and osteochondral regeneration, and lastly nanoparticle lubricants. We conclude by identifying opportunities for nanomedicine advances, and prospects for OA treatments.

3.2 Introduction

3.2.1 Medical Management

To date, initial treatments for patients suffering from OA include activity modification, weight loss, braces, exercise, and physical therapy in conjunction with anti-inflammatory drugs and/or intra-articular corticosteroid injections (**Table 3.1**). [1-6] Analgesics only relieve symptoms. Nonsteroidal anti-inflammatory drugs (NSAIDs), while both analgesic and anti-inflammatory, exhibit serious side effects over extended time periods. Predicated on the theory that supplementing hyaluronic acid in osteoarthritic synovial fluid will improve its viscous lubrication, viscosupplementation is the intra-articular injection of a cross-linked hyaluronic acid derivative into an osteoarthritic joint. While viscosupplements are generally safe, well tolerated by elderly patients, and demonstrated to provide moderate pain relief, they do no improve cartilage health and provide comparable outcomes to saline in several randomized controlled studies. Corticosteroids are recommended for short term (16-24 weeks) treatment of OA based on strong clinical and scientific evidence that glucocorticoids inhibit the expression and action of most cytokines.[7] Dexamethasone, the most potent of these, is chondroprotective in post-traumatic OA.[8] While systemically administered corticosteroids systemically prevent toxic side effects in off-target tissues and organ systems, intra-articular administration minimizes these unintended consequences. Although effective short-term, quarterly intra-articular steroid injections over two years do not reduce pain and compared to intra-articular saline,[9] result in greater cartilage volume loss.

3.2.2 Clinical Surgical Treatments

When medical management fails to ameliorate pain and OA progression begins to affect quality of life, surgical treatments are the next course of action. Surgical treatments are directed at correcting the inciting pathoanatomy from articular joint trauma, joint instability, ligamentous deficiency, skeletal malalignment or congenital deformity. Arthroscopy permits minimally invasive access to lavage the synovial joint, debride and/or repair injured structures including hyaline cartilage, menisci, and cruciate ligaments, but alone is ineffective at moderating the progression of OA.[10,11] Arthroscopy in conjunction with meniscal repairs, either full or partial, improves outcomes. Whereas meniscal repairs have a higher reoperation rate than partial meniscectomies, meniscal repairs are associated with better long-term outcomes.[12] A systematic review of the outcomes of meniscal repair >5 years postoperatively revealed similar rates (20-25%) of failure for all techniques investigated.[13] Cohort studies after meniscal transplantation with >10-year follow-up suggest that symptomatic relief is good and that progression to late stage OA is lower than natural history studies of meniscectomized knees.[14,15]

Full-thickness articular cartilage defects (Outerbridge grade III or IV)[16] possess limited regenerative potential, do not readily and spontaneously heal, and are associated with significant pain, swelling and stiffness.[17,18] Restoration of a discrete cartilage lesion with a lubricious cartilage-like tissue, able to withstand repetitive compressive and shear loads without degeneration and loss of function, remains a challenge because the endogenous repair tissue is unable to repopulate the type II collagen and aggrecan content of healthy hyaline cartilage.[17] Perforating the subchondral bone plate beneath the chondral

defect by micro-fracture aims to induce articular tissue reparation by allowing bone marrow elements (bone marrow mesenchymal stem cells) and blood products (fibrin clot) to fill the defect with fibrocartilaginous scar. While meta-analysis of the literature demonstrates clinically relevant improvement in pain and function, the cartilaginous repair tissue is generally fibrous (collagen I, II, III), is partly integrated with the surrounding hyaline cartilage, is mechanically softer, less lubricious, and deteriorates over time.[19,20]

Osteochondral allograft transfer (OATS or mosaicplasty) is a procedure where a cylinder of bone and cartilage is transferred into the defect from a lesser weight bearing region of the knee. The procedure suffers from donor site morbidity and limited availability of suitable anatomic donor sites. Tissue modulus mismatch between donor and surrounding host cartilage results in non-congruous tissue deformation and interfacial shear strains that interfere with graft integration at the host-graft interface. Systematic reviews of patients with long term follow-up treated by OATS show benefit in 70-75% of patients. Increased age, previous surgery, large defect size and patella femoral location associate with higher failure rates, whereas concomitant surgical procedures to address internal derangement, malalignment or instability improve outcomes.[21] OATS may achieve higher activity levels and lower failure rates compared to microfracture for cartilage lesions in the knee >3 cm^2, although at 3-year follow-up, there was no significant difference for lesions <3 cm^2.[21]

Autologous chondrocyte implantation is FDA approved for the treatment of discreet knee cartilage defects (>3 cm^2).[22] Chondrocytes, harvested from cartilage biopsy (200,000–300,000) and expanded in cell culture (12–48 million, depending on defect size), are injected into the defect and secured in place using a sutured periosteum, harvested from

the proximal tibia, or a synthetic collagen membrane.[22] Chondrocytes attach to the subchondral bone and produce cartilage matrix, filling the defect with hyaline-like cartilage. Successful transplantation depends on technique, rehabilitation protocol and anatomic site; complications include symptomatic hypertrophy, disturbed fusion, delamination, and graft failure

Finally, total joint arthroplasty is the most cost-effective and reliable intervention for improving quality of life, alleviating pain, and restoring function in articular joints compromised by end-stage OA.[23] Overall failure rates for total hip and knee replacement (most common total joint arthroplasty) are low at 1%/year. Risk of failure is higher in younger and more active patients as well as patients with medical co-morbidities. While short term failures tend to be related to imperfect surgical technique, longer term implant failures are a result of symptomatic loosening due to infection or polyethylene wear debris induced osteolysis,[24,25] an inflammatory foreign body reaction resulting in osteoclast mediated bone loss.[26] Improved surgical technique, aided by robotic assisted surgery, better implant designs that allow more functional joint kinematics, advanced materials that reduce wear and implant surface coatings that are antimicrobial and/or osteoinductive may enhance outcomes and decrease total joint arthroplasty failure rates.[27]

3.3 Drug Delivery Systems

Today, to treat arthritic conditions, therapeutics typically are administered systemically which entails high risk for systemic toxicity and minimally effective doses reaching the target joints.[28] As OA is a local joint disease, intra-articular (IA) administration increases local drug bioavailability, avoids physiologic barriers of

transportation, and decreases off target effects and risk for systemic toxicity. Rapid clearance from the synovial space and inadequate penetration throughout the cartilage layers hamper this strategy. Synovial fluid is constantly undergoing turnover thus requiring frequent IA injections to deliver sufficient drug, increasing patient discomfort, risk for infection, and doctor's office visits. Given the drawbacks and less than ideal clinical outcomes, significant research is devoted to drug delivery systems.[28,29]

Successes in cancer treatments using nanomedicines provide motivation to employ these technologies to address OA clinical challenges (**Figure 3.1**). Nanoparticles (NPs) are typically spherical in shape and between 10–1000nm in diameter. NP drug delivery systems improve pharmacologic characteristics of agents, enabling controlled delivery of poorly-water soluble agents and water-soluble small molecules, proteins, or nucleic acids. NP composition dictates what agent(s) can be encapsulated, the release profile, target tissue accumulation, and cellular mechanism of uptake. Additionally, NPs can penetrate the ECM and/or cell barriers, allowing for either extracellular or intracellular drug delivery, respectively.[30] NP drug delivery systems commonly contain an agent encapsulated within or chemically conjugated to the NP and a hydrophilic charged surface coating for aqueous colloidal stability. NP compositions range from solid core materials composed of polymers to water filled vessels surrounded by lipids. NP accumulation in target tissue employs either passive or active targeting. Passive targeting capitalizes on physicochemical properties and allows for non-specific localization in the negatively charged ECM, Coll II, or chondrocytes.[31] While, active targeting employs specific biochemical moieties such as an antibody.[31]

3.3.1 Polymeric NPs

For NPs, natural polymers are attractive materials due to their biodegradability and biocompatibility. Their drawbacks include ill-defined composition, batch-batch nonuniformity and impurities from harvest and isolation procedures. Chitosan, a prime example of a natural polymer, has positively charged amine groups lending itself useful for adherence to the anionic surfaces of cellular membranes, electrostatic complexation with anionic DNA or RNA, and chemical modification. Chitosan itself enhances chondrogenesis and shares structural similarities to GAG. Kartogenin is a small molecule that induces chondrogenesis by regulating the nuclear localization of Core Binding Factor -β. When conjugated to chitosan nanoparticles (150nm) or microparticles (1.8um) kartogenin is released over 7 weeks *in vitro*, and when administered intra-articularly affords less degenerative changes compared to untreated controls in a surgically induced rat OA model (**Figure 3.2**).[32] Similarly, genipin cross-linked chitosan microspheres containing flurbipofen, a commonly utilized NSAID with a very short *in vivo* half-life of 4 hours, release the agent for over 108 hours.[33]

Synthetic polymeric NPs offer defined chemical composition, reproducible synthetic procedures, lack of immunogenicity, and tunability. Aliphatic polyesters such as polylactide (PLA), polyglycolide (PGA), and their co-polymers are biocompatible, biodegradable, and widely used to engineer NPs. Degradation products of these polymers are lactic acid and glycolic acid, two metabolites of the citric acid cycle, *i.e.*, the Krebs cycle. Additionally, these polymers are components of a number of regulatory approved treatments - Lupronâ for prostate cancer, Bydureonâ for glycemic control, and Risperdal

Constaâ for schizophrenia and bipolar disorder.[34, 35] Notably, one such PLGA (poly(lactic-co-glycolic acid)) microspheres affords sustained release of a steroid, and this microtechnology is in phase 3 trials for patients with severe OA pain.[36]

Active and passive targeting techniques enhance specificity and retention in the joint space. For example, hyaluronate binds the CD44 surface receptor on chondrocytes t. Chondrocytes readily internalize nanoparticles functionalized with hyaluronate.[37] Self assembled amphiphilic block copolymer NPs, 300nm in diameter, tethered with a natural protein inhibitor of IL-1 (IL-Ra) reduce IL-1 mediated inflammation.[44] These NPs retain bioactivity *in vitro* and target synoviocytes, blocking the IL-1 signaling pathway, and remain in rat stifle joints over 14 days providing an extended IL-Ra half-life (3X) compared to soluble IL1-Ra (**Figure 3.2**).[38] Peptide ligands also enhance targeting specificity and lead to greater accumulation in target cells and higher retention in the ECM compared to non-targeted particles.[39] A cartilage affinity peptide, identified via phage display biopanning, when conjugated to polyethylenimine nanoparticles, caring DNA, exhibits a 9-fold higher transfection efficiency *in-vivo* in rabbits compared to scrambled peptide polyethylenimine /DNA complexes.[39]

Passive targeting techniques use both size and charge to increase accumulation of nanoparticles in the ECM and joint space. For example, 70nm PLGA and Eudaragit RL (a co-polymer of ethyl acrylate and methyl methacrylate) cationic NPs when injected in the joint space form micrometer sized clusters with hyaluronic acid, increasing localization of NPs to the cartilage surface. These cationic NPs reside in mice stifle joints for over 4 weeks following IA injection.[40] Other NPs form similar structures with hyaluronate, to include an

ionically cross-linked hydrogel following IA injection with increased *in vivo* retention times.[41] Apart from charge, NP size increases retention times. Singh et al. demonstrate size dependent prolonged retention of self-assembled nanoparticles. 900nm Nanoparticles composed of polyhydroxyethylmethacrylate), functionalized with bovine serum albumin and pyridine particles show sustained retention (~30% at 14d) in a rat stifle joint and a significantly longer retention than 500nm particles.[42]

3.3.2 Stimuli Responsive Nanoparticles

Stimuli responsive nanoparticles release their agent only when the appropriate environment conditions or triggers are present. Triggers include disease related changes in local environmental conditions such as temperature, pH or oxidative stress, enzyme activity, or external stimuli such as near infrared light.

To address the challenge of loading multiple drugs with independent release profiles, Kang et al. report a dual drug loaded thermo-responsive nanocapsule system composed of a chitosan modified pluronic. The hydrophobic small molecule drug kartogenin, which promotes chondrogenic differentiation of mesenchymal stem cells and induces regeneration of cartilage in OA, covalently links to the amine groups of chitosan, while the anti-inflammatory small molecule drug diclofenac, is contained within the core.[43] Drug release depends on temperature with an initial burst release of diclofenac after cold shock treatment, followed by sustained release of kartogenin. The nanocapsule system suppresses lipopolysaccharide-induced inflammation in chondrocytes and induces chondrogenesis in MSCs, enhanced via a cold shock treatment.[43] In a rat model, treatment with the thermoresponsive nanocapsules suppresses OA progression and reduces COX2

expression. The outcomes improve with a cold treatment.[43] Other strategies use temperature to directly control formation of nanoparticles. Hyaluronic acid conjugated to the thermoresponsive polymer, poly(*N*-isopropylacrylamide) (pNiPAM), described by Maudens et al., only forms NPs (247nm diameter) above the lower critical solution temperature, due to aggregation of hydrophobic polymer side chains, while below the lower critical solution temperature it is soluble. A hyaluronic acid-pNiPAM solution, which exhibits a lower critical solution temperature around body temperature. injected intra-articularly in an OA murine model, curtails pro-inflammatory cytokines and produces biocompatibility with prolonged (up to 2 months) intra-articular residence time.[44]

Reactive oxygen and reactive nitrogen species normally exist at low levels in chondrocytes but are upregulated during OA as a result of dysregulation of antioxidant mechanisms. In an *in-vivo* rodent OA model, administration of 112nm diameter melanin nanoparticles slow cartilage degradation, reduces reactive oxygen and reactive nitrogen species levels in cartilage, and enhances autophagy.[45]

Near infrared (NIR) light, which penetrates tissue with low tissue absorption, reduced scattering, and minimal autofluorescence, is an external stimuli of wide-spread interests.[46] Chitosan modified molybdenum disulfide nanosheets, as reported by Zhao et al., are NIR photo-responsive carriers of the dexamethasone.[46] Dexamethasone releases in response to NIR light via photothermal conversion, enabling remote control over drug release by adjusting the NIR light dose.[46] In a mouse model of OA, dexamethasone loaded chitosan modified molybdenum disulfide nanosheets remain within mice stifle joints (48h), avoiding rapid clearance via the lymphatic system, and lower the expression of

inflammatory factors (IL-1β, TNF-α, and IL-8) in the synovial membrane and serum. [46]

3.3.3 Micelles and Liposomes

Micelles, structures of 20-200nm in diameter, are composed of amphiphilic polymers and readily self-assemble in aqueous solvents. The micelle's core entraps hydrophobic drugs, while hydrophilic drugs can be tethered to the surface. Preferential uptake of micelles occurs via conjugation by peptides, antibodies, or other targeting ligands, while functionalization with poly(ethylene glycol) shields micelles from phagocytosis, and is a site for further modification.[35] Doxorubicin-conjugated block copolymer micelles are widely used in many preclinical and clinical anticancer agent studies.[47] Examples of micellar drug delivery systems for OA are common and include delivery of hydrophobic small molecules (*e.g.*, indomethacin, triamcinolone, and kartogenin) administered either locally or systemically. Indomethacin loaded poly(N-isopropylacrylamide)-polyphosphazene micelles, functionalized with ethyl 4-aminobenzoate, reported by Zhang et al., possess increased indomethacin loading efficiency compared to the non-functionalized micelles. IV administration of this micellar formulation in an OA rat ankle arthritis model affords prolonged indomethacin circulation time and reduces inflammation.[48] Saadat et al. report a polymeric micelle based on hyaluronic acid conjugated 1,2-distearoylphosphatidyl-ethanolamine for sustained delivery of triamcinolone, a common corticosteroid for OA and rheumatoid arthritis that suppresses production of COX1 and COX2.[49] *In vitro* release profiles of the micellar system show a small burst release during the first four hours with sustained release for the 72 hours following.[49] Micelles remain in the stifle joint up to three days post injection, as

revealed by real time NIR fluorescence imaging with cy-7.5 labeled micelles.[49] Self-assembling micelles constructed from amphiphilic polyurethane with pendant amino groups and covalently bound kartogenin, reported by Fan et al., reduce cartilage degradation in an anterior cruciate ligament transection rat model of OA.[50] Cartilage surfaces are intact with only mild superficial fibrillation, confirmed via histological staining, while immunohistochemistry reveal polyurethane-kartogenin treated groups increase Coll II production.[50] Kang et al. report self-assembled PEGylated kartogenin micelles covalently integrated into hyaluronic acid hydrogels.[51] *In vitro*, hydrogels with PEGylated kartogenin micelles show an initial burst release over 12 hours, followed by sustained release over 5 days, resulting in a cumulative drug loss of 32.4%, compared to PEGylated kartogenin micelles alone.[51] In an anterior cruciate ligament transection OA rat model, treatment with the hydrogel PEGylated kartogenin micelle system suppresses progression of OA compared to free-HA hydrogels via OARSI and Mankin scores.[51] Apart from drug delivery systems, micelles may contain vectors for gene therapy. Delivery of recombinant adeno-associated virus vectors (rAAV) via poly(ethylene oxide)-co-poly(propylene oxide) polymeric micelles, developed by Rey-Rico et al., to human chondrocytes increases TGF-β expression and cell proliferation.[52] Treatment to human osteochondral defect cultures *in situ* with rAAV-micelles increases TGF-β production and cell density in regions adjacent to defects, and enhances production of proteoglycan rich ECM.[52]

Like micelles, liposomes are self-assembled structures but possess an aqueous core surrounded by a lipid bilayer, and readily encapsulate hydrophilic or polar agents.

Liposomes vary from 50–5000nm depending on composition and formulation and are routinely used to deliver anti-cancer agents. Doxorubicin loaded liposomes are already used in the clinic with several additional clinical trials underway including PEGylated liposomal doxorubicin (Doxil/Caelyx), non-PEGylated liposomal doxorubicin (Myocet), liposomal daunorubicin (DaunoXome), and liposomal cytarabine (Depocyte).[53] Liposomes with a positive surface charge target the negatively charged ECM via electrostatic interaction. Bio-adhesive, multilamellar liposomes developed by Elron-Gross et al., encapsulate dexamethasone, diclofenac, or both.[54] Liposomes, surface functionalized with either hyaluronan or collagen, exhibit increased affinity for the ECM and CD44 membrane receptors on chondrocytes. In a monosodium iodoacetate induced OA rat model, these liposomes reduce inflammation volume compared to untreated animals.[54] The best performing liposome, one functionalized with hyaluronan co-encapsulating diclofenac and dexamethasone, reduces inflammation volume by 12.9% at 17 days post single injection.[54] Near infrared immuno-liposomes of 200nm, conjugated with type II collagen antibody, bind to exposed type II collagen in the ECM and enable quantitative analysis of cartilage damage. In a guinea pig spontaneous model of OA, the immune-liposome conjugates bind to the damaged cartilage and the fluorescence intensity corresponds to the extent of cartilage damage.[55]

3.3.4 Dendrimers

Dendrimers, repetitively branched molecules, are nano-scale carriers for small molecules, imaging agents, therapeutic proteins, peptides, and nucleic acids.[56-60] Their size spans from tens of nanometers to hundreds of nanometers, and their end group functionality

allows for attaching target ligands or peptides to increase retention times and accumulation. Recently, Geiger et al. describe a PEGylated polyamidoamine dendrimer to deliver insulin-like growth factor1 directly to chondrocytes within cartilage.[61] In a rat anterior cruciate ligament transection model of OA, dendrimers remain in the joint for 30 days and reduce cartilage degeneration by 60% relative to untreated rats at 4 weeks post-surgery.[61] Similarly, Hu et al. report a PEGylated polyamidoamine dendrimer for the cytoplasmic delivery of kartogenin, either conjugated to the surface or to the terminal end group of polyethylene glycol, to induce chondrogenesis of mesenchymal stem cells.[62] Kartogenin conjugated to PEG exhibits the highest expression of chondrogenic markers (Coll II, aggrecan and SOX9). IA injection of this formulation, in an *in vivo* model of papain induced OA, affords improved chondrogenic differentiation efficacy and remains in the joint for 21 days.[62]

3.4 Nanoparticle Gene Delivery Systems

Gene delivery, the transfer of exogenous nucleic acids from the extra-cellular environment to intracellular compartments *i.e.*, the nucleus for pDNA or cytoplasm for siRNA or miRNA, is an attractive technology for OA treatment as it targets specific disease related mechanisms, treating causes rather than symptoms. For successful gene therapy, an efficient and safe delivery system is required. Most gene therapy products in clinical trials use viral vectors due to their high transfection efficiency, but drawbacks include immunogenicity, complicated production, oncogenic effects,[63-71] and risks of potential pathogenicity and lethality. Recent advances have yielded promising non-viral delivery systems currently in different phases of clinical trials. These non-viral delivery systems

include for example PEG-polyethylenimine based systems for ovarian and lipid-based siRNA nanoparticle systems for treatment of advanced cancers to fibrosis.[72,73]

3.4.1 Cationic polymers for gene delivery

Chitosan's potential as a DNA delivery vehicle was discovered in 1998 by MacLaughlin et al.,[74] and reflects its biocompatibility,[75] biodegradability,[75] and non-toxicity[75] although is hampered by low transfection efficiency.[76] To identify an optimal NP formulation, Zhao et al. report transfection efficiency for chitosan-pEGFP nanoparticles as a function of NP size (100-300nm), zeta potential (+1 to +23 mV), culture media pH, chitosan molecular weight, and plasmid dosage.[77] Chitosan-pEGFP nanoparticles (*N/P* ratio of 3.8) prepared at pH 7 with 85 kDa chitosan and 8 µg/mL plasmid afford greater than 50% EGFP expression in primary chondrocytes.[77] Combining chitosan with cationic or anionic biopolymers further increases transfection efficiency. Lu et al. report a hybridized chitosan-hyaluronic acid system containing plasmid DNA.[78] Treatment of chondrocytes with the nanoparticles increases transfection efficiency compared to plasmid nanoparticles of purely chitosan/DNA, with an average cell viability of transfected cells over 90%.[78] More recently, a chitosan-graft-polyethylenimine/DNA nanoparticle with a chitosan-graft-polyethylenimine:DNA ratio of 8:1, carries pDNA to both chondrocytes and synoviocytes with improved transfection efficiency and lower cytotoxicity compared to chondroitin sulfate/DNA nanoparticles, polyethylenimine /DNA nanoparticles, or naked pDNA (**Figure 3.3**).[79] The polyethylenimine protects DNA from nuclease degradation, facilitates endosomal escape, and increase transfection efficiency, despite polyethylenimine having an inherently high level of toxicity *in vitro* and *in vivo*.[79]

Peptide ligands specific to cell surface receptors enhance target specificity and reduce off target responses when conjugated to non-viral delivery vectors. Chemical conjugation of a chondrocyte affinity peptide (CAP) to polyethylenimine /DNA particles increases transfection efficiency and affords higher NP concentrations in rabbit stifle cartilage following IA injection (**Figure 3.3**).[80] This same CAP- polyethylenimine nanoparticle system efficiently delivers siRNA to chondrocytes silencing HIF-2a expression, a transcription factor upregulated during OA that directly induces chondrocyte production of catabolic factors such as MMPs.[80] In an OA mouse model, IA administration of CAP- polyethylenimine particles decreases IL-1β concentration, synovial membrane inflammation, and expression of Hif-2a compared to control groups.[80] Yan et al., report a second method for siRNA delivery using the amphipathic, cationic, cell-penetrating peptide, melittin, targeting the p65 subunit of NF-kB to suppress inflammatory cytokine expression.[81] In a collagen induced arthritis mouse model, these peptide-nanoparticle complexes localize to inflamed joints after intraperitoneal injection, and suppress NF-kB expression.[81] Recently, IA administration of this siRNA loaded peptidic nanoparticle in a stifle-joint impact injury mouse model reduces chondrocyte apoptosis, injury length, and synovitis.[82] As a proof of concept for clinical translatability, human cartilage explants treated with the peptide-siRNA NPs penetrate the explants and persistence in chondrocyte lacunae for at least 2 weeks.[82]

PLGA based nanoparticles are also being explored for gene delivery. Crawford et al., report PLGA nanoparticles, complexed with polyethylenimine and a PLGA scaffold, to enhance transfection efficiency.[83] Specifically, treatment of an articular defect in a rabbit

model with the scaffold, seeded with BMP-4 transfected adipose derived stem cell, significantly improves *in vivo* chondrogenesis.[84] In a rabbit model of a critical size auricular cartilage defect, implantation of chondrocytes, transfected with a plasmid-encoding BMP using the non-viral Turbofect vector embedded within a gelatin-oxidized dextran scaffold, improve healing compared to non-transfected chondrocyte or control groups.[85]

3.4.2 Lipid based delivery systems for gene delivery

Lipid-based nanoparticle delivery systems, a relatively new class of delivery systems for siRNA and DNA, have only recently been investigated for the treatment of cartilage diseases.[86] Wang et al., report a novel lipid-based nanoparticle for siRNA, composed of dipalmitoyl phosphatidylcholine, cholesterol and c16 ceramide-mPEG2000, which efficiently transfects 100% of chondrocytes.[86] Intra-articular injection of lipid-based nanoparticle beacon into mouse stifle joint affords a positive signal by fluorescence molecular tomography up to 72 hours compared to IA administration of free beacon.[86] In a rat anterior cruciate ligament transection OA model, treatment with lipid-based nanoparticle-siRNA complexes correlates with stronger safranin-O staining, and increased cellularity.[86] A second lipid-based nanoparticle system uses the transfection reagent GenePORTE 2 to deliver an endostatin plasmid to mesenchymal stem cells via a collagen scaffold, overexpression of endostatin promotes cartilage repair.[87] Mesenchymal stem cells, seeded onto collagen scaffolds produce greater endostatin, monitored via ELISA, compared to those seeded on control scaffolds.[87]

3.5 Scaffolds for Osteochondral Regeneration

Generating well-integrated, stable cartilage and bone compartments presents a major challenge to tissue engineering. Not only are mechanical properties vastly different between native cartilage and bone, the cellular and biochemical content are distinct as well. Scaffolds play a key role in directing cells to appropriate lineage and location. The following are various approaches to the use of scaffolds in OA treatment: incorporation of nanoparticles within traditional scaffolds or hydrogels; modifying traditional scaffolds to generate nanoscale features; and direct fabrication of nanofibrous scaffolds.

3.5.1 Nano-scale bone scaffolds

Significant research focuses on incorporating osteogenic or mineral inducing nanoparticles, such as nano-hydroxyapatite , into scaffolds to induce mineralization and/or bone formation.[88] Nano-hydroxyapatite in conjunction with mesenchymal stem cells and other progenitor cells enhances mineralization, and is fabricated via a wide range of processing techniques including thermally induced phase separation,[89] 3D printing,[90] selective laser sintering,[91] and bioprinting.[92] Other nano-scale additives, such as mesoporous bioglass, increase osteogenic differentiation of mesenchymal stem cells, act as efficient drug carrier and release systems, and elicit a greater effect than non-mesoporous bioglass.[63,94]

Mineral inducing nanoparticles aid to the improvement total joint arthroplasty outcomes, which are often plagued by symptomatic loosening due to infection or polyethylene wear debris induced osteolysis. Modification of titanium, ceramics and hydroxyapatite with nano-scale additives facilitates biological activity and decrease

incidence of revisions.[95-98] Additionally, nanomodification of joint replacement surfaces reduces bacterial adherence, biofilm formation and disrupts bacterial cell homeostasis.[96]

3.5.2 Nano-scale scaffolds for cartilage repair

Nano- and micro-scale scaffolds, akin to osteogenic approaches, guide and enhance cartilage repair. Cell pellet culture systems, widely used in the study of mesenchymal stem cell chondrogenesis, are inherently disadvantageous with small sizes and weak mechanical properties, making the system impractical for cartilage defect repair. Early studies by Tuan et al., describe scaffolds of randomly oriented nanofibrous poly(e-caprolactone) which aid mesenchymal stem cell chondrogenesis, via the Wnt signaling pathway, when coupled with the chondrogenic growth factor TGF-β1.[99] Chondrogenesis levels are on par with levels observed in a cell pellet culture system, with the additional benefit of improved mechanical properties. These scaffolds possess limited porosity, reducing cell migration and nutrient transport. A low-density random nanofiber approach overcomes this issue by incorporating chondroitin sulfate into nanofibers, to promote chondrogenesis *in vitro* and *in vivo* in a rat osteochondral defect model. Although this repair tissue remains biomechanically inferior to native cartilage and produces significantly less proteoglycan and collagen II. Increased density of nanofibers further reinforces the hydrogels and improves mechanical properties, as well as MSC chondrogenesis of the resulting construct.[100,101] More recently, melt electrowriting affords nano-fiber scaffolds (down to <1 µm)[102] with precisely controlled pore sizes and geometries.[103] When combined with a hydrogel and cells, the dynamic mechanical properties more closely match native tissue and the cells maintain their chondrogenic phenotype.[104] Further, this printing process enables formation of mechanical

property gradients to mimic zonal properties of articular cartilage.[105] When cells are embedded in these constructs, mechanical properties further improve over time.[106]

There is a technological shift from melting or gluing together of bone and cartilage scaffold components, towards additive manufacturing technologies. Improvement in the latter, combined with knowledge from individual cartilage and bone studies, enables production of seamless composite osteochondral constructs which are a better anatomical match. Kon et al., describe a gradient scaffold with varying collagen I and nanoscale magnesium-hydroxyapatite formed *in situ* in separate layers. Scaffolds implanted into sheep femoral condyle osteochondral lesions aid bone regeneration and direct bone and hyaline-like cartilage regeneration.[107] In a pilot human clinical trial, these osteochondral scaffolds improve functional scores over 2 years as determined using the Magnetic Resonance Observation of Cartilage Repair Tissue scoring system.[108] Positive treatment outcomes remain consistent over 5 years post-surgery, while some abnormalities persisted in the repair tissues.[109] Ultimately, it will be critical to determine which scaffold-based strategies result in better functionality *in vivo* both in humans and in large animal studies, which are instrumental in evaluating promising approaches prior to clinical trials.

3.6 Nanoparticle-Based Lubricants

Nanoparticles aid lubrication by altering the tribology of contacting surfaces via small-gap infiltration to provide a protective layer and to act as interposed ball bearings between surfaces.[110,111] Adding nanoparticles to conventional oils results in a colloidal suspension, a nanolubricant, reducing coefficient of friction values up to 50%.[110] Addition of biocompatible tantalum oxide NPs to bovine synovial fluid , as described by Lawson et

al., improves boundary mode lubrication by reducing the coefficient of friction between cartilage articulating surfaces.[112] Anilkumar et al. describe a new nanoparticulate lubricant composed of soft, nanometer sized single hyperbranched glycerol polymers of millions of molecular weight (megaHPGs). These mega-polymers possess high water solubility, compact morphologies, low intrinsic viscosities, and exist as single polymer particles.[113] megaHPGs act as interposed ball-bearings when between both hard (*e.g.*, stainless steel) and soft (cartilage) surfaces to lower the coefficient of friction.

3.7 Conclusions and Perspectives

Nanotechnology offers significant potential to enhance current OA management through targeted therapeutics, smart scaffolds, and novel viscosupplements. As discussed above, several new technologies and materials are in pre-clinical development to address OA. With regards to drug delivery systems, nanoparticles composed of polymers, metals, lipids, etc., are enabling selective, targeted delivery of disease modifying OA drugs, nucleic acids, and growth factors. These approaches provide delayed, sustained, or triggered drug release, increased joint retention after administration, as well as reduced off-target side effects. Scaffolds incorporating nano-designs and structural features recapitulate cartilage, augment biochemical constituents, and enhance biomechanical properties. Strategies to repair early-stage disease with the use of lubricants and late-stage disease utilizing tissue engineered scaffolds, are also being pursued. Although nanotechnology in orthopaedics is still in its infancy, new research opportunities exists including: 1) stimuli-responsive drug delivery systems which deliver their payload in response to a biological cue or under appropriate environmental stimuli; 2) development of additional chondroprotective

treatments as opposed to just pain management; 3) long-term non-metal implants that integrate with host tissue, including the nervous system, to functional as artificial tissues; and, 4) nanomaterials to augment or control the immune system.

Clinically, nanotechnology is not a dream but a reality for OA patients. Nano-coatings for orthopaedic implants are already available and in clinical development to reduce or eliminate infection and biofilm formation and/or promote host bone integration. For example, silver nanoparticle surface modifications reduce prosthetic joint infection, with its antimicrobial properties and strong anti-biofilm potential.[114] To date, no orthopaedic implants that possess a silver nanotreatment are available for general use, but two manufacturers produce total joint arthroplasty implants treated by a galvanic deposition of elementary silver upon request (Implantcast GmbH–Medizintechnik, Buxtehude, Germany; Stanmore Implants, Borehamwood, UK) and clinical experiences are promising.[115] This approach is promising given the precedence of regulatory approved silver nanoparticle coated medical catheters (Silverline® and ON-Q Soaker™).[116] Other nano-based coatings include patented technology based on functionalized titanium dioxide to promote osteointegration and minimize bacterial infections.[117] While these examples are all in the bone space, they set a precedent for future developments in cartilage repair.

Nanotechnology has and will continue to unveil new fundamental material properties and activities, and these findings will catalyze advancements in patient care through collaborative efforts between engineers, scientists, and clinicians. We encourage all to collaborate, to form multidisciplinary teams, to perform mechanistically driven *in vitro*, *ex vivo*, and *in vivo* experiments, and to translate their findings to patient care.

3.8 References

1. Edmonds, S. Therapeutic targets for osteoarthritis. *Maturitas* **63**, 191–194 (2009).

2. Praveen Rao, P. N. & Knaus, E. E. Evolution of nonsteroidal anti-inflammatory drugs (NSAIDs): Cyclooxygenase (COX) inhibition and beyond. *Journal of Pharmacy and Pharmaceutical Sciences* **11**, (2008).

3. Kloppenburg, M. & Berenbaum, F. Osteoarthritis year in review 2019: epidemiology and therapy. *Osteoarthritis and Cartilage* **28**, 242–248 (2020).

4. Apostu, D. *et al.* Systemic drugs with impact on osteoarthritis. *Drug Metabolism Reviews* **51**, 498–523 (2019).

5. Goldring, S. R. Needs and opportunities in the assessment and treatment of osteoarthritis of the knee and hip: The view of the rheumatologist. in *Journal of Bone and Joint Surgery - Series A* **91**, 4–6 (2009).

6. Lo, G. H., LaValley, M., McAlindon, T. & Felson, D. T. Intra-articular Hyaluronic Acid in Treatment of Knee Osteoarthritis: A Meta-analysis. *Journal of the American Medical Association* **290**, 3115–3121 (2003).

7. Arroll, B. & Goodyear-Smith, F. Corticosteroid injections for osteoarthritis of the knee: meta-analysis. *BMJ (Clinical research ed.)* **328**, 869 (2004).

8. Grodzinsky, A. J., Wang, Y., Kakar, S., Vrahas, M. S. & Evans, C. H. Intra-articular dexamethasone to inhibit the development of post-traumatic osteoarthritis. *Journal of Orthopaedic Research* **35**, 406–411 (2017).

9. McAlindon, T. E. *et al.* Effect of intra-articular triamcinolone vs saline on knee cartilage volume and pain in patients with knee osteoarthritis a randomized clinical trial. *JAMA - Journal of the American Medical Association* **317**, 1967–1975 (2017).

10. Moseley, J. B. *et al.* A Controlled Trial of Arthroscopic Surgery for Osteoarthritis of the Knee. *New England Journal of Medicine* **347**, 81–88 (2002).

11. Kirkley, A. *et al.* A randomized trial of arthroscopic surgery for osteoarthritis of the knee.[Erratum appears in N Engl J Med. 2009 Nov 12;361(20):2004]. *New England Journal of Medicine* **359**, 1097–1107 (2008).

12. Paxton, E. S., Stock, M. v. & Brophy, R. H. Meniscal repair versus partial meniscectomy: A systematic review comparing reoperation rates and clinical outcomes. *Arthroscopy - Journal of Arthroscopic and Related Surgery* **27**, 1275–1288 (2011).

13. Nepple, J. J., Dunn, W. R. & Wright, R. W. Meniscal repair outcomes at greater than five years: A systematic literature review and meta-analysis. *Journal of Bone and Joint Surgery - Series A* **94**, 2222–2227 (2012).

14. Verdonk, P. C. M. *et al.* Meniscal allograft transplantation: Long-term clinical results with radiological and magnetic resonance imaging correlations. *Knee Surgery, Sports Traumatology, Arthroscopy* **14**, 694–706 (2006).

15. van der Wal, R. J. P., Thomassen, B. J. W. & van Arkel, E. R. A. Long-term clinical outcome of open Meniscal allograft transplantation. *American Journal of Sports Medicine* **37**, 2134–2139 (2009).

16. Lusic, H. & Grinstaff, M. W. X-ray-Computed Tomography Contrast Agents. *Chemical Reviews* **113**, 1641–1666 (2013).

17. Ding, C. *et al.* Natural history of knee cartilage defects and factors affecting change. *Archives of Internal Medicine* **166**, 651–658 (2006).

18. Shapiro, F., Koide, S. & Glimcher, M. J. Cell origin and differentiation in the repair of full-thickness defects of articular cartilage. *Journal of Bone and Joint Surgery - Series A* **75**, 532–553 (1993).

19. Negrin, L., Kutscha-Lissberg, F., Gartlehner, G. & Vecsei, V. Clinical outcome after microfracture of the knee: A meta-analysis of before/after-data of controlled studies. *International Orthopaedics* **36**, 43–50 (2012).

20. Bae, D. K., Yoon, K. H. & Song, S. J. Cartilage Healing After Microfracture in Osteoarthritic Knees. *Arthroscopy: The Journal of Arthroscopic & Related Surgery* **22**, 367–374 (2006).

21. Pareek, A. *et al.* Osteochondral Autograft Transfer Versus Microfracture in the Knee: A Meta-analysis of Prospective Comparative Studies at Midterm. *Arthroscopy - Journal of Arthroscopic and Related Surgery* **32**, 2118–2130 (2016).

22. Minas, T. *et al.* Autologous chondrocyte implantation for joint preservation in patients with early osteoarthritis. in *Clinical Orthopaedics and Related Research* **468**, 147–157 (2010).

23. Katz, J. N., Earp, B. E. & Gomoll, A. H. Surgical management of osteoarthritis. *Arthritis Care and Research* **62,** 1220–1228 (2010).

24. Evans, J. T. *et al.* How long does a knee replacement last? A systematic review and meta-analysis of case series and national registry reports with more than 15 years of follow-up. *The Lancet* **393**, 655–663 (2019).

25. Rolfson, O., Dahlberg, L. E., Nilsson, J. Å., Malchau, H. & Garellick, G. Variables determining outcome in total hip replacement surgery. *Journal of Bone and Joint Surgery - Series B* **91**, 157–161 (2009).

26. Goodman, S. B., Gibon, E. & Yao, Z. The basic science of periprosthetic osteolysis. *Instructional course lectures* **62**, 201–6 (2013).

27. Deirmengian, C. A. & Lonner, J. H. What's new in adult reconstructive knee surgery. *Journal of Bone and Joint Surgery - Series A* **90**, 2556–2565 (2008).

28. Larsen, C. *et al.* Intra-articular depot formulation principles: Role in the management of postoperative pain and arthritic disorders. *Journal of Pharmaceutical Sciences* **97**, 4622–4654 (2008).

29. Evans, C. H., Kraus, V. B. & Setton, L. A. Progress in intra-articular therapy. *Nature Reviews Rheumatology* **10**, 11–22 (2014).

30. Zhao, F. *et al.* Cellular Uptake, Intracellular Trafficking, and Cytotoxicity of Nanomaterials. *Small* **7**, 1322–1337 (2011).

31. Brown, S., Kumar, S. & Sharma, B. Intra-articular targeting of nanomaterials for the treatment of osteoarthritis. *Acta Biomaterialia* **93,** 239–257 (2019).

32. Kang, M. L., Ko, J. Y., Kim, J. E. & Im, G. il. Intra-articular delivery of kartogenin-conjugated chitosan nano/microparticles for cartilage regeneration. *Biomaterials* (2014)

33. Kawadkar, J. & Chauhan, M. K. Intra-articular delivery of genipin cross-linked chitosan microspheres of flurbiprofen: Preparation, characterization, in vitro and in vivo studies. *European Journal of Pharmaceutics and Biopharmaceutics* **81**, 563–572 (2012).

34. FDA's Regulatory Science Program for Generic PLA/ PLGA-Based Drug Products | American Pharmaceutical Review - The Review of American Pharmaceutical Business & Technology. https://www.americanpharmaceuticalreview.com/Featured-Articles/188841-FDA-s-Regulatory-Science-Program-for-Generic-PLA-PLGA-Based-Drug-Products/.

35. Kavanaugh, T. E., Werfel, T. A., Cho, H., Hasty, K. A. & Duvall, C. L. Particle-based technologies for osteoarthritis detection and therapy. *Drug Delivery and Translational Research* **6**, 132–147 (2016).

36. Kumar, A., Bendele, A. M., Blanks, R. C. & Bodick, N. Sustained efficacy of intra-articular FX006 in a rat model of osteoarthritis. *Osteoarthritis and Cartilage* **20**, S289 (2012).

37. Laroui, H. *et al.* Hyaluronate-covered nanoparticles for the therapeutic targeting of cartilage. *Biomacromolecules* **8**, 3879–3885 (2007).

38. Whitmire, R. E. *et al.* Self-assembling nanoparticles for intra-articular delivery of anti-inflammatory proteins. *Biomaterials* **33**, 7665–7675 (2012).

39. Rothenfluh, D. A., Bermudez, H., O'Neil, C. P. & Hubbell, J. A. Biofunctional polymer nanoparticles for intra-articular targeting and retention in cartilage. *Nature Materials* **7**, 248–254 (2008).

40. Kang, M. J. *et al.* Cationic PLGA/Eudragit RL nanoparticles for increasing retention time in synovial cavity after intra-articular injection in knee joint. *International Journal of Nanomedicine* **10**, 5263 (2015).

41. Morgen, M. *et al.* Nanoparticles for improved local retention after intra-articular injection into the knee joint. *Pharmaceutical Research* **30**, 257–268 (2013).

42. Singh, A. *et al.* Nanoengineered Particles for Enhanced Intra-Articular Retention and Delivery of Proteins. *Advanced Healthcare Materials* **3**, 1562–1567 (2014).

43. Kang, M.-L., Kim, J.-E. & Im, G.-I. Thermoresponsive nanospheres with independent dual drug release profiles for the treatment of osteoarthritis. *Acta Biomaterialia* **39**, 65–78 (2016).

44. Maudens, P., Meyer, S., Seemayer, C. A., Jordan, O. & Allémann, E. Self-assembled thermoresponsive nanostructures of hyaluronic acid conjugates for osteoarthritis therapy. **10**, 1845 (2018).

45. Zhong, G. *et al.* Dopamine-melanin nanoparticles scavenge reactive oxygen and nitrogen species and activate autophagy for osteoarthritis therapy. *Nanoscale* **24,** (2019)

46. Zhao, Y. *et al.* Drug Delivery System Based on Near-Infrared Light-Responsive Molybdenum Disulfide Nanosheets Controls the High-Efficiency Release of Dexamethasone To Inhibit Inflammation and Treat Osteoarthritis. *ACS applied materials and interfaces* **27**, 11587-11601(2019).

47. Yokoyama, M. *et al.* Preparation of Micelle-Forming Polymer-Drug Conjugates. *Bioconjugate Chem* **3**, 295-301 (1992).

48 Zhang, J. X. *et al.* Local delivery of indomethacin to arthritis-bearing rats through polymeric micelles based on amphiphilic polyphosphazenes. *Pharmaceutical Research* **24**, 1944–1953 (2007).

49. Saadat, E., Shakor, N., Gholami, M. & Dorkoosh, F. A. Hyaluronic acid based micelle for articular delivery of triamcinolone, preparation, in vitro and in vivo evaluation. *International journal of pharmaceutics* **489**, 218-225 (2015)

50. Fan, W. *et al.* Intra-articular injection of kartogenin-conjugated polyurethane nanoparticles attenuates the progression of osteoarthritis. *Drug Delivery* **25**, 1004–1012 (2018).

51. Kang, M.-L., Jeong, S.-Y. & Im, G.-I. Hyaluronic Acid Hydrogel Functionalized with Self-Assembled Micelles of Amphiphilic PEGylated Kartogenin for the Treatment of Osteoarthritis. *Tissue Engineering Part A* **23**, 630–639 (2017).

52. Rey-Rico, A. *et al.* rAAaaV-mediated overexpression of TGF-β via vector delivery in polymeric micelles stimulates the biological and reparative activities of human articular chondrocytes in vitro and in a human osteochondral defect model. *International Journal of Nanomedicine* **12**, 6985–6996 (2017).

53. Kavanaugh, T. E., Werfel, T. A., Cho, H., Hasty, K. A. & Duvall, C. L. Particle-based technologies for osteoarthritis detection and therapy. *Drug Delivery and Translational Research* **6**, 132–147 (2016).

54. Elron-Gross, I., Glucksam, Y. & Margalit, R. Liposomal dexamethasone-diclofenac combinations for local osteoarthritis treatment. *International Journal of Pharmaceutics* **376**, 84–91 (2009).

55. Cho, H. *et al.* Theranostic immunoliposomes for osteoarthritis. *Nanomedicine: Nanotechnology, Biology, and Medicine* **10**, 619–627 (2014).

56. Tripathi, P. K. & Tripathi, S. Dendrimers for anticancer drug delivery. in *Pharmaceutical Applications of Dendrimers* 131–150 (2020).

57. Chauhan, A., Krynicka, D. & Singh, M. K. Therapeutic dendrimers. in *Pharmaceutical Applications of Dendrimers* 275–287 (2020).

58. Bonam, S. R., Areti, A., Komirishetty, P. & Muller, S. Dendrimers in immunotherapy and hormone therapy. in *Pharmaceutical Applications of Dendrimers* 233–249 (2020).

59. Wolinsky, J. B. & Grinstaff, M. W. Therapeutic and diagnostic applications of dendrimers for cancer treatment. *Advanced Drug Delivery Reviews* **60**, 1037–1055 (2008).

60. Jain, K., Mehra, N. K., Jain, V. K. & Jain, N. K. IPN Dendrimers in Drug Delivery. *Interpenetrating Polymer Network: Biomedical Applications* 143–181 (2020).

61. Geiger, B. C., Wang, S., Padera, R. F., Grodzinsky, A. J. & Hammond, P. T. Cartilage-penetrating nanocarriers improve delivery and efficacy of growth factor treatment of osteoarthritis. *Science Translational Medicine* **10**, (2018).

62. Hu, Q. *et al.* Polyethylene glycol modified PAMAM dendrimer delivery of kartogenin to induce chondrogenic differentiation of mesenchymal stem cells. *Nanomedicine: Nanotechnology, Biology, and Medicine* **13**, 2189–2198 (2017).

63. Lungwitz, U., Breunig, M., Blunk, T. & Göpferich, A. Polyethylenimine-based non-viral gene delivery systems. *European Journal of Pharmaceutics and Biopharmaceutics* **60**, 247–266 (2005).

68. Zhao, Q. Q. *et al.* Combination of poly(ethylenimine) and chitosan induces high gene transfection efficiency and low cytotoxicity. *Journal of Bioscience and Bioengineering* **105**, 65–68 (2008).

69. Tae, H. K., Su, I. K., Akaike, T. & Chong, S. C. Synergistic effect of poly(ethylenimine) on the transfection efficiency of galactosylated chitosan/DNA complexes. *Journal of Controlled Release* **105**, 354–366 (2005).

70. Tripathi, S. K., Goyal, R., Kumar, P. & Gupta, K. C. Linear polyethylenimine-graft-chitosan copolymers as efficient DNA/siRNA delivery vectors in vitro and in vivo. *Nanomedicine: Nanotechnology, Biology, and Medicine* **8**, 337–345 (2012).

71. Gao, J. Q. *et al.* Gene-carried chitosan-linked-PEI induced high gene transfection efficiency with low toxicity and significant tumor-suppressive activity. *International Journal of Pharmaceutics* **387**, 286–294 (2010).

72. Barba, A. A., Bochicchio, S., Dalmoro, A. & Lamberti, G. Lipid delivery systems for nucleic-acid-based-drugs: From production to clinical applications. *Pharmaceutics* **11** (2019).

73. Áyen, Á., Martínez, Y. J., Marchal, J. A. & Boulaiz, H. Recent progress in gene therapy for ovarian cancer. *International Journal of Molecular Sciences* **19** (2018).

74. MacLaughlin, F. C. *et al.* Chitosan and depolymerized chitosan oligomers as condensing carriers for in vivo plasmid delivery. *Journal of controlled release : official journal of the Controlled Release Society* **56**, 259–72 (1998).

75. Zhang, J. *et al.* Chitosan Modification and Pharmaceutical/Biomedical Applications. *Marine Drugs* **8**, 1962–1987 (2010).

76. Mao, S., Sun, W. & Kissel, T. Chitosan-based formulations for delivery of DNA and siRNA. *Advanced Drug Delivery Reviews* **62**, 12–27 (2010).

77. Zhao, X., Yu, S. B., Wu, F. L., Mao, Z. bin & Yu, C. L. Transfection of primary chondrocytes using chitosan-pEGFP nanoparticles. *Journal of Controlled Release* **112**, 223–228 (2006).

78. Lu, H. D., Zhao, H. Q., Wang, K. & Lv, L. L. Novel hyaluronic acid-chitosan nanoparticles as non-viral gene delivery vectors targeting osteoarthritis. *International Journal of Pharmaceutics* **420**, 358–365 (2011).

79. Lu, H., Dai, Y., Lv, L. & Zhao, H. Chitosan-Graft-Polyethylenimine/DNA Nanoparticles as Novel Non-Viral Gene Delivery Vectors Targeting Osteoarthritis. *PLoS ONE* **9**, e84703 (2014).

80. Pi, Y. *et al.* Intra-articular delivery of anti-Hif-2α siRNA by chondrocyte-homing nanoparticles to prevent cartilage degeneration in arthritic mice. *Gene Therapy* **22**, 439–448 (2015).

81. Zhou, H. F. *et al.* Peptide-siRNA nanocomplexes targeting NF-κB subunit p65 suppress nascent experimental arthritis. *Journal of Clinical Investigation* **124**, 4363–4374 (2014).

82. Yan, H. *et al.* Suppression of NF-κB activity via nanoparticle-based siRNA delivery alters early cartilage responses to injury. *Proceedings of the National Academy of Sciences of the United States of America* **113**, E6199–E6208 (2016).

83. Crawford R, Dogdas B, Keough E, et al. 2011. Analysis of Lipid Nanoparticles by Cryo-EM for Characterizing SiRNA Delivery Vehicles. *International Journal of Pharmaceutics* **403**, 237–244.

84. Shi, J. *et al.* Nanoparticle delivery of the bone morphogenetic protein 4 gene to adipose-derived stem cells promotes articular cartilage repair in vitro and in vivo. *Arthroscopy - Journal of Arthroscopic and Related Surgery* **29**, 2001-2011.e2 (2013).

85. Odabas, S. *et al.* Auricular cartilage repair using cryogel scaffolds loaded with BMP-7-expressing primary chondrocytes. *Journal of Tissue Engineering and Regenerative Medicine* **7**, 831–840 (2013).

86. Wang, S. *et al.* A novel therapeutic strategy for cartilage diseases based on lipid nanoparticle-RNAi delivery systme. *International Journal of Nanomedicine* **13**, 617–631 (2018).

87. Sun, X. D., Jeng, L., Bolliet, C., Olsen, B. R. & Spector, M. Non-viral endostatin plasmid transfection of mesenchymal stem cells via collagen scaffolds. *Biomaterials* **30**, 1222–1231 (2009).

88. Venkatesan, J. & Kim, S. K. Nano-hydroxyapatite composite biomaterials for bone tissue engineering - A review. *Journal of Biomedical Nanotechnology* **10**, 3124–3140 (2014).

89. Wei, G. & Ma, P. X. Structure and properties of nano-hydroxyapatite/polymer composite scaffolds for bone tissue engineering. *Biomaterials* **25**, 4749–4757 (2004).

90. Esposito Corcione, C. *et al.* The feasibility of printing polylactic acid-nanohydroxyapatite composites using a low-cost fused deposition modeling 3D printer. *Journal of Applied Polymer Science* **134**, (2017).

91. Feng, P., Niu, M., Gao, C., Peng, S. & Shuai, C. A novel two-step sintering for nano-hydroxyapatite scaffolds for bone tissue engineering. *Scientific Reports* **4**, 1–10 (2014).

92. Wang, X. F. *et al.* Nano hydroxyapatite particles promote osteogenesis in a three-dimensional bio-printing construct consisting of alginate/gelatin/hASCs. *RSC Advances* **6**, 6832–6842 (2016).

93. Wu, C., Zhang, Y., Zhou, Y., Fan, W. & Xiao, Y. A comparative study of mesoporous glass/silk and non-mesoporous glass/silk scaffolds: Physiochemistry and in vivo osteogenesis. *Acta Biomaterialia* **7**, 2229–2236 (2011).

94. El-Fiqi, A., Kim, J. H. & Kim, H. W. Osteoinductive fibrous scaffolds of biopolymer/mesoporous bioactive glass nanocarriers with excellent bioactivity and long-term delivery of osteogenic drug. *ACS Applied Materials and Interfaces* **7**, 1140–1152 (2015).

95. Korkusuz, F. Editorial comment: Nanoscience in musculoskeletal medicine general. *Clinical Orthopaedics and Related Research* **471**, 2530–2531 (2013).

96. Gallo, J., Holinka, M. & Moucha, C. S. Antibacterial surface treatment for orthopaedic implants. *International Journal of Molecular Sciences* **15**, 13849–13880 (2014).

97. Rieger, E. *et al.* Controlled implant/soft tissue interaction by nanoscale surface modifications of 3D porous titanium implants. *Nanoscale* **7**, 9908–9918 (2015).

98. Zan, X., Kozlov, M., McCarthy, T. J. & Su, Z. Covalently Attached, Silver-Doped Poly(vinyl alcohol) Hydrogel Films on Poly(l -lactic acid). *Biomacromolecules* **11**, 1082–1088 (2010).

99. Li, W. J. *et al.* A three-dimensional nanofibrous scaffold for cartilage tissue engineering using human mesenchymal stem cells. *Biomaterials* **26**, 599–609 (2005).

100. Coburn, J. *et al.* Biomimetics of the extracellular matrix: An integrated three-dimensional fiber-hydrogel composite for cartilage tissue engineering. *Smart Structures and Systems* **7**, 213–222 (2011).

101. Coburn, J. M., Gibson, M., Monagle, S., Patterson, Z. & Elisseeff, J. H. Bioinspired nanofibers support chondrogenesis for articular cartilage repair. *Proceedings of the National Academy of Sciences of the United States of America* **109**, 10012–10017 (2012).

102. Dalton, P. D., Joergensen, T. & Groll, J. Additive manufacturing of scaffolds with sub-micron filaments via melt electrospinning writing Related content Patterned melt electrospun substrates for tissue engineering. *Biofabrication* (2015)

103. Brown, T. D., Dalton, P. D. & Hutmacher, D. W. Direct Writing By Way of Melt Electrospinning. *Advanced Materials* **23**, 5651–5657 (2011).

104. Visser, J. *et al.* Reinforcement of hydrogels using three-dimensionally printed microfibres. *Nature Communications* **6**, 1–10 (2015).

105. Bas, O. *et al.* Rational design and fabrication of multiphasic soft network composites for tissue engineering articular cartilage: A numerical model-based approach. *Chemical Engineering Journal* **340**, 15–23 (2018).

106. Pahoff, S. *et al.* Effect of gelatin source and photoinitiator type on chondrocyte redifferentiation in gelatin methacryloyl-based tissue-engineered cartilage constructs. *Journal of Materials Chemistry B* **7**, 1761–1772 (2019).

107. Kon, E. *et al.* Orderly osteochondral regeneration in a sheep model using a novel nano-composite multilayered biomaterial. *Journal of Orthopaedic Research* **28**, (2009).

108. Kon, E. *et al.* Novel nano-composite multilayered biomaterial for osteochondral regeneration: A pilot clinical trial. *American Journal of Sports Medicine* **39**, 1180–1190 (2011).

109. Kon, E. *et al.* Clinical results and MRI evolution of a nano-composite multilayered biomaterial for osteochondral regeneration at 5 years. *American Journal of Sports Medicine* **42**, 158–165 (2014).

110. Shahnazar, S., Bagheri, S. & Abd Hamid, S. B. Enhancing lubricant properties by nanoparticle additives. *International Journal of Hydrogen Energy* **41**, 3153–3170 (2016).

111. Hsu, S. M. Nano-lubrication: Concept and design. *Tribology International* **37**, 537–545 (2004).

112. Lawson, T. B., Joenathan, A. T., Snyder, B. D. & Grinstaff, M. W. A Theranostic Nanolubricant. **41**, 1–7 (2020).

113. Anilkumar, P. *et al.* Mega macromolecules as single molecule lubricants for hard and soft surfaces. *Nature Communications* **11**, 1–9 (2020).

114. Wafa, H. *et al.* Retrospective evaluation of the incidence of early periprosthetic infection with silver-treated endoprostheses in high-risk patients: Case-control study. *Bone and Joint Journal* **97-B**, 252–257 (2015).

115. Ge, L. *et al.* Nanosilver particles in medical applications: Synthesis, performance, and toxicity. *International Journal of Nanomedicine* **9**, 2399–2407 (2014).

116. Gallo, J. *et al.* Silver nanocoating technology in the prevention of prosthetic joint infection. *Materials* **9** (2016).

117. Bignozzi, C., Carinci, F. & Caramori, S. Use of nanomaterials based on titanium dioxide and zirconium diozide as coatings for osteointegrated biomedical prostheses, and osteointegrated biomedical prostheses prepared therewith. (2012).

Table 3.1. Medical Management strategies for OA.

Therapy	Description and Benefits	Disadvantages
Analgesics	An analgesic is any member of the diverse group of drugs used to relieve pain. Includes acetaminophen, propoxyphene hydrochloride, tramadol, salicylates, and capsaicin. Can effectively relieve mild to moderate pain short-term. Many available over-the counter (acetaminophen, etc.)	Does not relieve inflammation or swelling. Can cause liver damage with chronic use and overdosing. Typically, not used long-term. Opioids have the devastating potential for chemical dependency
Non-steroidal Anti-Inflammatory Drugs (NSAIDs)	NSAIDs are prescribed to reduce inflammation and swelling as well as aid in pain relief for patients who have moderate-to-severe pain and signs of inflammation. NSAIDs usually work well initially. NSAIDs are non-narcotic.	Increased or chronic use often leads to gastrointestinal and renal problems such as gastric ulcers, gastrointestinal bleeding and rarely death. 10-20% of NSAID patients experience dyspepsia; upper gastrointestinal adverse events estimated to result in 103,000 hospitalizations and 16,500 deaths per year in US (43% drug-related emergency visits). NSAIDs decrease in effectiveness over time until they no longer work, or the patient suffers from side effects.
COX-2 Inhibitors	NSAID that directly targets COX-2, an enzyme responsible for inflammation and pain. Selectivity for COX-2 reduces risk of peptic ulceration, and is the main feature of celecoxib, rofecoxib and other members of this drug class.	COX-2-selectivity does not reduce other adverse-effects of NSAIDs - most notably an increased risk of renal failure and potentially an increase in the risk for heart attack, thrombosis, and stroke. Several COx-2 inhibitors have been withdrawn from the market or have alerts by the FDA due to safety (Vioxx, Celebrex, etc.).

Injectable Glucocorticoids	Steroids injected intra-articularly for targeted pain relief. Alternative therapy for moderate-to-severe knee pain and signs of inflammation not mitigated by acetaminophen or NSAIDs. Strong clinical and scientific evidence that glucocorticoids inhibit expression and action of pro-inflammatory cytokines, stimulate matrix remodeling and synthesis.[7,8]	Must repeat intra-articular injections 3-4x/year. Corticosteroids associated with toxic side effects off-target tissues and organs Long term use may not reduce pain or reduce cartilage volume loss
Viscosupple-mentation with Hyaluronic Acid	Hyaluronic acid, or hyaluronan, is a gel-like polysaccharide substance Intra-articular viscosupplementation is a treatment in which hyaluronic acid is injected directly into the joint space to supplement the viscous properties of the synovial fluid.	Only pain relief, no clinical demonstration of chondroprotection Randomized, prospective clinical trials demonstrate no difference from saline for pain relief. No evidence that HA products improves viscous lubrication or ameliorates cartilage degradation. Synthesis is costly
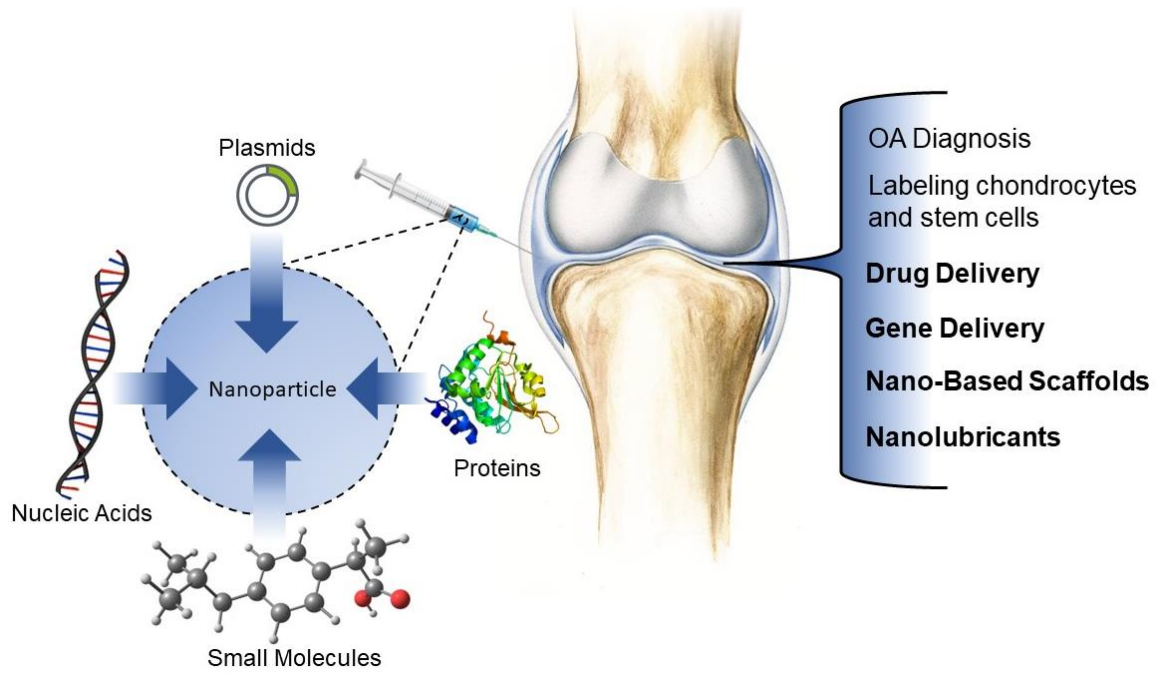
Figure 3.1. Facets of nanotechnology investigated for a multitude of applications for osteoarthritis, from nano-based drug delivery and gene delivery systems, along with nano-based scaffolds and nanolubricants.
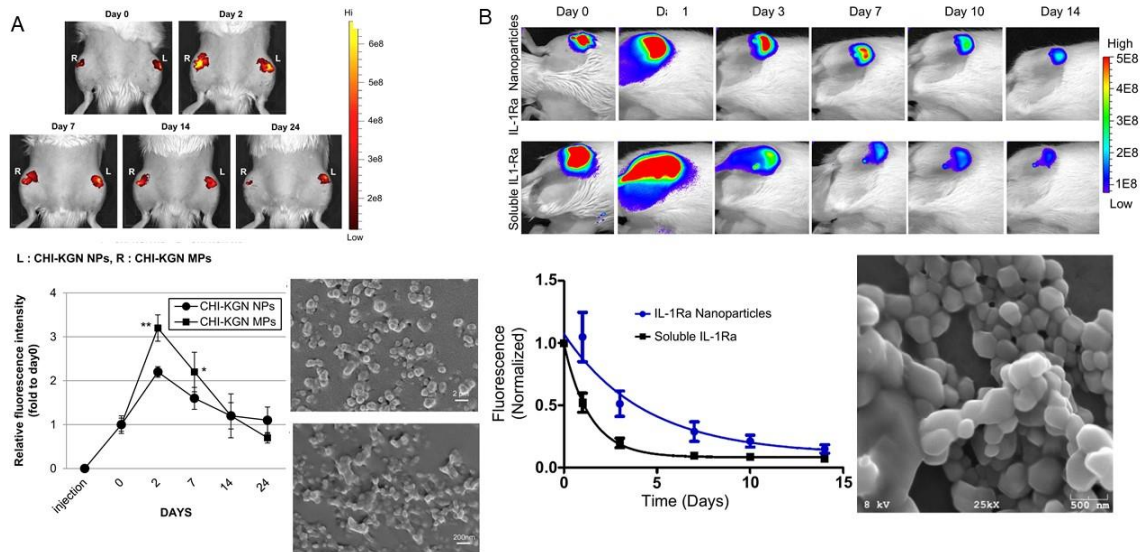
Figure 3.2. Whole joint retention profiles across different drug delivery nanoparticle systems, with a variety of structures, compositions, sizes, and shapes. Retention presented as fluorescence intensity. Joint retention prolonged by nanomaterials up to 14 days **A**) Chitosan nanoparticles (CHI-KGN NPs) or microparticles (CHI-KGN MPs) conjugated with kartogenin;[32] **B**) Tri-block polymeric nanoparticle.[38] All figures reprinted with permission.
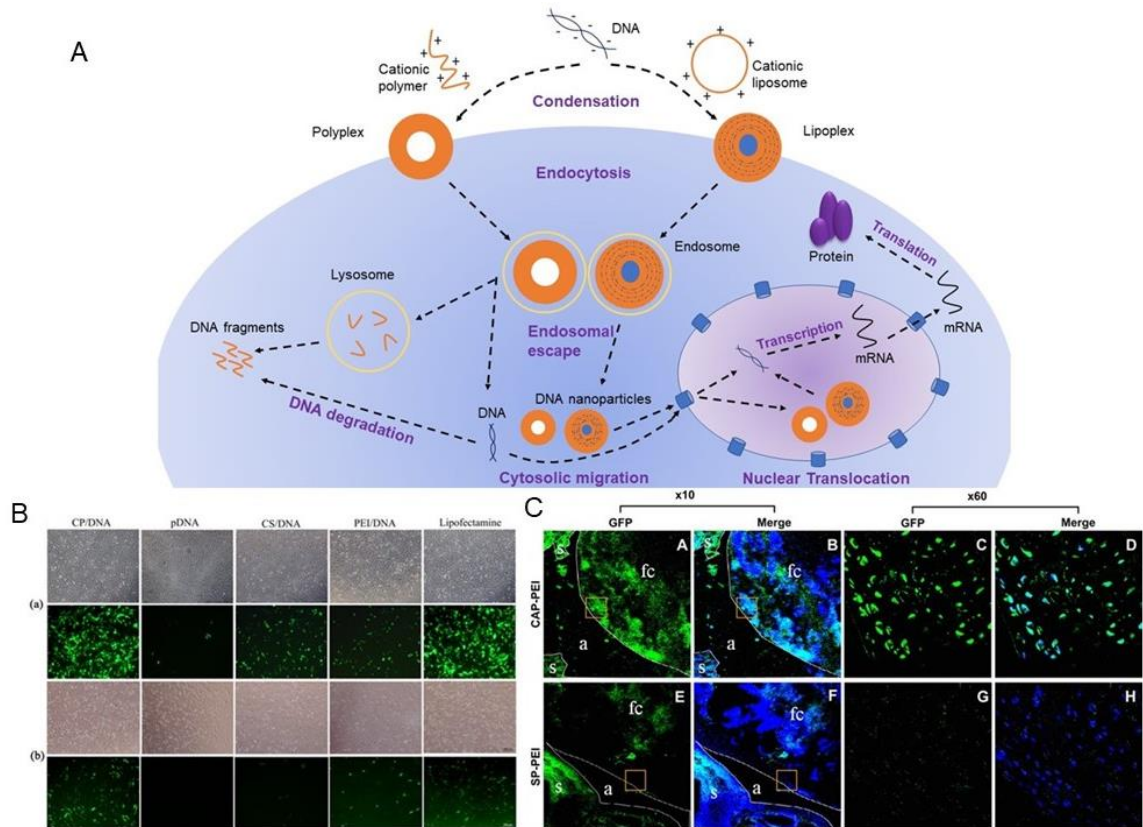
Figure 3.3. A) Basic mechanism of non-viral gene delivery via polymer (polyplex) or lipid based (lipoplex) delivery system. DNA condensed via interaction with cationic polymer or lipid and encapsulated to for a polyplex or lipoplex. **B**) Images of chondrocytes (a) or synoviocytes (b) transfected with CP/DNA nanoparticles, naked pDNA, CS/DNA nanoparticles, PEI (25 kDa)/DNA nanoparticles, and Lipofectamine™ 2000 as observed under fluorescence microscope or inverted phase contrast microscope.[79] **C**) Rabbit cartilage chondrocytes transfected by either chondrocyte affinity peptide/DNA (CAP/DNA) or scrambled peptide/DNA (SP/DNA), visualized under a confocal microscope. Blue: nuclear count-stained by Hoechst 33258; Green: GFP protein. Much higher GFP express level was observed inside the cartilage tissues transfected by CAP-PEI (A–D) than that transfected by SP-PEI (E–H). s: synovium; a: articular cavity; fc: femoral condyle.[80]

PART II: NANOPARTICULATE LUBRICANTS FOR ARTICULAR

CARTILAGE

CHAPTER IV: Strategies to Augment the Rheological and Tribological Properties of Synovial Fluid for the Treatment of Osteoarthritis

4.1 Abstract

Undergoing millions of articulations throughout an average lifetime, synovial joints require effective lubrication to provide a low coefficient of friction and prevent wear at the cartilage surface. Prolonged use or trauma results in osteoarthritis, a degenerative disease whose pathology is predominantly characterized by the breakdown of articular cartilage, concomitant with the degradation of synovial fluid biomacromolecules, hyaluronic acid and lubricin. This degradation decreases both the fluid and boundary lubricating capacity of synovial fluid, exacerbating tissue wear and disease progression. Viscosupplementation replaces degraded synovial fluid with a highly viscous supplement aimed at reestablishing rheological homeostasis to osteoarthritic joints. Current clinically approved viscosupplements provide minimal chondroprotection paired with ineffective joint residence times providing limited relief from disease progression. Thus, significant activities are ongoing to design and evaluate novel biolubricants to reduce the friction of articulating joints to prolong if not restore synovial joint function. This review highlights existing viscosupplements along with naturally occurring, partially, or fully synthetic biolubricant formulations and their relationship to cartilage theory of lubrication.

4.2 Introduction

4.2.1 Articular Cartilage Lubrication and Osteoarthritis

Articular cartilage is the primary bearing biomaterial of the body, lining the ends of bones within synovial joints and transmitting applied forces. Within the highly

organized, porous, and anisotropic structure of cartilage exists both a fluid and a solid phase. The fluid phase consists of interstitial water and dissolved ions, while the solid phase comprises primarily of collagen fibrils endowing cartilage with tensile strength, complemented by a matrix of negatively charged glycosaminoglycan (GAGs). The synergistic interactions between the solid and fluid phases grant cartilage a viscoelastic response to loading and highly specialized lubricating abilities. Being a porous structure, loading of cartilage leads to the entrapment of interstitial fluid within the pores of the solid collagen matrix and effectively supports >90% of applied joint load (i.e., interstitial fluid load support, IFLS).[1] Applied deformations induce efflux of fluid from the solid matrix to form an interposed fluid film that decreases the coefficient of friction (COF) and protects articulating joint surfaces from mechanical wear.[1]

Classically, for engineered systems such as bearings, Stribeck curves are used to describe how altering parameters of viscosity, velocity and load affect the COF and in turn the COF values are indicative of modes of lubrication – boundary, mixed and hydrodynamic. Boundary lubrication is characterized by a high COF and direct asperity contact between the two opposing surfaces with a molecularly thin layer of biomolecules separating opposing surfaces, accompanied by a high load and low speed, with the COF dictated based on surface characteristics of roughness, chemistry, and lubricant additives. It is during boundary lubrication where the COF values are the greatest, and material wear occurs by way of direct asperity-asperity contact of opposing surfaces and friction forces. Mixed mode lubrication occurs by means of slightly higher speeds or lower loads and is characterized by areas of boundary lubrication accompanied by areas where the height of

the fluid is greater than the asperities thereby separating the articulating surfaces entirely. Lastly, a thick film of fluid separates the articulating surfaces in hydrodynamic lubrication and occurs at low loads or high speeds.

While the Stribeck curve concisely places the three lubrication modes within well characterized boxes, lubrication modes of articular cartilage are more complex and not as easily defined. Unlike impermeable, non-derformable materials, boundary mode articular cartilage lubrication is also predicated on complex factors such as porosity and interstitial fluid. Other deviations from the classically ascribed Stribeck curve include the elastoviscous transition between boundary and hydrodynamic lubrication when the pressure in the self-generated hydrodynamic fluid film causes elastic deformation of the articulating surfaces. Furthermore, interstitial fluid pressurization enhances hydrodynamic lubrication. It is generally accepted that synovial joints operate under a combination and coexistence of boundary, mixed and elastohydrodynamic lubrication mechanisms.[1]

Synovial fluid (SF) is the naturally occurring lubricant in synovial joints, whose primary function is to provide shock absorption and lubrication which facilitates smooth, pain free ambulation and articulation. SF primarily consists of lubricin and hyaluronic acid, which act as boundary and fluid lubricants between opposing joint surfaces.[2,3] Hyaluronic acid (HA) is an anionic, non-sulfated, high molecular weight (MW 6 MDa) glycosaminoglycan, with repeating units of D-glucuronic acid and N-acetyl-D-glucosamine linked by a glucuronidic β (1->3) bond and contributes to viscosity and by extension, hydrodynamic lubrication (**Figure 4.1**). Lubricin, on the other hand, is a surface-active mucinous glycoprotein that aids in boundary lubrication (**Figure 4.1**).[3] Localized to

the cartilage surface, lubricin contains a central bottle brush like domain, coupled with somatomedin B and hemopexin like peptides.[4] Disulfide bridges between the somatomedin B domains allow lubricin multimerization, while the hemopexin domain facilitates hydrophobic interactions and promotes its binding to the articular cartilage surface. For these biomacromolecules of synovial fluid, function follows form. Synovial joint lubrication relies on the synergistic action of these components, none of which is solely responsible for the extremely low COF of articular cartilage. Recent studies indicate the entanglement and hydrophobic interaction of lubricin and HA contribute to mixed mode lubrication and shock absorption.[5–7] Although, the entanglement of HA and lubricin alone cannot account for the low COF of articular cartilage at high applied loads. Klein et al suggest a three-component system, where in conjunction with lubricin-immobilized-HA at the articular surface, HA complexes with phosphatidylcholine lipids exposing their charge groups at the cartilage interface[8,9] (8, 34) and allowing for "hydration lubrication", whereby lubrication occurs via hydration shells forming around the charged phosphatidyl choline molecules.[8]

Osteoarthritis (OA), a painful, chronic, condition, damages synovial joint function, and affects both the mechanical integrity and rheological behavior of synovial fluid. While the etiology of OA is multi-factorial, it is typically induced by mechanical injury as a consequence of trauma, joint instability, ligamentous deficiency, skeletal malalignment, obesity or anatomic deformity. Early-stage OA is characterized by the depletion of GAGS and subsequent collagen network degradation, instigating increased hydraulic permeability and decreased cartilage stiffness.[10] Integral to OA pathology are concomitant changes in

the biochemical composition of SF that cause deterioration of its rheological properties, resulting in increased cartilage wear. Specifically, HA decreases in molecular weight and viscosity, with degradation of lubricin occurring in parallel, decreasing the boundary lubricating capabilities of SF,[3,10] which is associated with early signs of articular cartilage wear.[11–13]

4.2.2 Viscosupplementation

To date, the two most common non-surgical treatment options for OA are non-steroidal-anti-inflammatory drugs and viscosupplementation. Viscosupplementation refers to the concept of augmenting osteoarthritic synovial fluid with solutions aimed to recapitulate the lubricating abilities of healthy SF. Current viscosupplementation targets HA concentration restoration, increasing viscosity, improving lubricity, and enhancing cushioning properties of the SF, while on the macroscopic scale providing pain relief and improved ambulation.

There are a handful of commercially available HA viscosupplements which vary with respect to molecular weight, crosslinking, zero shear rate viscosity, shear thinning ratio and cross over frequency. Made commercially available in 1986, Hyalgan and Artz are two of the oldest and lowest molecular weight supplements (**Table 4.1**). The efficacy of currently available viscosupplements is variable at best and significant debate exists surrounding the use of intra-articular (IA) HA injections, so much so that the guidelines of the American Academy of Orthopedic Surgeons do not recommend the use of HA injections to treat knee OA.[14]

While results are conflicting in terms of efficacy, there are a number of clinical

studies that indicate improvements in pain and joint function as a result of IA HA injections.[15–18] Miltner et al describe improvements in knee function following HA injections (2 mL Hyalart), as demonstrated by pain relief, and improved functional performance.[19] Similarly, following a single injection of Hylan G-F20 or a placebo in patients with symptomatic primary OA of the knee, patients who received the HA injection report significant improvements in WOMAC pain scores compared to the placebo up to 26 weeks post injection.[20] Likewise, in a comparison of functionality of IA HA injections and a placebo, it was found that while there was no appreciable difference in gait velocity, patients treated with the IA HA injections had improvements in WOMAC pain scores. Following 5 weekly injections of Hyalgan in patients with symptomatic knee OA, statistically significant improvements in knee joint function and maximum walking time for up to 12 months were observed, demonstrating long term efficacy for IA HA.[21]

A prime example of the tenuous link between IA HA injection and pain relief is the systematic review and meta-analysis by Rutjes et al., initially indicating no clinically significant reduction in pain following HA injections for OA, but a sub-analysis only including those studies using high molecular weight HA shows a statistically and clinically significant reduction in pain. The efficacy of varying HA molecular weight has been further investigated in a study of 1187 late-stage OA patients. Those injected with high molecular weight HA delayed, by an average of 2 years, total knee arthroplasty.[22] In a comparison of two differing molecular weight HA preparations, an intermediate (800-1500 kDa, GO-ON) and low (500-730 kDa, Hyalgan), Berenbaum et al. illustrate superior knee pain relief of the intermediate molecular weight supplement compared to the low (500-730 kDa,

Hyalgan) when administered to patients with primary knee OA.[23] Apart from pain reduction, studies indicate high molecular weight HA has a positive impact on cartilage biochemistry.[23] Following high molecular weight HA viscosupplementation, results from Shah et al show increased proteoglycan content at both 6 weeks and 3 months, concomitant with improvements in pain scores as measured by WOMAC.[24]

In contrast to studies indicating the positive effects of HA viscosupplementation several studies report none to minimal differences in measurable efficacy between IA HA injections and placebos or between varying MW of HA supplements. Weekly intra-articular injections for four weeks of sodium hyaluronate (Hyalgan) in comparison to IA injection of physiological saline, demonstrate no statistical difference between groups.[25] While a comparison of high and low molecular weight HA in symptomatic knee OA patients showed improvements in pain and WOMAC scores for both groups but not between groups, indicating similar efficacy regardless of MW.[26] These results are supported by a randomized control trial of IA HA injection of high molecular weight HA and a placebo, with no statistical difference in cartilage preservation observed between groups.[27] In tandem, a double blind randomized controlled trial comparing high molecular weight HA and saline found no improvements or differences in WOMAC pain scores in mild to moderate knee osteoarthritis.[28] Concomitantly, a study comparing 3 weekly injections of HA (MW 1.5 million Da) or a saline placebo indicate no significant difference between function and symptoms with respect to the saline placebo injection,[29] and a similar study consisting of 5 weekly IA injections of HA, illustrate no significant improvement in knee pain or function after 3-, 6-, 9- and 12-months following treatment.[30] Lending further

evidence to the nebulous efficacy of viscosupplementation, IA administration of high molecular weight HA (Artzal®), or crosslinked HA (Synvisc-One®) show no clinical benefit compared to a placebo.[31]

The contrasting results reflect the existing debate between clinical efficacy of viscosupplementation with hyaluronic acid. While there are studies indicating improvements in patients' pain, a similar number of studies conclude no differences between treatment with HA and saline. It is no surprise that given the polarizing conclusions on efficacy, the American Association of Orthopedic Surgeons guidelines do not recommend the use of HA injections to treat knee OA, and further studies concomitant with exploration of other lubricant materials apart from hyaluronic acid are warranted and explored in this review.

4.3 Naturally Occurring Lubricants for Tribosupplementation

4.3.1 Lubricin

Lubricin, a mucinous glycoprotein found in synovial fluid, protrudes from the cartilage surface, functioning as a boundary lubricant, while also acting to entangle and bind HA near the cartilage surface. These physical and chemical entanglements form a lubricious film on the surface of cartilage which contributes to cushioning applied forces and reducing the COF of articulating cartilage surfaces during mixed mode lubrication. Lubricin mimetic HA-binding peptides offer one approach to mimic lubricin's ability to bind HA and lubricate the cartilage surface. The HA-binding peptide, HABpep, covalently binds the cartilage surface upon reaction with free amines, or non-covalently binds to the surface through a collagen-binding peptide.[32] HABpep increases the *in vivo* joint retention

time of HA 12-fold compared to an untreated control. Cartilage-on-cartilage friction testing reveals that healthy cartilage treated with HABpep submerged in a solution of HA, significantly decreases the static and kinetic COFs compared to untreated cartilage, demonstrating the HA-binding peptide does not need HA to be continuously present for it to lubricate a surface (**Figure 4.2**). Similarly, mLub15, a lubricin-mimetic consisting of a chondroitin sulfate backbon e with type II collagen- and HA- binding peptides, demonstrates cartilage surface localization and when used to lubricate trypsin degraded cartilage-on-glass, restores the static and kinetic COF to values equal to non-degraded cartilage and comparable to the commercially available viscosupplement Synvisc-One® (**Figure 4.2**).[33] Notably, following IA injection of mLub15 into the patellar tendon of a spontaneous model of OA using Dunkin Hartley guinea pigs, mLub15 resides at the cartilage surface 6 hours post injection and is replaced by native lubricin 1- to 2-weeks post injection.[33]

Apart from mimicking the structure and function of lubricin, efforts are ongoing to develop recombinant lubricin for use in viscosupplementation.[34–37] Recombinant human lubricin (rhLub) shares 70% of its amino acid sequence with rat lubricin and reduces the COF of cartilage in a dose dependent manner up to ~50 µg/mL.[35,36] At this concentration, cartilage treated with rhLub affords an equilibrium coefficient of friction (0.093 ±0.011), significantly lower than PBS (0.281± 0.014), but not significantly different from equine synovial fluid (0.115±0.013).[36] Administration of rhLub in an OA rat medial collateral ligament and meniscus transection model, 1 or 3 times a week, decreases cartilage degradation scores compared to a PBS control.[35] In conjunction, immunostaining and

fluorescence *in situ* hybridization show that rhLub, increases native lubricin content and mRNA production, demonstrating lubricin administration during OA progression may have benefits beyond its lubricating abilities. Although in an OA rat anterior cruciate ligament transection (ACLT) model of OA, rhLub does not significantly improve Mankin scores when compared to cell culture derived lubricin and patient derived lubricin.[37]

Other lubricin related endeavors include modification of the naturally occurring molecule itself, offering a means to localize lubricin to the cartilage surface. One such modification is the addition of a reactive aldehyde to lubricin which then reacts with free amines on the cartilage surface to form a shift-base bond.[38,39] The aldehyde functionalization of lubricin, termed PRG4-CHO, does not significantly impact its function as a boundary lubricant and serves to increase the concentration of lubricin at the cartilage surface. Cartilage-on-cartilage friction tests show the static and kinetic COFs of PRG4-CHO are significantly lower than PBS and significantly higher than SF, however, were not significantly different from unmodified or sham modified lubricin.[38] Nevertheless, the aldehyde modification increases lubricin localization at the cartilage surface, with PRG4-CHO found at a 2- and 5-fold higher concentration at the cartilage surface compared to native lubricin and SDS treated cartilage samples, respectively.[39]

4.3.2 Micelles and Liposomes

Surface active phospholipids also play a role in synovial joint lubrication serving as boundary lubricants and with their highly hydrated headgroups reduce friction via hydration lubrication.[40–42] Phospholipid liposomes, derived from hydrogenated soy phosphatidylcholine (HSPC), form small unilamellar vesicles (SUVs) with an average

diameter between 65 and 75 nm and when absorbed onto mica surfaces, produce COF

values as low as 0.00002 and 0.0006, in pure water and a salt solution, respectively.[40,41]

The polar headgroups on the outer surface of the liposomes coordinate water molecules

and form hydration layers, leading to the low COFs observed, while the salt ions present

in the physiological solution compete with the polar headgroups of the liposomes for water

interactions, leading to an increase in COF of liposomes in the salt containing solution.[41]

Similarly, Sivan et al. describe five different phospholipid-based liposomes and their

ability to reduce friction in a cartilage-on-cartilage set up, with those composed of 1,2-

dimyristoyl-sn-glycero-3-phosphocholine (DMPC) producing the lowest static and kinetic

COFs across all loads tested.[42] Likewise, DMPC forms large multilamellar vesicles

(MLVs), with an average diameter greater than 800 nm, as well as SUVs, with an average

diameter less than 100 nm. When compared, the DMPC-MLVs yields lower static and

kinetic COFs than DMPC-SUVs when dispersed in the same buffer, and distillate at higher

concentration at the cartilage surface, a result of DMPC-SUVs penetrating and diffusing

throughout the layers of the cartilage.[42]

Akin to phospholipid liposomes, surfactant-based micelles are being explored,

albeit to a lesser degree, for their lubricating capabilities in aqueous solutions. Kampf et

al., report micelles of tri(dodecyldimethylammonioacetoxy) diethyltriamine trichloride

(DTAD), a trimeric surfactant, adsorbed onto mica surfaces. At low pressures, the DTAD-

micelle functionalized surface achieves an average coefficient of friction of 0.00013,

whereas increasing the pressure above 26 atms causes the average COF to increase to 0.01.

While the surfactant-based micelles lubricate through the same hydration mechanism as

phospholipid liposomes, they produce significantly higher coefficients of friction on the same articulating mica-on-mica surface, suggesting that phospholipid liposomes are a more promising viscosupplement.

4.3.3 Chitosan

Chitosan, a naturally occurring polymer with positively charged amine groups useful for adherence to anionic surfaces, enhances chondrogenesis, shares structural similarities to glycosaminoglycans (GAGs), and offers potential as a viscosupplement.[43–45] Scognamiglio et al. chronicle several sterilizable microgels based on lactose-modified chitosan. Rheological testing demonstrates the deleterious mechanical effects of autoclaving and tunability of the materials based on the chitosan to boric acid ratio. The lactose-modified chitosan hydrogels display a high resistance to degradation and at mildly higher pH the hydrogels exhibit an increase in elastic modulus in contrast to HA-hydrogels which degrade.[45] Of the hydrogels synthesized, those of 3 w/v% lactose-modified chitosan and 2 mM boric acid have storage (27.12 ± 0.21 Pa) and loss (19.44 ± 0.88 Pa) moduli akin to both commercially available viscosupplements (Synvisc-One®) and healthy SF.[45] In a rat bilateral medial partial meniscectomy model of OA, treatment with a thermo-responsive self-forming chitosan-hyaluronate hydrogel reduces pain as measured by increased load bearing of the joint.[43] This is coupled with histological evaluation indicating treated knees maintain thicker cartilage (170 ± 8 µm) compared to control knees (108 ± 10 µm) and prevent the formation of cysts. Similarly, IA injection of HA associated with lactose modified chitosan (Arty-Duo®) in a rat medial meniscotibial ligament transection model of OA, as compared to saline and HA, lowers both OARSI and Mankin scores. Arty-Duo®

injected knees show a decrease in the amount of matrixmetalloproteinase-3, matrixmetalloproteinase-13, Galectin-1 and Galectin-3 staining and increased Coll-II staining, compared to the saline control, demonstrating Arty-Duo's® ability to downregulate cartilage degrading proteins and promote cartilage regeneration during OA progression.[44]

4.3.4 Platelet Rich Plasma

Platelet rich plasma (PRP) offers a novel and effective treatment strategy for OA due to its high concentration of growth factors, which may promote chondrocyte differentiation and proliferation, and slow the progression of OA. The potential of PRP has led to several clinical studies comparing intraarticular injections of PRP to HA or saline.[46–51] Sakata et al., report both thrombin-activated and non-activated PRP produce COF values statistically significantly lower than those from saline and high-molecular weight HA.[52] Correspondingly, Russo et al. elucidate the rheological properties of HA solutions and HA solutions containing PRP. A frequency sweep conducted on the test solutions demonstrate that addition of PRP causes the storage and loss moduli of HA solutions to decrease, while increasing the crossover points.[53] However, similar trends are observed with addition of PBS to HA solutions, suggesting that the change in rheological properties are not due to the components of the PRP interfering with the lubricating ability of HA, but rather a change in the concentration of HA.[53] These preliminary studies hint that administration of a HA/PRP solution may have application as an effective viscosupplement for OA.

4.4 Synthetic Lubricants for Tribosupplementation

Synthetic biolubricants may overcome some of the disadvantages of naturally derived biolubricants such high compositional heterogeneity and undesirable physical properties related to poor oxidation stability, low temperature properties, and viscosity indexes. Despite the potential for naturally derived biolubricants, they are not widely commercialized due to high heterogeneity and undesirable physical properties related to poor oxidation stability, low temperature properties, and viscosity indexes.[54] The advantages of partially and fully synthetic lubricants include their ability to restore cartilage lubrication in conjunction with resistance to enzymatic degradation, superior stability, increased longer residence time, and ability to control tribological properties.[55]

With inspiration from hyaluronic acid and lubricin, researchers are developing both semi and fully synthetic biomimetic lubricants using two major approaches: either mimicking the 1) architecture or 2) chemistry (charge, functional groups, etc.) of biological macromolecules found in synovial fluid.

4.4.1 Proteoglycan Mimetics

The brush-like design of lubricin plays a vital role in lubrication. Following this lead, several groups are synthesizing and optimized brush-like diblock copolymers that bind and localize at the cartilage surface, reducing the COF during boundary mode lubrication to values comparable to native cartilage. Putnam et al., report an AB diblock copolymer consisting of a cationic cartilage-binding domain and a brush like lubricating domain that reduce the COF of cartilage in boundary mode conditions to naturally occurring lubricin (0.088 ± 0.039 and 0.093 ± 0.011, respectively). Further, the polymer

exhibits a cartilage-binding time constant comparable to purified human and recombinant lubricin.[56] As in lubricin, the composition is key to successful performance as the same polymer as a random copolymer or the individual polymer blocks fails to lubricate the articular surface. A second study of this AB diblock copolymer, further demonstrates the interdependence of form and function by altering the block lengths of the polymer.[57] The cartilage-binding block length influences degree of lubrication under boundary mode conditions, with twenty-four cartilage binding groups providing the lowest COF. Whereas the length of the actual lubricating block does not affect the degree of lubrication, providing key quantitative values for future designs of synthetic lubricants. With the same aim of designing and fabricating a biomimetic lubricant, Morgese et al., describe graft copolymers of a polyglutamic acid backbone onto which poly(2-methyl-2-oxazoline) (PMOXA) and hydroxybenzaldehyde are alternatively grafted.[58] The graft copolymers bind to bovine articular cartilage surfaces and cartilage-on-cartilage tribology experiments show a statistically significant reduction in friction using the graft copolymers, with COF values reaching those of native cartilage. The lubricity of the graft copolymer improves with higher concentrations of PMOXA side chains and by replacing the linear PMOXA side chains with cyclic side chains.[59]

Water absorption and coordination within synovial fluid plays a major role during boundary mode lubrication. As such, water-coordinating polyelectrolytes are a promising class of viscosupplementation material. For example, grafting surfaces with poly(2-methacryloyloxyethyl phosphorylcholine) (pMPC) reduces COF and provides chondroprotection.[60–62] Using water as a lubricant alone, grafting of pMPC polymer

brushes onto surfaces maintain the COF as low as 0.0004 at pressures as high as 8 MPa.[60,62] These results suggest the low COF arises due to formation of the hydration shells surrounding the phosphocholine monomers, thus providing lubricity via hydration lubrication. Likewise, physisorbed pMPC bottlebrush structures with positively charged terminal domains on charged mica surfaces afford COF values lower than naturally occurring lubricin over a wide range of applied loads and speeds. Tangentially, bottlebrush like polymers using polyacrylic acid-graft poly(ethylene glycol) and a thiol terminating backbone onto lubricin depleted cartilage surfaces, lower the COF, though not to values found within native cartilage.

This brush like strategy also applies to nanoparticles or microparticles as lubricants. For example, a microgel possessing a polyelectrolyte shell composed of polymer brushes grafted onto hollow silica nanoparticles, functions both as a lubricant and a drug delivery vehicle. The system, composed of poly(N-isopropylacrylamide) (PNIPAAm) microgels functionalized with a poly(3-sulfopropyl methacrylate potassium salt) shell, yield COF values akin to native cartilage when used to lubricate PDMS vs. silcon wafer.[63] On top of their lubricating capabilities, the microgels carry a drug payload which releases at different rates by way of the thermoresponsive properties of the PNIPAAm core.[63] Along this same vein, pMPC grafted mesoporous silica nanospheres synthesized via photopolymerization, encapsulate diclofenac sodium (DS), a commonly used anti-inflammatory for osteoarthritis pain relief, and lubricate the cartilage surface. In an *in vivo* medial meniscectomy rat model of OA, the pMPC grafted nanospheres loaded with DS preserve joint space, decrease volume of osteophyte formation, and improve OARSI scores as compared to controls.[64,65]

Concomitantly, hyaluronic acid-mimetic polymers synthesized to increase joint residence times and reintroduce anionic charged species to synovial fluid, outperform lubricin during boundary mode lubrication.[66] To increase the hyaluronic acid residence time in knee joints, the tribological properties of crosslinked or chemically modified hyaluronic acid microgels of vinyl sulfone-modified HA are crosslinked via dithiol-terminated poly(ethylene glycol) (HA-VS/SH-2-pEG).[67] The microgels increase viscosity and decrease COF compared to unmodified HA, while maintaining drug loading capabilities.[67] A second approach to modification of HA is via chemical modification. Zheng et al., describe grafting 2-methacryloyloxyethyl phosphorylcholine (MPC) onto HA, reducing the COF by 60% compared to endogenous HA, which is mechanistically attributed to hydration lubrication between water and the zwitterionic MPC.[68] Along those same lines, Wathier et al., describe a (poly(7-oxanorbornene-2-carboxylate) polymer to highlight the importance of the hydrophilicity and negatively charged moieties of HA on lubrication.[69] The polymers resist enzymatic degradation in vivo, display similar non-Newtonian behaviors to healthy synovial fluid, and demonstrate superior tribological, wear-preventative, and chondroprotection compared to native HA.[69]

4.4.2 Hydrogels

As osteoarthritis progresses, the viscoelastic and rheological properties of synovial fluid, crucial to maintaining the fluid barrier between articulating surfaces, deteriorate as HA and lubricin degrade. With many desirable properties such as localized drug delivery, tunable mechanical properties, biocompatibility, and environmentally responsive structures, hydrogels offer promise to improve lubrication strategies. Spontaneous

organization of hydrogel nanofibers with an inner core of cationic peptide amphiphiles surrounded by anionic high molecular weight HA entrap endogenous HA.[70] Tissue staining demonstrate that this scaffold approach was effective at maintaining cartilage tissue, increasing cellularity, enhancing cartilage specific GAG deposition, and increasing collagen II abundance.[70] Along those same lines, hydrogels synthesized via simple click chemistry, covalently bond HA to divinyl sulfone with thiol-terminated PEG.[67] Using various weight ratios of HA, the hydrogels demonstrate tunable viscoelasticity and controllable degradation rates, coupled with resistance to hyaluronidase and sustained release of the disease modified OA drug, triamcinolone acetonide.[67] When intra-articularly injected in an ACLT rabbit model of osteoarthritis the hydrogel decreases macroscopic scores of OA paired with decreased Mankin scores.[67] An HA-based hydrogel with covalently bound micelles of PEG and kartogenin (KGN), a small molecule that promotes chondrocyte differentiation of mesenchymal stem cells, sustains release of KGN and when intra-articularly injected into an ACLT and medial meniscectomy rat model of OA significantly suppresses disease progression.[71]

The use of naturally occurring polysaccharides as hydrogels is not limited to HA.[72–76] Analogous to previously mentioned endeavors to combine naturally occurring lubricants with chitosan, groups are using this naturally occurring polysaccharide to synthesize chitosan-based hydrogels and synthetic polymers for lubrication. Faivre et al., describe a hydrogel of chitosan coupled with HA and a bottle brush polymethylmethacrylate polymer, which substantially resists wear induced degradation following articulation and increases deposition of endogenous HA. Likewise, Arunkumar et al., report a dual-purpose

composite gelling system of a chitosan gel loaded with poly(caprolactone) microparticles for use as a viscosupplement and an intra-articular drug delivery depot of the COX-2 inhibitor Etoricoxib, which poses severe cardiovascular toxicity when administered orally.[73] The microparticle-hydrogel system demonstrates similar viscoelastic properties to HA, and *in vivo* fluorescence imaging reveal improved joint residence times, compared to bare chitosan gels or microparticles alone, and allow for sustained release of Etoricoxib.[73] Apart from chitosan, other polysaccharide-based hydrogel systems include one of gellan gum, a linear, anionic extracellular polysaccharide, coated with crosslinked polyvinyl alcohol, shows resistance to degradation when sterilized and elastic and viscous moduli values higher than the commercially available Synvisc indicating improvements in resistance to shear and compression.[77] Similarly, a hydrogel based on the naturally occurring polysaccharide guar gum, described by Cunha et al., demonstrates shear thinning behavior and viscosity on par with commercially available Hylan G-F 20.[78]

4.5 Conclusion

In OA, the capacity for SF to effect elastohydrodynamic cartilage lubrication is altered by decreases in the Mw of HA that deplete the viscoelastic properties of SF, along with deprivation of lubricin that reduces boundary lubrication. As a result, articular cartilage exhibits a higher COF, increasing mechanical wear, coupled with elevated cytokine levels, which stimulate matrix metalloproteinase production, further propagating degradation of the cartilage ECM.

FDA approved intra-articular injection of HA for viscosupplementation as a device is predicated on the theory that reconstituting high MW HA concentration will recuperate

SF viscosity and rejuvenate the elastohydrodynamic lubrication properties of SF. However, the safety and efficacy of viscosupplements as a "device" was established on attaining analgesia equivalent to non-steroidal anti-inflammatory drugs administered enterally, rather than proof of chondroprotective or chondroregenerative effectiveness. As such, the efficacy of currently available viscosupplements is variable, limited by failure of these treatments to modify OA cartilage pathology as a consequence of short intra-articular residence time due to enzymatic degradation by hyaluronidase, and persistence of elevated cytokine levels in OA SF.

Currently, no device or pharmacological treatment has been demonstrated to impart chondroprotection after the induction of OA. Therefore, to address these deficits, researchers are developing bio-lubricants that reduce friction between articulating joint surfaces and cartilage wear by recapitulating the non-Newtonian, tribological properties of healthy SF and imparting boundary lubrication. As a general strategy, these biolubricants use bio-inspired polymer networks based on HA and/or lubricin, incorporating the hydrophilic phosphorylcholine headgroup, exploiting its ability to attract and coordinate water molecules to induce hydration lubrication. Chemical or physical alterations to HA so as to resist enzymatic degradation in the hostile environment of an OA afflicted synovial joint include vinyl sulfone-modified HA crosslinked via dithiol-terminated poly(ethylene glycol) (HA-VS/SH-2-pEG),[67] or grafting the zwitterionic monomer 2-methacryloyloxyethyl phosphorylcholine onto HA.[68] Efforts to create boundary lubricants range from transforming naturally occurring lubricin, by attaching an HA-binding peptide, to chemical modification of the molecule itself via aldehyde functionalization to increase

cartilage surface localization. Research involving naturally occurring polysaccharides, such as chitosan,[73] gellan gum,[77] and guar gum,[78] are being explored for use as fluid film lubricants. While boundary lubricants are a final defensive guard against cartilage wear, this treatment will not repair degraded cartilage ECM. Therefore, multifunctional SF supplements are being developed that not only augment SF viscoelasticity and resist enzymatic degradation, but incorporate nanoparticles, micelles and/or hydrogels that are depots for the sustained release of disease modifying OA drugs and/or small therapeutic molecules. However, the challenge to the clinical efficacy of recuperating elastohydrodynamic lubrication in diseased joints with synovial fluid supplements is diagnosing OA at a stage where chondroprotective biolubricants are capable of mitigating cartilage destruction *before* irreversible damage has transpired. Imaging methods to identify early-stage biochemical and structural changes indicative of OA pathology, before pathoanatomy is apparent must be developed in tandem with the tribosupplementation endeavors described herein.

4.6 References

1. Neu, C. P., Komvopoulos, K. & Reddi, A. H. The interface of functional biotribology and regenerative medicine in synovial joints. *Tissue Engineering - Part B: Reviews* **14**, 235–247 (2008).

2. Jahn, S., Seror, J. & Klein, J. Lubrication of Articular Cartilage. *Annual Review of Biomedical Engineering* **18**, 235–258 (2016).

3. Furmann, D. *et al.* The effect of synovial fluid composition, speed and load on frictional behaviour of articular cartilage. *Materials* **13**, (2020).

4. Morgese, G., Benetti, E. M. & Zenobi-Wong, M. Molecularly Engineered Biolubricants for Articular Cartilage. *Advanced Healthcare Materials* **7**, 1701463 (2018).

5.   Ludwig, T. E., Hunter, M. M. & Schmidt, T. A. Cartilage boundary lubrication synergism is mediated by hyaluronan concentration and PRG4 concentration and structure. *BMC Musculoskeletal Disorders* **16**, 386 (2015).

6.   Bonnevie, E. D., Galesso, D., Secchieri, C., Cohen, I. & Bonassar, L. J. Elastoviscous Transitions of Articular Cartilage Reveal a Mechanism of Synergy between Lubricin and Hyaluronic Acid. (2015).

7.   Greene, G. W. *et al.* Adaptive mechanically controlled lubrication mechanism found in articular joints. *Proceedings of the National Academy of Sciences of the United States of America* **108**, 5255-5259

8.   Jahn, S. & Klein, J. Hydration Lubrication: The Macromolecular Domain. *Macromolecules* **48**, 5059–5075 (2015).

9.   Seror, J., Zhu, L., Goldberg, R., Day, A. J. & Klein, J. ARTICLE Supramolecular synergy in the boundary lubrication of synovial joints. *Nature Communications* (2015).

10. Chen, D. *et al.* Osteoarthritis: Toward a comprehensive understanding of pathological mechanism. *Bone Research* **5**, 16044 (2017).

11. Guilak, F. The slippery slope of arthritis. *Arthritis & Rheumatism* **52**, 1632–1633 (2005).

12. Elsaid, K. A., Jay, G. D., Warman, M. L., Rhee, D. K. & Chichester, C. O. Association of articular cartilage degradation and loss of boundary-lubricating ability of synovial fluid following injury and inflammatory arthritis. *Arthritis and Rheumatism* **52**, 1746–1755 (2005).

13. Schmidt, T. A., Gastelum, N. S., Nguyen, Q. T., Schumacher, B. L. & Sah, R. L. Boundary lubrication of articular cartilage: role of synovial fluid constituents. *Arthritis and Rheumatism* **56**, 882–891 (2007).

14. AAOS.com. https://www.orthoguidelines.org/go/cpg/detail.cfm?id=1214.

15. Adams, M. E. *et al.* The role of viscosupplementation with hylan G-F 20 (Synvisc ®) in the treatment of osteoarthritis of the knee: a Canadian multicenter trial comparing hylan G-F 20 alone, hylan G-F 20 with non-steroidal anti-inflammatory drugs (NSAIDs) and NSAIDs alone. *Osteoarthritis and Cartilage* **3**, (1995).

16. Altman, R. D., Rosen, J. E., Bloch, D. A., Hatoum, H. T. & Korner, P. A Double-Blind, Randomized, Saline-Controlled Study of the Efficacy and Safety of EUFLEXXA® for Treatment of Painful Osteoarthritis of the Knee, With an Open-Label Safety Extension (The FLEXX Trial). *Seminars in Arthritis and Rheumatism* **39**, 1–9 (2009).

17. Kirchner, M. & Marshall, D. A double-blind randomized controlled trial comparing alternate forms of high molecular weight hyaluronan for the treatment of osteoarthritis of the knee. *Osteoarthritis and Cartilage* **14**, 154–162 (2006).

18. Wobig, M., Dickhut, A., Maier, R. & Vetter, G. Viscosupplementation with Hylan G-F 20: A 26-week controlled trial of efficacy and safety in the osteoarthritic knee. *Clinical Therapeutics* **20**, 410–423 (1998).

19. Miltner, O., Schneider, U., Siebert, C. H., Niedhart, C. & Niethard, F. U. Efficacy of intraarticular hyaluronic acid in patients with osteoarthritis - A prospective clinical trial. *Osteoarthritis and Cartilage* **10**, 680–686 (2002).

20. Chevalier, X. *et al.* Single, intra-articular treatment with 6 ml hylan G-F 20 in patients with symptomatic primary osteoarthritis of the knee: A randomised, multicentre, double-blind, placebo controlled trial. *Annals of the Rheumatic Diseases* **69**, 113–119 (2010).

21. Kolarz, G., Kotz, R. & Hochmayer, I. Long-term benefits and repeated treatment cycles of intra-articular sodium hyaluronate (Hyalgan) in patients with osteoarthritis of the knee. *Seminars in Arthritis and Rheumatism* **32**, 310–319 (2003).

22. Waddell, D. D. & Bricker, D. W. C. Total knee replacement delayed with hylan G-F 20 use in patients with grade IV osteoarthritis. *Journal of Managed Care Pharmacy* **13**, 113–121 (2007).

23. Berenbaum, F. *et al.* A randomised, double-blind, controlled trial comparing two intra-articular hyaluronic acid preparations differing by their molecular weight in symptomatic knee osteoarthritis. *Annals of the Rheumatic Diseases* **71**, 1454–1460 (2012).

24. Shah, R. P. *et al.* T1Rho magnetic resonance imaging at 3t detects knee cartilage changes after viscosupplementation. *Orthopedics* **38**, e604–e610 (2015).

25. Lundsgaard, C., Dufour, N., Fallentin, E., Winkel, P. & Gluud, C. Intra-articular sodium hyaluronate 2 mL versus physiological saline 20 mL versus physiological saline 2 mL for painful knee osteoarthritis: a randomized clinical trial. *Scandinavian Journal of Rheumatology* **37**, 142–150 (2008).

26. Gigis, I., Fotiadis, E., Nenopoulos, A., Tsitas, K. & Hatzokos, I. Comparison of two different molecular weight intra-articular injections of hyaluronic acid for the treatment of knee osteoarthritis. *Hippokratia* **20**, 26–31 (2016).

27. Wang, Y. *et al.* Effects of Hylan G-F 20 supplementation on cartilage preservation detected by magnetic resonance imaging in osteoarthritis of the knee: A two-year single-blind clinical trial. *BMC Musculoskeletal Disorders* **12**, 1–9 (2011).

28. van der Weegen, W., Wullems, J. A., Bos, E., Noten, H. & van Drumpt, R. A. M. No Difference Between Intra-Articular Injection of Hyaluronic Acid and Placebo for Mild to Moderate Knee Osteoarthritis: A Randomized, Controlled, Double-Blind Trial. *Journal of Arthroplasty* **30**, 754–757 (2015).

29. Kul-Panza, E. & Berker, N. Is hyaluronate sodium effective in the management of knee osteoarthritis? A placebo-controlled double-blind study. *Minerva Medica* **101**, 63–72 (2010).

30. Jørgensen, A. *et al.* Intra-articular hyaluronan is without clinical effect in knee osteoarthritis: A multicentre, randomised, placebo-controlled, double-blind study of 337 patients followed for 1 year. *Annals of the Rheumatic Diseases* **69**, 1097–1102 (2010).

31. Karlsson, J. Comparison of two hyaluronan drugs and placebo in patients with knee osteoarthritis. A controlled, randomized, double-blind, parallel-design multicentre study. *Rheumatology* **41**, 1240–1248 (2002).

32. Singh, A. *et al.* Enhanced lubrication on tissue and biomaterial surfaces through peptide-mediated binding of hyaluronic acid. *Nature Materials* **13**, 988–995 (2014).

33. Lawrence, A. *et al.* Synthesis and characterization of a lubricin mimic (mLub) to reduce friction and adhesion on the articular cartilage surface. *Biomaterials* **73**, 42–50 (2015).

34. Jones, A. R. C. *et al.* Binding and localization of recombinant lubricin to articular cartilage surfaces. *Journal of Orthopaedic Research* **25**, 283–292 (2007).

35. Flannery, C. R. *et al.* Prevention of cartilage degeneration in a rat model of osteoarthritis by intraarticular treatment with recombinant lubricin. *Arthritis & Rheumatism* **60**, 840–847 (2009).

36. Gleghorn, J. P., Jones, A. R. C., Flannery, C. R. & Bonassar, L. J. Boundary mode lubrication of articular cartilage by recombinant human lubricin. *Journal of Orthopaedic Research* **27**, 771–777 (2009).

37. Jay, G. D. *et al.* Prevention of cartilage degeneration and restoration of chondroprotection by lubricin tribosupplementation in the rat following anterior cruciate ligament transection. *Arthritis & Rheumatism* **62**, 2382–2391 (2010).

38. Abubacker, S., Ham, H. O., Messersmith, P. B. & Schmidt, T. A. Cartilage boundary lubricating ability of aldehyde modified proteoglycan 4 (PRG4-CHO). *Osteoarthritis and Cartilage* **21**, 186–189 (2013).

39. Chawla, K., Ham, H. O., Nguyen, T. & Messersmith, P. B. Molecular resurfacing of cartilage with proteoglycan 4. *Acta Biomaterialia* **6**, 3388–3394 (2010).

40. Goldberg, R. *et al.* Boundary Lubricants with Exceptionally Low Friction Coefficients Based on 2D Close-Packed Phosphatidylcholine Liposomes. *Advanced Materials* **23**, 3517–3521 (2011).

41. Goldberg, R., Schroeder, A., Barenholz, Y. & Klein, J. Interactions between adsorbed hydrogenated soy phosphatidylcholine (HSPC) vesicles at physiologically high pressures and salt concentrations. *Biophysical Journal* **100**, 2403–2411 (2011).

42. Sivan, S. *et al.* Liposomes act as effective biolubricants for friction reduction in human synovial joints. *Langmuir* **26**, 1107–1116 (2010).

43. Patchornik, S., Ram, E., ben Shalom, N., Nevo, Z. & Robinson, D. Chitosan-Hyaluronate Hybrid Gel Intraarticular Injection Delays Osteoarthritis Progression and Reduces Pain in a Rat Meniscectomy Model as Compared to Saline and Hyaluronate Treatment. *Advances in Orthopedics* **2012**, 1–5 (2012).

44. Salamanna, F. *et al.* Effects of intra-articular hyaluronic acid associated to Chitlac (arty-duo®) in a rat knee osteoarthritis model. *Journal of Orthopaedic Research* **37**, 867–876 (2019).

45. Scognamiglio, F., Travan, A., Donati, I., Borgogna, M. & Marsich, E. A hydrogel system based on a lactose-modified chitosan for viscosupplementation in osteoarthritis. *Carbohydrate Polymers* **248**, 116787 (2020).

46. Kon, E. *et al.* Platelet-rich plasma intra-articular injection versus hyaluronic acid viscosupplementation as treatments for cartilage pathology: From early degeneration to osteoarthritis. *Arthroscopy - Journal of Arthroscopic and Related Surgery* **27**, 1490–1501 (2011).

47. Cole, B. J., Karas, V., Hussey, K., Pilz, K. & Fortier, L. A. Hyaluronic Acid Versus Platelet-Rich Plasma. *American Journal of Sports Medicine* **45**, 339–346 (2017).

48. Sánchez, M. *et al.* A randomized clinical trial evaluating plasma rich in growth factors (PRGF-Endoret) versus hyaluronic acid in the short-term treatment of symptomatic knee osteoarthritis. *Arthroscopy - Journal of Arthroscopic and Related Surgery* **28**, 1070–1078 (2012).

49. Spaková, T., Rosocha, J., Lacko, M., Harvanová, D. & Gharaibeh, A. Treatment of Knee Joint Osteoarthritis with Autologous Platelet-Rich Plasma in Comparison with Hyaluronic Acid. *American Journal of Physical Medicine & Rehabilitation* **91**, 411–417 (2012).

50. Patel, S., Dhillon, M. S., Aggarwal, S., Marwaha, N. & Jain, A. Treatment with platelet-rich plasma is more effective than placebo for knee osteoarthritis: A prospective,

double-blind, randomized trial. *American Journal of Sports Medicine* **41**, 356–364 (2013).

51. Filardo, G. *et al.* Platelet-rich plasma vs hyaluronic acid to treat knee degenerative pathology: Study design and preliminary results of a randomized controlled trial. *BMC Musculoskeletal Disorders* **13**, 229 (2012).

52. Sakata, R. *et al.* Stimulation of the Superficial Zone Protein and Lubrication in the Articular Cartilage by Human Platelet-Rich Plasma. *American Journal of Sports Medicine* **43**, 1467–1473 (2015).

53. Russo, F. *et al.* Platelet Rich Plasma and Hyaluronic Acid Blend for the Treatment of Osteoarthritis: Rheological and Biological Evaluation. *PLOS ONE* **11**, e0157048 (2016).

54. Nagendramma, P. & Kaul, S. Development of ecofriendly/biodegradable lubricants: An overview. *Renewable and Sustainable Energy Reviews* **16**, 764–774 (2012).

55. Hayes, A. J. & Melrose, J. Glycosaminoglycan and Proteoglycan Biotherapeutics in Articular Cartilage Protection and Repair Strategies: Novel Approaches to Visco-supplementation in Orthobiologics. *Advanced Therapeutics* **2**, 1900034 (2019).

56. Sun, Z. *et al.* Boundary mode lubrication of articular cartilage with a biomimetic diblock copolymer. *Proceedings of the National Academy of Sciences of the United States of America* **116**, 12437–12441 (2019).

57. Sun, Z., Bonassar, L. J. & Putnam, D. Influence of Block Length on Articular Cartilage Lubrication with a Diblock Bottle-Brush Copolymer. *ACS Applied Materials and Interfaces* **12**, 330–337 (2020).

58. Morgese, G., Cavalli, E., Müller, M., Zenobi-Wong, M. & Benetti, E. M. Nanoassemblies of Tissue-Reactive, Polyoxazoline Graft-Copolymers Restore the Lubrication Properties of Degraded Cartilage. *ACS Nano* **11**, 2794–2804 (2017).

59. Morgese, G., Cavalli, E., Rosenboom, J.-G., Zenobi-Wong, M. & Benetti, E. M. Cyclic Polymer Grafts That Lubricate and Protect Damaged Cartilage. *Angewandte Chemie International Edition* **57**, 1621–1626 (2018).

60. Chen, M., Briscoe, W. H., Armes, S. P., Cohen, H. & Klein, J. Robust, biomimetic polymer brush layers grown directly from a planar mica surface. *ChemPhysChem* **8**, 1303–1306 (2007).

61. Chen, M., Briscoe, W. H., Armes, S. P. & Klein, J. Lubrication at physiological pressures by polyzwitterionic brushes. *Science* **323**, 1698–1701 (2009).

62. Chen, M., Briscoe, W. H., Armes, S. P., Cohen, H. & Klein, J. Polyzwitterionic brushes: Extreme lubrication by design. (2011).

63. Liu, G., Cai, M., Zhou, F. & Liu, W. Charged polymer brushes-grafted hollow silica nanoparticles as a novel promising material for simultaneous joint lubrication and treatment. *Journal of Physical Chemistry B* **118**, 4920–4931 (2014).

64. Chen, H. *et al.* Cartilage matrix-inspired biomimetic superlubricated nanospheres for treatment of osteoarthritis. *Biomaterials* **242**, 119931 (2020).

65. Wan, L. *et al.* Biodegradable lubricating mesoporous silica nanoparticles for osteoarthritis therapy. *Friction* 1–12 (2020).

66. Wathier, M. *et al.* A synthetic polymeric biolubricant imparts chondroprotection in a rat meniscal tear model. *Biomaterials* **182**, 13–20 (2018).

67. Cai, Z., Zhang, H., Wei, Y., Wu, M. & Fu, A. Shear-thinning hyaluronan-based fluid hydrogels to modulate viscoelastic properties of osteoarthritis synovial fluids. *Biomaterials Science* **7**, 3143–3157 (2019).

68. Zheng, Y. *et al.* Bioinspired Hyaluronic Acid/Phosphorylcholine Polymer with Enhanced Lubrication and Anti-Inflammation. *Biomacromolecules* **20**, 4135–4142 (2019).

69. Wathier, M. *et al.* A large-molecular-weight polyanion, synthesized via ring-opening metathesis polymerization, as a lubricant for human articular cartilage. *Journal of the American Chemical Society* **135**, 4930–4933 (2013).

70. Arslan, E. *et al.* Protective therapeutic effects of peptide nanofiber and hyaluronic acid hybrid membrane in in vivo osteoarthritis model. *Acta Biomaterialia* **73**, 263–274 (2018).

71. Kang, M.-L., Jeong, S.-Y. & Im, G.-I. Hyaluronic Acid Hydrogel Functionalized with Self-Assembled Micelles of Amphiphilic PEGylated Kartogenin for the Treatment of Osteoarthritis. *Tissue Engineering Part A* **23**, 630–639 (2017).

72. Milcovich, G. *et al.* Modulating carbohydrate-based hydrogels as viscoelastic lubricant substitute for articular cartilages. *International Journal of Biological Macromolecules* **102**, 796–804 (2017).

73. Arunkumar, P., Indulekha, S., Vijayalakshmi, S. & Srivastava, R. Poly (caprolactone) microparticles and chitosan thermogels based injectable formulation of etoricoxib for the potential treatment of osteoarthritis. *Materials Science and Engineering C* **61**, 534–544 (2016).

74. Cunha, P. L. R., Castro, R. R., Rocha, F. A. C., de Paula, R. C. M. & Feitosa, J. P. A. Low viscosity hydrogel of guar gum: Preparation and physicochemical characterization. *International Journal of Biological Macromolecules* **37**, 99–104 (2005).

75. Leone, G. *et al.* Enriched Gellan Gum hydrogel as visco-supplement. *Carbohydrate Polymers* **227**, 115347 (2020).

76. Chejara, D. *et al.* Synthesis and Evaluation of a Sodium Alginate-4-Aminosalicylic Acid Based Microporous Hydrogel for Potential Viscosupplementation for Joint Injuries and Arthritis-Induced Conditions. *Marine Drugs* **15**, 257 (2017).

77. Leone, G. *et al.* Enriched Gellan Gum hydrogel as visco-supplement. *Carbohydrate Polymers* **227**, 115347 (2020).

78. Cunha, P. L. R., Castro, R. R., Rocha, F. A. C., de Paula, R. C. M. & Feitosa, J. P. A. Low viscosity hydrogel of guar gum: Preparation and physicochemical characterization. *International Journal of Biological Macromolecules* **37**, 99–104 (2005).

Table 4.1. FDA Approved, clinically used viscosupplements.

Name	Injections per week	Molecular Weight (kDa)
Euflexxa	3	2400 - 3600
Synvisc	3	6000 - 7000
Synvisc-One	1	6000 - 7000
Gel-One	1	Crosslinked, infinite MW
Synojoynt	3	2500
Monovisc	1	1000 - 2900
Gel-Syn	3	1100
Orthovisc	3 to 4	1000 - 2900
Supartz	3 to 4	620 - 1170
Durolane	1	1000
Ostenil	3	1000 - 2000
Visco-3	3	620 - 1170
Suplasyn	1	500 - 730
Hyalgan	5	500 - 730
Hymovis	2	500 - 730
Triluron	3	500 - 730
GenVisc	3 - 5	850
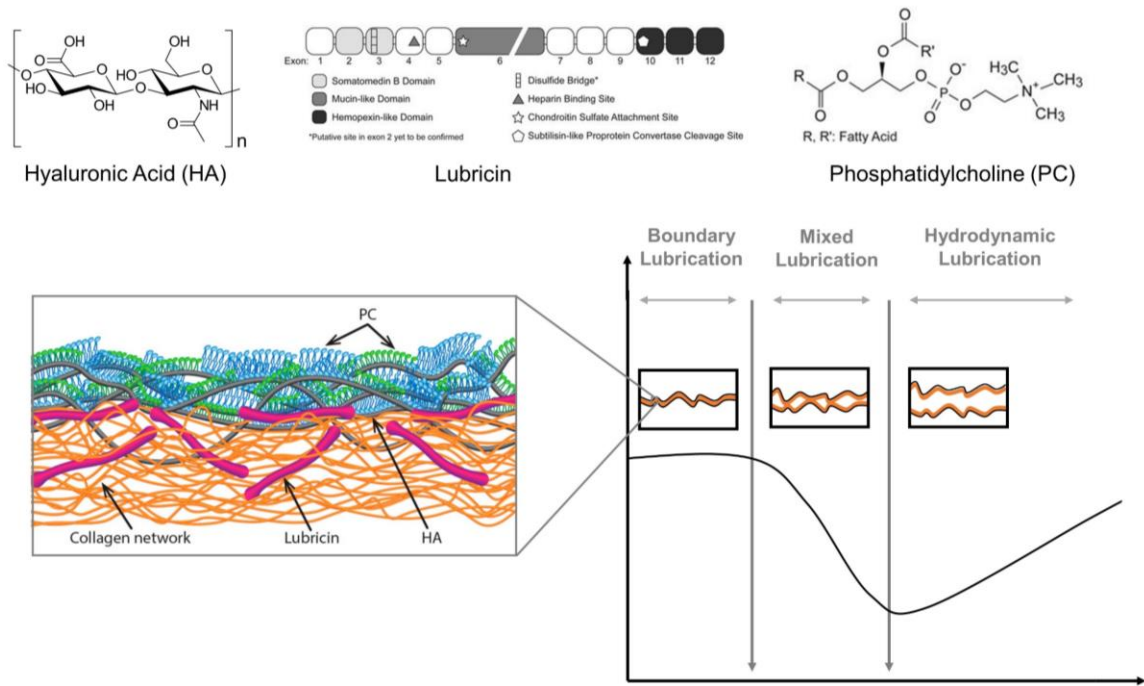
Figure 4.1. Macromolecules of synovial fluid and their synergistic interactions at the cartilage surface. The lubrication mode which this organized surface layer of macromolecules impacts, boundary mode lubrication.
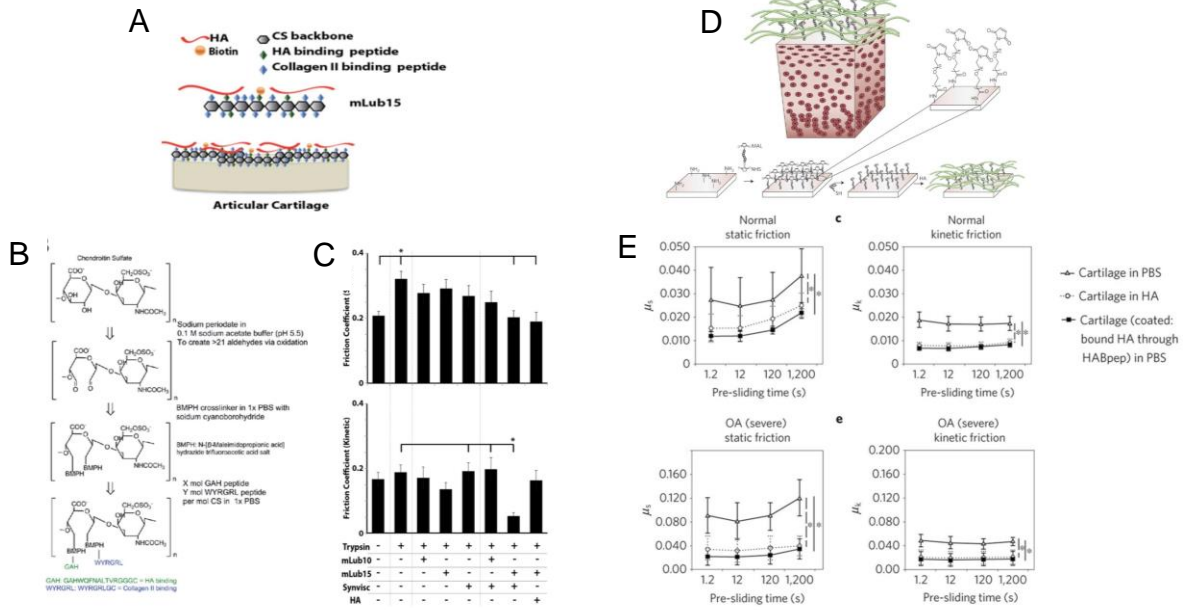
Figure 4.2. A) Schematic of mLub15 binding to the articular surface and HA in the synovial fluid. **B**) Reaction schematic for the synthesis of mLub15 with the addition of HA and type II collagen binding peptides to a chondroitin sulfate backbone. **C**) Calculated static and kinetic coefficient of friction values of each treatment group ($n \geq 9$). In static COF, there is statistical difference ($p < 0.05$) between the trypsin treated plug and the WT, mLub15 + Synvisc, and mLub15 + HA treatments. In kinetic friction, there is statistical difference ($p < 0.05$) between the mLub15 + Synvisc treatment and the trypsin, Synvisc, and mlub10 + Synvisc treatments. Standard error bars are shown.[33] **D**) Schematic of a cartilage surface modified with a HABpep designed to interact with and bind HA in surrounding fluid. E) HA-recruiting molecules able to reduce the COF of healthy OA cartilage for both static and kinetic friction.[32] All figures reprinted with permission.
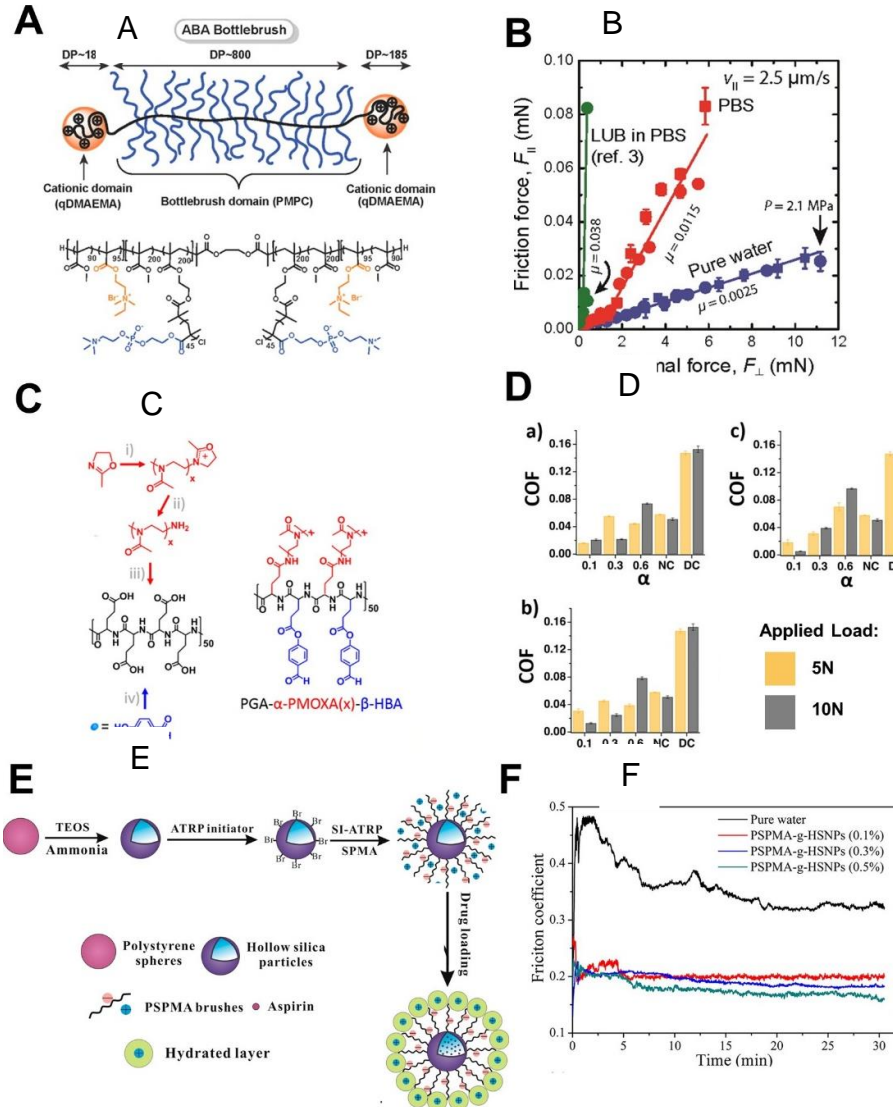
Figure 4.3. A) Schematic representations of the bottle-brush polymer mimicking LUB. **B**) Experimental data showing that the friction coefficient μ is independent of the applied load. C) PGA-α-PMOXA(*x*)-β-HBA synthesis via cationic ring-opening polymerization of 2-methyl-2-oxazoline **D**) Degraded cartilage slices were coated with PGA-PMOXA-HBA graft-copolymers, and the COF values were measured sliding them against each other using a bovine synovial fluid solution of the corresponding graft-copolymer at 5 mm/s (a–b–c), the recorded values of COF are reported for the different copolymer grafting densities (α) and a fixed side-chain length: *x* = 30 for (a), *x* = 100 for (b), *x* = 120 for (c). Native cartilage (NC) and digested cartilage (DC) were chosen as positive and negative controls, respectively. **E**) Fabrication of PSPMA-g-HSNPs, and drug loading. **F**) Friction curves for steel–steel contacts lubricated by pure water and PSPMA-*g*-HSNP suspension with different solid contents (0.1, 0.3, and 0.5 wt %). DOI: (10.1021/jp500074g). All figures reprinted with permission.

CHAPTER V: Mega-Macromolecules as Single Molecule Lubricants for Hard and Soft Surfaces

5.1 Abstract

A longstanding goal in science and engineering is to mimic the size, structure, and functionality present in biology with synthetic analogs. Today, synthetic globular polymers of several million molecular weight are unknown, and, yet these structures are expected to exhibit unanticipated properties due to their size, compactness, and low inter-chain interactions. Here we report the gram-scale synthesis of dendritic polymers, mega hyperbranched polyglycerols (mega HPGs), in million daltons. The mega HPGs are highly water soluble, soft, nanometer-scale single polymer particles that exhibit low intrinsic viscosities. Further, the mega HPGs are lubricants acting as interposed single molecule ball bearings to reduce the coefficient of friction between both hard and soft natural surfaces in a size dependent manner. We attribute this result to their globular and single particle nature together with its exceptional hydration. Collectively, these results set the stage for new opportunities in the design, synthesis, and evaluation of mega polymers.

5.2 Introduction

As our mastery of polymerization reactions advances, macromolecules of increasing complexity and size are readily synthesized. Dendrimers clearly showcase this advancement; specific structural or compositional features are introduced at defined locations within a 3D globular structure.[1-6] Linear polymers of a few million Dalton molecular weight also exhibit interesting properties and are prepared via judicious choice of monomer and under carefully controlled reaction conditions including reversible

deactivation radical polymerization[7], atom transfer radical polymerization,[8] reversible addition-fragmentation chain transfer[9], ring-opening metathesis[10] and Lewis pair polymerizations.[11] Synthesizing globular polymers of several million molecular weight has not been previously achieved and will, similarly, afford unexpected properties as one single polymer itself occupies a size of tens of nanometers owing to its compact structure. A path to such mega-macromolecules of several million Dalton molecular weight represents a significant synthetic challenge. During a polymerization reaction, the viscosity of the polymerization medium increases, which leads to quenching of propagation species, poor control of molecular weight, polydispersity, and branching.

Herein, we report the synthesis and characterization of semi-dendritic hyperbranched polyglycerols of 1, 3, and 9 million Dalton (MDa) (i.e., mega HPGs), and their performance as single molecule soft ball bearing lubricants on hard and soft surfaces. The mega HPGs reduce the coefficient of friction between both hard and soft surfaces and exhibit rheological properties similar to a fluid lubricant. The high-water solubility, low intrinsic viscosity, compactness, nearly molecular weight independent intrinsic viscosity, and hydration of the mega HPGs are responsible for their performance as single molecule ball bearings.

5.3 Methods

5.3.1 Materials

All solvents and reagents were purchased from Sigma-Aldrich, Canada, unless otherwise mentioned. Glycidol was vacuum distilled over CaH_2 at 40-50 °C and stored over 4 Å molecular sieves. Anhydrous DMF and dioxane from Sigma Aldrich were used

without further purification. Deuterated solvent (D_2O, 99.8%D) was purchased from Cambridge Isotope Laboratories, Inc. Standard regenerated cellulose (RC) membranes (MWCO-50 and 10 kDa) were purchased from Spectrum, Inc., USA. NMR spectra (^{1}H, ^{13}C, and ^{13}C inverse-gated (IG)) were recorded on a Bruker Avance 300 and 400 MHz NMR spectroameters. Degree of branching of polymers was measured in deuterated water (D_2O) with a relaxation delay of 6 s, and it, and it was calculated as per the reported procedure from the equation, $DB = 2D/(2D + L)$, where D and L represent the intensities of the signals corresponding to the dendritic and linear units respectively).[12,13] The absolute molecular weights of the polymers were determined by gel permeation chromatography (GPC) on a Waters 2695 separation module fitted with a DAWN HELEOS II multi angle laser light scattering detector coupled with Optilab T-rEX refractive index detector, both from Wyatt Technology, Inc., Santa Barbara, CA. GPC analysis was performed using Waters ultrahydrogel columns (guard, linear and 120) and 0.1 N $NaNO_3$ buffer (pH = 7.0) was used a mobile phase, and dn/dc value for mega HPG used was 0.12 mL/g. The dn/dc values of the mega HPGs were determined independently; there was no molecular weight dependence. The hydrodynamic radii (R_h) of the polymers were obtained by quasi elastic light scattering (QELS) detector using a Wyatt Internal QELS instrument (angle of measurement, 99.9°, laser λ = 620 nm). The intrinsic viscosity measurements were performed on viscometer-II from Wyatt technologies in which 0.1 N $NaNO_3$ buffer (pH = 7.0) was used a mobile phase. Hydration of the polymers was determined using differential scanning calorimetry (DSC) (TA instruments, New Castle, DE, USA.[14] Cryo-scanning electron microscopes (SEM) size measurements were made on the FEI (Field Electron and

Ion Company) Helios NanoLab 650 SEM with a focused ion beam (SEM-FIB) facility at 4D LABS, Simon Fraser University, Burnaby, Canada. Tc28a2 juvenile chondrocytes were purchased from EMD Millipore. MTT cell proliferation assay was purchased from ATCC. Absorbance readings for cell viability studies were measured at 570 nm on a SpectraMax 190 microplate reader from Molecular Devices.

5.3.2 Synthesis of high molecular weight HPG macro-initiator[15]

Trimethylolpropane (TMP) (120 mg, 0.894 mmol) was added to a flame dried three neck flask and dried under melting conditions (60 °C) and vacuum for 5 h. The dried TMP was partially deprotonated (33% of the total OH groups of TMP) with potassium methylate (25% MeOH, 70 μL, 0.237 mmol) under argon, and stirred for 30 min at room temperature. Methanol was evaporated at 70 °C for 4 h under vacuum. The flask was connected to an overhead stirrer and dry dioxane (24 mL) was added followed by slow addition of glycidol (12 mL, flow rate of 0.5 mL/hr) with a syringe pump under argon. After the addition of glycidol, the reaction mixture was stirred (rpm-150) for an additional 5 h. The reaction mixture was quenched with 0.5 mL of methanol after cooling it to RT. After decanting the supernatant (dioxane), the polymer was dissolved in 60 mL of methanol and precipitated from acetone (240 mL). The precipitation process was repeated twice (Caution: Make sure that a homogenous solution of the polymer in methanol was obtained before proceeding to precipitation with acetone. If it is taking long time for the dissolution of macro-initiator in methanol, the volume of methanol can be increased, however, same ratio of methanol and acetone should be maintained). The precipitated polymer was dissolved in deionized water (100 mL), neutralized by adding a few drops of 0.1 M HCl and further purified by dialysis

against water in a cellulose membrane (MWCO-10 kDa) for 2 days (with water replacement every 4-5 h). The polymer was freeze-dried and characterized by NMR (^{1}H and ^{13}C NMR; **Figure 5.1**) and GPC-MALS analyses (conversion of monomer-100%, yield-70%; M_w-840 kDa, Đ-1.2, **Figure 5.1**).

5.3.3 Synthesis of mega HPG-1

All the mega HPGs were synthesized by a modified macro-initiator approach.[16] The HPG macroinitiator (M_w-840 kDa, Đ-1.2) (2.5 g, 0.034 mols of OH groups) was dissolved in MeOH (5.0 mL) in a flame dried three neck flask and a polymer film was made on the walls of the flask by slowly evaporating the solution under vacuum. The flask containing the polymer film was further dried under vacuum at 100 °C for overnight to completely remove traces water and methanol. Thermogravimetric analysis was used to make sure that the polymer film was completely dried. The dried polymer was dissolved in dry DMF (35 mL) under Ar and KH suspension in oil (30 %) (80 mg, 270 µL, 1 eq) was added. The flask was heated to 95 °C and stirred for 50 min to ensure that all the polymer was completely dissolved and turned into a yellow-colored solution. The reaction flask was connected to an overhead stirrer under argon and the stirring speed was set at 150 rpm. To this homogenous solution, dried glycidol (8 mL) was added slowly (0.5 mL/h). After completion of glycidol addition, reaction was continued for 10 more hours, then cooled it to RT. The solution was turned into a clear pale red colored solution. The conversion of the monomer was almost 100%, confirmed by ^{1}H NMR spectroscopy. The polymer was dissolved in methanol (70-100 mL, make sure that no precipitate was found on the bottom of the flask) and precipitated in acetone (500 mL). The precipitation process was repeated

two more times to remove the small molecular weight fractions. The obtained precipitate was dissolved in water (100 mL), neutralized (pH-7) by dropwise addition of 0.1 M HCl and was further purified by dialysis (regenerated cellulose dialysis membrane, MWCO-50,000 Da) against water for 5 days (water replacements every 8 h). The polymer was stored as aqueous solution at 4 °C (yield-80 %). The experiment was repeated at least three times to determine the reproducibility (yield-81±3.6%). The polymer was characterized by NMR, GPC-MALS, viscosity measurements, and quasielastic light scattering measurements (Table 5.1 and 5.2). Caution: For the deprotonation of macroinitiator, the base, KH (in oil), is highly recommended. The KH solution should be homogenous before adding to the macroinitiator solution. Considering the pKa of the reagents involved in this deprotonation process, usage of either base KOMe or KH would be appropriate. However, if KOMe (25% in methanol) is used, the trace amounts of methanol can influence the polymer growth process resulting a bimodal distribution of HPG formed.

5.3.4 Synthesis of mega HPG-2

The HPG macroinitiator (M_w-840 kDa, Đ-1.2) (2.5 g, 0.034 mols of OH groups) was dissolved in MeOH (5.0 mL) in a flame dried three neck flask and a polymer film was made on the walls of the flask by slowly evaporating the solution under vacuum. The flask containing the polymer film was further dried under vacuum at 95 °C for 24 h to completely remove the traces water and methanol. Thermogravimetric analysis was used to make sure that the polymer film was completely dried. The dried polymer was dissolved in dry DMF (35 mL) under Ar and KH (30% suspension in oil, 80 mg, 270 µL) was added. The flask was heated to 95 °C and stirred for 60 min to ensure that all the polymer was completely

dissolved. The reaction flask was connected to an overhead stirrer under argon and the stirring speed was set up at 150 rpm. The solution color was turned to yellow. To this homogenous solution, dried glycidol (24 mL) was added slowly (1.4 mL/h). After completion of glycidol addition, reaction was continued for 10 more hours, then cooled to RT. The color of the solution was turned into pale red. The conversion of the monomer was almost 100% confirmed by ^{1}H NMR spectroscopy. Methanol (100 mL) was added to dissolve the polymer. A small amount of the precipitate was not soluble. 10 mL of DMF was added to completely to dissolve the polymer (make sure that no precipitate was found on the bottom of the flask). The polymer was precipitated from acetone (500 mL). The precipitation process was repeated two more times to remove the small molecular weight fractions. The obtained polymer was dissolved in water (100 mL), neutralized by dropwise addition of 0.1M HCl and was further purified by dialysis (regenerated cellulose dialysis membrane, MWCO-50,000 Da) against water for 5 days (water replacements every 8 h). The polymer was stored as aqueous solution at 4 °C (yield-85 %). The experiment was repeated at least three times to determine the reproducibility (yield-78 ± 6.5%). The polymer was characterized by NMR, GPC-MALS, solubility, viscosity measurements, and quasi elastic light scattering measurements (**Table 5.1, 5.2, 5.3**).

5.3.5 Synthesis of mega HPG-3

The HPG macroinitiator (M_w-840 kDa, Đ-1.2) (2.5 g, 0.034 mols of OH groups) was dissolved in MeOH (5.0 mL) in a flame dried three neck flask and a polymer film was made on the walls of the flask by slowly evaporating the solution under vacuum. The flask containing the polymer film was further dried under vacuum at 95 °C for 24 h to completely

remove the traces of water and methanol. Thermogravimetric analysis was used to make sure that the polymer film was completely dried. The dried polymer was dissolved in dry DMF (35 mL) under Ar and KH suspension in oil (30 %) (~80 mg, 270 µL) was added. The flask was heated to 95 °C and stirred for 30 min to ensure that all the polymer was completely dissolved. The reaction flask was connected to an overhead stirrer under argon and the stirring speed was set up at 200 rpm. To this homogenous solution, dried glycidol (50 mL) was added slowly (1.4 mL/h). After completion of glycidol addition, reaction was continued for 10 more hours, then cooled it to RT. The conversion of the monomer was almost 100% confirmed by ^{1}H NMR spectroscopy. Methanol (100 mL) was added to dissolve the polymer. A small amount of the precipitate was not soluble. 10-20 mL of DMF was added to completely to dissolve the polymer (make sure that no precipitate was found on the bottom of the flask). The polymer was precipitated from acetone (500 mL). The precipitation process was repeated two more times, dissolved in water (100 mL), neutralized (pH-7) by dropwise addition of 0.1M HCl and was further purified by dialysis (regenerated cellulose dialysis membrane, MWCO-50,000 Da) against water for 5 days (water replacements every 8 h). The polymer was stored as aqueous solution at 4 °C (yield-74 %). The experiment was repeated at least three times to determine the reproducibility of the synthesis of mega-HPG-3 (yield-74 ± 0.21%). The polymer was characterized by NMR, GPC-MALS, solubility, viscosity measurements, and quasi elastic light scattering measurements (**Table 5.1** and **5.2**).

5.3.6 Solubility measurements

The solubility of mega HPGs in water was measured and compared with other linear polymers (polyethylene oxide, polyvinyl alcohol purchased from Sigma-Aldrich, ON). The mega HPGs were initially dissolved in water (100 mg in 1 mL) using vortex mixing. Additional amount of mega HPGs were added until the solution reached saturation (Table 5.2). The solution was equilibrated overnight to measure consistency. The similar protocol was repeated for the other linear polymers until the solution become a stable gel.

5.3.7 Determination of hydration of mega HPG

Hydration of the polymers was determined using differential scanning calorimetry (DSC).[17] The mega-HPG solution was prepared in water (10% W/W). 20 μL of the solution was loaded into a Tzero aluminum hermetic sample pan and closed with appropriate lids. The sample pan was cooled down to −20 °C and warmed to −5 °C at the rate of 2 °C/min. Heating of the sample was further continued from −5 °C to +5 °C at the rate of 0.2 °C/min and to +20 °C at the rate of 2 °C/min. The enthalpy of fusion of polymer solution or pure water was determined by integrating the area under the respective peak on DSC trace (**Table 5.3**). An empty pan was used as a reference. The number of water molecules bound per polymer was calculated using the following equation.

$$[\mathbf{N_{bw}}] = [\Delta\mathbf{H_{fo}}\,(\mathbf{Wt_w} - \mathbf{Wt}_p) - \Delta\mathbf{H_{fps}} \times \mathbf{Wt_{ps}}] \,/\, [\Delta\mathbf{H_{fo}} \times \mathbf{MW_{H2O}} \times \mathbf{Np}]$$

N_{bw} = number of water molecules bound per polymer

ΔH_{fps}, ΔH_{fo} = fusion enthalpy of polymer solution and pure water respectively

Wt_w, Wt_p, Wt_{ps} = weight of the pure water, pure polymer alone and polymer solution respectively,

Np = number of moles of polymer taken.

5.3.8 Cryo-scanning electron microscopy (cryo-SEM) measurements

The morphology of the mega HPGs were visualized using cryo-SEM assembled with a focused ion beam SEM-FIB equipped with Quorum PP3010T cryo sample preparation system. A small volume of sample (10 µL) solution was loaded onto the sample carrier and immersed in slush liquid nitrogen for rapid freezing. The carrier with the frozen solution pellet is quickly vacuum transferred to the sample preparation stage cooled at -140 °C for fracturing the pellet. The fractured pellet was further transferred to the SEM stage cooled also at -140 °C for imaging the fractured surface, with an electron beam of 1 keV and 13 pA. The optimal concentration of the mega HPGs in Millipore water was 0.1 mg/mL. The average size of the mega HPGs were calculated from the 10 images with approximately 500 particles.

5.3.9 Cell viability measurements

Cell viability was assessed in Tc28a2 juvenile human chondrocytes and 3T3 murine fibroblast cells using the (3-(4,5-dimethylthiazol-2-yl)-2,5-diphenyltetrazolium bromide) tetrazolium reduction (MTT) assay as per previously reported protocol.[10] Cells were seeded at 10,000 cells/well and allowed to settle and adhere for 24 hours before addition of mega HPG or control samples. Mega HPG samples (10 µL) were prepared in regular growth media (DMEM) for (90 µL) to obtain a final polymer concentration of 1.25 mg/mL. Cells were incubated with the mega HPG samples for 48 h at 37 ºC. Wells containing 50% DMSO was used as a positive control. Wells containing saline and media in similar

volumes to the polymer samples were used as normal controls. After incubation, cells were washed with PBS 3 times followed by the addition of 100 µL of fresh media and 10 µL of 12 mM MTT reagent (from ATCC). After 4 h, 100 µL of sodium dodecyl sulphate (SDS)-HCl was added to solubilize the generated formazan. After solubilization for 2–24 hours, absorbance at 570 nm was read on a SpectraMax 190 microplate reader (Molecular Devices) and compared to saline controls. Three technical replicates were conducted per sample, and each study was independently repeated in triplicate. Average values and standard deviation are reported.

5.3.10 Lubrication measurements

Viscosity measurements were performed on a TA Instrument AR2000 rheometer using a 2° aluminum cone and a 47 µm gap at 25°C. Viscosity was then averaged across shear rates from 10 to 100 s^{-1}. Stribeck curves were constructed on a DHR-2 rheometer (TA instruments) with a stainless-steel ring on plate tribology geometry attachment. 300 µL of each lubricant were applied to the stainless-steel surface and a 5N load was applied, radial velocity increased from 0.001 rad/s to 50 rad/s while the load was held constant. This test was replicated three times for each lubricant, using fresh lubricant for all measurements. Average COF values and Hersey numbers, along with standard deviation were used to construct Stribeck curves for all formulations of mega HPG along with Synvisc One and BSF as controls. The values of 7 and 23% for mega HPGs were chosen as to ensure a 3X difference in amounts to better observe potential differences. Cartilage on cartilage coefficient of friction measurements, using 7 mm diameter bovine osteochondral plugs, were performed on a Bose Electro force 3200. Cartilage plugs were

cored from skeletally mature bovine knees using a diamond tipped drill bit. Plugs were incubated in 0.5 mL of lubricant at room temperature overnight prior to testing. An 8 N (200 kPa) creep load was applied to paired osteochondral plugs. After 3 hours of compression to equilibrate the tissue in creep, equilibrium friction measurement was made. Friction measurements used an angular velocity of 360°/s (effective velocity = 14.7 mm/s) for 120 seconds. Coefficient of friction (μ) was calculated from $\mu = (3/2) \cdot (\tau/Nr)$, where: τ = torque, N = load, r = plug radius.[17] Sampling frequency was 10 Hz.

5.3.11 AFM measurements

Atomic force microscopy (AFM) was performed using an MFP-3D microscope (Asylum Research; Santa Barbara, CA). The contact mode was applied using a silicon nitride tip with a nominal spring constant of 40 pN/nm. mega HPG-3 was chemically adhered to the surface of epoxide functionalized glass slides. 5 mg of mega HPG-3 was diluted in 50 mL of dimethylformamide. Stoichiometric amount of sodium hydride was then added. Ten microliters of this solution at concentration of (0.1 mg/mL) was dropped on the surface of the epoxide glass slide and kept at 60 °C overnight. The glass surface was rehydrated in PBS just before experimentation. The tip was slowly lowered to the surface to confirm contact without damage. Tip calibration was done on the bare glass surface, which acts as an infinitely hard surface, to set both a baseline deflection and virtual deflection correction. This determines the cantilever's inverse optical lever sensitivity (InvOLS; unit: m/V). The spring constant was verified via thermal tuning and was always within the range dictated by Bruker (within 30 pN/nm). After calibration, an area scan was performed in tapping mode prior to indentation to confirm the presence and density of the

polymer. Clumps of polymer were chosen for indentation based on shape and size. Force spectroscopy was then obtained over a 2 μm extension length and a 1000 nm/s approaching and retreating velocity. The tip was triggered at a set-point of 0.75 V of deflection. Once an indentation was performed, the raw distance of the tip along the z-direction was converted into an indentation depth using the InvOLS.

5.4 Results

5.4.1 Synthesis and structural characterization of mega HPGs

To overcome the challenges and prepare a large globular polymer, we used a homogenous polymerization method along with a macroinitiator to obtain ultra large dendritic polymers possessing a globular shape. As our interests lie in the polymers of potential use for environmentally responsible high-performance and biomedical applications, the selection of building blocks that are degradable, green, biocompatible, or natural metabolites is an additional key design criterion.[18,19] Polymers possessing a glycerol backbone are of significant interest for biomedical and environmental-green applications due to their chemical tuneability, degradability, and biocompatibility.[20-27] We synthesized the mega HPGs, in the million Dalton range (up to 10 million Dalton), *via* ring opening multibranching polymerization (ROMBP) in a single pot using a combined macro-initiator as and solvent based solution polymerization approach (**Figure 5.2**).[16] Specifically, we used the partially deprotonated (10%) high molecular weight HPG (KH in DMF, M_w - 840 kDa, Đ - 1.2) as the macroinitiator (**Figure 5.1**). The high solubility of the deprotonated macroinitiator in the polymerization medium, dry conditions and the use of KH as deprotonating base are critical to afford uniform polymer growth from the

macroinitiator. The slow addition of the monomer glycidol at 95 °C produced predetermined molecular weights of mega HPGs in a controlled manner in good yields (Fig. 5a, Table 5.1). We synthesized three different molecular weight mega HPGs (mega HPG-1 (M_w - 1.3 MDa, Đ - 1.2), mega HPG-2 (M_w - 2.9 MDa, Đ - 1.2), and mega HPG-3 (M_w - 9.3 MDa, Đ - 1.4)) by changing the glycidol to macroinitiator ratio (Table 5.1). The mega HPGs exhibit a monomodal distribution as demonstrated using gel permeation chromatography with multi angle light scattering (GPC-MALS) (**Figure 5.2d**, **5.3, Table 5.1**). Homogeneous polymerization conditions in dry solvent and the maintenance of uniform stirring using an overhead stir are important determinants in synthesizing mega HPGs with low polydispersity in good yield (~74 to 85%). For example, the current protocol affords ~42 g of isolated mega HPG-3 in a single batch. We repeated all of the reactions at least twice and obtained similar results (for example, average M_w for mega HPG-3 from three different batches was 9.3 ± 0.03 MDa and the yield was 74 ± 0.21%). This is significant, considering the difficulty in synthesizing semidendritic/hyperbranched polymers of such high molecular weights in large quantities using anionic ring opening polymerization.

We further characterized the mega HPGs by nuclear magnetic resonance (NMR) analysis for structure and branching density (**Figure 5.2** and **Figure 5.4**). A representative NMR spectra of mega HPG-3 shows the characteristic peaks of the polyglycerol backbone (**Figure 5.2b** and **5.2c**).[28] The degree of branching of mega HPGs, determined by C Inverse gated NMR spectroscopy, is between 53 and 57%, and similar to HPGs reported previously (Fig. 5c, Table 5.1 and 5.2) prepared by the ROMBP method.[15, 19] The molecular weights

achieved are the highest reported for dendritic polymers and as such these polymers display

unique characteristics. For example, mega HPG-3 possesses >87000 hydroxyl groups per

polymer on average influencing properties and amenable to modification. The mega HPGs

are highly hydrated, as determined by differential scanning calorimetry; mega HPG-3

possesses ~389,300 bound water molecules per polymer (**Figure 5.5** and **Table 5.2**). As

suspected, the mega HPGs are highly water soluble (> 380 mg/mL) in contrast to similarly

sized linear polymers (e.g., polyethylene oxide, polyvinyl alcohol) which form gels at high

concentrations (**Table 5.3**).[29]

Mega HPGs are highly compact nanostructures as demonstrated by their

hydrodynamic diameters (determined by dynamic light scattering) which range from 21

nm for the 1.3 MDa to 43 nm for the 9.3 MDa polymer (**Table 5.1**). We further investigated

the size of mega HPGs using cryogenic scanning electron microscopy (cryo-SEM). A

representative cryo-SEM of mega HPG-3 shows the spherical and single particle nature of

the mega HPGs (**Figure 5.6**). The average size of the mega HPGs are 28, 34, and 51 nm

for mega HPG-1, 2, and 3, respectively, and slightly higher than the data obtained from

DLS likely due to the frozen hydrated shell of the mega HPG in the cryo-SEM preparations

(**Figure 5.6**). Importantly, individual mega HPGs are nanometer-scale singular polymer

particles and easily visualized. The low hydrodynamic sizes of mega HPGs confirms their

stability in water without aggregation,[30, 31] and the size does not scale with molecular

weight as with linear polymers[32] and low molecular weight HPG (**Figure 5.7a** and **Table

5.2**). The size of the mega HPGs lies between linear polymers (e.g., PEG) and dendrimers

(e.g., PAMAM) (**Figure 5.7a**). The data further indicate that mega HPGs are more compact

than linear polymers and less compact in comparison to dendrimers, and this might be advantageous in terms of offering more 'interior room' between branching units.

The mega HPGs possess exceptionally low intrinsic viscosity in comparison to other polymeric systems. The intrinsic viscosity, [η], of the mega HPGs does not change considerably with molecular weight (**Table 5.1**); this small change in intrinsic viscosity of mega HPGs also does not follow the Mark-Houwink-Sakurada equation and instead falls in line with the Einstein viscosity theory's prediction of almost minimal change in [η] with molecular weight for "hard" globular shaped polymers.[31] This result is in striking contrast to dendrimers (PAMAM, generation G1-G10), which show an unusual bell shape dependence of [η] with increasing molecular weight (Fig. 5.7b).[33] Published simulation and experimental studies validate that the PAMAM dendrimer has almost zero asphericity with increasing generation number (G1→9) which indicates substantial back folding of terminal groups into the interior core of the dendrimer structure.[34] This conformational change may be occurring with mega HPGs to some degree as evident from their nearly molecular weight independent intrinsic viscosity, however, additional studies are needed to confirm this notion. Interestingly, the intrinsic viscosities of the mega HPGs are slightly increased with molecular weight compared to their lower molecular counterparts; the increase in size of the mega HPGs might be attributing to this rise.[35] The intrinsic viscosity values of mega HPGs are significantly lower than linear water-soluble polymers of similar molecular weight (e.g., polyethylene oxide, hyaluronic acid, and dextran sulfate),[29, 36-39] and this observation further confirms the compact nature of the mega HPGs. For example, the mega HPG-3 (9.3 MDa) possesses an intrinsic viscosity of 6.15 mL/g which is similar to most of

the globular proteins in aqueous solutions,[40-42] whereas a linear PEG (M_w-11 MDa) has a value of 2600 mL/g.[32] Thus, mega HPGs show a unique combination of ultra-high molecular weight, compact size, and very low intrinsic viscosity almost independent of molecular weight.

5.4.2 Lubrication properties

To take advantage of the unique solution properties of mega HPGs (high solubility, compactness, and low intrinsic viscosity), we investigated the lubrication properties of mega HPGs on hard synthetic and soft natural surfaces. Considering the globular and single particle nature of the mega HPGs, we anticipated that the rheological properties of mega HPGs will be quite different from their linear counter parts. We first determined the performance and lubrication characteristics of mega HPGs on stainless steel by generating Stribeck curves. Stribeck curves describe the coefficient of friction (COF) of a system across different lubrication modes: boundary, mixed, and hydrodynamic lubrication. Generally, boundary lubrication exists under conditions of low speed, high load and is characterized by a high COF while conversely hydrodynamic lubrication occurs under conditions of high speed and low load and is characterized by a low COF. Using a DHR-2 Rheometer (TA Instruments), we applied a 5N load and held it constant, while the radial velocity increased from 0.001 rads[-1] to 50 rads[-1]. Stribeck curves for all six mega HPGs formulations along with three controls, Pennzoil 80W-90 motor oil, Synvisc One, and bovine synovial fluid, were constructed by plotting COF against the Hersey number (velocity*viscosity/load) (**Figure 5.8**). Synvisc One and bovine synovial fluid (BSF) were selected as controls based on their different compositions (a lightly crosslinked linear

polymer of hyaluronic acid of high viscosity versus a low viscous, natural lubricating solution) and relevance to the soft natural surface next investigated. Pennzoil was chosen in order to verify our method of Stribeck curve construction.[43] Additionally, Synvisc One and BSF lubricate via different mechanisms, BSF aids in mixed mode lubrication within joints, while Synvisc One is a fluid lubricant. The mega HPGs-1, -2, and -3, at both 7 and 23 w/v%, possess viscosities on the order of BSF and display boundary mode lubrication. The higher weight percent mega HPGs exhibit boundary mode lubrication at a consistently higher velocity with a molecular weight and concentration dependence. At 23 w/v%, the mega HPGs transition into mixed mode lubrication from boundary mode at increasing Hersey number with increasing molecular weight and with COFs equal to but speeds greater than BSF, despite their similarities in viscosities to BSF (**Figure 5.8a** and **5.8b**). Consequently, mega HPGs demonstrate Stribeck curves similar to the hyaluronic acid solution, Synvisc, except that the mega HPGs are 100X less viscous.

For the natural soft surface, we selected articular cartilage for evaluation of the mega HPGs as lubrication of this surface is key for bodily movement, protection from wear, and prevention of osteoarthritis.[10, 44-48] Previously, linear[10, 49] and brush polymers[44, 50,51] have been explored for lubricating cartilage as these materials present controlled electrostatic interactions and hydration. Additionally with the brush structures, the tilting and/or the physical thinning of the polymer chains improves the lubricant properties.[52,53] Cartilage is a hydrated porous elasto-hydrodynamic material,[12,13] where upon initial loading interstitial aqueous fluid supports most of the applied load by creating an interposed lubricating layer between the articulating surfaces. At creep equilibrium, most

of the interstitial fluid has extruded, the deformed cartilage is softer and weeping lubrication is depleted. We conducted mechanical friction tests (BOSE Electroforce 3200) on harvested mated bovine osteochondral plug pairs (7 mm diameter, N = 6 pairs) in unconfined geometry (**Figure 5.9**).[10] After incubating the samples in the test groups (saline, healthy bovine synovial fluid, human osteoarthritic synovial fluid, and 1, 3, and 9 MDa mega HPGs at 7 and 23 w/v%), the opposing cartilage surfaces were pressed against each other (200 kPa creep load) for three hours while submerged in the test solutions. Then, while under load, rotation was applied for 120s at an angular speed of 360°/s and the equilibrium COF was determined.

All of the mega HPGs lubricate the cartilage surface. The COF values for the mega HPGs are statistically equivalent to healthy bovine synovial fluid (positive control) and, importantly, significantly lower than the COF value obtained with human osteoarthritic synovial fluid (Fig. 4, p<0.0001, one-way ANOVA). Between the different molecular weights of the mega HPGs, the 9 MDa mega HPG-3 exhibits a slightly lower COF, albeit not statistically significant. The performance of the mega HPG-3 is more consistent than the smaller mega HPG-1 and -2 lubricants as evident by the lower standard deviation bars. With regards to the relative COF performance of the 9 MDa mega HPG-3 to other lubricants, it is challenging to compare as the extracted absolute values depends on the measurement geometry and protocol, as well as tissue type. Given the above caveats, the COF values of the mega HPGs are roughly an order of magnitude lower than the values reported for some bottle-brush copolymer lubricants between cartilage and glass surfaces[51,54] while on par with linear polyelectrolyte polymers between cartilage and

cartilage surfaces.[55] (Comparative study results presented in **Table 5.4**). Analysis of the flow data reveals only the solution of mega HPG-1 (1 MDa) at 23% shear thins mimicking that of Synvisc, although with a smaller change in viscosity as a function of shear rate (**Figure 5.10**). We surmise that the mega HPG-2 and 3 (3 and 9 MDa polymers) are denser than the mega HPG-1. The hydrodynamic diameter of the mega HPG-3, for example, is only twice the size of the mega HPG-1 polymer, and therefore is less likely to entangle with itself. The mega HPG-1 extends into solution, shear thins, and is a non- Newtonian fluid. The mega HPG-3 maintains a constant viscosity across shear rate and acts as a Newtonian fluid. A Newtonian fluid lubricant is advantageous over a non-Newtonian one because the viscosity of the non-Newtonian lubricant reduces as a function of shear, displacing it from the surface and increasing the contact area between the surfaces. The mega HPGs exhibit viscosities similar to natural healthy synovial fluid, which are markedly lower than Synvisc (1226 mPas). Practically, this is advantageous as an 18G needle is used to intra-articularly administer Synvisc while mega HPGs easily flow through a 25 G needle. Finally, the cell compatibility of the mega HPGs against human chondrocytes and fibroblasts was evaluated at 48 hours. The different molecular weight mega HPGs show close to 80% cell viability demonstrating high cytocompatibility of these ultra-high molecular weight dendritic polymers with results similar to the saline control (**Figure 5.11**).

The mega HPGs acted as additive for enhanced liquid lubrication and join a class of tribological altering nanomaterials applied in lubrication engineering. The mechanism of anti-wear and friction reduction of these nano-lubricants include mending effect,

colloidal effect, protective film, and third body material transfer.[56,57] The mega HPGs are 20-40 nm in diameter and in the size range of most metal nanoparticle additives, albeit they are softer materials and more compressible with a Young's Modulus of 7.9 kPa determined by atomic force microscopy measurements (**Figure 5.12**).[57] No correlation is seen between COF and viscosity values suggesting that mega HPGs lubricate via a different mechanism than the extremely viscous Synvisc One. We propose that the mega HPGs, specifically the 3 and 9 MDa Newtonian fluid lubricants, function as interposed molecular ball-bearings in water to reduce the COF between the stainless-steel surfaces. We hypothesize a few modes of lubrication may be in effect during lubrication of cartilage with mega HPGs, particularly hydration shell lubrication described by Klein *et al.,*[58-60] where our highly hydrated, water dense structures of the mega HPGs maintain a molecular water film at the cartilage surface, supporting heavy loads without being squeezed out while simultaneously rapidly relaxing.[61] Additionally, we suspect the 9 MDa mega HPG-3 is better retained on the tissue surface and does not get washed off, providing constant and lower COF compared to PBS, or other lubricants. This proposal is supported by experiments that show no shear thinning with the mega HPG-3 as it is a Newtonian lubricant and follows the scenario in which Greene suggests[62] that a mechanical trapping mechanism maintains a layer of immobilized HA between surfaces. This is similar to the 'ultra-filtration' hypothesis from Walker *et al.,*[63] where water preferentially flows into the articular surface through the ~10 nm bovine cartilage pores,[64] leaving larger molecules, such as the 20 – 40 nm diameter mega HPGs to aggregate at the leading edge of contact. How these proposed mechanisms relate to the mode of lubrication on cartilage — boundary, mixed, or hydrodynamic — requires further

investigation.

In summary, we report the synthesis of ultra large dendritic polymers in the million Dalton range with high degrees of branching. The polymers are single molecule nanoscale objects with unique properties. The synthetic route affords control over the molecular weight and provides grams of material for study. The high-water solubility, low intrinsic viscosity, compactness, nearly molecular weight independent intrinsic viscosity, hydration and cell compatibility are important characteristics justifying investigation of these new polymers. The mega HPGs, we propose, are new nanoparticulate lubricants acting as interposed ball-bearings to reduce the COF between both hard and soft surfaces and demonstrate rheological properties similar to a fluid lubricant. This unexpected result arises from the unique size and structure of the polymers. Size, structure, and composition dictate function and this is highlighted in the largest known protein, titin, at 3.7 MDa which exhibits elastic properties and functions in muscle contraction.[65] Advances in synthetic polymer chemistry are providing routes to unique polymers and polymer architectures of unprecedented size and properties. These advances will propel our capability to prepare large single entity molecular structures as well as to conceive of self-assembled higher order complexes and to study the interactions of these materials with synthetic and natural substrates.

5.5 References

1. Lee, C. C., Mackay, J. A. & Szoka, F. Designing Dendrimers for Biological Applications. Nature Biotechnology. 23, 1517–1526 (2005).

2. Grayson, S. M. & Fréchet, J. M. J. Convergent Dendrons and Dendrimers: from Synthesis to Applications. Chemistry Reviews 101, 3819–3868 (2001).

3.   Svenson, S. & Tomalia, D. A. Dendrimers in Biomedical Applications—Reflections on the Field. Advanced Drug Delivery Reviews 64, 102–115 (2012).

4.   Bosman, A. W., Janssen, H. M. & Meijer, E. W. About Dendrimers: Structure, Physical Properties, and Applications. Chemical Reviews 99, 1665–1688 (1999).

5.   Fréchet, J. M. J. Dendrimers and Supramolecular Chemistry. Proceedings of the National Academy of Sciences of the United States of America 99, 4782–4787 (2002).

6.   Hawker, C. J., Farrington, P. J., Mackay, M. E., Wooley, K. L. & Frechet, J. M. J. Molecular Ball Bearings: The Unusual Melt Viscosity Behavior of Dendritic Macromolecules. Journal of the American Chemical Society 117, 4409–4410 (1995).

7.   Kamigaito, M. & Satoh, K. Light Leads to Ultra-Long Polymer Chains in Water. Chemistry 2, 13–15 (2017).

8.   Arita, T., Kayama, Y., Ohno, K., Tsujii, Y. & Fukuda, T. High-pressure Atom Transfer Radical Polymerization of Methyl Methacrylate for Well-Defined Ultrahigh Molecular-Weight Polymers. Polymer (Guildf). 49, 2426–2429 (2008).

9.   Truong, N. P., Dussert, M. V., Whittaker, M. R., Quinn, J. F. & Davis, T. P. Rapid Synthesis of Ultrahigh Molecular Weight and Low Polydispersity Polystyrene Diblock Copolymers by Raft-Mediated Emulsion Polymerization. Polymer Chemistry 6, 3865–3874 (2015).

10. Wathier, M. et al. A Large-Molecular-Weight Polyanion, Synthesized via Ring-Opening Metathesis Polymerization, as a Lubricant for Human Articular Cartilage. Journal of the American Chemical Society 135, 4930–4933 (2013).

11. Bai, Y., He, J. & Zhang, Y. Ultra-High-Molecular-Weight Polymers Produced by the Immortal Phosphine-Based Catalyst System. Angewandte Chemie. 57, 17230–17234 (2018).

12. Kawaguchi, S. *et al.* Aqueous Solution Properties of Oligo- and Poly(Ethylene Oxide) by Static Light Scattering and Intrinsic Viscosity. *Polymer (Guildf).* **38**, 2885–2891 (1997).

13. Kainthan, R. K., Muliawan, E. B., Hatzikiriakos, S. G. & Brooks, D. E. Synthesis, Characterization, and Viscoelastic Properties of High Molecular Weight Hyperbranched Polyglycerols. *Macromolecules* **39**, 7708–7717 (2006).

14. Alizadeh Noghani, M. & Brooks, D. E. Progesterone Binding Nano-Carriers Based on Hydrophobically Modified Hyperbranched Polyglycerols. *Nanoscale* **8**, 5189–5199 (2016).

15. Imran ul-haq, M., Shenoi, R. A., Brooks, D. E. & Kizhakkedathu, J. N. Solvent-Assisted Anionic Ring Opening Polymerization of Glycidol: Toward Medium and High Molecular Weight Hyperbranched Polyglycerols. *Journal of Polym. Science Part A Polymer Chemistry* **51**, 2614–2621 (2013).

16. Wilms, D. *et al.* Hyperbranched Polyglycerols with Elevated Molecular Weights: A Facile Two-Step Synthesis Protocol Based on Polyglycerol Macroinitiators. *Macromolecules* **42**, 3230–3236 (2009).

17. Schmidt, T. A. & Sah, R. L. Effect of Synovial Fluid on Boundary Lubrication of Articular Cartilage. *Osteoarthritis and Cartilage* **15**, 35–47 (2007).

18. Ricapito, N. G., Ghobril, C., Zhang, H., Grinstaff, M. W. & Putnam, D. Synthetic Biomaterials from Metabolically Derived Synthons. *Chemical Reviews* **116**, 2664–2704 (2016).

19. Grinstaff, M. W. Biodendrimers: New Polymeric Biomaterials for Tissue Engineering. *Chemistry—A European Journal* **8**, 2838 (2002).

20. Zhang, H. & Grinstaff, M. W. Synthesis of Atactic and Isotactic Poly(1,2-glycerol carbonate)s: Degradable Polymers for Biomedical and Pharmaceutical Applications. *Journal of the American Chemical Society* **135**, 6806–6809 (2013).

21. Imran ul-haq, M., Lai, B. F. L., Chapanian, R. & Kizhakkedathu, J. N. Influence of Architecture of High Molecular Weight Linear and Branched Polyglycerols on their Biocompatibility and Biodistribution. *Biomaterials* **33**, 9135–9147 (2012).

22. Zhang, H., Lin, X., Chin, S. & Grinstaff, M. W. Synthesis and Characterization of Poly(glyceric Acid Carbonate): A Degradable Analogue of Poly(acrylic Acid). *Journal of the American Chemical Society* **137**, 12660–12666 (2015).

23. Shenoi, R. A. *et al.* Affinity-Based Design of a Synthetic Universal Reversal Agent for Heparin Anticoagulants. *Science Translational Medicine* **6**, 260ra150 (2014).

24. Ray, W. C. & Grinstaff, M. W. Polycarbonate and Poly(carbonate−ester)s Synthesized from Biocompatible Building Blocks of Glycerol and Lactic Acid. *Macromolecules* **36**, 3557–3562 (2003).

25. Abbina, S. *et al.* Hyperbranched Polyglycerols: Recent Advances in Synthesis, Biocompatibility and Biomedical Applications. *Journal of Materials Chemistry B* **5**, 9249–9277 (2017).

26. Zhang, H. & Grinstaff, M. W. Recent Advances in Glycerol Polymers: Chemistry and Biomedical Applications. *Macromolecular Rapid Communications* **35**, 1906–1924 (2014).

27. Beharaj, A., Ekladious, I. & Grinstaff, M. W. Poly(Alkyl Glycidate Carbonate)s as Degradable Pressure-Sensitive Adhesives. *Angewandte Chemie* **58**, 1407–1411 (2019).

28. Sunder, A., Hanselmann, R., Frey, H. & Mülhaupt, R. Controlled Synthesis of Hyperbranched Polyglycerols by Ring-Opening Multibranching Polymerization. *Macromolecules* **32**, 4240–4246 (1999).

29. Liu, F. *et al.* Crystallization and Rheology of Poly(ethylene oxide) in Imidazolium Ionic Liquids. *Macromolecules* **49**, 6106–6115 (2016).

30. Li, J. *et al.* Visualization and Characterization of Poly(amidoamine) Dendrimers by Atomic Force Microscopy. *Langmuir* **16**, 135613–5616 (2000).

31. Lim, J. *et al.* Synthesis of Large Dendrimers with the Dimensions of Small Viruses. *Journal of the American Chemical Society* **135**, 4660–4663 (2013).

32. Armstrong, J. K., Wenby, R. B., Meiselman, H. J. & Fisher, T. C. The Hydrodynamic Radii of Macromolecules and their Effect on Red Blood Cell Aggregation. *Biophysical Journal* **87**, 4259–70 (2004).

33. Stechemesser, S. & Eimer, W. Solvent-Dependent Swelling of Poly(amido amine) Starburst Dendrimers. *Macromolecules* **30**, 2204–2206 (1997).

34. Maiti, P. K., Cagin, T., Wang, G. & Goddard, W. A. Structure of PAMAM Dendrimers: Generations 1 through 11. *Macromolecules* **37**, 6236–6254 (2004).

35. Flory, P. J. Spatial Configuration of Macromolecular Chains. *Science* **188**, 1268–1276 (1975).

36. Pillai, C. K. S., Paul, W. & Sharma, C. P. Chitin and Chitosan Polymers: Chemistry, Solubility and Fiber Formation. *Progress in Polymer Science* **34**, 641–678 (2009).

37. Senti, F. R. *et al.* Viscosity, Sedimentation, and Light-Scattering Properties of Fraction of an Acid-Hydrolyzed Dextran. *Journal of Polymer Science* **17**, 527–546 (1955).

38. Vega, J. F., Rastogi, S., Peters, G. W. M. & Meijer, H. E. H. Rheology And Reptation of Linear Polymers. Ultrahigh Molecular Weight Chain Dynamics in the Melt. *Journal of Rheology* **48**, 663–678 (2004).

39. Shimada, E. & Matsumura, G. Viscosity and Molecular Weight of Hyaluronic Acids. *Journal of Biochemistry* **78**, 513–517 (1975).

40. Hess, E. & Cobure, A. The Intrinsic Viscosity of Mixed Protein Systems, Including Studies of Plasma and Serum. *The Journal of General Physiology* **33**, 511–523 (1950).

41. Curvale, R., Masuelli, M. & Padilla, A. P. Intrinsic Viscosity of Bovine Serum Albumin Conformers. *International Journal of Biological Macromolecules* **42**, 133–137 (2008).

42. Hahn, D. K. & Aragon, S. R. Intrinsic Viscosity of Proteins and Platonic Solids by Boundary Element Methods. *Journal of Chemical Theory and Computation* **2**, 1416–1428 (2006).

43. Kavehpour, H. P. & Mckinley, G. H. Tribo-Rheometry: From Gap-Dependent Rheology to Tribology. *Tribology Letters* **17**, 327–3335 (2004).

44. Sun, Z. *et al.* Boundary Mode Lubrication of Articular Cartilage with a Biomimetic Diblock Copolymer. *Proceedings of the National Academy of Sciences of the United States of America* **116**, 12437–12441 (2019).

45. Morgese, G., Cavalli, E., Rosenboom, J. G., Zenobi-Wong, M. & Benetti, E. M. Cyclic Polymer Grafts That Lubricate and Protect Damaged Cartilage. *Angewandte Chemie* **57**, 57(6):1621-1626 (2018).

46. Gagnier, J. J. Patient Reported Outcomes in Orthopaedics. *Journal of Orthopaedic Research* **35**, 2098–2108 (2017).

47. Elsaid, K. A., Machan, J. T., Waller, K., Fleming, B. C. & Jay, G. D. The Impact of Anterior Cruciate Ligament Injury on Lubricin Metabolism and the Effect of Inhibiting Tumor Necrosis Factor A on Chondroprotection in an Animal Model. *Arthritis and Rheumatology* **60**, 2997–3006 (2009).

48. Malcor, J.-D. *et al.* Coupling of A Specific Photoreactive Triple-Helical Peptide to Crosslinked Collagen Films Restores Binding and Activation of DDR2 And VWF. *Biomaterials* **182**, 21–34 (2018).

49. Wathier, M. *et al.* A Synthetic Polymeric Biolubricant Imparts Chondroprotection in a Rat Meniscal Tear Model. *Biomaterials* **182**, 13–20 (2018).

50. Banquy, X., Burdyńska, J., Lee, D. W., Matyjaszewski, K. & Israelachvili, J. Bioinspired Bottle-Brush Polymer Exhibits Low Friction and Amontons-like Behavior. *Journal of the American Chemical Society* **136**, 6199–6202 (2014).

51. Samaroo, K. J., Tan, M., Putnam, D. & Bonassar, L. J. Binding and Lubrication of Biomimetic Boundary Lubricants on Articular Cartilage. *Journal of Orthopaedic Research* **35**, 548–557 (2017).

52. Doyle, P. S., Shaqfeh, E. S. G. & Gast, A. P. Rheology of Polymer Brushes: A Brownian Dynamics Study. *Macromolecules* **311**, 5474–5486 (1998).

53. Müller, M. T., Yan, X., Lee, S., Scott S. Perry, A. & Nicholas D. Spencer. Lubrication Properties of a Brushlike Copolymer as a Function of the Amount of Solvent Absorbed within the Brush. *Macromolecules* **38**, 5706–5713 (2005).

54. Coles, J. M., Chang, D. P. & Zauscher, S. Molecular Mechanisms of Aqueous Boundary Lubrication by Mucinous Glycoproteins. *Current Opinion in Colloid & Interface Science* **15**, 406–416 (2010).

55. Lakin, B. A. *et al.* A Synthetic Bottle-Brush Polyelectrolyte Reduces Friction and Wear of Intact and Previously Worn Cartilage. *ACS Biomaterials Science and Engineering* **5**, 3060–3067 (2019).

56. Shahnazar, S., Bagheri, S., Abd Hamid, S. B. & Hamid, S. S. B. Enhancing Lubricant Properties by Nanoparticle Additives. *International Journal of Hydrogen Energy* **41**, 3153–3170 (2016).

57. M Hsu, S. Nano-Lubrication: Concept and Design. *Tribology International* **37**, 537–545 (2004).

58. Ma, L., Gaisinskaya-Kipnis, A., Kampf, N. & Klein, J. Origins of Hydration Lubrication. *Nature Communications* **6**, 6060 (2015).

59. Raviv, U. *et al.* Lubrication by Charged Polymers. *Nature* **425**, 163–165 (2003).

60. Briscoe, W. H. *et al.* Boundary Lubrication under Water. *Nature* **444**, 191–194 (2006).

61. Tavakoli Nia, H. *et al.* Aggrecan Nanoscale Solid–Fluid Interactions Are a Primary Determinant of Cartilage Dynamic Mechanical Properties. *ACS Nano* **9**, 2614–2625 (2015).

62. Greene, G. W. *et al.* Adaptive Mechanically Controlled Lubrication Mechanism Found in Articular Joints. *Proceedings of the National Academy of Sciences of the United States of America* **108**, 5255-5259 (2011).

63. Walker, P. S., Dowson, D., Longfield, M. D. & Wright, V. 'Boosted lubrication' in Synovial Joints by Fluid Entrapment and Enrichment. *Annals of the Rheumatic Diseases* **27**, 512–520 (1968).

64. Majda, D. *et al.* New Approach for Determining Cartilage Pore Size Distribution: NaCl-Thermoporometry. *Microporous Mesoporous Materials* **241**, 238–245 (2017).

65. Herzog, W. The Multiple Roles of Titin in Muscle Contraction and Force Production. *Biophysical Reviews* **10**, 1187–1199 (2018).

Table 5.1. Physical characteristics of mega HPGs. Absolute molecular weight (Mw) and distribution (Đ) of mega HPGs was confirmed size exclusion chromatography coupled with light scattering detector (MALS). Degree of branching (DOB- 53-57%) supports the semi dendritic nature of the polymers and it was determined by 13C IG NMR spectroscopy. Mega HPGs are compact in size and have low intrinsic viscosity [η], determined by quasi elastic light scattering (QELS) detector and viscometer-II detector respectively which are coupled to a gel permeation chromatography system.

Polymer	M_w (Da)	Đ	DOB	Size (nm)	$[\eta]$ (mL/g)
mega HPG-1	1.3×10^6	1.2	0.57	21.2 ± 0.4	4.67
mega HPG-2	2.9×10^6	1.2	0.54	30.6 ± 0.6	5.26
mega HPG-3	9.3×10^6	1.4	0.53	43.0 ± 0.4	6.15

Table 5.2. Hydrodynamic diameters, degree of branching, and hydration of the mega HPGs and comparison with low molecular weight analogues.

Polymer	M_w ($Đ$)	Degree of Branching[a]	Hydrodynamic diameter (nm)[b]	Hydration (number of water molecules per polymer)[c]
HPG-1	120 kDa (1.15)	0.56	9.20[3]	-
HPG-2	491 kDa (1.40)	0.57	12.60[4]	-
HPG-3	840 kDa (1.20)	0.56	20.4 ± 0.5	-
mega HPG-1	1300 kDa (1.20)	0.57	21.2 ± 0.4	68600
mega HPG-2	2900 kDa (1.20)	0.54	30.6 ± 0.6	125500
mega HPG-3	9300 kDa (1.40)	0.53	43.0 ± 0.4	389300

[a]Determined by quasi-elastic light scattering (QELS) analysis. [b]Measured by ^{13}C inverse gated NMR spectroscopy. [c]Determined by DSC.

Table 5.3. Comparison of solubility of mega HPGs with other linear synthetic polymers

Sample (*M*n)	Solubility (mg/mL)
mega HPG-2 (2.5 MDa)	380
PEO (8 MDa)	20
PEO (4 MDa)	25
PVA (0.205 MDa)	200

Table 5.4. COF for other biomimetic lubricants.

Lubricant	System specifics	COF
Lubricin	Bovine cartilage on glass; 40% compressive strain imposed on each plug to ensure boundary mode, and 60min allowed for hydrostatic pressure to equilibrate	0.093
Inflamed SF 24oC	Human cartilage on cartilage; 30N load, 1 mm/s speed	0.109 (static)/ 0.089 (dynamic)
Inflamed SF 37oC	Human cartilage on cartilage; 30N load, 1 mm/s speed	0.06 (static)/ 0.055 (dynamic)
Water	Human cartilage on cartilage; 30N load, 1 mm/s speed	0.059 (static)/ 0.05 (dynamic)
NaCl 15mM	Human cartilage on cartilage; 30N load, 1 mm/s speed	0.07 (static)/ 0.06 (dynamic)
NaCl 150mM	Human cartilage on cartilage; 30N load, 1 mm/s speed	0.089 (static)/ 0.067 (dynamic)
PBS	Early OA human cartilage on cartilage, 6.27 N load, 1 mm/s sliding speed, 900s test duration	0.134 +/- 0.034
PBS	Late OA human cartilage on cartilage, 6.27 N load, 1 mm/s sliding speed, 900s test duration	0.106 +/- 0.053
Human SF	Early OA human cartilage on cartilage, 6.27 N load, 1 mm/s sliding speed, 900s test duration	0.04 +/- 0.018
Human SF	Late OA human cartilage on cartilage, 6.27 N load, 1 mm/s sliding speed, 900s test duration	0.042 +/- 0.015
PBS	Early OA human cartilage on glass, 6.27 N load, 1 mm/s sliding speed, 3600s test duration	0.026 +/- 0.009
PBS	Late OA human cartilage on glass, 6.27 N load, 1 mm/s sliding speed, 3600s test duration	0.024 +/- 0.009
Human SF	Early OA human cartilage on glass, 6.27 N load, 1 mm/s sliding speed, 3600s test duration	0.02 +/- 0.07

Human SF	Late OA human cartilage on glass, 6.27 N load, 1 mm/s sliding speed, 3600s test duration	0.19 +/- 0.001
Poly-oxanorbornane carboxylate	Bovine cartilage on cartilage; torsional friction for 10,080 rotations at 22 mm/s, 0.78 MPa compressive strain	0.015 ± 0.01
Poly-oxanorbornane carboxylate containing pendent triethylene glycol chains	Bovine cartilage on cartilage; torsional friction for 10,080 rotations at 22 mm/s, 0.78 MPa compressive strain	0.0316 ± 0.0005
High-molecular-weight lubricious polymer with poly(2-methyl-2-oxazoline) side chains	Immature bovine cartilage mounted on a ball-on-disc microtribometer; 5 mm/s speed; 0.5, 0.7 and 0.9 MPa pressure for 10 minutes each	0.02 - 0.1
Lubricin mimetic - chondroitin sulfate backbone with type II collagen and HA binding peptides	Trypsin treated cartilage on glass with lubricin mimetic AND purified, commercially available HA; 0.0873 rad/sec sliding speed; 2 min test duration	0.1 - 0.3
pAA:PEG lubricant library with varying backbone lengths and ratios of the two polymers	Bovine cartilage on XX; 40% compressive strain imposed on each plug to ensure boundary mode, and 60min allowed for hydrostatic pressure to equilibrate	0.14 - 0.248
sodium poly(7-oxanorbornene-2-carboxylate)	Cartilage on cartilage equilibrated for 60 min and then subjected to a relative rotation of +2 revolutions (720°) at 5 deg/s (an effective velocity of 0.3 mm/ s)	0.06+-0.02
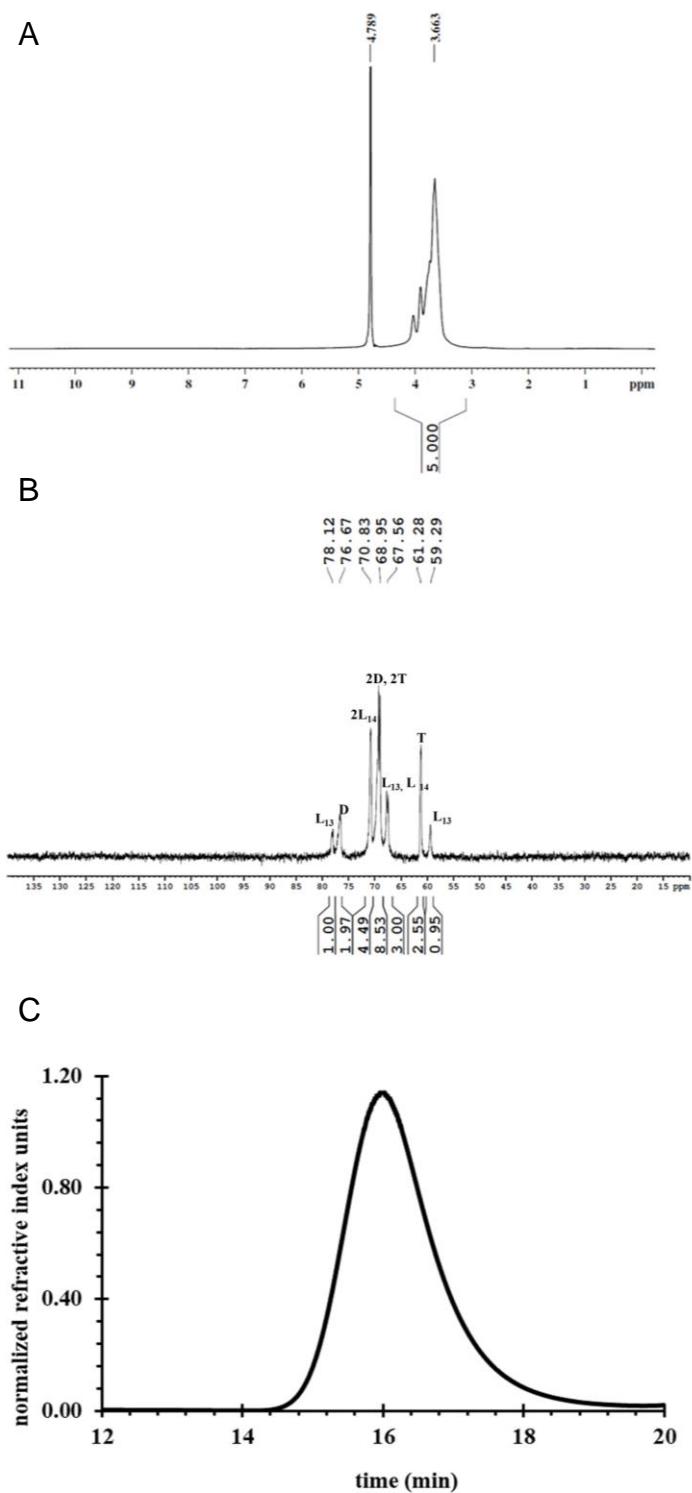
Figure 5.1. A) ^{1}H NMR spectrum (D$_2$O, 400 MHz) of the HPG macroinitiator. B) ^{13}C NMR spectrum (D$_2$O, 100 MHz) of the HPG macroinitiator. C) GPC-MALS chromatogram (0.1 M NaNO$_3$ buffer, pH 7.4) of the HPG macroinitiator.
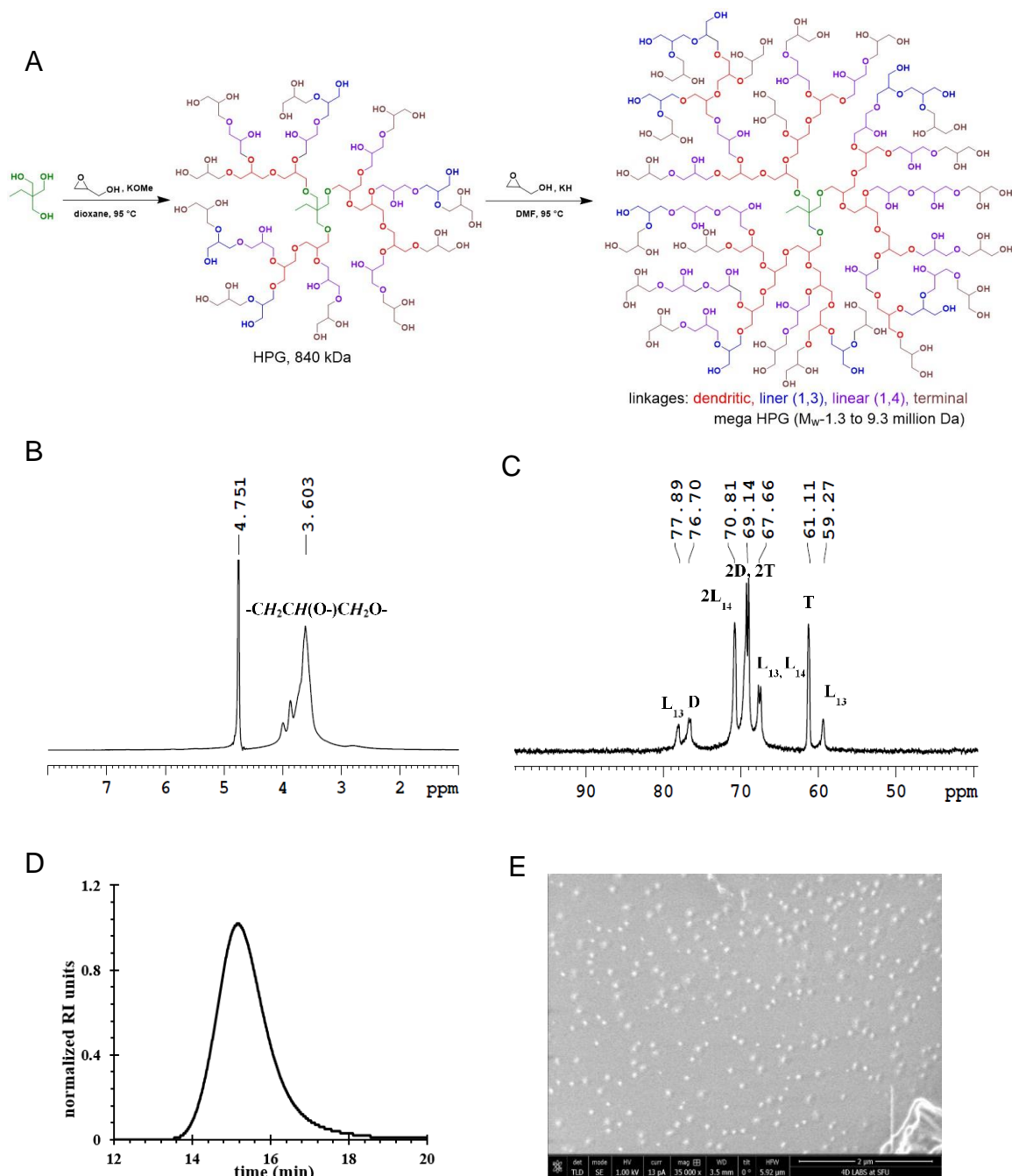
Figure 5.2. Synthesis and characterization of mega HPGs. A) Schematic representation of synthesis of mega HPGs (M_w: 1.3-9.3 million Dalton) by a macroinitiator approach in combination with solvent based ring opening multibranching polymerization. B) ^{1}H NMR and C) ^{13}C inverse gated (IG) NMR characterization confirmed the structural features of the mega HPG-3. D) Gel permeation chromatography analysis shows the monomodal distribution of mega HPG-3. E) Formation of single particles and globular shape of mega HPG-3 was confirmed by cryo-scanning electron microscopy (cryo-SEM).
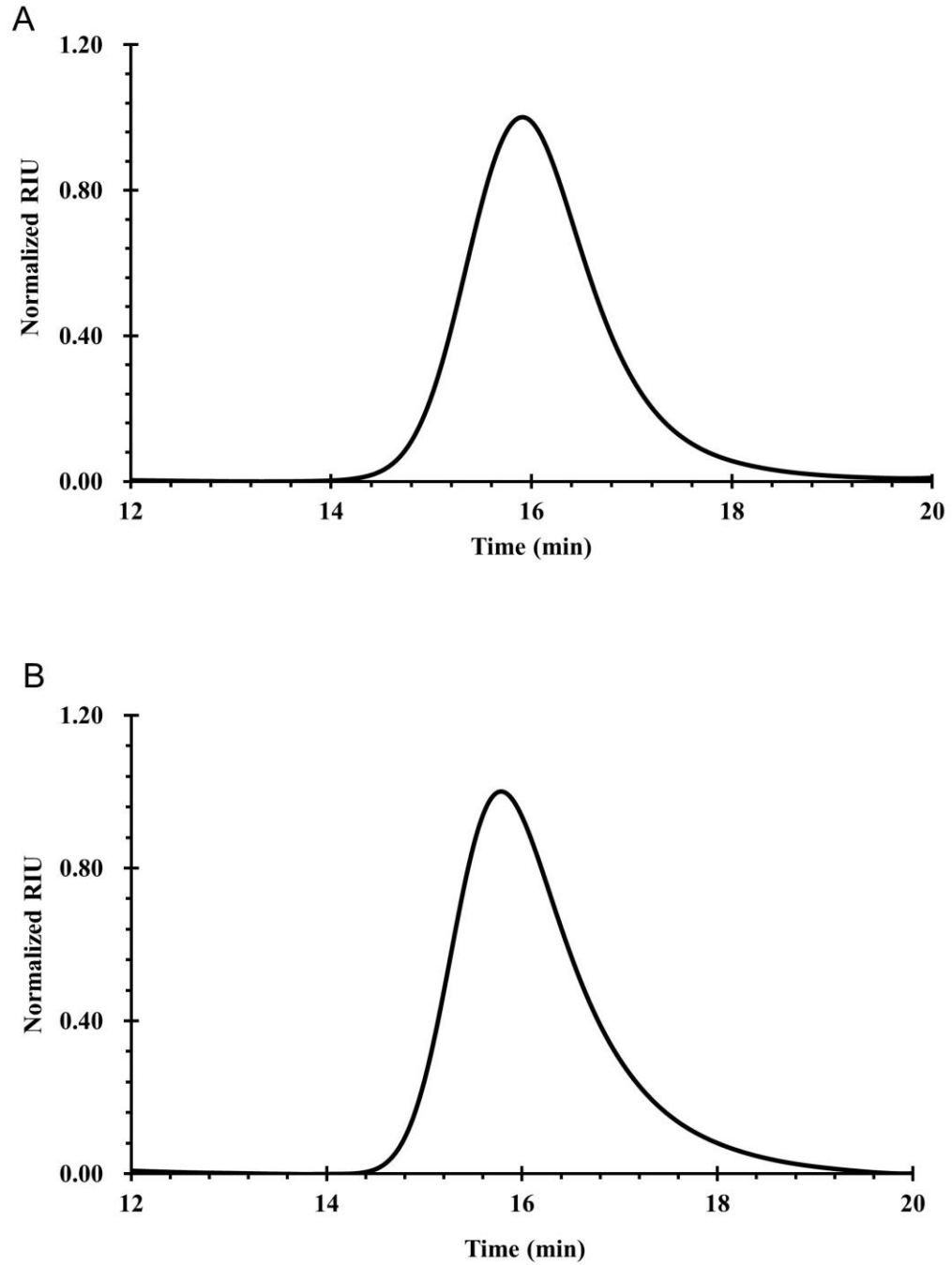
Figure 5.3. A) GPC-MALS chromatogram (0.1 M NaNO$_3$ buffer, pH 7.4) of the *mega* HPG-1 (*M*$_w$-1.3 MDa). **B**) GPC-MALS chromatogram (0.1 M NaNO$_3$ buffer, pH 7.4) of the *mega* HPG-2 (*M*w-2.9 MDa).
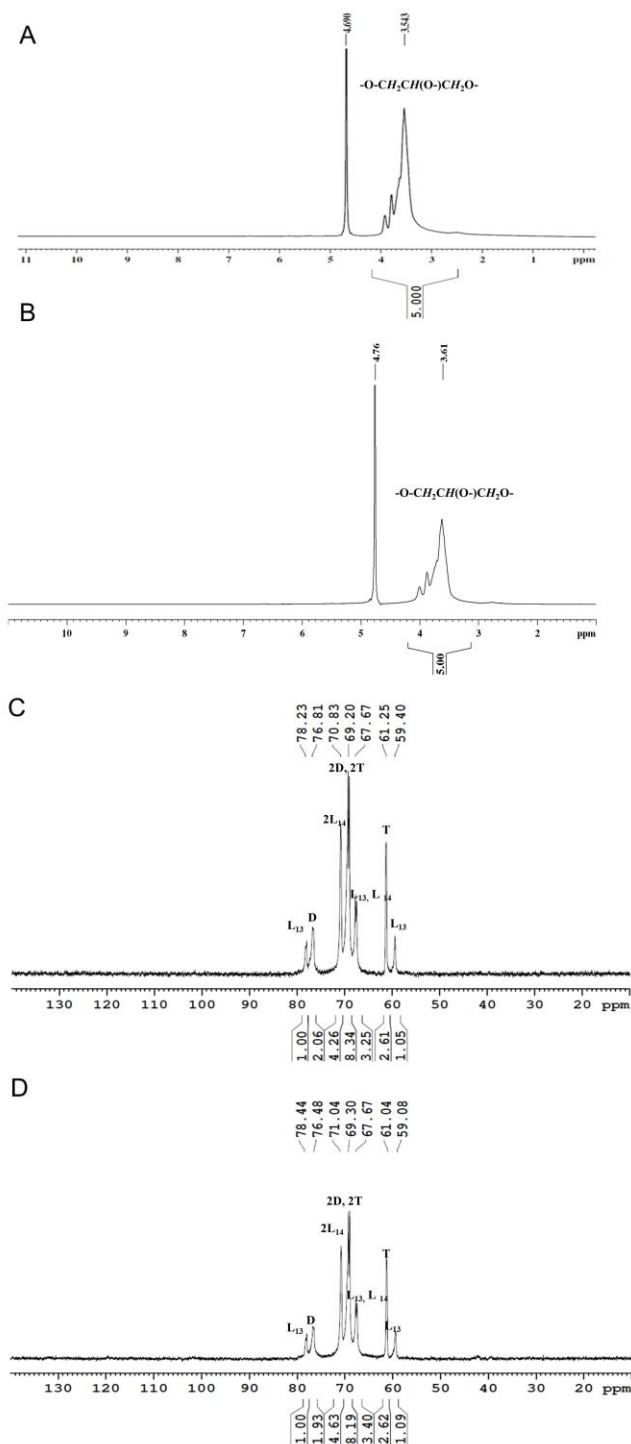
Figure 5.4. A) ^{1}H NMR spectrum (D$_2$O, 400 MHz) of the *mega* HPG-1 (*M*$_w$-1.3 MDa). **B**) ^{1}H NMR spectrum (D$_2$O, 400 MHz) of the *mega* HPG-2 (*M*$_w$-2.9 MDa). **C**) ^{13}C NMR spectrum (D$_2$O, 100 MHz) of the *mega* HPG-1 (*M*$_w$-1.3 MDa). **D**) ^{13}C NMR spectrum (D$_2$O, 100 MHz) of the *mega* HPG-2 (*M*$_w$-2.9 MDa).
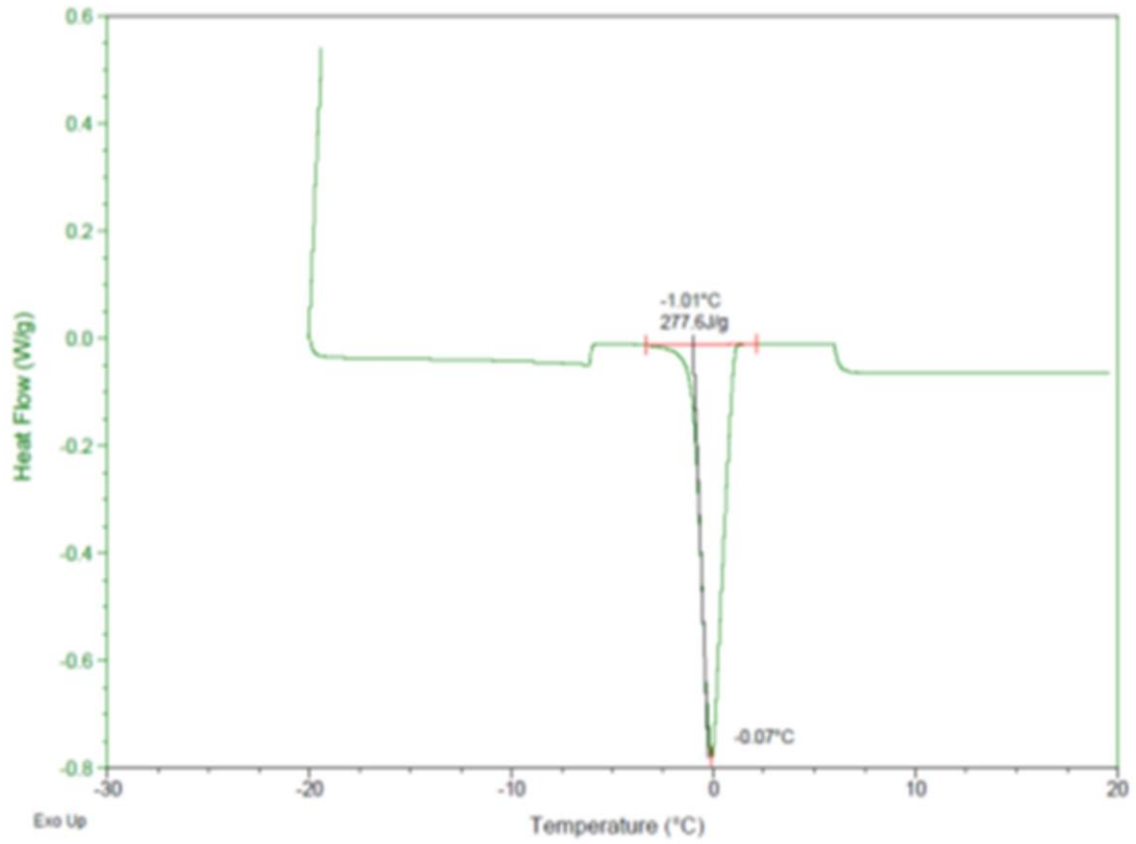
Figure 5.5. Differential scanning calorimetry (DSC) thermogram of the *mega* HPG-3.
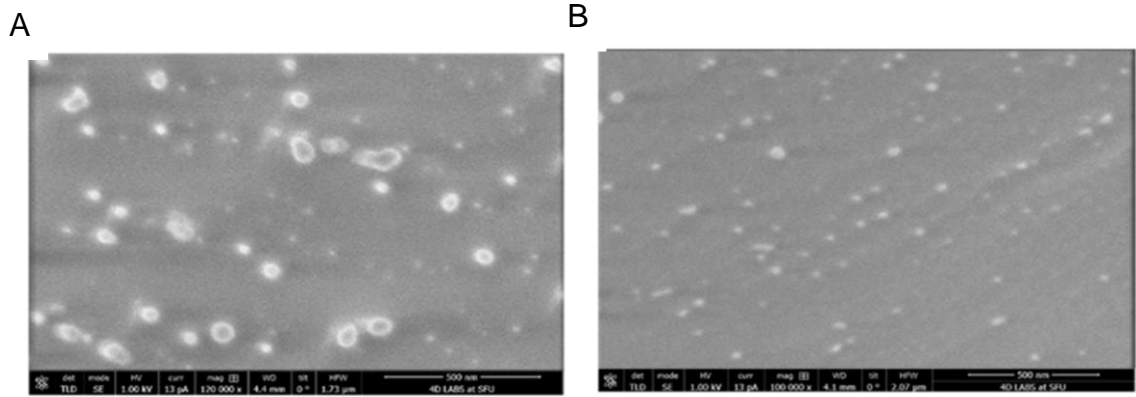
Figure 5.6. Cryo SEM images of *mega* HPG-1 (**A**) and *mega* HPG-2 (**B**).
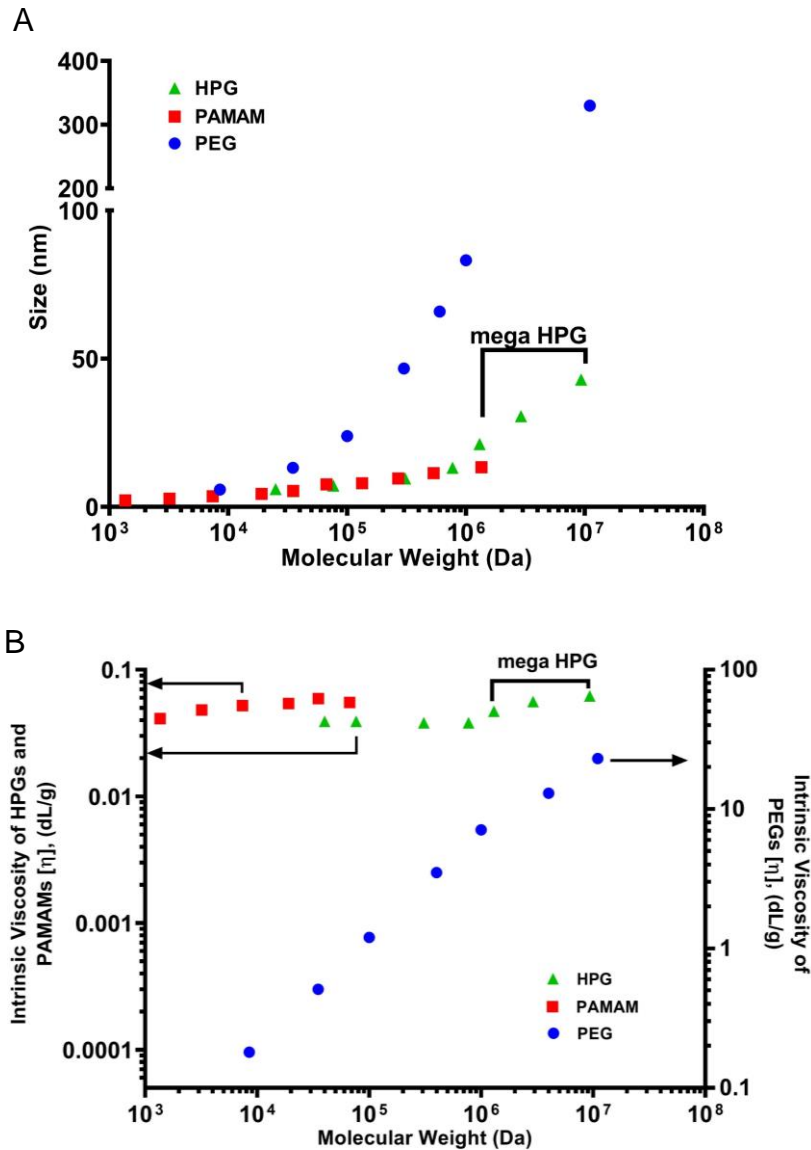
Figure 5.7. Comparison of solution properties of mega HPGs with PEG and PAMAM dendrimers. **A**) Variation of hydrodynamic size of the polymer with molecular weight. mega HPGs and their low molecular weight counterparts (first four data points), and PAMAM dendrimers are compact in size compared to PEG polymers. The values for high molecular weight HPGs (76.5, 307, and 771 kDa) are obtained from literature.[12] For PEGs, the size of PEG-4 (11 million Dalton) was derived from R_g and simulation studies.[13] **B**) Dependence of intrinsic viscosity of the polymers with molecular weight (arrow shows the representative Y-axis). Mega HPGs showed similar intrinsic viscosity behavior as that of PAMAM dendrimers, however, slight increment with molecular weight might was observed. The PEG systems showed liner dependency with molecular weight.
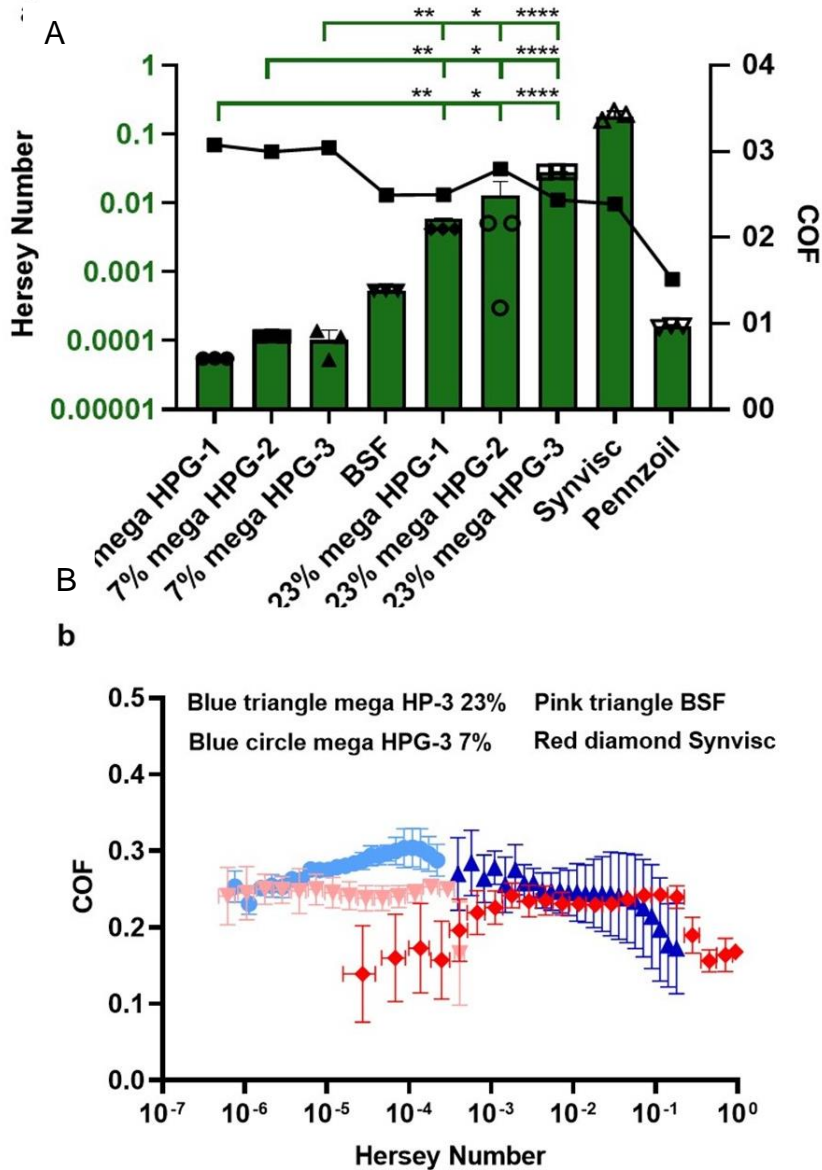
Figure 5.8. Lubrication characteristics of mega HPGs. **A**) Graph of the Hersey number at which each group transitions from boundary mode to mixed mode lubrication (left y-axis and green bars). The COF at the time each lubricant transition from boundary to mixed mode lubrication. Error bars represent standard deviation, N = 3 replicates; one-way ANOVA used to compare groups, statistical differences indicated by asterisk where p<0.05 =*, p<0.01=**, p<0.0001 =****. For full list of statistical results see SI. b. Stribeck curves for best preforming mega HPG (mega HPG-3) at both 7 and 23 w/v% as well as two controls, BSF and Synvisc One (right y-axis, black symbols). Error bars represent standard deviation, N = 3 replicates. **B**) Stribeck curves for best preforming mega HPG (mega HPG-3) at both 7 and 23 w/v%, as well as two controls, BSF and Synvisc One. Error bars represent standard deviation, *N* = 3 replicates.
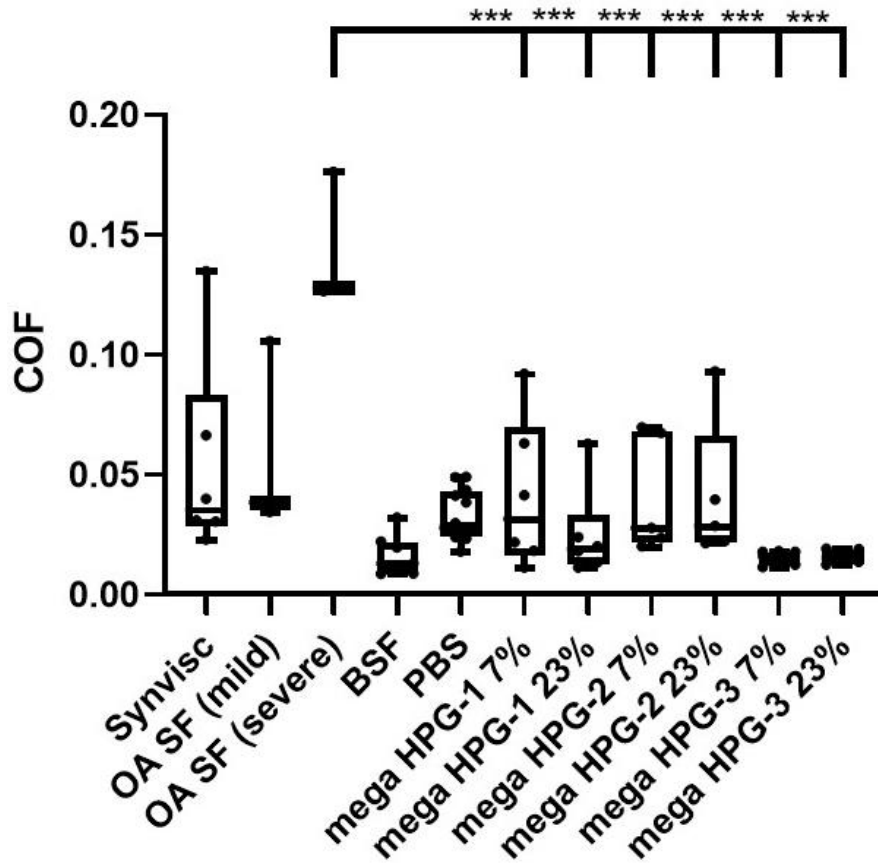
Figure 5.9. Determination of coefficient of friction of mega HPGs. Coefficient of friction values for cartilage on cartilage with each lubricant after equilibrating in creep, as shown with box-and-whiskers plot. Whiskers represent (min to max), bounds of box represent lower (25th percentile) and upper quartile (75th percentile), and center line represents median. Error bars represent standard deviation, N = 3 or greater replicates; one-way ANOVA used to compare groups, statistical differences indicated by asterisk where $p<0.05$ =*, $p<0.01$=**, $p<0.0001$ =****.
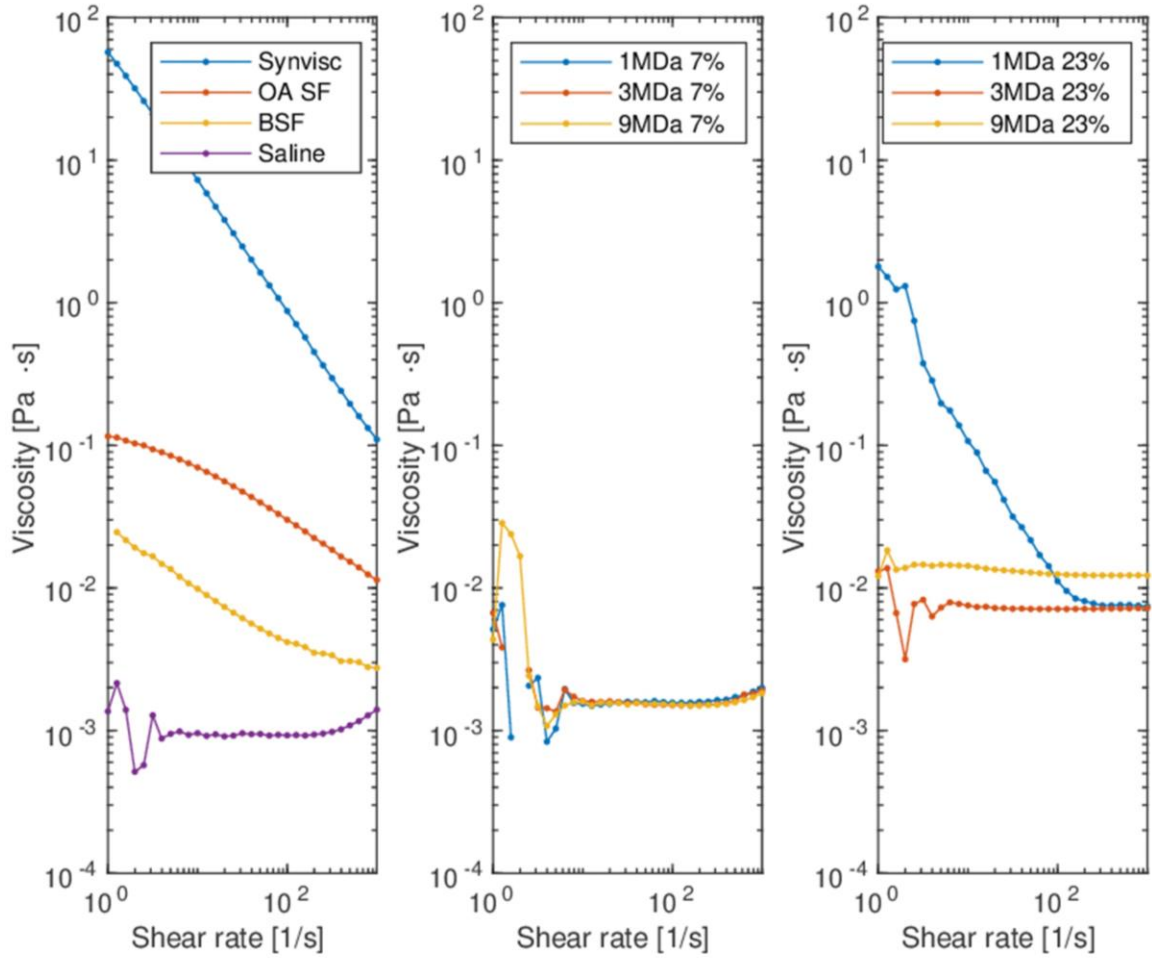
Figure 5.10. The viscosity-shear rate behavior of *mega* HPGs at two different concentrations (7 and 23 wt%) and compared with Synvisc One (Synvisc), osteoarthritic synovial fluid (OA SF), bovine synovial fluid (BSF), and saline.
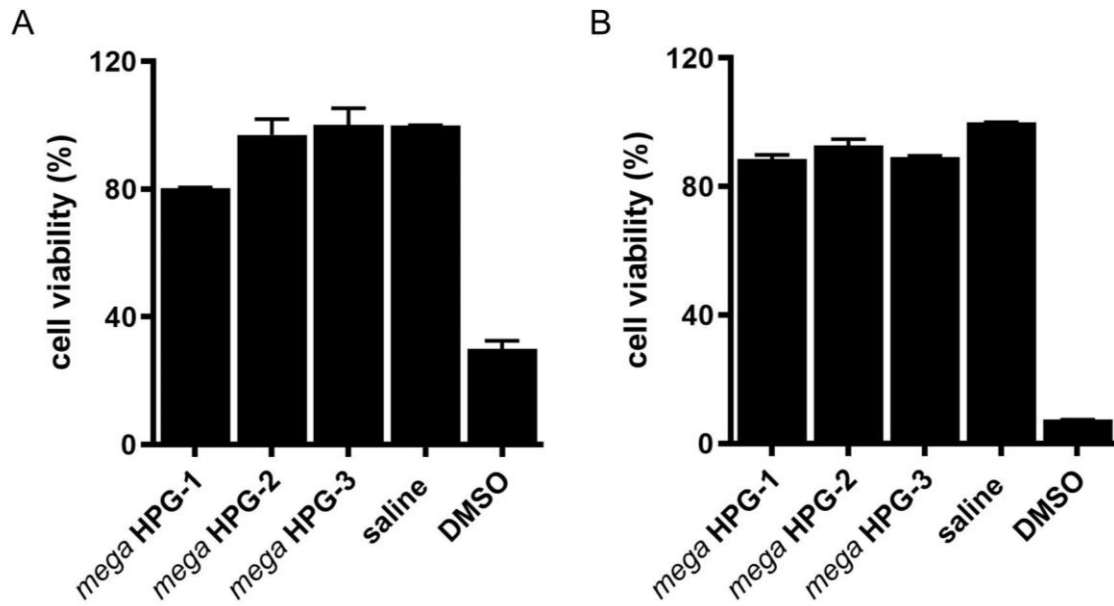
Figure 5.11. Cell viability of *mega* HPGs-1, 2, and 3 (1.25 mg/ml) towards Tc28a2 juvenile human chondrocytes (**A**) and 3T3 murine fibroblast cells (**B**). Cells were incubated with either *mega* HPGs, saline, or DMSO for 48 h at 37 °C. After washings, the metabolic activity of the cells was assessed by MTT assay.[5] Six replicates were performed and each study was repeated in quadruplicates. Average values and standard deviation are reported. Cell viability of *mega* HPGs (≥80%) irrespective of the cell line confirmed the high cell compatibility of the *mega* HPGs.

175
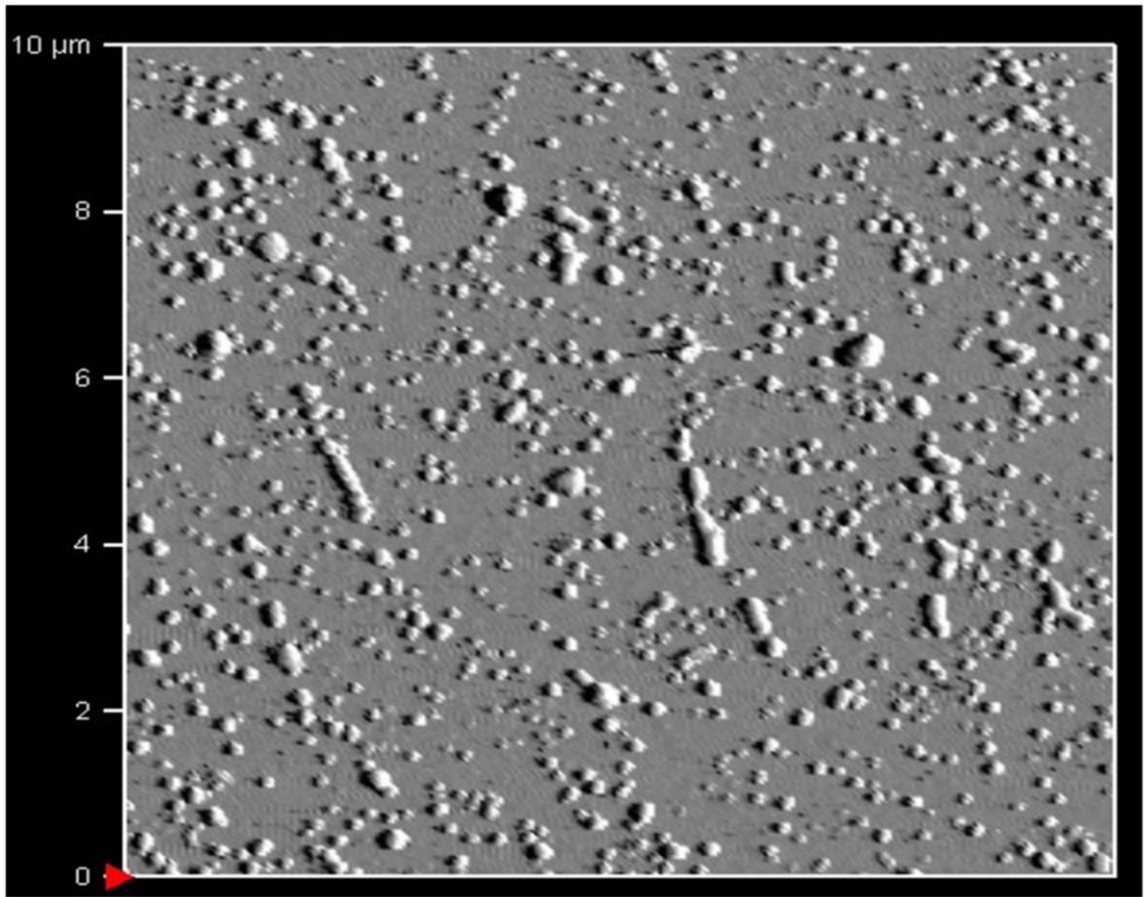
Figure 5.12. AFM image of *mega* HPG-3 chemically adhered to the surface of an epoxide functionalized glass slide in 2D.

CHAPTER VI: A Biocompatible Nanolubricant

6.1 Abstract

Osteoarthritis is a degenerative disease whose pathology is predominantly characterized by the breakdown of articular cartilage, concomitant with the degradation of synovial fluid macromolecules, hyaluronic acid and lubricin. Macromolecule degradation decreases both the fluid and boundary lubricating capacity of synovial fluid, exacerbating tissue wear and disease progression. The chemical and physical nature of both the lubricant and articulating surfaces are important determinants of wear. Classically, the mode of lubrication (i.e., boundary, mixed or fluid film) for rigid articulating surfaces is determined from the Stribeck curve: a plot of the non-dimensional Hersey number [(angular velocity of a rotating bearing x viscosity of lubricating fluid) / applied stress per unit length] vs. COF. Boundary lubrication, characterized by high load and low speed, is defined as that where apposing articulating surfaces are separated by a very thin film of lubricant molecules absorbed onto the bearing surfaces. It is particularly relevant during "stiction", the friction threshold that must be overcome to enable sliding between articulating surfaces after prolonged static contact; during this regime the COF is greatest. Nanoparticles (NPs) aid in boundary mode lubrication by altering the tribology of the contacting surfaces via introduction of a rolling ball element and infiltration of small gaps between bearing surfaces to provide a protective layer. By adding biocompatible tantalum oxide NPs to bovine synovial fluid (BSF), we propose a biocompatible nanolubricant that improves boundary mode lubrication by reducing the COF between articulating surfaces comprised of either rigid or poroelastic deformable materials such as hyaline cartilage

6.2 Introduction

Nanoparticles dispersed within a base fluid result in a colloidal suspension termed a nanolubricant.[1] Adding nanoparticles to conventional oils enhances performance by reducing the COF up to 50%, while purely introducing a rolling element between two surfaces in contact decreases the friction, producing frictional forces $10^2 - 10^3$ times lower than those from sliding alone.[1–3] Lubricants play an integral role in the operation of several technologies, including internal combustion engines, vehicles, gear systems, compressors, turbines, and the bearings of the body, synovial joints, whose main function is to reduce friction and material wear of hyaline cartilage.

In healthy synovial joints, hyaline cartilage supports mechanical loads and provides a smooth, nearly frictionless gliding surface with a coefficient of friction (COF) 20% that of ice on ice.[4] Hyaline cartilage is comprised of a collagen fibril network that provides structure and tensile strength, complemented by a glycosaminoglycan (GAG) matrix of negatively charged polysaccharides that regulate interstitial fluid transport such that >90% of applied joint load is supported by pressurization of entrapped interstitial fluid (i.e. interstitial fluid load support, IFLS).[5] Applied deformations induce efflux of fluid from the hyaline cartilage to form an interposed fluid film that decreases the COF and protects articulating joint surfaces from mechanical wear.[5–7] Synovial fluid (SF) contains polymers (e.g., hyaluronic acid and lubricin) that act as boundary lubricants between opposing joint surfaces.[8,9] Hyaluronan within synovial fluid contribute to viscosity and fluid lubrication, while surface zone proteins such as lubricin aid in boundary lubrication.[9]

Osteoarthritis (OA), a painful, chronic, condition is characterized by the depletion

of cartilage GAG and subsequent collagen network degradation that increase hydraulic permeability and decrease cartilage stiffness.[10] Integral to OA pathology are concomitant changes in the biochemical composition of SF that result in deterioration of its rheological and lubricious properties, which contribute to increased cartilage wear - hyaluronan decrease in molecular weight, decreasing viscosity, and surface zone proteins are degraded, decreasing boundary lubricating abilities.[9,10] Early signs of articular cartilage are associated with loss of the boundary lubrication function of synovial fluid.[11–13]

Lubrication is classically divided into three modes for non-deformable materials: boundary, mixed and hydrodynamic. Lubrication in the presence of an incompressible fluid lubricant is characterized and displayed on a Stribeck curve.[14] A Stribeck plots the non-dimensional Hersey number [(angular velocity of a rotating bearing x viscosity of lubricating fluid) / applied stress per unit length] vs. COF and displays three distinct modes of lubrication.[14] The COF within boundary and mixed is particularly high, causing wear and debridement. Lubricant additives, such as nanoparticles, are particularly relevant during "stiction", the friction threshold that must be overcome to enable sliding between articulating surfaces after prolonged static contact and in turn boundary lubrication. To date, a large number of nanomaterials are used as additives for lubricating oils such as carbon materials, carbon nanotubes, graphene eoxide, boron nitrides, and silicon oxide.[3] The mechanisms of action for nanoparticle lubrication are: 1) formation of tribo-films or adsorption films that change the surface properties and separate the two friction surfaces[15]; 2) added NPs are rolled between two articulating surfaces, reducing COF and wear[15]; and,

3) NPs are compacted on the wear track due to heat and pressure generated during the friction process, called sintering or the repair effect.[15]

By adding biocompatible tantalum oxide NPs to bovine synovial fluid (BSF), we propose a biocompatible nanolubricant. The goal of this study is to elucidate the effectiveness of a novel synthetic nanolubricant compared to saline, BSF and hyaluronic viscosupplement (Synvisc One) to reduce wear along of articulating surfaces comprised of poroelastic materials and improve boundary and hydration lubrication (and by extension, provide chondroprotection).

6.3 Methods

6.3.1 Nanoparticle Synthesis and Characterization

Tantalum oxide (Ta_2O_5) nanoparticles were synthesized by adding tantalum ethoxide (1.20 mL) dropwise at 0.2 mL/min to a stirring solution of n-propanol (34 mL), isobutyric acid (0.440 mL), and deuterium oxide (0.500 mL). This solution was stirred for 48 hours at room temperature after which, solutions of n-propanol (20 mL), N-trimethoxysilylpropyl-N,N,N-trimethylammonium chloride (2.343 mL), and 2-[methoxy(polyethyleneoxy)$_{6-9}$propyl]trimethoxysilane (2.5 mL) were subsequently added to the reaction vessel at 1 mL/min. The reaction was refluxed for 2 hours at 103°C, and cooled to room temperature. 0.1 M NH_4OH (0.250 mL) was added to the vessel and stirred for 18 hours. At 1 mL/min, deionized water (40 mL) and 1.2 M hydrochloric acid (10 mL) were added to the solution and stirred at 50°C for 48 hours. The reaction was then cooled to room temperature, adjusted to a pH of 7 using Na_2CO_3, and filtered using a 0.22 um PTFE filter. The filtered solution was then dialyzed for 72 hours, with frequent water

changes, followed by lyophilization to yield a white powder. ^{1}H NMR (500 MHz, D2O): δ = 0.10 (br s), 1.15 (br s), 1.37 (br s), 2.5–3.3 (br m). FTIR (cm^{-1}): 2871 (strong), 1647 (medium), 1479 (medium).

Nanoparticle size was evaluated using dynamic light scattering (DLS) and transmission electron microscopy (TEM). DLS size characterization was conducted using the Brookhaven Nanobrook Omni Particle Sizer (Brookhaven Instruments, Holstville, NY). Samples were prepared by suspending nanoparticles in either deionized water or bovine synovial fluid, and the hydrodynamic size of the nanoparticles was subsequently measured at room temperature. Samples for TEM were prepared by depositing 0.010 mL droplet of 0.1 mg/mL nanoparticles solution to dry on a glassy C-coated Cu TEM grid. Imaging was performed using a Hitachi 780 TEM at 80 kV.

Zeta potential of the nanoparticles was measured Brookhaven Nanobrook Omni Particle Sizer (Brookhaven Instruments, Holstville, NY), using the samples prepared with deionized water used for DLS size characterization. Zeta potential was recorded for each sample after three runs of ten cycles. Ta$_2$O$_5$ NPs were suspended in deuterium oxide and NMR spectra were obtained using the Agilent 500 MHz VNMRS spectrometer with a Varian ultra-shielded magnet. FTIR spectra were obtained on dried Ta2O5 NPs samples, using Thermo-Nicolet Nexus 670 FTIR E.S.P. instrument, equipped with Miracle ZnSe ATR prism (Thermo Sci., Billerica, MA).

6.3.2 Cytotoxicity

NIH3T3 murine fibroblast cells were maintained in Dulbecco's Modified Eagle Media, with 10% fetal bovine serum and 1% penicillin/streptomycin. Cells were

maintained in a humidified atmosphere at 37 °C and 5% CO2. Sub-confluent cells were harvested and seeded on 96 well plates at 3,000 cells/well for use in in vitro cytotoxicity studies. After 24-hours, the cells were treated with nanoparticles suspended in nanopure water, starting at 120 mg/mL and serially diluted by 1/3 until a final concentration of 0.002 mg/mL. After a 24-hour exposure, cell viability was tested using a colorimetric MTS [3-(4,5-dimethylthiazol-2-yl)-5-(3-   carboxymethoxyphenyl)-2-(4-sulfophenyl)-2H-tetrazolium] cell proliferation assay (Sigma, St. Louis, MO) and absorbance read at 490 nm on a Biotek Synergy HT Plate Reader (Winooski, VT). Cell viability in each well was calculated as the percentage of the positive control absorbance.

6.3.3 Classical Tribological Testing

Viscosity measurements were performed on a TA Instrument AR2000 rheometer using a 2° aluminum cone and a 47 µm gap at 25 °C. Viscosity was then averaged across shear rates from 10 to 100 per s. Rigid body Stribeck curves to evaluate the modes of rigid body lubrication were constructed using a DHR-2 rheometer (TA instruments) with a stainless steel ring articulating on a stainless-steel plate, bathed in 300 µL of each lubricant: 100 nm diameter NP in BSF were prepared at a range of concentrations 0.01, 0.1, 1, 3, 8 and 11 wt% to first determine a dose response curve. Next stribeck curves of the nanolubricant at 11 wt%, Synvisc, and BSF were conducted. Tribologic testing was conducted in triplicate for each lubricant at a constant 5N applied compressive load and progressively increasing radial velocity 0.001 rad/s to 50 rad/s. Stribeck curves were derived from the mean and standard deviation for Hersey number vs. COF for each lubricant.

6.3.4 Sample preparation

Bovine osteochondral plugs (7 mm diam.; N=9) were cored from skeletally mature cows (Green Village packing, Green Village, NJ) using a diamond tipped drill bit and stored at 4°C in 400 mOsm saline supplemented with protease inhibitors and antibiotics. Sample degradation was performed by placing osteochondral plugs in a Trypsin solution containing PBS and 0.1 mg Trypsin at pH 7.5 for two hours at 37 °C.[16]

6.3.5 Biotribological Testing

Cartilage on cartilage tribology testing using paired bovine osteochondral plugs in unconfined compression was performed for saline, BSF and nanoparticles suspended in BSF at 11 wt%. A static 8N (200kPa) compressive load was applied (Bose Electroforce 3200), followed by 3 hours of tissue creep to reach equilibrium, while submerged in the test solutions. Equilibrium COF was determined at an angular velocity of 360°/s (effective velocity = 14.7 mm/s) for 120 seconds. A second tribology test was then preformed after increasing the compressive load to 30N and decreasing the angular velocity to 36°/s. Dynamic and equilibrium COF were calculated using a custom MATLAB program.

6.3.6 Wear Testing

A static 30N load was held constant for 105 minutes while submerged in a bath of lubricant; saline BSF, or nanolubricant at a concentration 11 wt% nanoparticles. While the static load was applied, cartilage surfaces were articulated at 180°/s for the entire test duration. Cartilage wear was quantified by measuring tissue volume via microcomputed tomography before and after the wear test. The samples were scanned via microcomputed

tomography at an isotropic voxel resolution of 36 um, 70-kVp, 113-uAmp, 300 ms integration time (µCT40, Scanco Medical AG). µCT data were converted into DICOM format and imported into Analyze for post-processing analysis as previously described. The mean cartilage thickness at the apex was determined by a custom MATLAB program.

6.3.7 Animal Model

A mouse model was utilized for this study, specifically destabilization of the medical meniscus (DMM) as it is an accepted model of post-traumatic osteoarthritis for evaluation of novel therapeutics. After medial parapatellar arthrotomy, the infrapatellar fat pad (IFP) was temporarily repositioned laterally, allowing access to the anterior medial meniscotibial ligament. This ligament was severed using a #11 blade. The IFP was repositioned, and the incision closed using 5-0 PDS or similar absorbable suture. Mice were monitored daily throughout the study period for any signs of adverse events or complications to evaluate pain, lameness, incisional site, and ambulatory function as well as general health status, any animal noted to have abnormal clinical findings during routine daily monitoring, a complete physical examination will be performed by a veterinarian and a diagnostic plan and therapeutic plan will be implemented. All animals will receive intra-articular injections at 14-, 28-, and 42-days post-op. For each time-point, mice received a single intra-articular injection (10uL of Ta nanoparticles in sterile saline) in the injured knee under general anesthesia. Delivery occurred via a 27-gauge syringe into the cranial aspect of the knee just medial to the patellar tendon. Sham treatment animals received a needle puncture without an intra-articular injection. For recovery, animals were returned to their home cage. At 56 days post-op blood was collected immediately pre-euthanasia via

cardiac puncture using a 25G needle while the animal is under general anesthesia. All blood samples were centrifuged at 2,000xg for 10 minutes, and the serum removed and stored at -20˚C. All animals were humanely euthanized by CO2 inhalation and confirmatory cervical dislocation, following blood collection via cardiac puncture in accordance with the American Veterinary Medical Association (AVMA) guidelines. All hind-limb samples were processed for decalcified histological analysis. Following fixation in 10% NBF, specimens were decalcified in 10% EDTA. Specimens were processed using standard techniques (Tissue-Tek VIP, Sakura, Torrance, CA), embedded in paraffin, and one (1) 5um thin coronal section was taken from each knee joint. All sections were then be stained for toluidine blue and imaged under bright field light.

6.3.8 Statistics

Univariate linear regression (GraphPad Prism 8) was used to examine the relationship between boundary coefficient of friction and nanoparticle concentration. The coefficient of determination (R^2) was used to assess the strength of correlation. Brown-Forsythe, one-way repeated measure ANOVA, was used to examine the relationship between BSF, Synvisc, and nanolubricant. A dose-response curve was fit to evaluate the nanoparticle concentration response curve. The coefficient of determination (R^2) was used to assess the strength of correlation. For all analyses, significance was set as two-tailed $p < 0.05$.

6.4 Results

6.4.1 Characterization

1 H NMR showed the characteristic peaks and confirmed the silane coating on the particle (**Figure 6.2**). As shown in **Table 6.1**, the hydrodynamic size of the nanoparticles confirmed via dynamic light scattering (DLS) begin at 101.16 nm in DI water and grow in diameter to 285.91 nm when in bovine synovial fluid. The nanoparticles possess an overall positive charge of 8.9 +/- 2.1 mV as measured using Brookhaven Instruments ZetaPALS Zeta Potential Analyzer.

6.4.2 Dose response curve

Concentration is an important factor in development of a nanolubricant, demonstrating efficacy at concentrations below 1 wt % and above 2 wt%,[3] indicative that there is no ideal concentration and no predictable relationship between the concentration and the effect of the NP additive on friction and wear. Therefore, we determined the lowest concentration at which the tantalum oxide nanolubricant became efficacious compared to BSF alone, and if efficacy increased with concentration using our non-deformable body set up. At the lowest concentration of nanoparticle additive, the nanolubricant demonstrated an average boundary coefficient of friction lower than BSF alone (0.33 and 0.40, respectively). The measured boundary COF varied linearly with nanoparticle concentration (**Figure 6.4**). The highest concentration, 11 wt%, produced the lowest boundary mode COF (0.20), and was the concentration carried forward in the following experiments.

6.4.3 Tribological characterization

The nanolubricant displayed a viscosity on the order of BSF (0.0114 Pa.s and 0.0149 Pa.s, respectively), both an order of magnitude less than Synvisc (0.290 Pa.s) (**Figure 6.6**). All controls along with the nanolubricant demonstrate a shear thinning behavior and are therefore non-Newtonian fluids. Elastic and viscous effects for BSF (0.7898 and 0.4458, respectively) are slightly higher than the nanolubricant (0.5255 and 0.3384) but not to a statistically significant amount. Storage and loss moduli at a frequency of 2.5Hz. Moduli averaged over 11 logarithmically spaced data points spanning stress 1-10 Pa within linear viscoelastic region

6.4.4 Cytotoxicity

The nanoparticle concentration response curve was fit with a dose response curve in order to obtain an IC50 value. IC50 value for the tantalum oxide nanoparticle is 21.76 mg/mL. Nanoparticles demonstrate 90% viability at 11wt%, the concentration which demonstrated the most efficacy in reducing the boundary COF.

6.4.5 Rigid body Stribeck curves

BSF demonstrated an inflection point at the highest COF (0.473) and lowest Hersey number ($5.97*10^{-6}$). The nanolubricant demonstrated an inflection point at a Hersey number multiple orders of magnitude higher ($2.4*10^{-4}$) and at a COF half that of BSF (0.24). Consequently, the nanolubricant exhibited a Stribeck curve similar to the hyaluronic acid solution, Synvisc, except that the nanolubricant is 100× less viscous. Boundary mode COF for the nanolubricant was reduced to a value (0.20) statistically significantly less than

both Synvisc (0.30) (*p = 0.001*) and BSF alone (0.40) (*p = 0.0038*) (**Figure 6.5**).

6.4.6 Deformable body COF

Lubricant type had little to no effect on dynamic COF, with little variation between lubricant types. Upon instantaneous loading, fluid pressurization within the cartilage and exudation at the cartilage-cartilage interface governs dynamic equilibrium with an insensitivity to boundary lubricating and viscosity modifying entities in the lubricant. When fluid pressurization reaches equilibrium, the lubrication mode is sensitive to the operating parameters – specifically viscosity, strain, and co-planarity, and not dominated by tissue pressurization parameters. At equilibrium conditions at two different loads, 8N and 30N, the nanolubricant's ability to modulate the COF is apparent. At the 8N load and 0% interstitial fluid load, with a rotational speed of 360 °/second, the COF values for the nanolubricant (0.018) were statistically equivalent to healthy BSF (0.021)   and, importantly, significantly lower than the COF value obtained with saline (0.15) (*p = 0.018*) (Figure 7). With the goal of better emulating mixed mode lubrication, the load was increased by 375% to 30N and the speed decreased by an order of magnitude to 36°/second. Under these conditions at 0% interstitial fluid load support, the nanolubricant outperformed, BSF having a COF value of 0.135 compared to BSF at 0.039 (*p = 0.0219*) (Figure 6.X).

6.4.7 Cartilage Wear

Using healthy, native bovine cartilage, the nanolubricant allowed for a mere 3% reduction in tissue volume following a supraphysiologic wear cycle. Using BSF, the

cartilage volume was decreased by 13% and with saline by 17%. Bovine tissue was then degraded with Trypsin to remove surface level phospholipids and lubricin which aid in boundary lubrication, in conjunction with decreasing surface zone GAG content.[16] Using these degraded samples, the nanolubricant preserved tissue to an even greater extent, allowing for only 2% decrease in total cartilage volume following the supra-physiologic wear cycle, compared to saline and BSF which allowed for a decrease of 6.93% and 13.67% respectively (*p = 0.0029*) (**Figure 6.8**).

6.5 Discussion

Viscosupplementation is one of the most common non-surgical treatment options for OA, accompanied only by nonsteroidal anti-inflammatory drugs, both aimed at pain control and improved joint function. Current viscosupplementation endeavors aim at restoring concentrations of hyaluronic acid to increase viscosity, improve lubricity, and modulate hydrodynamic lubrication, while on the macroscopic scale provide pain relief and improved ambulation. Yet, to date, viscosupplementation efficacy remains under scrutiny, with ample recommendations both for and against its use. Its lack of chondroprotection, poor lubricity and a short *in vivo* half-life are shortcomings.

We describe a novel, biocompatible nanolubricant for modulating the coefficient of friction and wear of deformable, poroelastic, biphasic materials such as articular cartilage. This novel nanolubricant joins a class of tribological altering nanomaterials most commonly employed for lubrication of machinery (i.e., metal bearings and automotive applications)[17,18], but now demonstrating applicability to the living bearings of the body, synovial joints.

To investigate changes in tribological behavior from addition of nanoparticles to synovial fluid, we performed basic rheological characterization. Synvisc One and bovine synovial fluid (BSF) were selected as controls based on their different compositions (a lightly crosslinked linear polymer of hyaluronic acid of high viscosity versus a low viscous, natural lubricating solution) and relevance to the hard and soft natural surfaces investigated. Concomitantly, Synvisc One and BSF lubricate via different mechanisms, BSF aids in boundary and mixed mode lubrication, while Synvisc One is a fluid lubricant, operating during hydrodynamic lubrication. The nanolubricant, in comparison to the base fluid alone, BSF, reveals no apparent changes in viscous or elastic properties. The nanolubricant retains the same viscosity as pure BSF, in conjunction with the same storage and loss moduli. Tangentially, both BSF and nanolubricant present much lower viscosity and storage and loss moduli in comparison to the commercially available viscosupplement, Synvisc-One ®.

We first created Stribeck curves in order to determine the performance and modes of lubrication of the nanolubricant on non-deformable materials, specifically stainless steel. Stribeck curves describe the COF of a system composed of non-deformable materials across different lubrication modes: boundary, mixed, and hydrodynamic lubrication. Generally, boundary lubrication exists under conditions of low speed, high load, and is characterized by a high COF while conversely hydrodynamic lubrication occurs under conditions of high speed and low load, and is characterized by a low COF, with inflection points indicating thresholds for the transition from boundary to mixed mode lubrication. Mixed mode straddles conditions of both boundary and hydrodynamic lubrication, with

some areas of the articulating surfaces in direct contact where others are fully separated by a film of fluid.

Stribeck curves are a property of the whole system. Hersey number being (velocity * viscosity)/load, and are created by varying only one parameter, in this case, velocity. Both BSF and the nanolubricant possess similar viscosities (0.0115 Pa.s and 0.0149 Pa.s, respectively), yet they span different regions of the Stribeck plot , with BSF spanning fewer Hersey numbers (10^{-7} – 10^{-4}) in comparison to the nanolubricant (10^{-7} – 10^{-2}), concurrent with much higher COF values through all modes of lubrication for BSF. While the nanolubricant Stribeck curve differs from that of BSF, it more closely mimics that of Synvisc. Syncisc-One ®, a highly crosslinked supplement of hyaluronic acid possess a viscosity an order of magnitude greater than the nanolubricant and BSF (0.29 Pa.s), in parallel with larger viscous and elastic properties. Higher viscosity values increase Hersey numbers, effectively shifting Stribeck curves to the right on the Y-axis. Despite its fractional viscosity value compared to Synvisc, the nanolubricant's Stribeck curve spans similar Hersey numbers and COF values. The only parameter altered between Stribeck curves is the lubricant itself, with the load and velocity parameters held constant between groups. Thus the vastly different Stribeck footprint despite identical testing parameters to BSF (same viscosity, velocity and load) indicates the nanolubricant is lubricating via a different mechanism.

We propose the mechanisms of action for nanolubricant reduction in the COF are multifaceted and include – rolling effects, mending effects, and polishing effects. Rolling effect occurs when spherical and quasi spherical nanoparticles function as tiny ball

bearings rolling into the contact zone and changing sliding friction to a combination of sliding and rolling.[19] The mending effect is characterized by nanoparticle deposition on friction surfaces and mass loss compensation, filling scars and grooves to reduce abrasion.[20] The polishing effect manifests itself when roughness of lubricating surface is reduced by abrasive treatment with nanoparticles. Nanoparticles fill gaps acting as reservoirs of solid lubricants and this artificial smoothing results in improved tribological characteristics owing to reduced surface roughness.[21] With our current model it is impossible to parse out if all or only some of these mechanisms are responsible for the reduction in COF, and determining which mechanisms are present requires further investigation.

In addition to these mechanisms of action, we hypothesize a different mode of lubrication to be in effect during lubrication with our nanolubricant, which involves charge effects and hydration shell lubrication. For the macromolecules of synovial fluid, function follows form; hyaluronic acid, lubricin and phosphatidylcholine lipids all playing very specific roles in cartilage lubrication as dictated by their form and chemical composition. It is the synergistic interaction of these eloquently designed macromolecules and the extracellular matrix, which give rise to the extremely low COF of articular cartilage. Recent studies indicate the entanglement and hydrophobic interaction of lubricin and HA contribute to mixed mode lubrication and shock absorption.[22–24] Although, the entanglement of HA and lubricin alone do not account for the low COF of articular cartilage at high applied loads. Klein et al suggest a three-component system, where in conjunction with lubricin-immobilized-HA at the articular surface, HA complexes with

phosphatidylcholine lipids exposing their charge groups at the cartilage interface and allowing for "hydration lubrication", whereby lubrication occurs via hydration shells forming around the charged phosphatidyl choline molecules.[25–28]

We hypothesize that our hybrid tantalum oxide nanoparticles coupled with hyaluronic acid aggregate on the surface to maintain a lubricious, hydrated film, aiding to support heavy loads and decreasing the COF of articulating surfaces, able to act as both a fluid film or boundary lubricant, depending on the operating conditions. That tantalum oxide nanoparticles described herein are cationic, possessing multiple positive charges per nanoparticle, whereas lubricating constituents within SF, including hyaluronic acid, are negatively charged.[29] When suspended in DI water, DLS measurements reveal the nanoparticles to be a size 101.16 nm in diameter, yet when suspended in BSF, the nanoparticle size increases to 285.91nm, supporting the hypothesis that when these cationic particles are suspended in BSF, the aggregation of negatively charged SF constituents occurs. Aggregation of SF constituents affords the nanoparticles within our nanolubricant a hybrid structure, a synergistic combination of a rigid internal shape and a slippery fluid-like surface. We envision these hybrid structures function to maintain a lubricious film near the anionic cartilage surface during mixed mode lubrication. This proposal is supported by results that show when used to lubricate poroelastic, biphasic materials such as hyaline cartilage, the nanolubricant acts to modulate the coefficient of friction under mixed mode operating conditions, (higher load, lower speed), generating COF values much lower than BSF, but in hydrodynamic lubrication, when the COF is dominated by the viscous effects of the lubricant, the nanoparticles produce COF values on par with BSF (**Figure 6.7**).

Being cationic, we hypothesize that during boundary mode lubrication, when other synovial fluid constituents have been squeezed out from between the surfaces, the cationic nanoparticles lubricate via hydration shell lubrication and a mechanical trapping mechanism. Cartilage being an anionic material, creates hydration layers of charge bound water molecules when exposed to a bath solution of saline at high salt concentrations, when ions condense over ionizable sites.[30,31] These charge bound water molecules form hydration layers, and when there is overlap of layers, water moves freely, effectively acting as a low viscosity lubricant.[30–32] In our scenario with the cationic nanoparticles, we postulate the cationic nanoparticles condense over the ionizable sites on the anionic cartilage, while simultaneously forming hydration shell around the particles themselves, thereby creating similar hydration layers and allowing water to move freely in overlapping regions. This entrapment of a lubricious layer of nanoparticles coated with HA and water molecules also follows the scenario in which Greene et al suggest a mechanical trapping mechanism maintains a layer of immobilized HA between articulating surfaces.[33] Where rather than HA alone, as the nanoparticles are ionically bound to the HA, they too become mechanically trapped between the articulating surfaces. Purely introducing a rolling ball element between surfaces reduces the COF [REF], independent of the presence of lubricating macromolecules, suggesting a second mechanism by which the nanoparticles act to reduce the COF during boundary mode operating conditions. The ability of the nanolubricant to modulate boundary mode COF values is supported by results from the non-deformable materials, where the nanolubricant reduces the boundary mode COF to values lower than either the fluid lubricant, Synvisc, or the boundary lubricant, BSF.

High friction causes increased shear strain, vitally important when it comes to articular cartilage and the disease pathogenesis of OA, as strains transmits themselves to the chondrocytes embedded within cartilage, causing upregulation of cartilage degrading enzymes via mechanotransduction.[34–36] Degraded tissue is then abraded and removed by friction upon articulation, damaging the cartilage surface causing higher friction, increasing shear strain and so on in a self-reinforcing cycle.[37] In a healthy joint, synovial fluid and its constituents aid to mitigate shear strains on the tissue, but with OA pathogenesis this functionality decreases, making viscosupplementation an attractive solution to elongating the lifespan of hyaline cartilage.[38] Viscosupplementation standard of care utilizes solutions of highly crosslinked hyaluronic acid, which demonstrate nebulous efficacy, are susceptible to enzymatic degradation via hyaluronidase and possess minimal joint residence time.[38,39] Previously, linear[40,41] and brush polymers[41–43] have been explored for lubricating cartilage as these materials present controlled electrostatic interactions and hydration, yet none to date have employed nanoparticles.

In summary, we report the synthesis of cationic, tantalum oxide nanoparticles suspended in bovine synovial fluid as a first of its kind, biocompatible nanolubricant. The nanolubricant acts as interposed ball bearings to reduce the COF between both hard and soft surfaces, without altering the rheological properties of the base synovial fluid. It possesses the capacity to operate and improve the COF under both hydrodynamic and mixed lubrication modes. A function that arises due to the hybrid nature of the particles with a hard, core shell of tantalum oxide, which act as load bearing ball bearings during boundary lubrication when surfaces have direct contact, and soft, lubricious outer, formed

via the aggregation of negatively charged synovial fluid constituents (*e.g.* hyaluronic acid),

to facilitate hydration shell lubrication.

6.6 References

1. Hsu, S. M. Nano-lubrication: Concept and design. *Tribology International* **37**, 537–545 (2004).

2. Vilt, S. G., Martin, N., McCabe, C. & Kane Jennings, G. Frictional performance of silica microspheres. *Tribology International* **44**, 180–186 (2011).

3. Uflyand, I. E., Zhinzhilo, V. A. & Burlakova, V. E. Metal-containing nanomaterials as lubricant additives: State-of-the-art and future development. *Friction* **7**, 93–116 (2019).

4. Sophia Fox, A. J., Bedi, A. & Rodeo, S. A. The basic science of articular cartilage: Structure, composition, and function. *Sports Health* **1**, 461–468 (2009).

5. Ateshian, G. A. The Role of Interstitial Fluid Pressurization in Articular Cartilage Lubrication. *Journal of Biomechanics* **42**, 1173-1176 (2009)

6. Krishnan, R., Kopacz, M. & Ateshian, G. A. Experimental verification of the role of interstitial fluid pressurization in cartilage lubrication. *Journal of Orthopaedic Research* **22**, 565–570 (2004).

7. Caligaris, M. & Ateshian, G. A. Effects of sustained interstitial fluid pressurization under migrating contact area, and boundary lubrication by synovial fluid, on cartilage friction. *Osteoarthritis and Cartilage* **16**, 1220–1227 (2008).

8. Jahn, S., Seror, J. & Klein, J. Lubrication of Articular Cartilage. *Annual Review of Biomedical Engineering* **18**, 235–258 (2016).

9. Furmann, D. *et al.* The effect of synovial fluid composition, speed and load on frictional behaviour of articular cartilage. *Materials* **13**, (2020).

10. Chen, D. *et al.* Osteoarthritis: Toward a comprehensive understanding of pathological mechanism. *Bone Research* **5**, 16044 (2017).

11. Schmidt, T. A., Gastelum, N. S., Nguyen, Q. T., Schumacher, B. L. & Sah, R. L. Boundary lubrication of articular cartilage: Role of synovial fluid constituents. *Arthritis & Rheumatism* **56**, 882–891 (2007).

12. Elsaid, K. A., Jay, G. D., Warman, M. L., Rhee, D. K. & Chichester, C. O. Association of articular cartilage degradation and loss of boundary-lubricating ability of

synovial fluid following injury and inflammatory arthritis. *Arthritis and Rheumatism* **52**, 1746–1755 (2005).

13. Guilak, F. The slippery slope of arthritis. *Arthritis & Rheumatism* **52**, 1632–1633 (2005).

14. Lu, X., Khonsari, M. M. & Gelinck, E. R. M. The Stribeck curve: Experimental results and theoretical prediction. *Journal of Tribology* **128**, 789–794 (2006).

15. Ali, M. K. A. *et al.* Friction and wear reduction mechanisms of the reciprocating contact interfaces using nanolubricant under different loads and speeds. *Journal of Tribology* **140**, (2018).

16. Moody, H. R. *et al.* In vitro degradation of articular cartilage: Does trypsin treatment produce consistent results? *Journal of Anatomy* **209**, 259–267 (2006).

17. Wang, X.-B. & Liu, W.-M. Nanoparticle-Based Lubricant Additives. in *Encyclopedia of Tribology* 2369–2376 (Springer US, 2013).

18. Zou, Q. Nanoparticles in Automotive Applications. in *Encyclopedia of Tribology* 2376–2381 (Springer US, 2013).

19. Luo, T., Wei, X., Zhao, H., Cai, G. & Zheng, X. Tribology properties of Al2O3/TiO2 nanocomposites as lubricant additives. *Ceramics International* **40**, 10103–10109 (2014).

20. He, X., Xiao, H., Kyle, J. P., Terrell, E. J. & Liang, H. Two-dimensional nanostructured Y2O3 particles for viscosity modification. *Applied Physics Letters* **104**, 163107 (2014).

21. Kotia, A., Borkakoti, S. & Ghosh, S. K. Wear and performance analysis of a 4-stroke diesel engine employing nanolubricants. *Particuology* **37**, 54–63 (2018).

22. Greene, G. W. *et al.* Adaptive mechanically controlled lubrication mechanism found in articular joints. *Proceedings of the National Academy of Sciences of the United States of America* **108**, 5255-5259.

23. Bonnevie, E. D., Galesso, D., Secchieri, C., Cohen, I. & Bonassar, L. J. Elastoviscous Transitions of Articular Cartilage Reveal a Mechanism of Synergy between Lubricin and Hyaluronic Acid. *Plos One* (2015)

24. Ludwig, T. E., Hunter, M. M. & Schmidt, T. A. Cartilage boundary lubrication synergism is mediated by hyaluronan concentration and PRG4 concentration and structure. *BMC Musculoskeletal Disorders* **16**, 386 (2015).

25. Jahn, S. & Klein, J. Hydration Lubrication: The Macromolecular Domain. *Macromolecules* **48**, 5059–5075 (2015).

26. Ma, L., Gaisinskaya-Kipnis, A., Kampf, N. & Klein, J. Origins of hydration lubrication. *Nature Communications* **6** (2015).

27. Seror, J., Zhu, L., Goldberg, R., Day, A. J. & Klein, J. Supramolecular synergy in the boundary lubrication of synovial joints. *Nature Communications* (2015).

28. Jahn, S., Seror, J. & Klein, J. Lubrication of Articular Cartilage. *Annual Review of Biomedical Engineering* **18**, 235–258 (2016).

29. Horkay, F., Basser, P. J., Londono, D. J., Hecht, A. M. & Geissler, E. Ions in hyaluronic acid solutions. *Journal of Chemical Physics* **131**, (2009).

30. Jahn, S. & Klein, J. Hydration Lubrication: The Macromolecular Domain. *Macromolecules* **48**, 5059–5075 (2015).

31. Ma, L., Gaisinskaya-Kipnis, A., Kampf, N. & Klein, J. Origins of hydration lubrication. *Nature Communications* **6**, 1–6 (2015).

32. Raviv, U. & Klein, J. Fluidity of bound hydration layers. *Science* **297**, 1540–1543 (2002).

33. Greene, G. W. *et al.* Adaptive mechanically controlled lubrication mechanism found in articular joints. *Proceedings of the National Academy of Sciences of the United States of America* **108**, 5255-5259.

34. Leong, D. J., Hardin, J. A., Cobelli, N. J. & Sun, H. B. Mechanotransduction and cartilage integrity. *Annals of the New York Academy of Sciences* **1240**, 32–37 (2011).

35. Bader, D. L., Salter, D. M. & Chowdhury, T. T. Biomechanical Influence of Cartilage Homeostasis in Health and Disease. *Arthritis* **2011**, 1–16 (2011).

36. Sanchez-Adams, J., Leddy, H. A., McNulty, A. L., O'Conor, C. J. & Guilak, F. The Mechanobiology of Articular Cartilage: Bearing the Burden of Osteoarthritis. *Current Rheumatology Reports* **16**, 1–9 (2014).

37. Man, G. S. & Mologhianu, G. Osteoarthritis pathogenesis - a complex process that involves the entire joint. *Journal of medicine and life* **7**, 37–41 (2014).

38. Henrotin, Y. *et al.* Consensus statement on viscosupplementation with hyaluronic acid for the management of osteoarthritis. *Seminars in Arthritis and Rheumatism* **45**, 140–149 (2015).

39. Rutjes, A. W. S. *et al. Viscosupplementation for Osteoarthritis of the Knee A Systematic Review and Meta-analysis*. *Annals of internal medicine* **157**, 180-91 (2012).

40. Wathier, M. *et al.* A synthetic polymeric biolubricant imparts chondroprotection in a rat meniscal tear model. *Biomaterials* **182**, 13–20 (2018).

41. Wathier, M. *et al.* A large-molecular-weight polyanion, synthesized via ring-opening metathesis polymerization, as a lubricant for human articular cartilage. *Journal of the American Chemical Society* **135**, 4930–4933 (2013).

42. Banquy, X., Burdyńska, J., Lee, D. W., Matyjaszewski, K. & Israelachvili, J. Bioinspired bottle-brush polymer exhibits low friction and amontons-like behavior. *Journal of the American Chemical Society* **136**, 6199–6202 (2014).

43. Samaroo, K. J., Tan, M., Putnam, D. & Bonassar, L. J. Binding and lubrication of biomimetic boundary lubricants on articular cartilage; Binding and lubrication of biomimetic boundary lubricants on articular cartilage. *Journal of Orthopaedic Research* **35**, 548–557 (2017).

Table 6.1. Zeta Potential and Nanoparticle Size in deionized water and BSF as determined by DLS.

Charge	Zeta Potential in Deionized water*	Size in Deionized Water (nm)	Size in BSF (nm)
Positive	8.9 ± 2.1	101.16	285.91
Neutral	0.20 ± 1.5	89.14	110.32
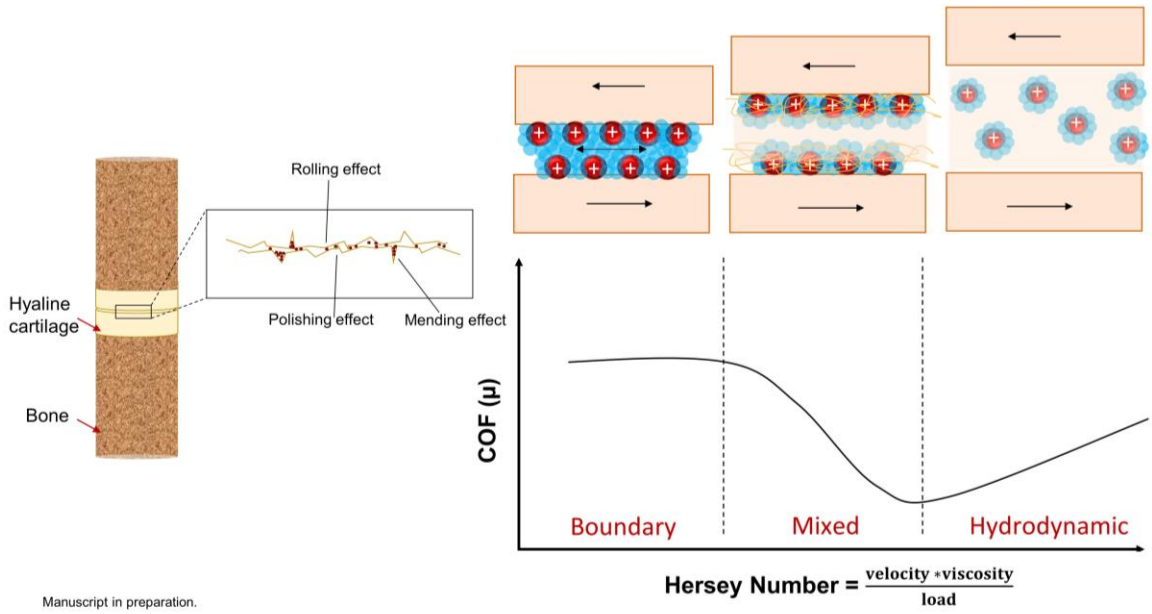
Figure 6.1. Mechanisms of action and Stribeck curve A) Schematic representing nanoparticle lubrication mechanism of action, lubricating the deformable material, hyaline cartilage. B) Stribeck curve representing coefficient of friction vs. hersey number depicting three modes of lubrication.
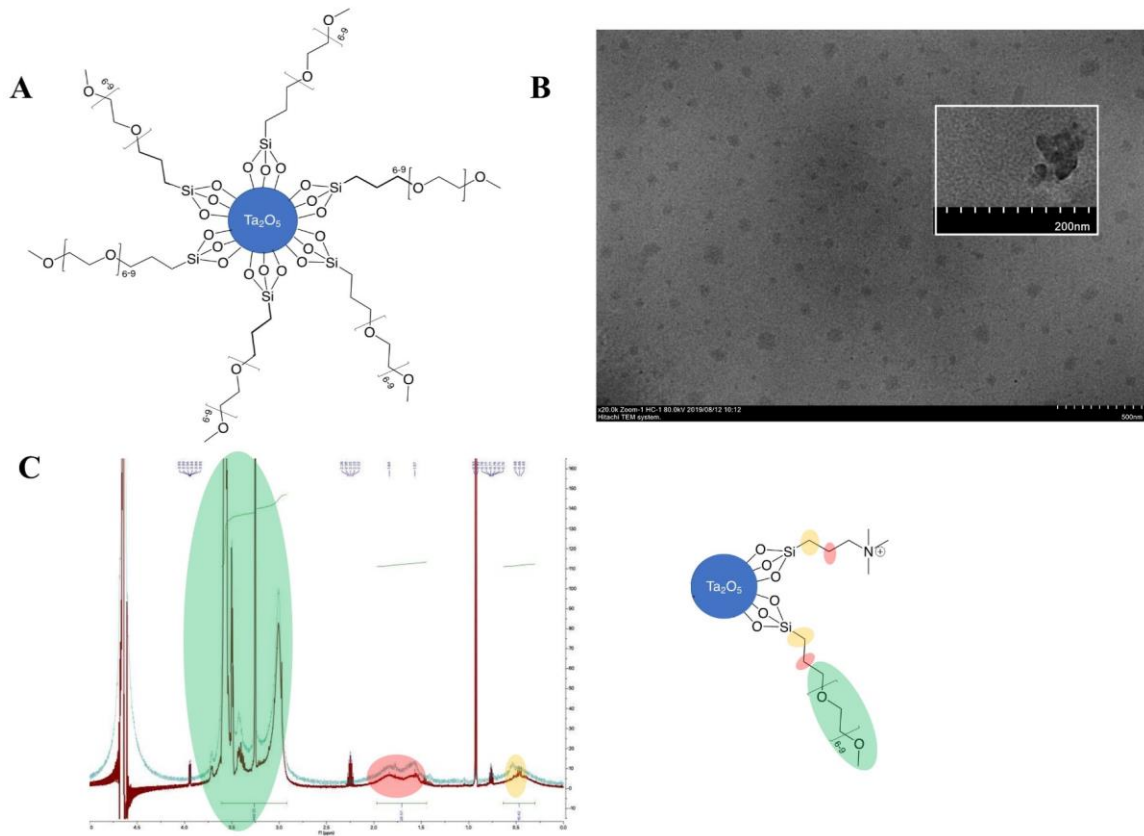
Figure 6.2. Characterization of tantalum oxide nanoparticles. **A**) schematic representation of nanoparticles synthesized. **B**) TEM image of synthesized nanoparticles. **C**) 1 H NMR showed the characteristic peaks and confirmed the silane coating on the particle.
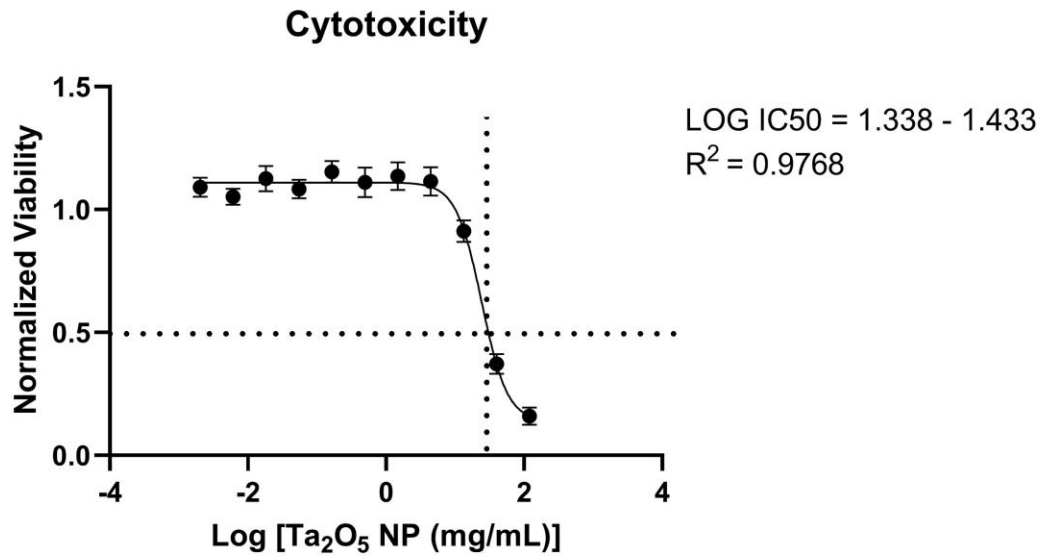
Figure 6.3. Tantalum oxide nanoparticle concentration response curve. IC50 of tantalum oxide nanoparticles determined by measuring cell viability of NIH 3T3 fibroblasts after 24 hours of exposure to varying concentrations, ranging from 120 mg/mL to 0.002 mg/mL of particles.
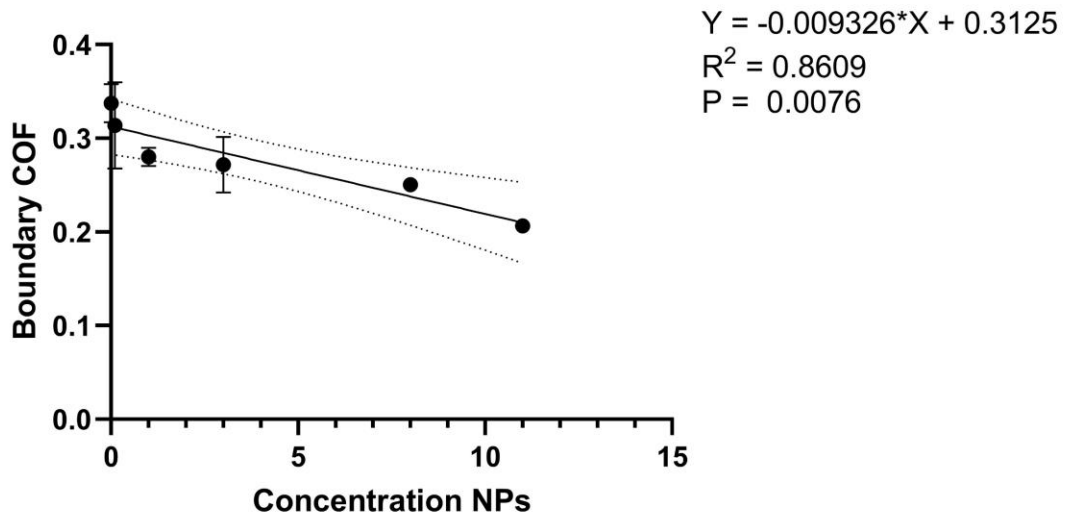
Figure 6.4. Nanolubricant Dose Response Curve. 100 nm diameter NP in BSF were prepared at a range of concentrations 0.01, 0.1, 1, 3, 8 and 11 wt%. The measured boundary COF varied linearly with nanoparticle concentration. N = 3 replicates, linear regression analysis, p = 0.0076, dashed lines indicate 95% confidence bands of best fit line.
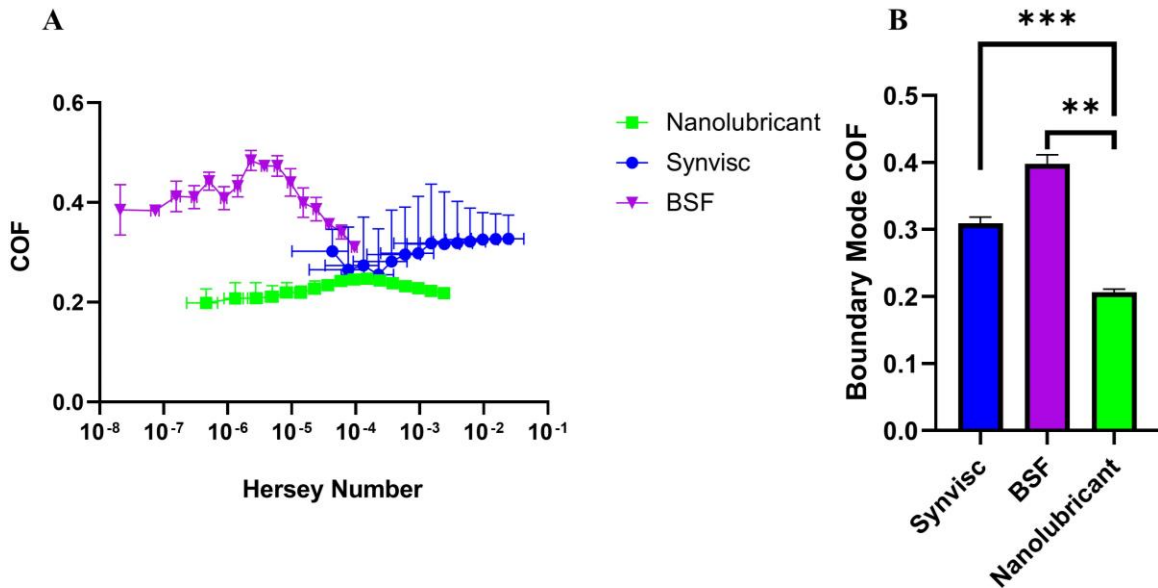
Figure 6.5. Non-deformable Body Stribeck Curves. **A**) Stribeck curves for nanolubricant with nanoparticles suspended at a concentration of 11 wt%, as well as two controls, BSF and Synvisc. Error bars represent standard deviation, N = 3 replicates. **B**) Average boundary mode coefficient of friction for the nanolubricant at 11 wt% nanoparticles and two controls, BSF and Synvisc. Error bars represent standard deviation, N = 3 replicates; one-way ANOVA used to compare groups, statistical difference indicated by asterisk, where ** $p<0.01$, *** $p<0.0001$.
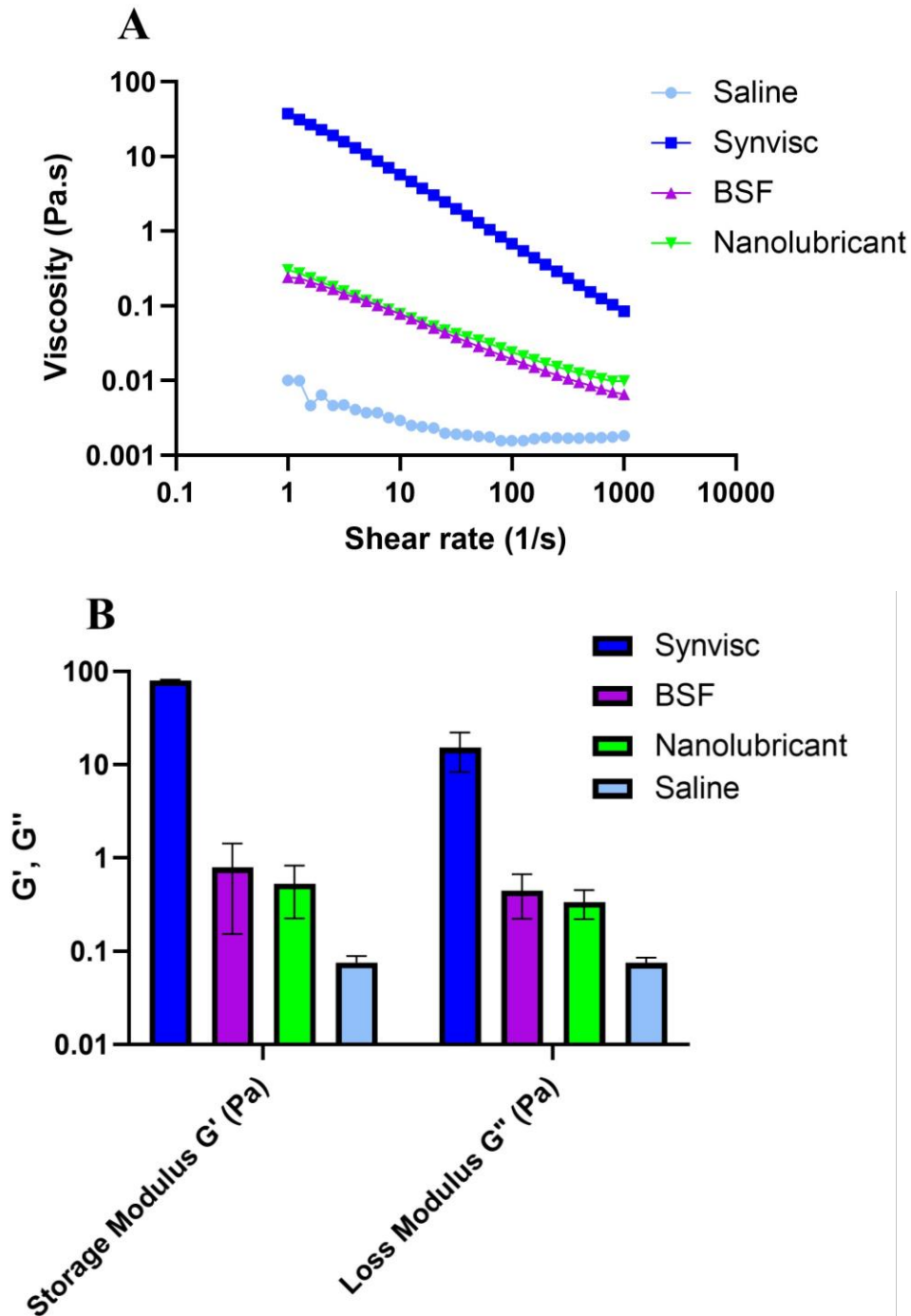
Figure 6.6. A) Viscosity values for controls, Synvisc and BSF, and nanolubricant at 11 wt%, viscosity as a function of shear rate. **B**) Storage and loss moduli Storage and loss moduli at a frequency of 2.5Hz. Moduli averaged over 11 logarithmically spaced data points spanning stress 1-10 Pa within linear viscoelastic region.
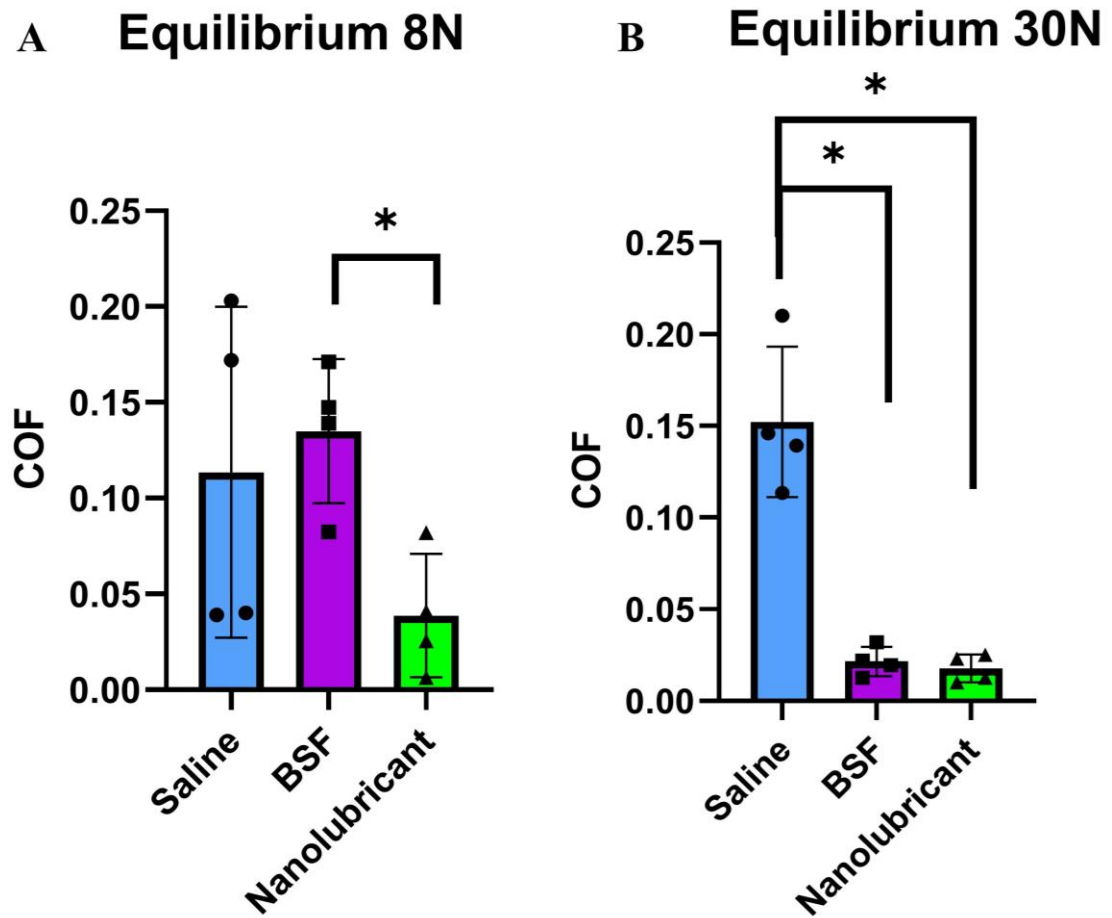
Figure 6.7. Cartilage Lubrication. **A**) Equilibrium coefficient of friction with an 8N load and rotational speed of 36 deg/second, for controls, saline and BSF, and nanolubricant at 11wt% concentration. **B**) Equilibrium coefficient of friction with a 30N load and rotational speed of 360 deg/second for controls, saline and BSF, and nanolubricant at 11wt% concentration. Error bars represent standard deviation, N = 4 replicates; one-way ANOVA used to compare groups, statistical difference indicated by asterisk, where $*$ $p<0.05$.
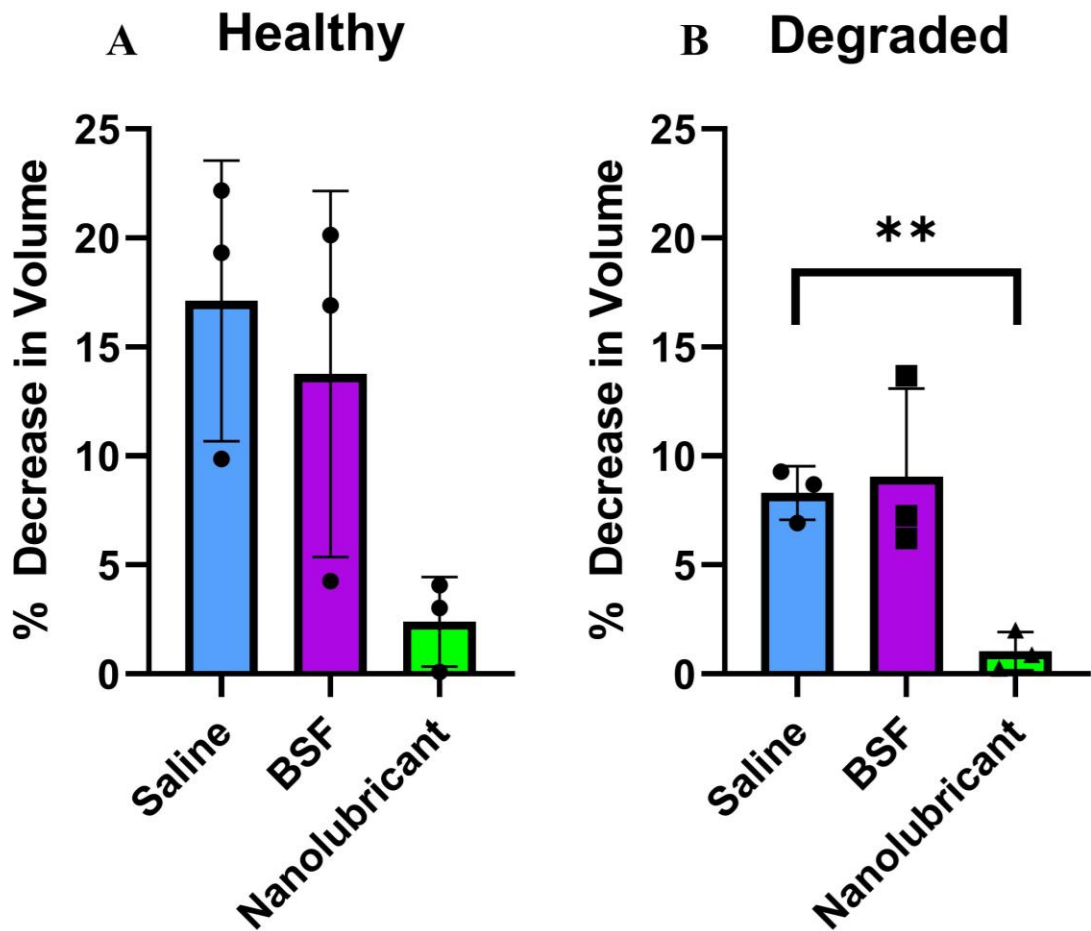
Figure 6.8. Cartilage Wear. **A**) Percent decrease in tissue volume using healthy bovine cartilage subject to a wear cycle of articulations for 105 minutes with a 30N load, lubricated with either controls, saline and BSF, or nanolubricant at 11 wt%. **B**) Percent decrease in tissue volume using trypsin degraded bovine cartilage subject to aforementioned wear cycle. Error bars represent standard deviation, N = 4 replicates; one-way ANOVA used to compare groups, statistical difference indicated by asterisk, where ** $p < 0.01$.

CHAPTER VII: Conclusion

7.1 Part I.

Plain radiography remains the most accessible tool and the current standard of care to diagnose OA. While it is accessible and inexpensive, it cannot directly visualize soft tissues or cartilage, and diagnoses are based solely on boney changes such as joint space narrowing, osteophytes, sclerosis, joint incongruity, and malalignment. Nanotechnology offers significant potential to enhance current OA management through new diagnostic capabilities. And while application of nanotechnology in orthopaedics remains in its infancy, a number of new technologies are in pre-clinical development to address the many facets of OA.

Specifically, nanoparticles of various compositions are explored in **Chapter 1** for their use as 1) MRI and CT contrast agents to provide quantitative assessment of a tissue component other than GAG; 2) functional MRI or CT agents that provide information on the biochemical or metabolic state of the tissue; 3) nanotracers for specific cells types; and 4) theranostics, which act simultaneously as a diagnostic agent and a therapy. However, there is currently no FDA approved nanotechnology for the diagnosis or treatment of OA and while advances in the synthesis of nanoparticles are yielding various types of nanoparticles for medical imaging, their use as has been restricted to non-quantitative imaging of soft tissues.

To advance the capabilities of contrast-enhanced CT imaging of articular cartilage for OA diagnosis, this work presents further development of a nanoparticle-based contrast agent for minimally invasive assessment of cartilage biochemical content (e.g., GAG

content) and mechanical integrity (e.g., E). Specifically, the ability of the cationic and neutral nanoparticle formulations to disseminate throughout the layers of cartilage to allow direct visualization of the soft tissue is initially established using an ex vivo human metacarpal phalangeal joint model (**Chapter 2**). The contrast-enhanced CT (CECT) with either of the nanoparticle contrast agents, cationic or neutral, is effective at determining GAG content and equilibrium modulus. Furthermore, in tandem with the sensitivity of the nanoparticle contrast agents for quantitative metrics of cartilage health, CT retains the ability to examine boney changes, presenting the potential for comparative studies of the crosstalk between cartilage and bone. CECT's sensitivity to biochemical and biomechanical properties, in conjunction with its ability to evaluate boney changes, signifies its utility as a diagnostic and monitoring agent for progression of OA, and potential as a research tool for both in vivo animal and human use. Additionally, results indicate the nanoparticle formulations described function to assess cartilage health minimally invasively.

In vivo experiments are warranted to next establish this technique as a potential alternative to histology. Specifically, an *in vivo* study that assesses NP enhanced attenuation to accurately measure cartilage properties throughout the progression of OA, with groups of animals euthanized at time points beginning from the very-early stages of OA. Diffusion kinetics of the three separate cartilage layers indicate the passive diffusion of the neutral nanoparticles does not follow an exponential model, and further experiments and modeling are necessary to parse out the effects of water, collagen, and glycosaminoglycan content on the diffusion kinetics. Tangentially, the cationic

nanoparticles actively diffuse into the cartilage due to electrostatic interactions with the negatively charged glycosaminoglycans. How glycosaminoglycan, collagen, and water content impact the active diffusion of the cationic particles requires further experimentation. Specifically, diffusion experiments for both nanoparticle formulations, using cartilage degraded with enzymes that target specific parts of the cartilage extracellular matrix, collagenase to degrade the collagen and hyaluronidase to degrade glycosaminoglycans, coupled with finite element modeling.

Early-stage treatment options are not yet a fully realized reality, as OA is typically detected its late stage when little cartilage is left to salvage and any reversible changes are long gone. Functional measures of tissue health apart from patient pain, such as the imaging technique described herein offer avenues potential to identify early-stage OA when early-stage treatments and preventative measures may be employed improve patient outcomes and the functional lifetime of their synovial joints.

7.2 Part II

Nanotechnology offers significant potential to enhance current OA management through targeted therapeutics, smart scaffolds, and novel viscosupplements. **Chapter 3** describes nano-based approaches to 1) provide delayed, sustained, or triggered drug release with increased joint retention, 2) reduce off-target side effects, 3) construct scaffolds incorporating nano-designs and structural features to recapitulate cartilage, augment biochemical constituents, and enhance biomechanical properties, and 4) to repair osteoarthritic tissue with the use of lubricants and engineered scaffolds. However, these nano-based treatments have yet to reach clinical use.

To date, the two most common, clinically utilized, non-surgical treatment options for OA are nonsteroidal anti-inflammatory drugs and viscosupplementation. Current viscosupplementation targets HA concentration restoration, increasing viscosity, improving lubricity, and enhancing cushioning properties of the SF, while on the macroscopic scale providing pain relief and improved ambulation. Viscosupplementation effectiveness remains debated, an equal number of studies supporting and rejecting its efficacy. **Chapter 4** highlights existing viscosupplements along with natural, partial, or full synthetic biolubricant formulations and their relationship to cartilage theory of lubrication.

Through this research an intricate understanding of biolubrication and biotribology has been gained, and lessons learned have informed the development of lubricants based on the concept of ball bearings between articulating surfaces — one out of single macromolecules (**Chapter 5**) and the other from nanoparticles (**Chapter 6**). The lubrication strategies presented in this dissertation have been tribologically and mechanically investigated for their ability to reduce friction and prevent wear between non-deformable and deformable materials. The macromolecule lubricant appears to be the first example of a lubricant composed of single particle, ultra-high molecular weight, macromolecules. Tribological results indicate these polymers lubricate via a mechanism independent of viscosity and by a method separate from a traditional mixed mode lubricant (i.e., synovial fluid) or a fluid lubricant (i.e., the HA viscosupplement Synvisc-One ®), functioning as small, interposed ball bearings between articulating surfaces to reduce friction and wear.

This tribological of ball bearings between articulating surfaces was further probed through the development of a biocompatible nanolubricant (**Chapter 6**). The nanolubricant described herein is capable of multimodal lubrication for non-deformable materials, in conjunction with reducing friction and wear between articulating poroelastic materials (e.g., articular cartilage). The nanolubricant functions under boundary and mixed mode lubrication mechanisms. We suggest the nanolubricant operates by hydration shell lubrication, where overlapping regions of water molecules surrounding the cationic nanoparticles function as a low viscosity lubricant, and by maintaining a hydrated, lubricious layer of associated water and HA molecules at the cartilage surface. It joins a class of tribological altering nanomaterials most commonly employed for lubrication of machinery (i.e., metal bearings and automotive applications)[17,18], but now demonstrates applicability to the living bearings of the body, synovial joints.

There are numerous remaining questions pertaining to these novel lubricants ranging from fundamental scientific questions to clinically relevant, biomechanical engineering questions. Future studies are required for translation of this device into clinical application. Specifically, joint space residence time course studies are necessary to validate the long-term presence and efficacy of the described lubricants in an *in vivo* OA animal model. Pertaining to the nanolubricant specifically, ascertaining what synovial fluid constituents specifically are adhering to the surface and how this is affecting the lubricating abilities requires further investigation. Firstly, we propose adding neutral nanoparticles to bovine synovial fluid (BSF) to ascertain if this formulation behaves differently than plain BSF or the nanolubricant. Secondly, we propose confirming it is HA aggregating around

the cationic particles by suspending the particles in BSF and allowing aggregation of the SF constituents, removing the particles from solution and staining what we postulate is HA surrounding the particles via hyaluronic acid binding protein coupled with a streptavidin 488 fluorophore and confocal imaging.

BIBLIOGRAPHY

AAOS.com. https://www.orthoguidelines.org/go/cpg/detail.cfm?id=1214.

Abbina, S. et al. Hyperbranched Polyglycerols: Recent Advances in Synthesis, Biocompatibility and Biomedical Applications. *Journal of Materials Chemistry B* **5**, 9249–9277 (2017).

Abubacker, S., Ham, H. O., Messersmith, P. B. & Schmidt, T. A. Cartilage boundary lubricating ability of aldehyde modified proteoglycan 4 (PRG4-CHO). *Osteoarthritis and Cartilage* **21**, 186–189 (2013).

Adams, M. E. et al. The role of viscosupplementation with hylan G-F 20 (Synvisc ®) in the treatment of osteoarthritis of the knee: a Canadian multicenter trial comparing hylan G-F 20 alone, hylan G-F 20 with non-steroidal anti-inflammatory drugs (NSAIDs) and NSAIDs alone. *Osteoarthritis and Cartilage* **3**(4), 213–225 (1995).

Aigner, T. et al. Large-scale gene expression profiling reveals major pathogenetic pathways of cartilage degeneration in osteoarthritis. *Arthritis and Rheumatism* **54**, 3533–3544 (2006).

Aigner, T., McKenna, L. Molecular Pathology and Pathobiology of Osteoarthritic Cartilage. *Cellular and Molecular Life Sciences* **59**, 5–18 (2002).

Ali, M. K. A. et al. Friction and wear reduction mechanisms of the reciprocating contact interfaces using nanolubricant under different loads and speeds. *Journal of Tribology* **140**, (2018).

Alizadeh Noghani, M. & Brooks, D. E. Progesterone Binding Nano-Carriers Based on Hydrophobically Modified Hyperbranched Polyglycerols. *Nanoscale* **8**, 5189–5199 (2016).

Altman, R. D., Rosen, J. E., Bloch, D. A., Hatoum, H. T. & Korner, P. A Double-Blind, Randomized, Saline-Controlled Study of the Efficacy and Safety of EUFLEXXA® for Treatment of Painful Osteoarthritis of the Knee, With an Open-Label Safety Extension (The FLEXX Trial). *Seminars in Arthritis and Rheumatism* **39,** 1–9 (2009).

Amin, S.; LaValley, M. P.; Guermazi, A.; Grigoryan, M.; Hunter, D. J.; Clancy, M.; Niu, J.; Gale, D. R.; Felson, D. T. The Relationship between Cartilage Loss on Magnetic Resonance Imaging and Radiographic Progression in Men and Women with Knee Osteoarthritis. Arthritis and Rheumatism **52**, 3152–3159 (2005).

Anilkumar, P. et al. Mega macromolecules as single molecule lubricants for hard and soft surfaces. *Nature Communications* **11**, 1–9 (2020).

Apostu, D. et al. Systemic drugs with impact on osteoarthritis. *Drug Metabolism Reviews* **51** 498–523 (2019).

Arita, T., Kayama, Y., Ohno, K., Tsujii, Y. & Fukuda, T. High-pressure Atom Transfer Radical Polymerization of Methyl Methacrylate for Well-Defined Ultrahigh Molecular-Weight Polymers. *Polymer* **49**, 2426–2429 (2008).

Armstrong, J. K., Wenby, R. B., Meiselman, H. J. & Fisher, T. C. The Hydrodynamic Radii of Macromolecules and their Effect on Red Blood Cell Aggregation. *Journal of Biophysics* **87**, 4259–70 (2004).

Arroll, B. & Goodyear-Smith, F. Corticosteroid injections for osteoarthritis of the knee: meta-analysis. *British Medical Journal* (Clinical research edition) **328**, 869 (2004).

Arslan, E. et al. Protective therapeutic effects of peptide nanofiber and hyaluronic acid hybrid membrane in in vivo osteoarthritis model. *Acta Biomaterialia* **73**, 263–274 (2018).

Arunkumar, P., Indulekha, S., Vijayalakshmi, S. & Srivastava, R. Poly (caprolactone) microparticles and chitosan thermogels based injectable formulation of etoricoxib for the potential treatment of osteoarthritis. *Materials Science and Engineering C* **61**, 534–544 (2016).

Ashton, J. R., West, J. L. & Badea, C. T. In vivo small animal micro-CT using nanoparticle contrast agents. *Frontiers in Pharmacology* **6**, 256 (2015).

Ateshian, G. A. The Role of Interstitial Fluid Pressurization in Articular Cartilage Lubrication. *Journal of Biomechanics* **42**, 1163-1176 (2009)

Attia, M. F., Wallyn, J., Anton, N. & Vandamme, T. F. Inorganic nanoparticles for X-ray computed tomography imaging. *Critical Reviews in Therapeutic Drug Carrier Systems* **35**, 391–432 (2018).

Au, J. T.; Craig, G.; Longo, V.; Zanzonico, P.; Mason, M.; Fong, Y.; Allen, P. J. Gold Nanoparticles Provide Bright Long-Lasting Vascular Contrast for CT Imaging. *American Journal of Roentgenology* **200**, 1347–1351 (2013).

Avouris, P., Freitag, M. & Perebeinos, V. Carbon-nanotube photonics and optoelectronics. *Nature Photonics* **2**, 341–350 (2008).

Áyen, Á., Martínez, Y. J., Marchal, J. A. & Boulaiz, H. Recent progress in gene therapy for ovarian cancer. *International Journal of Molecular Sciences* **19,** 1930 (2018).

Azzazy, H. M. E.; Mansour, M. M. H. In Vitro Diagnostic Prospects of Nanoparticles. *Clinica Chimica Acta* **403**(1–2), 1–8 2009.

Bader, D. L., Salter, D. M. & Chowdhury, T. T. Biomechanical Influence of Cartilage Homeostasis in Health and Disease. *Arthritis* 1–16 (2011).

Bae, D. K., Yoon, K. H. & Song, S. J. Cartilage Healing After Microfracture in Osteoarthritic Knees. *Arthroscopy: The Journal of Arthroscopic & Related Surgery* **22**, 367–374 (2006).

Bai, Y., He, J. & Zhang, Y. Ultra-High-Molecular-Weight Polymers Produced by the Immortal Phosphine-Based Catalyst System. *Angewandte Chemie (International Edition)* **57**, 17230–17234 (2018).

Banquy, X., Burdyńska, J., Lee, D. W., Matyjaszewski, K. & Israelachvili, J. Bioinspired bottle-brush polymer exhibits low friction and amontons-like behavior. *Journal of the American Chemical Society* **136**, 6199–6202 (2014).

Bansal, P. N., Stewart, R. C., Entezari, V., Snyder, B. D. & Grinstaff, M. W. Contrast agent electrostatic attraction rather than repulsion to glycosaminoglycans affords a greater contrast uptake ratio and improved quantitative CT imaging in cartilage. *Osteoarthritis and Cartilage* **19**, 970–976 (2011).

Barba, A. A., Bochicchio, S., Dalmoro, A. & Lamberti, G. Lipid delivery systems for nucleic-acid-based-drugs: From production to clinical applications. *Pharmaceutics* **11**(8), 360 (2019).

Bas, O. et al. Rational design and fabrication of multiphasic soft network composites for tissue engineering articular cartilage: A numerical model-based approach. *Chemical Engineering Journal* **340**, 15–23 (2018).

Bashir, A., Gray, M. L. & Burstein, D. Gd-DTPA2− as a measure of cartilage degradation. *Magnetic Resonance in Medicine* **36**, 665–673 (1996).

Bashir, A., Gray, M. L., Hartke, J. & Burstein, D. Nondestructive imaging of human cartilage glycosaminoglycan concentration by MRI. *Magnetic Resonance in Medicine* **41**, 857–865 (1999).

Beharaj, A., Ekladious, I. & Grinstaff, M. W. Poly(Alkyl Glycidate Carbonate)s as Degradable Pressure-Sensitive Adhesives. *Angewandte Chemie (International Edition)* **58**, 1407–1411 (2019).

Berenbaum, F. et al. A randomised, double-blind, controlled trial comparing two intra-articular hyaluronic acid preparations differing by their molecular weight in symptomatic knee osteoarthritis. *Annals of the Rheumatic Diseases* **71**, 1454–1460 (2012).

Bhattarai, A. et al. Dual contrast in computed tomography allows earlier characterization of articular cartilage over single contrast. *Journal of Orthopaedic Research* **38**, 2230–2238 (2020).

Bhave, G.; Lewis, J. B.; Chang, S. S. Association of Gadolinium Based Magnetic Resonance Imaging Contrast Agents and Nephrogenic Systemic Fibrosis. *Journal of Urology* **180**(3), 830–835 (2008).

Bignozzi, C., Carinci, F. & Caramori, S. Use of nanomaterials based on titanium dioxide and zirconium diozide as coatings for osteointegrated biomedical prostheses, and osteointegrated biomedical prostheses prepared therewith. (2012). US Patent US-20090270997-A1, https://portal.unifiedpatents.com/patents/patent/US-20090270997-A1

Bogdanov, A. A. et al. Synthesis and Testing of Modular Dual-Modality Nanoparticles for Magnetic Resonance and Multispectral Photoacoustic Imaging. *Bioconjugate Chemistry* **27**, 383–390 (2016).

Bonam, S. R., Areti, A., Komirishetty, P. & Muller, S. Dendrimers in immunotherapy and hormone therapy. In A. Chauhan and H. Kulhari (eds.) *Pharmaceutical Applications of Dendrimers,* pp. 233–249 (2020). Elsevier.

Bonitatibus, P. J.; Torres, A. S.; Goddard, G. D.; Fitzgerald, P. F.; Kulkarni, A. M. Synthesis, Characterization, and Computed Tomography Imaging of a Tantalum Oxide Nanoparticle Imaging Agent. *Chemical Communications* **46**, 8956–8958 (2010).

Bonitatibus, P. J.; Torres, A. S.; Kandapallil, B.; Lee, B. D.; Goddard, G. D.; Colborn, R. E.; Marino, M. E. Preclinical Assessment of a Zwitterionic Tantalum Oxide Nanoparticle X-Ray Contrast Agent. *ACS Nano* **6**, 6650–6658 (2012).

Bonnevie, E. D., Galesso, D., Secchieri, C., Cohen, I. & Bonassar, L. J. Elastoviscous Transitions of Articular Cartilage Reveal a Mechanism of Synergy between Lubricin and Hyaluronic Acid. *PLoS One* 10(11): e0143415 (2015). https://doi.org/10.1371/journal.pone.0143415

Bosman, A. W., Janssen, H. M. & Meijer, E. W. About Dendrimers: Structure, Physical Properties, and Applications. *Chemical Reviews* **99**, 1665–1688 (1999).

Botter, S. M.; van Osch, G. J. V. M.; Clockaerts, S.; Waarsing, J. H.; Weinans, H.; van Leeuwen, J. P. T. M. Osteoarthritis Induction Leads to Early and Temporal Subchondral Plate Porosity in the Tibial Plateau of Mice: An in Vivo Microfocal Computed Tomography Study. *Arthritis and Rheumatism* **63**, 2690–2699 (2011).

Botter, S. M.; van Osch, G. J. V. M.; Waarsing, J. H.; Day, J. S.; Verhaar, J. A. N.; Pols, H. A. P.; van Leeuwen, J. P. T. M.; Weinans, H. Quantification of Subchondral Bone

Changes in a Murine Osteoarthritis Model Using Micro-CT. *Biorheology* **43**, 379–388 (2006).

Braun, H. J.; Gold, G. E. Diagnosis of Osteoarthritis: Imaging. *Bone* **51**, 278–288 (2012).

Briscoe, W. H. et al. Boundary Lubrication under Water. *Nature* **444**, 191–194 (2006).

Brown, S., Kumar, S. & Sharma, B. Intra-articular targeting of nanomaterials for the treatment of osteoarthritis. *Acta Biomaterialia* **93**, 239–257 (2019).

Brown, T. D., Dalton, P. D. & Hutmacher, D. W. Direct Writing By Way of Melt Electrospinning. *Advanced Materials* **23**, 5651–5657 (2011).

Buckwalter, K. A. CT Arthrography. *Clinical Journal of Sport Medicine* **25**, 899–915 (2006).

Cai, Z., Zhang, H., Wei, Y., Wu, M. & Fu, A. Shear-thinning hyaluronan-based fluid hydrogels to modulate viscoelastic properties of osteoarthritis synovial fluids. *Biomaterials Science* **7**, 3143–3157 (2019).

Caligaris, M. & Ateshian, G. A. Effects of sustained interstitial fluid pressurization under migrating contact area, and boundary lubrication by synovial fluid, on cartilage friction. *Osteoarthritis and Cartilage* **16**, 1220–1227 (2008).

Chaisson, C. E.; Zhang, Y.; McAlindon, T. E.; Hannan, M. T.; Aliabadi, P.; Naimark, A.; Levy, D.; Felson, D. T. Radiographic Hand Osteoarthritis: Incidence, Patterns, and Influence of Pre-Existing Disease in a Population Based Sample. *The Journal of Rheumatology* **24**, 1337–1343 (1997).

Chang, G.; Xia, D.; Chen, C.; Madelin, G.; Abramson, S. B.; Babb, J. S.; Saha, P. K.; Regatte, R. R. 7T MRI Detects Deterioration in Subchondral Bone Microarchitecture in Subjects with Mild Knee Osteoarthritis as Compared with Healthy Controls. *Journal of Magnetic Resonance Imaging* **41**, 1311–1317 (2015)

Chauhan, A., Krynicka, D. & Singh, M. K. Therapeutic dendrimers. In A. Chauhan and H. Kulhari (eds.) *Pharmaceutical Applications of Dendrimers*, pp. 275–287 (2020). Elsevier.

Chawla, K., Ham, H. O., Nguyen, T. & Messersmith, P. B. Molecular resurfacing of cartilage with proteoglycan 4. *Acta Biomaterialia* **6**, 3388–3394 (2010).

Chejara, D. et al. Synthesis and Evaluation of a Sodium Alginate-4-Aminosalicylic Acid Based Microporous Hydrogel for Potential Viscosupplementation for Joint Injuries and Arthritis-Induced Conditions. *Marine Drugs* **15**, 257 (2017).

Chen, D.; Shen, J.; Zhao, W.; Wang, T.; Han, L.; Hamilton, J. L.; Im, H. J. Osteoarthritis: Toward a Comprehensive Understanding of Pathological Mechanism. *Bone Research* **5**, 16044 (2017)

Chen, H. et al. Cartilage matrix-inspired biomimetic superlubricated nanospheres for treatment of osteoarthritis. *Biomaterials* **242**, 119931 (2020).

Chen, J. et al. In Vivo MRI Tracking of Polyethylenimine-Wrapped Superparamagnetic Iron Oxide Nanoparticle-Labeled BMSCs for Cartilage Repair: A Minipig Model. *Cartilage* **4**, 75–82 (2013).

Chen, J. et al. In vivo tracking of superparamagnetic iron oxide nanoparticle labeled chondrocytes in large animal model. *Annals of Biomedical Engineering* **40**, 2568–2578 (2012).

Chen, L. et al. Cationic poly-l-lysine-encapsulated melanin nanoparticles as efficient photoacoustic agents targeting to glycosaminoglycans for the early diagnosis of articular cartilage degeneration in osteoarthritis. *Nanoscale* **10**, 13471–13484 (2018).

Chen, M., Briscoe, W. H., Armes, S. P. & Klein, J. Lubrication at physiological pressures by polyzwitterionic brushes. *Science* **323**, 1698–1701 (2009).

Chen, M., Briscoe, W. H., Armes, S. P., Cohen, H. & Klein, J. Polyzwitterionic brushes: Extreme lubrication by design. *European Polymer Journal* **47**, 511-523 (2011).

Chen, M., Briscoe, W. H., Armes, S. P., Cohen, H. & Klein, J. Robust, biomimetic polymer brush layers grown directly from a planar mica surface. *ChemPhysChem* **8**, 1303–1306 (2007).

Chen, Z. et al. Non-invasive monitoring of in vivo hydrogel degradation and cartilage regeneration by multiparametric MR imaging. *Theranostics* **8**, 1146–1158 (2018).

Chevalier, X. et al. Single, intra-articular treatment with 6 ml hylan G-F 20 in patients with symptomatic primary osteoarthritis of the knee: A randomised, multicentre, double-blind, placebo controlled trial. *Annals of the Rheumatic Diseases* **69**, 113–119 (2010).

Cho, H. et al. Theranostic immunoliposomes for osteoarthritis. *Nanomedicine: Nanotechnology, Biology, and Medicine* **10**, 619–627 (2014).

Clements, K. M., Hollander, A. P., Sharif, M. & Adams, M. A. Cyclic loading can denature type II collagen in articular cartilage. *Connective Tissue Research* **45**, 174–180 (2004).

Coburn, J. et al. Biomimetics of the extracellular matrix: An integrated three-dimensional fiber-hydrogel composite for cartilage tissue engineering. *Smart Structures and Systems* **7**, 213–222 (2011).

Coburn, J. M., Gibson, M., Monagle, S., Patterson, Z. & Elisseeff, J. H. Bioinspired nanofibers support chondrogenesis for articular cartilage repair. *Proceedings of the National Academy of Sciences of the United States of America* **109**, 10012–10017 (2012).

Cole, B. J., Karas, V., Hussey, K., Pilz, K. & Fortier, L. A. Hyaluronic Acid Versus Platelet-Rich Plasma. *American Journal of Sports Medicine* **45**, 339–346 (2017).

Cole, L. E.; Ross, R. D.; Tilley, J. M.; Vargo-Gogola, T.; Roeder, R. K. Gold Nanoparticles as Contrast Agents in X-Ray Imaging and Computed Tomography. *Nanomedicine* **10**, 321–341 (2015).

Coles, J. M., Chang, D. P. & Zauscher, S. Molecular Mechanisms of Aqueous Boundary Lubrication by Mucinous Glycoproteins. *Current Opinion in Colloid & Interface Science* **15**, 406–416 (2010).

Cormode, D. P.; Naha, P. C.; Fayad, Z. A. Nanoparticle Contrast Agents for Computed Tomography: A Focus on Micelles. *Contrast Media and Molecular Imaging* **9**, 37–52 (2014)

Crawford R, Dogdas B, Keough E, et al. Analysis of Lipid Nanoparticles by Cryo-EM for Characterizing SiRNA Delivery Vehicles. *International Journal of Pharmaceutics* **403**, 237–244 (2011).

Cunha, P. L. R., Castro, R. R., Rocha, F. A. C., de Paula, R. C. M. & Feitosa, J. P. A. Low viscosity hydrogel of guar gum: Preparation and physicochemical characterization. *International Journal of Biological Macromolecules* **37**, 99–104 (2005).

Curvale, R., Masuelli, M. & Padilla, A. P. Intrinsic Viscosity of Bovine Serum Albumin Conformers. *International Journal of Biological Macromolecules* **42**, 133–137 (2008).

Dalton, P. D., Joergensen, T. & Groll, J. Additive manufacturing of scaffolds with sub-micron filaments via melt electrospinning writing Related content Patterned melt electrospun substrates for tissue engineering. *Biofabrication* **7**, (2015)

Deirmengian, C. A. & Lonner, J. H. What's new in adult reconstructive knee surgery. *Journal of Bone and Joint Surgery - Series A* **90**, 2556–2565 (2008).

DiMicco, M. A. et al. Mechanisms and Kinetics of Glycosaminoglycan Release Following In Vitro Cartilage Injury. *Arthritis and Rheumatism* **50**, 840–848 (2004).

Ding, C. et al. Natural history of knee cartilage defects and factors affecting change. *Archives of Internal Medicine* **166**, 651–658 (2006).

Doyle, P. S., Shaqfeh, E. S. G. & Gast, A. P. Rheology of Polymer Brushes: A Brownian Dynamics Study. *Macromolecules* **311**, 5474–5486 (1998).

Eckstein Reiser M, Englmeier KH, Putz R., F. In vivo morphometry and functional analysis of human articular cartilage with quantitative magnetic resonance imaging - from image to data, from data to theory. *Anatomy and Embryology* **203**, 147–173 (2001).

Edmonds, S. Therapeutic targets for osteoarthritis. *Maturitas* **63**, 191–194 (2009).

Egger, P.; Cooper, C.; Hart, D. J.; Doyle, D. v.; Coggon, D.; Spector, T. D. Patterns of Joint Involvement in Osteoarthritis of the Hand: The Chingford Study. *Journal of Rheumatology* **22**, 1509–1513 (1995).

El-Fiqi, A., Kim, J. H. & Kim, H. W. Osteoinductive fibrous scaffolds of biopolymer/mesoporous bioactive glass nanocarriers with excellent bioactivity and long-term delivery of osteogenic drug. *ACS Applied Materials and Interfaces* **7**, 1140–1152 (2015).

Elron-Gross, I., Glucksam, Y. & Margalit, R. Liposomal dexamethasone-diclofenac combinations for local osteoarthritis treatment. *International Journal of Pharmaceutics* **376**, 84–91 (2009).

Elsaid, K. A., Jay, G. D., Warman, M. L., Rhee, D. K. & Chichester, C. O. Association of articular cartilage degradation and loss of boundary-lubricating ability of synovial fluid following injury and inflammatory arthritis. *Arthritis and Rheumatism* **52**, 1746–1755 (2005).

Elsaid, K. A., Machan, J. T., Waller, K., Fleming, B. C. & Jay, G. D. The Impact of Anterior Cruciate Ligament Injury on Lubricin Metabolism and the Effect of Inhibiting Tumor Necrosis Factor A on Chondroprotection in an Animal Model. *Arthritis and Rheumatology* **60**, 2997–3006 (2009).

Esposito Corcione, C. et al. The feasibility of printing polylactic acid-nanohydroxyapatite composites using a low-cost fused deposition modeling 3D printer. *Journal of Applied Polymer Science* **134**(13), (2017). https://doi.org/10.1002/app.44656

Evans, C. H., Kraus, V. B. & Setton, L. A. Progress in intra-articular therapy. *Nature Reviews. Rheumatology* **10**, 11–22 (2014).

Evans, J. T. et al. How long does a knee replacement last? A systematic review and meta-analysis of case series and national registry reports with more than 15 years of follow-up. *The Lancet* **393**, 655–663 (2019).

Fan, W. et al. Intra-articular injection of kartogenin-conjugated polyurethane nanoparticles attenuates the progression of osteoarthritis. *Drug Delivery* **25**, 1004–1012 (2018).

Farka, Z.; Juřík, T.; Kovář, D.; Trnková, L.; Skládal, P. Nanoparticle-Based Immunochemical Biosensors and Assays: Recent Advances and Challenges. *Chemical Reviews*. **117**, 9973–10042 (2017).

Farrell, E. et al. Cell labelling with superparamagnetic iron oxide has no effect on chondrocyte behaviour. *Osteoarthritis and Cartilage* **17**, 961–967 (2009).

FDA's Regulatory Science Program for Generic PLA/ PLGA-Based Drug Products | American Pharmaceutical Review - The Review of American Pharmaceutical Business & Technology. https://www.americanpharmaceuticalreview.com/Featured-Articles/188841-FDA-s-Regulatory-Science-Program-for-Generic-PLA-PLGA-Based-Drug-Products/.

Feng, P., Niu, M., Gao, C., Peng, S. & Shuai, C. A novel two-step sintering for nano-hydroxyapatite scaffolds for bone tissue engineering. *Scientific Reports* **4**, 1–10 (2014).

Feng, Y. et al. In vitro targeted magnetic delivery and tracking of superparamagnetic iron oxide particles labeled stem cells for articular cartilage defect repair. *Journal of Huazhong University of Science and Technology - Medical Science* **31**, 204–209 (2011).

Filardo, G. et al. Platelet-rich plasma vs hyaluronic acid to treat knee degenerative pathology: Study design and preliminary results of a randomized controlled trial. *BMC Musculoskeletal Disorders* **13**, 229 (2012).

Fitzgerald, P. F. et al. Proposed computed tomography contrast agent using carboxybetaine zwitterionic tantalum oxide nanoparticles imaging, biological, and physicochemical performance. *Investigative Radiology* **51**, 786–796 (2016).

Fitzgerald, P. F.; Butts, M. D.; Roberts, J. C.; Colborn, R. E.; Torres, A. S.; Lee, B. D.; Yeh, B. M.; Bonitatibus, P. J. Proposed Computed Tomography Contrast Agent Using Carboxybetaine Zwitterionic Tantalum Oxide Nanoparticles Imaging, Biological, and Physicochemical Performance. *Investigative Radiology* **51**, 786–796 (2016).

Flannery, C. R. et al. Prevention of cartilage degeneration in a rat model of osteoarthritis by intraarticular treatment with recombinant lubricin. *Arthritis and Rheumatism* **60**, 840–847 (2009).

Flory, P. J. Spatial Configuration of Macromolecular Chains. *Science* **188**, 1268–1276 (1975).

Fréchet, J. M. J. Dendrimers and Supramolecular Chemistry. *Proceedings of the National Academy of Sciences of the United States of America* **99**, 4782–4787 (2002).

Freedman, J. D.; Lusic, H.; Snyder, B. D.; Grinstaff, M. W. Tantalum Oxide Nanoparticles for the Imaging of Articular Cartilage Using X-Ray Computed Tomography: Visualization of Ex Vivo/in Vivo Murine Tibia and Ex Vivo Human Index Finger Cartilage. *Angewandte Chemie - International Edition* **53**, 8406–8410 (2014).

Fu, Q., Zhu, R., Song, J., Yang, H. & Chen, X. Photoacoustic Imaging: Contrast Agents and Their Biomedical Applications. *Advanced Materials* **31**, 1805875 (2018).

Furmann, D. et al. The effect of synovial fluid composition, speed and load on frictional behaviour of articular cartilage. *Materials* **13**, 1334 (2020). https://dx.doi.org/10.3390%2Fma13061334

Gagnier, J. J. Patient Reported Outcomes in Orthopaedics. *Journal of Orthopaedic Research* **35**, 2098–2108 (2017).

Gallo, J. et al. Silver nanocoating technology in the prevention of prosthetic joint infection. *Materials* **9**(5), 337 (2016). https://dx.doi.org/10.3390%2Fma9050337

Gallo, J., Holinka, M. & Moucha, C. S. Antibacterial surface treatment for orthopaedic implants. *International Journal of Molecular Sciences* **15**, 13849–13880 (2014).

Gao, J. Q. et al. Gene-carried chitosan-linked-PEI induced high gene transfection efficiency with low toxicity and significant tumor-suppressive activity. *International Journal of Pharmaceutics* **387**, 286–294 (2010).

Garnero, P. et al. Cross sectional evaluation of biochemical markers of bone, cartilage, and synovial tissue metabolism in patients with knee osteoarthritis: Relations with disease activity and joint damage. *Annals of the Rheumatic Diseases* **60**, 619–626 (2001).

Ge, L. et al. Nanosilver particles in medical applications: Synthesis, performance, and toxicity. *International Journal of Nanomedicine* **9**, 2399–2407 (2014).

Geiger, B. C., Wang, S., Padera, R. F., Grodzinsky, A. J. & Hammond, P. T. Cartilage-penetrating nanocarriers improve delivery and efficacy of growth factor treatment of osteoarthritis. *Science Translational Medicine* **10**(469), eaat8800 (2018). doi: 10.1126/scitranslmed.aat8800

Gigis, I., Fotiadis, E., Nenopoulos, A., Tsitas, K. & Hatzokos, I. Comparison of two different molecular weight intra-articular injections of hyaluronic acid for the treatment of knee osteoarthritis. *Hippokratia* **20**, 26–31 (2016).

Gleghorn, J. P., Jones, A. R. C., Flannery, C. R. & Bonassar, L. J. Boundary mode lubrication of articular cartilage by recombinant human lubricin. *Journal of Orthopaedic Research* **27**, 771–777 (2009).

Goldberg, R. et al. Boundary Lubricants with Exceptionally Low Friction Coefficients Based on 2D Close-Packed Phosphatidylcholine Liposomes. *Advanced Materials* **23**, 3517–3521 (2011).

Goldberg, R., Schroeder, A., Barenholz, Y. & Klein, J. Interactions between adsorbed hydrogenated soy phosphatidylcholine (HSPC) vesicles at physiologically high pressures and salt concentrations. *Biophysical Journal* **100**, 2403–2411 (2011).

Goldring, S. R. Needs and opportunities in the assessment and treatment of osteoarthritis of the knee and hip: The view of the rheumatologist. *Journal of Bone and Joint Surgery - Series A* **91**, 4–6 (2009).

Goodman, S. B., Gibon, E. & Yao, Z. The basic science of periprosthetic osteolysis. *Instructional course lectures* **62**, 201–6 (2013).

Gray, M. L., Burstein, D., Kim, Y.-J. & Maroudas, A. Magnetic resonance imaging of cartilage glycosaminoglycan: Basic principles, imaging technique, and clinical applications. *Journal of Orthopaedic Research* **26**, 281–291 (2008).

Grayson, S. M. & Fréchet, J. M. J. Convergent Dendrons and Dendrimers: from Synthesis to Applications. *Chemical Reviews* **101**, 3819–3868 (2001).

Greene, G. W. et al. Adaptive Mechanically Controlled Lubrication Mechanism Found in Articular Joints. *Proceedings of the National Academy of Sciences of the United States of America* **108**(13), 5255–5259 (2011).

Grinstaff, M. W. Biodendrimers: New Polymeric Biomaterials for Tissue Engineering. *Chemistry – A European Journal* **8**, 2838 (2002).

Grobner, T. Gadolinium - A Specific Trigger for the Development of Nephrogenic Fibrosing Dermopathy and Nephrogenic Systemic Fibrosis. *Nephrology Dialysis Transplantation* **21**, 1104–1108 (2006).

Grodzinsky, A. J., Wang, Y., Kakar, S., Vrahas, M. S. & Evans, C. H. Intra-articular dexamethasone to inhibit the development of post-traumatic osteoarthritis. *Journal of Orthopaedic Research* **35,** 406–411 (2017).

Guilak, F. Biomechanical factors in osteoarthritis. *Best Practice and Research: Clinical Rheumatology* **25**, 815–823 (2011).

Guilak, F. The slippery slope of arthritis. *Arthritis and Rheumatism* **52**, 1632–1633 (2005).

Hahn, D. K. & Aragon, S. R. Intrinsic Viscosity of Proteins and Platonic Solids by Boundary Element Methods. *Journal of Chemical Theory and Computation* **2**, 1416–1428 (2006).

Han, X.; Xu, K.; Taratula, O.; Farsad, K. Applications of Nanoparticles in Biomedical Imaging. *Nanoscale* **11**(3), 799–819 (2019). https://doi.org/10.1039/C8NR07769J

Hawker, C. J., Farrington, P. J., Mackay, M. E., Wooley, K. L. & Frechet, J. M. J. Molecular Ball Bearings: The Unusual Melt Viscosity Behavior of Dendritic Macromolecules. *Journal of the American Chemical Society* **117**, 4409–4410 (1995).

Hayami, T.; Pickarski, M.; Zhuo, Y.; Wesolowski, G. A.; Rodan, G. A.; Duong, L. T. Characterization of Articular Cartilage and Subchondral Bone Changes in the Rat Anterior Cruciate Ligament Transection and Meniscectomized Models of Osteoarthritis. *Bone* **38**, 234–243 (2006)

Hayashi, D., Roemer, F. W. & Guermazi, A. Imaging for osteoarthritis. *Annals of Physical and Rehabilitation Medicine* **59**, 161–169 (2016).

Hayes, A. J. & Melrose, J. Glycosaminoglycan and Proteoglycan Biotherapeutics in Articular Cartilage Protection and Repair Strategies: Novel Approaches to Visco-supplementation in Orthobiologics. *Advanced Therapeutics* **2**, 1900034 (2019).

He, X., Xiao, H., Kyle, J. P., Terrell, E. J. & Liang, H. Two-dimensional nanostructured Y2O3 particles for viscosity modification. *Applied Physics Letters* **104**, 163107 (2014).

Henrotin, Y. et al. Consensus statement on viscosupplementation with hyaluronic acid for the management of osteoarthritis. *Seminars in Arthritis and Rheumatism* **45**, 140–149 (2015).

Herzog, W. The Multiple Roles of Titin in Muscle Contraction and Force Production. *Biophysical Reviews* **10**, 1187–1199 (2018).

Hess, E. & Cobure, A. The Intrinsic Viscosity of Mixed Protein Systems, Including Studies of Plasma and Serum. *The Journal of General Physiology* **33**, 511–523 (1950).

Hills, B. A. & Monds, M. K. Deficiency of lubricating surfactant lining the articular surfaces of replaced hips and knees. *British Journal of Rheumatology* **37**, 143–147 (1998).

Holzinger, M.; Goff, A. le; Cosnier, S. Nanomaterials for Biosensing Applications: A Review. *Frontiers in Chemistry* **2**, 63 (2014). https://doi.org/10.3389/fchem.2014.00063

Honkanen, M. K. M. et al. Triple Contrast CT Method Enables Simultaneous Evaluation of Articular Cartilage Composition and Segmentation. *Annals of Biomedical Engineering* **48**, 556–567 (2020).

Honkanen, M. K. M.; Saukko, A. E. A.; Turunen, M. J.; Xu, W.; Lovric, G.; Honkanen, J. T. J.; Grinstaff, M. W.; Lehto, V. P.; Töyräs, J. Triple Contrast CT Method Enables Simultaneous Evaluation of Articular Cartilage Composition and Segmentation. *Annals of Biomedical Engineering* **48**, 556–567 (2020)

Horkay, F., Basser, P. J., Londono, D. J., Hecht, A. M. & Geissler, E. Ions in hyaluronic acid solutions. *Journal of Chemical Physics* **131**, (2009).

Hsu, S. M. Nano-lubrication: Concept and design. *Tribology International* **37**, 537–545 (2004).

Hu, Q. et al. Polyethylene glycol modified PAMAM dendrimer delivery of kartogenin to induce chondrogenic differentiation of mesenchymal stem cells. *Nanomedicine: Nanotechnology, Biology, and Medicine* **13**, 2189–2198 (2017).

Huber, M, Trattnig, S. & Lintner, F. Anatomy, Biochemistry and Physiology of Articular Cartilage. *Investigative Radiology* **35**, 573–580 (2000).

Hunter D Grainger G, et al., G. D., Hunter, D., Gale, D. & Grainger, G. The reliability of a new scoring system for knee osteoarthritis MRI and the validity of bone marrow lesion assessment: BLOKS (Boston Leeds Osteoarthritis Knee Score). *Annals of the Rheumatic Diseases* **67**, 206–211 (2008).

Ibrahim, M. A. & Dublin, A. B. Magnetic Resonance Imaging (MRI), Gadolinium. StatPearls (StatPearls Publishing, 2018).

Imran ul-haq, M., Lai, B. F. L., Chapanian, R. & Kizhakkedathu, J. N. Influence of Architecture of High Molecular Weight Linear and Branched Polyglycerols on their Biocompatibility and Biodistribution. *Biomaterials* **33**, 9135–9147 (2012).

Imran ul-haq, M., Shenoi, R. A., Brooks, D. E. & Kizhakkedathu, J. N. Solvent-Assisted Anionic Ring Opening Polymerization of Glycidol: Toward Medium and High Molecular Weight Hyperbranched Polyglycerols. *Journal of Polymer Science Part A: Polymer Chemistry* **51**, 2614–2621 (2013).

Ishihara, M. et al. Usefulness of photoacoustic measurements for evaluation of biomechanical properties of tissue-engineered cartilage. *Tissue Engineering* **11** 1234–1243 (2005).

Jahn, S. & Klein, J. Hydration Lubrication: The Macromolecular Domain. *Macromolecules* **48**, 5059–5075 (2015).

Jahn, S., Seror, J. & Klein, J. Lubrication of Articular Cartilage. *Annual Review of Biomedical Engineering* **18**, 235–258 (2016).

Jain, K., Mehra, N. K., Jain, V. K. & Jain, N. K. IPN Dendrimers in Drug Delivery. In: Jana S., Jana S. (eds.) *Interpenetrating Polymer Network: Biomedical Applications*. Springer, Singapore. (2020) https://doi.org/10.1007/978-981-15-0283-5_6

Jasmin et al. Labeling stem cells with superparamagnetic iron oxide nanoparticles: Analysis of the labeling efficacy by microscopy and magnetic resonance imaging. *Methods in Molecular Biology* **906**, 239–252 (2012).

Jay, G. D. et al. Prevention of cartilage degeneration and restoration of chondroprotection by lubricin tribosupplementation in the rat following anterior cruciate ligament transection. *Arthritis and Rheumatism* **62**, 2382–2391 (2010).

Jiang, Y. & Pu, K. Advanced Photoacoustic Imaging Applications of Near-Infrared Absorbing Organic Nanoparticles. *Small* **13**, 1700710 (2017).

Jo, J. et al. A Functional Study of Human Inflammatory Arthritis Using Photoacoustic Imaging. *Scientific Reports* **7**, 15026 (2017).

Jones, A. R. C. et al. Binding and localization of recombinant lubricin to articular cartilage surfaces. *Journal of Orthopaedic Research* **25**, 283–292 (2007).

Jørgensen, A. et al. Intra-articular hyaluronan is without clinical effect in knee osteoarthritis: A multicentre, randomised, placebo-controlled, double-blind study of 337 patients followed for 1 year. *Annals of the Rheumatic Diseases* **69**, 1097–1102 (2010).

Kainthan, R. K., Muliawan, E. B., Hatzikiriakos, S. G. & Brooks, D. E. Synthesis, Characterization, and Viscoelastic Properties of High Molecular Weight Hyperbranched Polyglycerols. *Macromolecules* **39**, 7708–7717 (2006).

Kalichman, L.; Hernández-Molina, G. Hand Osteoarthritis: An Epidemiological Perspective. *Seminars in Arthritis and Rheumatism* **39**(6), 465–476 (2010).

Kamigaito, M. & Satoh, K. Light Leads to Ultra-Long Polymer Chains in Water. *Chem* **2**, 13–15 (2017). https://doi.org/10.1016/j.chempr.2016.12.010

Kang, M. J. et al. Cationic PLGA/Eudragit RL nanoparticles for increasing retention time in synovial cavity after intra-articular injection in knee joint. *International Journal of Nanomedicine* **10**, 5263 (2015).

Kang, M.-L., Ko, J. Y., Kim, J. E. & Im, G.-I. Intra-articular delivery of kartogenin-conjugated chitosan nano/microparticles for cartilage regeneration. *Biomaterials* **35**(37), 9984–9994 (2014). https://doi.org/10.1016/j.biomaterials.2014.08.042

Kang, M.-L., Jeong, S.-Y. & Im, G.-I. Hyaluronic Acid Hydrogel Functionalized with Self-Assembled Micelles of Amphiphilic PEGylated Kartogenin for the Treatment of Osteoarthritis. *Tissue Engineering Part A* **23**, 630–639 (2017).

Kang, M.-L., Kim, J.-E. & Im, G.-I. Thermoresponsive nanospheres with independent dual drug release profiles for the treatment of osteoarthritis. *Acta Biomaterialia* **39**, 65–78 (2016).

Karlsson, J. Comparison of two hyaluronan drugs and placebo in patients with knee osteoarthritis. A controlled, randomized, double-blind, parallel-design multicentre study. *Rheumatology* **41**, 1240–1248 (2002).

Katz, J. N., Earp, B. E. & Gomoll, A. H. Surgical management of osteoarthritis. *Arthritis Care and Research* **62**, 1220–1228 (2010).

Kauffmann, C., Gravel, P., Godbout, B., al. Et & Kauffmann C Godbout B, et al., G. P. Computer-aided method for quantification of cartilage thickness and volume changes using MRI: validation study using a synthetic model. *IEEE Transactions on Biomedical Engineering* **50**, 978–988 (2003).

Kavanaugh, T. E., Werfel, T. A., Cho, H., Hasty, K. A. & Duvall, C. L. Particle-based technologies for osteoarthritis detection and therapy. *Drug Delivery and Translational Research* **6**, 132–147 (2016).

Kavehpour, H. P. & Mckinley, G. H. Tribo-Rheometry: From Gap-Dependent Rheology to Tribology. *Tribology Letters* **17**, 327–3335 (2004).

Kawadkar, J. & Chauhan, M. K. Intra-articular delivery of genipin cross-linked chitosan microspheres of flurbiprofen: Preparation, characterization, in vitro and in vivo studies. *European Journal of Pharmaceutics and Biopharmaceutics* **81**, 563–572 (2012).

Kawaguchi, S. et al. Aqueous Solution Properties of Oligo- and Poly(Ethylene Oxide) by Static Light Scattering and Intrinsic Viscosity. *Polymer* **38**, 2885–2891 (1997).

Kim, D.; Park, S.; Jae, H. L.; Yong, Y. J.; Jon, S. Antibiofouling Polymer-Coated Gold Nanoparticles as a Contrast Agent for in Vivo X-Ray Computed Tomography Imaging. *Journal of the American Chemical Society* **129**, 7661–7665 (2007).

Kirchner, M. & Marshall, D. A double-blind randomized controlled trial comparing alternate forms of high molecular weight hyaluronan for the treatment of osteoarthritis of the knee. *Osteoarthritis and Cartilage* **14**, 154–162 (2006).

Kirkley, A. et al. A randomized trial of arthroscopic surgery for osteoarthritis of the knee. *New England Journal of Medicine* **359**, 1097–1107 (2008).

Kloppenburg, M. & Berenbaum, F. Osteoarthritis year in review 2019: epidemiology and therapy. *Osteoarthritis and Cartilage* **28**, 242–248 (2020).

Kolarz, G., Kotz, R. & Hochmayer, I. Long-term benefits and repeated treatment cycles of intra-articular sodium hyaluronate (Hyalgan) in patients with osteoarthritis of the knee. *Seminars in Arthritis and Rheumatism* **32**, 310–319 (2003).

Kon, E. et al. Clinical results and MRI evolution of a nano-composite multilayered biomaterial for osteochondral regeneration at 5 years. *American Journal of Sports Medicine* **42**, 158–165 (2014).

Kon, E. et al. Novel nano-composite multilayered biomaterial for osteochondral regeneration: A pilot clinical trial. *American Journal of Sports Medicine* **39**, 1180–1190 (2011).

Kon, E. et al. Orderly osteochondral regeneration in a sheep model using a novel nano-composite multilayered biomaterial. *Journal of Orthopaedic Research* **28**(1), 116–124 (2009). https://doi.org/10.1002/jor.20958

Kon, E. et al. Platelet-rich plasma intra-articular injection versus hyaluronic acid viscosupplementation as treatments for cartilage pathology: From early degeneration to osteoarthritis. *Arthroscopy - Journal of Arthroscopic and Related Surgery* **27**, 1490–1501 (2011).

Korkusuz, F. Editorial comment: Nanoscience in musculoskeletal medicine general. *Clinical Orthopaedics and Related Research* **471**, 2530–2531 (2013).

Kotia, A., Borkakoti, S. & Ghosh, S. K. Wear and performance analysis of a 4-stroke diesel engine employing nanolubricants. *Particuology* **37**, 54–63 (2018).

Krishnan, R., Kopacz, M. & Ateshian, G. A. Experimental verification of the role of interstitial fluid pressurization in cartilage lubrication. *Journal of Orthopaedic Research* **22**, 565–570 (2004).

Kul-Panza, E. & Berker, N. Is hyaluronate sodium effective in the management of knee osteoarthritis? A placebo-controlled double-blind study. *Minerva Medica* **101**, 63–72 (2010).

Kumar, A., Bendele, A. M., Blanks, R. C. & Bodick, N. Sustained efficacy of intra-articular FX006 in a rat model of osteoarthritis. *Osteoarthritis and Cartilage* **20**, S289 (2012).

Labens, R., Daniel, C., Hall, S., Xia, X. R. & Schwarz, T. Effect of intra-articular administration of superparamagnetic iron oxide nanoparticles (SPIONs) for MRI assessment of the cartilage barrier in a large animal model. *PLoS ONE* **12**, (2017).

Lakin, B. A. et al. A Synthetic Bottle-Brush Polyelectrolyte Reduces Friction and Wear of Intact and Previously Worn Cartilage. *ACS Biomaterials Science and Engineering* **5**, 3060–3067 (2019).

Lakin, B. A. et al. Cationic agent contrast-enhanced computed tomography imaging of cartilage correlates with the compressive modulus and coefficient of friction. *Osteoarthritis and Cartilage* **21**, 60–68 (2013).

Lakin, B. A. et al. Contrast-enhanced CT facilitates rapid, non-destructive assessment of cartilage and bone properties of the human metacarpal. *Osteoarthritis and Cartilage* **23**, 2158–2166 (2015).

Lakin, B. A. et al. Contrast-enhanced CT using a cationic contrast agent enables non-destructive assessment of the biochemical and biomechanical properties of mouse tibial plateau cartilage. *Journal of Orthopaedic Research* **34**, 1130–1138 (2016).

Larguinho, M.; Baptista, P. V. Gold and Silver Nanoparticles for Clinical Diagnostics - From Genomics to Proteomics. *Journal of Proteomics* **75**(10), 2811–2823 (2012). https://doi.org/10.1016/j.jprot.2011.11.007.

Laroui, H. et al. Hyaluronate-covered nanoparticles for the therapeutic targeting of cartilage. *Biomacromolecules* **8**, 3879–3885 (2007).

Larsen, C. et al. Intra-articular depot formulation principles: Role in the management of postoperative pain and arthritic disorders. *Journal of Pharmaceutical Sciences* **97**, 4622–4654 (2008).

Lawrence, A. et al. Synthesis and characterization of a lubricin mimic (mLub) to reduce friction and adhesion on the articular cartilage surface. *Biomaterials* **73**, 42–50 (2015).

Lawson, T. B., Joenathan, A. T., Snyder, B. D. & Grinstaff, M. W. A Theranostic Nanolubricant. *ORS Annual Meeting* **41**, 1–7 (2020).

Lawson, T. B.; Mäkelä, J. T. A.; Klein, T.; Snyder, B. D.; Grinstaff, M. W. Nanotechnology and Osteoarthritis. Part 1: Clinical Landscape and Opportunities for Advanced Diagnostics. *Journal of Orthopaedic Research* **39**, 465-472 (2020).

Lawson, T. B.; Mäkelä, J. T. A.; Klein, T.; Snyder, B. D.; Grinstaff, M. W. Nanotechnology and Osteoarthritis. Part 2: Opportunities for Advanced Devices and Therapeutics. *Journal of Orthopaedic Research* **39**, 473-484 (2020).

Lee, C. C., Mackay, J. A. & Szoka, F. Designing Dendrimers for Biological Applications. *Nature Biotechnology* **23**, 1517–1526 (2005).

Lee, N., Choi, S. H. & Hyeon, T. Nano-Sized CT Contrast Agents. *Advanced Materials* **25**, 2641–2660 (2013).

Leone, G. et al. Enriched Gellan Gum hydrogel as viscosupplement. *Carbohydrate Polymers* **227**, 115347 (2020).

Leong, D. J., Hardin, J. A., Cobelli, N. J. & Sun, H. B. Mechanotransduction and cartilage integrity. *Annals of the New York Academy of Sciences* **1240**, 32–37 (2011).

Li, G.; Yin, J.; Gao, J.; Cheng, T. S.; Pavlos, N. J.; Zhang, C.; Zheng, M. H. Subchondral Bone in Osteoarthritis: Insight into Risk Factors and Microstructural Changes. *Arthritis Research and Therapy* **15**(6), 223 (2013). https://doi.org/10.1186/ar4405

Li, J. et al. Visualization and Characterization of Poly(amidoamine) Dendrimers by Atomic Force Microscopy. *Langmuir* **16**, 135613–5616 (2000).

Li, L. et al. Superparamagnetic iron oxide nanoparticles as MRI contrast agents for non-invasive stem cell labeling and tracking. *Theranostics* **3**, 595–615 (2013).

Li, W. & Chen, X. Gold nanoparticles for photoacoustic imaging. *Nanomedicine* **10**, 299–320 (2015).

Li, W. J. et al. A three-dimensional nanofibrous scaffold for cartilage tissue engineering using human mesenchymal stem cells. *Biomaterials* **26**, 599–609 (2005).

Lim, J. et al. Synthesis of Large Dendrimers with the Dimensions of Small Viruses. *Journal of the American Chemical Society* **135**, 4660–4663 (2013).

Lin, J., Chen, X. & Huang, P. Graphene-based nanomaterials for bioimaging. *Advanced Drug Delivery Reviews* **105**, 242–254 (2016).

Ling, W., Regatte, R. R., Navon, G. & Jerschow, A. Assessment of glycosaminoglycan concentration in vivo by chemical exchange-dependent saturation transfer. *Proceedings of the National Academy of Sciences of the United States of America* **105**, 2266–2270 (2008).

Liu, F. et al. Crystallization and Rheology of Poly(ethylene oxide) in Imidazolium Ionic Liquids. *Macromolecules* **49**, 6106–6115 (2016).

Liu, G., Cai, M., Zhou, F. & Liu, W. Charged polymer brushes-grafted hollow silica nanoparticles as a novel promising material for simultaneous joint lubrication and treatment. *Journal of Physical Chemistry B* **118**, 4920–4931 (2014).

Liu, Y., Wang, Y. & Yuan, Z. Dual-Modality Imaging of the Human Finger Joint Systems by Using Combined Multispectral Photoacoustic Computed Tomography and Ultrasound Computed Tomography. *Biomed Research International* **2016**, 1453272 (2016). https://doi.org/10.1155/2016/1453272

Lo, G. H., LaValley, M., McAlindon, T. & Felson, D. T. Intra-articular Hyaluronic Acid in Treatment of Knee Osteoarthritis: A Meta-analysis. *JAMA: The Journal of the American Medical Association* **290**, 3115–3121 (2003).

Lu, H. D., Zhao, H. Q., Wang, K. & Lv, L. L. Novel hyaluronic acid-chitosan nanoparticles as non-viral gene delivery vectors targeting osteoarthritis. *International Journal of Pharmaceutics* **420**, 358–365 (2011).

Lu, H., Dai, Y., Lv, L. & Zhao, H. Chitosan-Graft-Polyethylenimine/DNA Nanoparticles as Novel Non-Viral Gene Delivery Vectors Targeting Osteoarthritis. *PLoS ONE* **9**, 84703 (2014).

Lu, X., Khonsari, M. M. & Gelinck, E. R. M. The Stribeck curve: Experimental results and theoretical prediction. *Journal of Tribology* **128**, 789–794 (2006).

Ludwig, T. E., Hunter, M. M. & Schmidt, T. A. Cartilage boundary lubrication synergism is mediated by hyaluronan concentration and PRG4 concentration and structure. *BMC Musculoskeletal Disorders* **16**, 386 (2015).

Lundsgaard, C., Dufour, N., Fallentin, E., Winkel, P. & Gluud, C. Intra-articular sodium hyaluronate 2 mL versus physiological saline 20 mL versus physiological saline 2 mL for painful knee osteoarthritis: a randomized clinical trial. *Scandinavian Journal of Rheumatology* **37**, 142–150 (2008).

Lungwitz, U., Breunig, M., Blunk, T. & Göpferich, A. Polyethylenimine-based non-viral gene delivery systems. *European Journal of Pharmaceutics and Biopharmaceutics* **60** 247–266 (2005).

Luo, T., Wei, X., Zhao, H., Cai, G. & Zheng, X. Tribology properties of Al2O3/TiO2 nanocomposites as lubricant additives. *Ceramics International* **40**, 10103–10109 (2014).

Lusic, H. & Grinstaff, M. W. X-ray-Computed Tomography Contrast Agents. *Chemical Reviews* **113**, 1641–1666 (2013).

Ma, L., Gaisinskaya-Kipnis, A., Kampf, N. & Klein, J. Origins of hydration lubrication. *Nature Communications* **6**, 6060 (2015).

MacLaughlin, F. C. et al. Chitosan and depolymerized chitosan oligomers as condensing carriers for in vivo plasmid delivery. *Journal of Controlled Release* **56**, 259–72 (1998).

Maiti, P. K., Cagin, T., Wang, G. & Goddard, W. A. Structure of PAMAM Dendrimers: Generations 1 through 11. *Macromolecules* **37**, 6236–6254 (2004).

Majda, D. et al. New approach for determining cartilage pore size distribution: NaCl-thermoporometry. *Microporous and Mesoporous Materials* **241**, 238–245 (2017).

Malcor, J.-D. et al. Coupling of A Specific Photoreactive Triple-Helical Peptide to Crosslinked Collagen Films Restores Binding and Activation of DDR2 And VWF. *Biomaterials* **182**, 21–34 (2018).

Man, G. S. & Mologhianu, G. Osteoarthritis pathogenesis - a complex process that involves the entire joint. *Journal of Medicine and Life* **7**, 37–41 (2014).

Mankin, H. J. Biochemical and Metabolic Aspects of Osteoarthritis. *Orthopedic Clinics of North America* **2**, 19–31 (1971).

Mao, S., Sun, W. & Kissel, T. Chitosan-based formulations for delivery of DNA and siRNA. *Advanced Drug Delivery Reviews* **62**, 12–27 (2010).

Markides, H. et al. Ex vivo MRI cell tracking of autologous mesenchymal stromal cells in an ovine osteochondral defect model. *Stem Cell Research and Therapy* **10**, 25 (2019).

Martel-Pelletier, J., Battista, J. di & Lajeunesse, D. Biochemical Factors in Joint Articular Tissue Degradation in Osteoarthritis. In: *Osteoarthritis,* pp. 156–187. Springer, Berlin, Heidelberg. (1999) https://doi.org/10.1007/978-3-642-60026-5_9

Maudens, P., Meyer, S., Seemayer, C. A., Jordan, O. & Allémann, E. Self-assembled thermoresponsive nanostructures of hyaluronic acid conjugates for osteoarthritis therapy. *Nanoscale* **10**, 1845 (2018).

Mazor, M.; Best, T. M.; Cesaro, A.; Lespessailles, E.; Toumi, H. Osteoarthritis Biomarker Responses and Cartilage Adaptation to Exercise: A Review of Animal and Human Models. *Scandinavian Journal of Medicine and Science in Sports* **29**(8), 1072–1082 (2019).

McAlindon, T. E. et al. Effect of intra-articular triamcinolone vs saline on knee cartilage volume and pain in patients with knee osteoarthritis a randomized clinical trial. *JAMA: The Journal of the American Medical Association* **317**, 1967–1975 (2017).

McNulty, A. L., Rothfusz, N. E., Leddy, H. A. & Guilak, F. Synovial fluid concentrations and relative potency of interleukin-1 alpha and beta in cartilage and meniscus degradation. *Journal of Orthopaedic Research* **31**, 1039–1045 (2013).

Milcovich, G. et al. Modulating carbohydrate-based hydrogels as viscoelastic lubricant substitute for articular cartilages. *International Journal of Biological Macromolecules* **102**, 796–804 (2017).

Miltner, O., Schneider, U., Siebert, C. H., Niedhart, C. & Niethard, F. U. Efficacy of intraarticular hyaluronic acid in patients with osteoarthritis - A prospective clinical trial. *Osteoarthritis and Cartilage* **10**, 680–686 (2002).

Minas, T. et al. Autologous chondrocyte implantation for joint preservation in patients with early osteoarthritis. *Clinical Orthopaedics and Related Research* **468**, 147–157 (2010).

Mitchell, M. J.; Billingsley, M. M.; Haley, R. M.; Wechsler, M. E.; Peppas, N. A.; Langer, R. Engineering Precision Nanoparticles for Drug Delivery. *Nature Reviews Drug Discovery* 20(2), 101–124 (2021). https://doi.org/10.1038/s41573-020-0090-8

Moody, H. R. et al. In vitro degradation of articular cartilage: Does trypsin treatment produce consistent results? *Journal of Anatomy* **209**, 259–267 (2006).

Morgen, M. et al. Nanoparticles for improved local retention after intra-articular injection into the knee joint. *Pharmaceutical Research* **30**, 257–268 (2013).

Morgese, G., Benetti, E. M. & Zenobi-Wong, M. Molecularly Engineered Biolubricants for Articular Cartilage. *Advanced Healthcare Materials* **7**, 1701463 (2018).

Morgese, G., Cavalli, E., Müller, M., Zenobi-Wong, M. & Benetti, E. M. Nanoassemblies of Tissue-Reactive, Polyoxazoline Graft-Copolymers Restore the Lubrication Properties of Degraded Cartilage. *ACS Nano* **11**, 2794–2804 (2017).

Morgese, G., Cavalli, E., Rosenboom, J.-G., Zenobi-Wong, M. & Benetti, E. M. Cyclic Polymer Grafts That Lubricate and Protect Damaged Cartilage. *Angewandte Chemie International Edition* **57**, 1621–1626 (2018).

Moseley, J. B. et al. A Controlled Trial of Arthroscopic Surgery for Osteoarthritis of the Knee. *New England Journal of Medicine* **347**, 81–88 (2002).

Mow, V. C., Ratcliffe, A. & Poole, A. R. Cartilage and diarthrodial joints as paradigms for hierarchical materials and structures. *Biomaterials* **13**, (1992).

Mow, V. C.; Holmes, M. H.; Michael Lai, W. Fluid Transport and Mechanical Properties of Articular Cartilage: A Review. *Journal of Biomechanics* **17**(5), 377–394 (1984).

Müller, M. T., Yan, X., Lee, S., Scott S. Perry, A. & Nicholas D. Spencer. Lubrication Properties of a Brushlike Copolymer as a Function of the Amount of Solvent Absorbed within the Brush. *Macromolecules* **38**, 5706–5713 (2005).

Muller-Borer, B. J., Collins, M. C., Gunst, P. R., Cascio, W. E., Kypson, A. P. Quantum dot labeling of mesenchymal stem cells. *Journal of Nanobiotechnology* **5**, 9 (2007).

Murr, L. E. & Murr, L. E. Serendipitous Nanotechnology in Antiquity. *Handbook of Materials Structures, Properties, Processing and Performance* 703–717 (2015).

Myller, K. A. H. et al. In Vivo Contrast-Enhanced Cone Beam CT Provides Quantitative Information on Articular Cartilage and Subchondral Bone. *Annals of Biomedical Engineering* **45**, 811–818 (2017).

Nagendramma, P. & Kaul, S. Development of ecofriendly/biodegradable lubricants: An overview. *Renewable and Sustainable Energy Reviews* **16**, 764–774 (2012).

Nanotechnology is ancient history | Nanotechnology world | The Guardian. https://www.theguardian.com/nanotechnology-world/nanotechnology-is-ancient-history.

Negrin, L., Kutscha-Lissberg, F., Gartlehner, G. & Vecsei, V. Clinical outcome after microfracture of the knee: A meta-analysis of before/after-data of controlled studies. *International Orthopaedics* **36**, 43–50 (2012).

Nepple, J. J., Dunn, W. R. & Wright, R. W. Meniscal repair outcomes at greater than five years: A systematic literature review and meta-analysis. *Journal of Bone and Joint Surgery - Series A* **94**, 2222–2227 (2012).

Neu, C. P., Komvopoulos, K. & Reddi, A. H. The interface of functional biotribology and regenerative medicine in synovial joints. *Tissue Engineering - Part B: Reviews* **14**, 235–247 (2008).

Ngen, E. J. & Artemov, D. Advances in monitoring cell-based therapies with magnetic resonance imaging: Future perspectives. *International Journal of Molecular Sciences* **18** (2017).

NIS Database Documentation. https://hcup-us.ahrq.gov/db/nation/nis/nisdbdocumentation.jsp.

Odabas, S. et al. Auricular cartilage repair using cryogel scaffolds loaded with BMP-7-expressing primary chondrocytes. *Journal of Tissue Engineering and Regenerative Medicine* **7**, 831–840 (2013).

Oh, M. H.; Lee, N.; Kim, H.; Park, S. P.; Piao, Y.; Lee, J.; Jun, S. W.; Moon, W. K.; Choi, S. H.; Hyeon, T. Large-Scale Synthesis of Bioinert Tantalum Oxide Nanoparticles for X-Ray Computed Tomography Imaging and Bimodal Image-Guided Sentinel Lymph Node Mapping. *Journal of the American Chemical Society* **133**, 5508–5515 (2011)

Oungoulian, S. R. et al. Articular cartilage wear characterization with a particle sizing and counting analyzer. *Journal of Biomechanical Engineering* **135**, 024501 (2013).

Pahoff, S. et al. Effect of gelatin source and photoinitiator type on chondrocyte redifferentiation in gelatin methacryloyl-based tissue-engineered cartilage constructs. *Journal of Materials Chemistry B* **7**, 1761–1772 (2019).

Palmer, A. W., Guldberg, R. E., Levenston, M. E. Analysis of cartilage matrix fixed charge density and three-dimensional morphology via contrast-enhanced microcomputed tomography. *Proceedings of the National Academy of Sciences of the United States of America* **103**, 19255–19260 (2006).

Pang, P. et al. An MRI-Visible Non-Viral Vector Bearing GD2 Single Chain Antibody for Targeted Gene Delivery to Human Bone Marrow Mesenchymal Stem Cells. *PLoS ONE* **8**, 76612 (2013).

Pareek, A. et al. Osteochondral Autograft Transfer Versus Microfracture in the Knee: A Meta-analysis of Prospective Comparative Studies at Midterm. *Arthroscopy - Journal of Arthroscopic and Related Surgery* **32**, 2118–2130 (2016).

Park, S.; Krishnan, R.; Nicoll, S. B.; Ateshian, G. A. Cartilage Interstitial Fluid Load Support in Unconfined Compression. *Journal of Biomechanics* **36**, 1785–1796 (2003)

Patchornik, S., Ram, E., ben Shalom, N., Nevo, Z. & Robinson, D. Chitosan-Hyaluronate Hybrid Gel Intraarticular Injection Delays Osteoarthritis Progression and Reduces Pain in a Rat Meniscectomy Model as Compared to Saline and Hyaluronate Treatment. *Advances in Orthopedics* **2012**, 1–5 (2012).

Patel, S., Dhillon, M. S., Aggarwal, S., Marwaha, N. & Jain, A. Treatment with platelet-rich plasma is more effective than placebo for knee osteoarthritis: A prospective, double-blind, randomized trial. *American Journal of Sports Medicine* **41**, 356–364 (2013).

Patra, J. K.; Das, G.; Fraceto, L. F.; Campos, E. V. R.; Rodriguez-Torres, M. D. P.; Acosta-Torres, L. S.; Diaz-Torres, L. A.; Grillo, R.; Swamy, M. K.; Sharma, S.; Habtemariam, S.; Shin, H. S. Nano Based Drug Delivery Systems: Recent Developments and Future Prospects. *Journal of Nanobiotechnology* **16**(1), 71 (2018).

Paxton, E. S., Stock, M. v. & Brophy, R. H. Meniscal repair versus partial meniscectomy: A systematic review comparing reoperation rates and clinical outcomes. *Arthroscopy - Journal of Arthroscopic and Related Surgery* **27**, 1275–1288 (2011).

Peterfy C Janzen D, et al., van D. C., Peterfy, C., van Dijke, C., Janzen, D. Quantification of articular cartilage in the knee with pulsed saturation transfer subtraction and fat-suppressed MR imaging: optimization and validation. *Radiology* **193**, 485–491 (1994).

Peterfy, C.; Kothari, M. Imaging Osteoarthritis: Magnetic Resonance Imaging Versus X-Ray. *Current Rheumatology Reports* **8**, 16 – 21 2006.

Petersson, I. F., Boegård, T., Svensson, B., Heinegård, D. & Saxne, T. Changes in cartilage and bone metabolism identified by serum markers in early osteoarthritis of the knee joint. *British Journal of Rheumatology* **37**, 46–50 (1998).

Pi, Y. et al. Intra-articular delivery of anti-Hif-2α siRNA by chondrocyte-homing nanoparticles to prevent cartilage degeneration in arthritic mice. *Gene Therapy* **22**, 439–448 (2015).

Pillai, C. K. S., Paul, W. & Sharma, C. P. Chitin and Chitosan Polymers: Chemistry, Solubility and Fiber Formation. *Progress in Polymer Science* **34**, 641–678 (2009).

Potter, H. G.; Schachar, J. High Resolution Noncontrast MRI of the Hip. *Journal of Magnetic Resonance Imaging* **31**, 268–278 (2010).

Praveen Rao, P. N. & Knaus, E. E. Evolution of nonsteroidal anti-inflammatory drugs (NSAIDs): Cyclooxygenase (COX) inhibition and beyond. *Journal of Pharmacy and Pharmaceutical Sciences* **11**(2), 81s–110s (2008). https://doi.org/10.18433/j3t886

Rabin, O.; Perez, J. M.; Grimm, J.; Wojtkiewicz, G.; Weissleder, R. An X-Ray Computed Tomography Imaging Agent Based on Long-Circulating Bismuth Sulphide Nanoparticles. *Nature Materials* **5**, 118–122 (2006)

Raghava Reddy, K. et al. Functionalized magnetic nanoparticles/biopolymer hybrids: Synthesis methods, properties and biomedical applications. *Methods in Microbiology* **46**, 227–254 (2019).

Ramaswamy, S. et al. Magnetic resonance imaging of chondrocytes labeled with superparamagnetic iron oxide nanoparticles in tissue-engineered cartilage. *Tissue Engineering - Part A* **15**, 3899–3910 (2009).

Raviv, U. & Klein, J. Fluidity of bound hydration layers. *Science* **297**, 1540–1543 (2002).

Raviv, U. et al. Lubrication by Charged Polymers. *Nature* **425**, 163–165 (2003).

Ray, W. C. & Grinstaff, M. W. Polycarbonate and Poly(carbonate−ester)s Synthesized from Biocompatible Building Blocks of Glycerol and Lactic Acid. *Macromolecules* **36**, 3557–3562 (2003).

Rey-Rico, A. et al. rAAaaV-mediated overexpression of TGF-β via vector delivery in polymeric micelles stimulates the biological and reparative activities of human articular chondrocytes in vitro and in a human osteochondral defect model. *International Journal of Nanomedicine* **12**, 6985–6996 (2017).

Ricapito, N. G., Ghobril, C., Zhang, H., Grinstaff, M. W. & Putnam, D. Synthetic Biomaterials from Metabolically Derived Synthons. *Chemical Reviews* **116**, 2664–2704 (2016).

Rieger, E. et al. Controlled implant/soft tissue interaction by nanoscale surface modifications of 3D porous titanium implants. *Nanoscale* **7**, 9908–9918 (2015).

Roduner, E. Size Matters: Why Nanomaterials Are Different. *Chemical Society Reviews*. **35,** 583–592 (2006).

Roemer, F. W.; Eckstein, F.; Hayashi, D.; Guermazi, A. The Role of Imaging in Osteoarthritis. *Best Practice and Research: Clinical Rheumatology* **28**(1), 31–60 (2014). https://doi.org/10.1016/j.berh.2014.02.002

Rolfson, O., Dahlberg, L. E., Nilsson, J. Å., Malchau, H. & Garellick, G. Variables determining outcome in total hip replacement surgery. *Journal of Bone and Joint Surgery - Series B* **91**, 157–161 (2009).

Rothenfluh, D. A., Bermudez, H., O'Neil, C. P. & Hubbell, J. A. Biofunctional polymer nanoparticles for intra-articular targeting and retention in cartilage. *Nature Materials* **7**, 248–254 (2008).

Russo, F. et al. Platelet Rich Plasma and Hyaluronic Acid Blend for the Treatment of Osteoarthritis: Rheological and Biological Evaluation. *PLoS ONE* **11**, 0157048 (2016).

Rutjes, A. W. S. et al. Viscosupplementation for Osteoarthritis of the Knee A Systematic Review and Meta-analysis. *Annals of Internal Medicine* **7**, 180–191 (2012).

Saadat, E., Shakor, N., Gholami, M. & Dorkoosh, F. A. Hyaluronic acid based micelle for articular delivery of triamcinolone, preparation, in vitro and in vivo evaluation. *International Journal of Pharmaceutics* **15**, 218–225 (2015).

Sakata, R. et al. Stimulation of the Superficial Zone Protein and Lubrication in the Articular Cartilage by Human Platelet-Rich Plasma. *American Journal of Sports Medicine* **43**, 1467–1473 (2015).

Salamanna, F. et al. Effects of intra-articular hyaluronic acid associated to Chitlac (arty-duo®) in a rat knee osteoarthritis model. *Journal of Orthopaedic Research* **37**, 867–876 (2019).

Samaroo, K. J., Tan, M., Putnam, D. & Bonassar, L. J. Binding and Lubrication of Biomimetic Boundary Lubricants on Articular Cartilage. *Journal of Orthopaedic Research* **35**, 548–557 (2017).

Sánchez, M. et al. A randomized clinical trial evaluating plasma rich in growth factors (PRGF-Endoret) versus hyaluronic acid in the short-term treatment of symptomatic knee osteoarthritis. *Arthroscopy - Journal of Arthroscopic and Related Surgery* **28**, 1070–1078 (2012).

Sanchez-Adams, J., Leddy, H. A., McNulty, A. L., O'Conor, C. J. & Guilak, F. The Mechanobiology of Articular Cartilage: Bearing the Burden of Osteoarthritis. *Current Rheumatology Reports* **16**, 1–9 (2014).

Saukko, A. E. A. et al. Dual Contrast CT Method Enables Diagnostics of Cartilage Injuries and Degeneration Using a Single CT Image. *Annals of Biomedical Engineering* **45**, 2857–2866 (2017).

Saukko, A. E. A.; Honkanen, J. T. J.; Xu, W.; Väänänen, S. P.; Jurvelin, J. S.; Lehto, V. P.; Töyräs, J. Dual Contrast CT Method Enables Diagnostics of Cartilage Injuries and Degeneration Using a Single CT Image. *Annals of Biomedical Engineering* **45**(12), 2857–2866 (2017). https://doi.org/10.1007/s10439-017-1916-3

Schmidt, T. A. & Sah, R. L. Effect of Synovial Fluid on Boundary Lubrication of Articular Cartilage. *Osteoarthritis and Cartilage* **15**, 35–47 (2007).

Schmidt, T. A., Gastelum, N. S., Nguyen, Q. T., Schumacher, B. L. & Sah, R. L. Boundary lubrication of articular cartilage: role of synovial fluid constituents. *Arthritis and Rheumatism* **56**, 882–891 (2007).

Scognamiglio, F., Travan, A., Donati, I., Borgogna, M. & Marsich, E. A hydrogel system based on a lactose-modified chitosan for viscosupplementation in osteoarthritis. *Carbohydrate Polymers* **248**, 116787 (2020).

Senti, F. R. et al. Viscosity, Sedimentation, and Light-Scattering Properties of Fraction of an Acid-Hydrolyzed Dextran. *Journal of Polymer Science* **17**, 527–546 (1955).

Seror, J., Zhu, L., Goldberg, R., Day, A. J. & Klein, J. Supramolecular synergy in the boundary lubrication of synovial joints. *Nature Communications* **6**, 6497 (2015).

Setton, L. A.; Elliott, D. M.; Mow, V. C. Altered Mechanics of Cartilage with Osteoarthritis: Human Osteoarthritis and an Experimental Model of Joint Degeneration. *Osteoarthritis and Cartilage* **7**(1), 2–14 (1999). https://doi.org/10.1053/joca.1998.0170

Shah, R. P. et al. T1Rho magnetic resonance imaging at 3t detects knee cartilage changes after viscosupplementation. *Orthopedics* **38**, e604–e610 (2015).

Shahnazar, S., Bagheri, S. & Abd Hamid, S. B. Enhancing lubricant properties by nanoparticle additives. *International Journal of Hydrogen Energy* **41**, 3153–3170 (2016).

Shapiro, F., Koide, S. & Glimcher, M. J. Cell origin and differentiation in the repair of full-thickness defects of articular cartilage. *Journal of Bone and Joint Surgery - Series A* **75**, 532–553 (1993).

Shenoi, R. A. et al. Affinity-Based Design of a Synthetic Universal Reversal Agent for Heparin Anticoagulants. *Science Translational Medicine* **6**, 260 (2014).

Shi, J. et al. Nanoparticle delivery of the bone morphogenetic protein 4 gene to adipose-derived stem cells promotes articular cartilage repair in vitro and in vivo. *Arthroscopy - Journal of Arthroscopic and Related Surgery* **29**, 2001-2011.e2 (2013).

Shimada, E. & Matsumura, G. Viscosity and Molecular Weight of Hyaluronic Acids. *Journal of Biochemistry* **78**, 513–517 (1975).

Shreffler, J. W.; Pullan, J. E.; Dailey, K. M.; Mallik, S.; Brooks, A. E. Overcoming Hurdles in Nanoparticle Clinical Translation: The Influence of Experimental Design and Surface Modification. *International Journal of Molecular Sciences* **20**(23), 6056 (2019). https://dx.doi.org/10.3390%2Fijms20236056

Singh, A. et al. Enhanced lubrication on tissue and biomaterial surfaces through peptide-mediated binding of hyaluronic acid. *Nature Materials* **13**, 988–995 (2014).

Singh, A. et al. Nanoengineered Particles for Enhanced Intra-Articular Retention and Delivery of Proteins. *Advanced Healthcare Materials* **3**, 1562–1567 (2014).

Sivan, S. et al. Liposomes act as effective biolubricants for friction reduction in human synovial joints. *Langmuir* **26**, 1107–1116 (2010).

Solloway, S., Hutchinson, C. E., Waterton, J. C. & Taylor, C. J. The use of active shape models for making thickness measurements of articular cartilage from MR images. *Magnetic Resonance in Medicine* **37**, 943–952 (1997).

Sophia Fox, A. J.; Bedi, A.; Rodeo, S. A. The Basic Science of Articular Cartilage: Structure, Composition, and Function. *Sports Health* **1**, 461–468 (2009).

Spaková, T., Rosocha, J., Lacko, M., Harvanová, D. & Gharaibeh, A. Treatment of Knee Joint Osteoarthritis with Autologous Platelet-Rich Plasma in Comparison with Hyaluronic Acid. *American Journal of Physical Medicine and Rehabilitation* **91**, 411–417 (2012).

Stechemesser, S. & Eimer, W. Solvent-Dependent Swelling of Poly(amido amine) Starburst Dendrimers. *Macromolecules* **30**, 2204–2206 (1997).

Steinmeyer, J., Knue, S., Raiss, R. X. & Pelzer, I. Effects of intermittently applied cyclic loading on proteoglycan metabolism and swelling behaviour of articular cartilage explants. *Osteoarthritis and Cartilage* **7**, 155–164 (1999).

Stewart, R. C. et al. Contrast-enhanced CT with a high-affinity cationic contrast agent for imaging ex vivo bovine, intact ex vivo rabbit, and in vivo rabbit cartilage. *Radiology* **266**, 141–150 (2013).

Strickland, C. D. & Kijowski, R. Morphologic imaging of articular cartilage. *Magnetic Resonance Imaging Clinics of North America* **19**, 229–248 (2011).

Su, J.-Y., Chen, S.-H., Chen, Y.-P. & Chen, W.-C. Evaluation of Magnetic Nanoparticle-Labeled Chondrocytes Cultivated on a Type II Collagen–Chitosan/Poly(Lactic-co-Glycolic) Acid Biphasic Scaffold. *International Journal of Molecular Sciences* **18**, 87 (2017).

Sun, X. D., Jeng, L., Bolliet, C., Olsen, B. R. & Spector, M. Non-viral endostatin plasmid transfection of mesenchymal stem cells via collagen scaffolds. *Biomaterials* **30**, 1222–1231 (2009).

Sun, Y., Sobel, E. S. & Jiang, H. First assessment of three-dimensional quantitative photoacoustic tomography for in vivo detection of osteoarthritis in the finger joints. *Medical Physics* **38**, 4009–4017 (2011).

Sun, Z. et al. Boundary mode lubrication of articular cartilage with a biomimetic diblock copolymer. *Proceedings of the National Academy of Sciences of the United States of America* **116**, 12437–12441 (2019).

Sun, Z., Bonassar, L. J. & Putnam, D. Influence of Block Length on Articular Cartilage Lubrication with a Diblock Bottle-Brush Copolymer. *ACS Applied Materials and Interfaces* **12**, 330–337 (2020).

Sunder, A., Hanselmann, R., Frey, H. & Mülhaupt, R. Controlled Synthesis of Hyperbranched Polyglycerols by Ring-Opening Multibranching Polymerization. *Macromolecules* **32**, 4240–4246 (1999).

Svenson, S. & Tomalia, D. A. Dendrimers in Biomedical Applications—Reflections on the Field. *Advanced Drug Delivery Reviews* **64**, 102–115 (2012).

Tae, H. K., Su, I. K., Akaike, T. & Chong, S. C. Synergistic effect of poly(ethylenimine) on the transfection efficiency of galactosylated chitosan/DNA complexes. *Journal of Controlled Release* **105**, 354–366 (2005).

Tavakoli Nia, H. et al. Aggrecan Nanoscale Solid–Fluid Interactions Are a Primary Determinant of Cartilage Dynamic Mechanical Properties. *ACS Nano* **9**, 2614–2625 (2015).

Theruvath, A. J. et al. Tracking stem cell implants in cartilage defects of minipigs by using ferumoxytol-enhanced MRI. *Radiology* **292**, 129–137 (2019).

Tiderius, C. J., Jessel, R., Kim, Y. J. & Burstein, D. Hip dGEMRIC in asymptomatic volunteers and patients with early osteoarthritis: The influence of timing after contrast injection. *Magnetic Resonance in Medicine* **57**, 803–805 (2007).

Tiderius, C. J.; Olsson, L. E.; Leander, P.; Ekberg, O.; Dahlberg, L. Delayed Gadolinium-Enhanced MRI of Cartilage (DGEMRIC) in Early Knee Osteoarthritis. *Magnetic Resonance in Medicine* **49**, 488–492 (2003).

Torres, A. S.; Bonitatibus, P. J.; Colborn, R. E.; Goddard, G. D.; Fitzgerald, P. F.; Lee, B. D.; Marino, M. E. Biological Performance of a Size-Fractionated Core-Shell Tantalum Oxide Nanoparticle X-Ray Contrast Agent. *Investigative Radiology* **47**, 578–587 (2012).

Tripathi, P. K. & Tripathi, S. Dendrimers for anticancer drug delivery. In A. Chauhan and H. Kulhari (eds.) *Pharmaceutical Applications of Dendrimers*, pp. 131–150 (2020). Elsevier.

Tripathi, S. K., Goyal, R., Kumar, P. & Gupta, K. C. Linear polyethylenimine-graft-chitosan copolymers as efficient DNA/siRNA delivery vectors in vitro and in vivo. *Nanomedicine: Nanotechnology, Biology, and Medicine* **8**, 337–345 (2012).

Truong, N. P., Dussert, M. V., Whittaker, M. R., Quinn, J. F. & Davis, T. P. Rapid Synthesis of Ultrahigh Molecular Weight and Low Polydispersity Polystyrene Diblock Copolymers by Raft-Mediated Emulsion Polymerization. *Polymer Chemistry* **6**, 3865–3874 (2015).

Uflyand, I. E., Zhinzhilo, V. A. & Burlakova, V. E. Metal-containing nanomaterials as lubricant additives: State-of-the-art and future development. *Friction* **7**, 93–116 (2019).

van Buul, G. M. et al. Clinically translatable cell tracking and quantification by MRI in cartilage repair using superparamagnetic iron oxides. *PLoS ONE* **6**, e17001 (2011).

van den Berg, W. B., van de Loo, F. A. J., Zwarts, W. A. & Otterness, I. G. Effects of murine recombinant interleukin 1 on intact homologous articular cartilage: A quantitative and autoradiographic study. *Annals of the Rheumatic Diseases* **47**, 855–863 (1988).

van der Wal, R. J. P., Thomassen, B. J. W. & van Arkel, E. R. A. Long-term clinical outcome of open Meniscal allograft transplantation. *American Journal of Sports Medicine* **37**, 2134–2139 (2009).

van der Weegen, W., Wullems, J. A., Bos, E., Noten, H. & van Drumpt, R. A. M. No Difference Between Intra-Articular Injection of Hyaluronic Acid and Placebo for Mild to Moderate Knee Osteoarthritis: A Randomized, Controlled, Double-Blind Trial. *Journal of Arthroplasty* **30**, 754–757 (2015).

Vega, J. F., Rastogi, S., Peters, G. W. M. & Meijer, H. E. H. Rheology And Reptation of Linear Polymers. Ultrahigh Molecular Weight Chain Dynamics in the Melt. *Journal of Rheology* **48**, 663–678 (2004).

Venkatesan, J. & Kim, S. K. Nano-hydroxyapatite composite biomaterials for bone tissue engineering - A review. *Journal of Biomedical Nanotechnology* **10**, 3124–3140 (2014).

Verdonk, P. C. M. et al. Meniscal allograft transplantation: Long-term clinical results with radiological and magnetic resonance imaging correlations. *Knee Surgery, Sports Traumatology, Arthroscopy* **14**, 694–706 (2006).

Vilt, S. G., Martin, N., McCabe, C. & Kane Jennings, G. Frictional performance of silica microspheres. *Tribology International* **44**, 180–186 (2011).

Visser, J. et al. Reinforcement of hydrogels using three-dimensionally printed microfibres. *Nature Communications* **6**, 1–10 (2015).

Waddell, D. D. & Bricker, D. W. C. Total knee replacement delayed with hylan G-F 20 use in patients with grade IV osteoarthritis. *Journal of Managed Care Pharmacy* **13**, 113–121 (2007).

Wafa, H. et al. Retrospective evaluation of the incidence of early periprosthetic infection with silver-treated endoprostheses in high-risk patients: Case-control study. *Bone and Joint Journal* **97**, 252–257 (2015).

Walker, P. S., Dowson, D., Longfield, M. D. & Wright, V. 'Boosted lubrication' in Synovial Joints by Fluid Entrapment and Enrichment. *Annals of the Rheumatic Diseases* **27**, 512–520 (1968).

Wan, L. et al. Biodegradable lubricating mesoporous silica nanoparticles for osteoarthritis therapy. *Friction* 1–12 (2020). https://doi.org/10.1007/s40544-020-0391-2

Wang, S. et al. A novel therapeutic strategy for cartilage diseases based on lipid nanoparticle-RNAi delivery system. *International Journal of Nanomedicine* **13**, 617–631 (2018).

Wang, X. F. et al. Nano hydroxyapatite particles promote osteogenesis in a three-dimensional bio-printing construct consisting of alginate/gelatin/hASCs. *RSC Advances* **6**, 6832–6842 (2016).

Wang, X.-B. & Liu, W.-M. Nanoparticle-Based Lubricant Additives. In *Encyclopedia of Tribology* 2369–2376 (Springer US, 2013).

Wang, Y. et al. Effects of Hylan G-F 20 supplementation on cartilage preservation detected by magnetic resonance imaging in osteoarthritis of the knee: A two-year single-blind clinical trial. *BMC Musculoskeletal Disorders* **12**, 1–9 (2011).

Wathier, M. et al. A large-molecular-weight polyanion, synthesized via ring-opening metathesis polymerization, as a lubricant for human articular cartilage. *Journal of the American Chemical Society* **135**, 4930–4933 (2013).

Wathier, M. et al. A Synthetic Polymeric Biolubricant Imparts Chondroprotection in a Rat Meniscal Tear Model. *Biomaterials* **182**, 13–20 (2018).

Weber, J., Beard, P. C. & Bohndiek, S. E. Contrast agents for molecular photoacoustic imaging. *Nature Methods* **13**, 639–650 (2016).

Wei, B.; Zhang, X.; Zhang, C.; Jiang, Y.; Fu, Y. Y.; Yu, C.; Sun, S. K.; Yan, X. P. Facile Synthesis of Uniform-Sized Bismuth Nanoparticles for CT Visualization of Gastrointestinal Tract in Vivo. *ACS Applied Materials and Interfaces* **8**(20), 12720–12726 (2016). https://doi.org/10.1021/acsami.6b03640

Wei, G. & Ma, P. X. Structure and properties of nano-hydroxyapatite/polymer composite scaffolds for bone tissue engineering. *Biomaterials* **25**, 4749–4757 (2004).

Wei, L.; Fleming, B. C.; Sun, X.; Teeple, E.; Wu, W.; Jay, G. D.; Elsaid, K. A.; Luo, J.; Machan, J. T.; Chen, Q. Comparison of Differential Biomarkers of Osteoarthritis with and without Posttraumatic Injury in the Hartley Guinea Pig Model. *Journal of Orthopaedic Research* **28**, 900–906 (2010)

Wheaton, A. J. et al. Proteoglycan loss in human knee cartilage: Quantitation with sodium MR imaging - Feasibility study. *Radiology* **231**, 900–905 (2004).

Wheaton, A. J., Dodge, G. R., Elliott, D. M., Nicoll, S. B. & Reddy, R. Quantification of cartilage biomechanical and biochemical properties viaT1ρ magnetic resonance imaging. *Magnetic Resonance in Medicine* **54**, 1087–1093 (2005).

Whitmire, R. E. et al. Self-assembling nanoparticles for intra-articular delivery of anti-inflammatory proteins. *Biomaterials* **33**, 7665–7675 (2012).

Wick, M. C.; Kastlunger, M.; Weiss, R. J. Clinical Imaging Assessments of Knee Osteoarthritis in the Elderly: A Mini-Review. *Gerontology* **60**(5), 386–394 (2014).

Williams, A.; Sharma, L.; McKenzie, C. A.; Prasad, P. v.; Burstein, D. Delayed Gadolinium-Enhanced Magnetic Resonance Imaging of Cartilage in Knee Osteoarthritis: Findings at Different Radiographic Stages of Disease and Relationship to Malalignment. *Arthritis and Rheumatism* **52**, 3528–3535 (2005).

Williams, F. M. K.; Spector, T. D. *Osteoarthritis. Medicine* 364–368 (2006)

Wilms, D. et al. Hyperbranched Polyglycerols with Elevated Molecular Weights: A Facile Two-Step Synthesis Protocol Based on Polyglycerol Macroinitiators. *Macromolecules* **42**, 3230–3236 (2009).

Wimpenny, I., Markides, H. & el Haj, A. J. Orthopaedic applications of nanoparticle-based stem cell therapies. *Stem Cell Research and Therapy* **3**, 13 (2012).

Wobig, M., Dickhut, A., Maier, R. & Vetter, G. Viscosupplementation with Hylan G-F 20: A 26-week controlled trial of efficacy and safety in the osteoarthritic knee. *Clinical Therapeutics* **20**, 410–423 (1998).

Wolinsky, J. B. & Grinstaff, M. W. Therapeutic and diagnostic applications of dendrimers for cancer treatment. *Advanced Drug Delivery Reviews* **60**, 1037–1055 (2008).

Workman, J., Thambyah, A. & Broom, N. The influence of early degenerative changes on the vulnerability of articular cartilage to impact-induced injury. *Clinical Biomechanics* **43**, 40–49 (2017).

Wu, C., Zhang, Y., Zhou, Y., Fan, W. & Xiao, Y. A comparative study of mesoporous glass/silk and non-mesoporous glass/silk scaffolds: Physiochemistry and in vivo osteogenesis. *Acta Biomaterialia* **7**, 2229–2236 (2011).

Xi, D. et al. Gold nanoparticles as computerized tomography (CT) contrast agents. *RSC Advances* **2**, 12515–12524 (2012).

Xiao, Q.; Bu, W.; Ren, Q.; Zhang, S.; Xing, H.; Chen, F.; Li, M.; Zheng, X.; Hua, Y.; Zhou, L.; Peng, W.; Qu, H.; Wang, Z.; Zhao, K.; Shi, J. Radiopaque Fluorescence-Transparent TaOx Decorated Upconversion Nanophosphors for in Vivo CT/MR/UCL Trimodal Imaging. *Biomaterials* **33**, 7530–7539 (2012)

Yan, H. et al. Suppression of NF-κB activity via nanoparticle-based siRNA delivery alters early cartilage responses to injury. *Proceedings of the National Academy of Sciences of the United States of America* **113**, E6199–E6208 (2016).

Yarmola, E. G., Shah, Y., Arnold, D. P., Dobson, J. & Allen, K. D. Magnetic Capture of a Molecular Biomarker from Synovial Fluid in a Rat Model of Knee Osteoarthritis. *Annals of Biomedical Engineering* **44**, 1159–1169 (2016).

Yokoyama, M. et al. Preparation of Micelle-Forming Polymer-Drug Conjugates. *Bioconjugate Chemistry* **3**, 295-301 (1992).

Yoshioka, T. et al. Fate of bone marrow mesenchymal stem cells following the allogeneic transplantation of cartilaginous aggregates into osteochondral defects of rabbits. *Journal of Tissue Engineering and Regenerative Medicine* **5**, 437–443 (2011).

Zan, X., Kozlov, M., McCarthy, T. J. & Su, Z. Covalently Attached, Silver-Doped Poly(vinyl alcohol) Hydrogel Films on Poly(l -lactic acid). *Biomacromolecules* **11**, 1082–1088 (2010).

Zare, S. et al. MRI-Tracking of Dental Pulp Stem Cells In Vitro and In Vivo Using Dextran-Coated Superparamagnetic Iron Oxide Nanoparticles. *Journal of Clinical Medicine* **8**, 1418 (2019).

Zhang, H. & Grinstaff, M. W. Recent Advances in Glycerol Polymers: Chemistry and Biomedical Applications. *Macromolecular Rapid Communications* **35**, 1906–1924 (2014).

Zhang, H. & Grinstaff, M. W. Synthesis of Atactic and Isotactic Poly(1,2-glycerol carbonate)s: Degradable Polymers for Biomedical and Pharmaceutical Applications *Journal of the American Chemical Society* **135**, 6806–6809 (2013).

Zhang, H., Lin, X., Chin, S. & Grinstaff, M. W. Synthesis and Characterization of Poly(glyceric Acid Carbonate): A Degradable Analogue of Poly(acrylic Acid). *Journal of the American Chemical Society* **137**, 12660–12666 (2015).

Zhang, J. et al. Chitosan Modification and Pharmaceutical/Biomedical Applications. *Marine Drugs* **8**, 1962–1987 (2010).

Zhang, J. X. et al. Local delivery of indomethacin to arthritis-bearing rats through polymeric micelles based on amphiphilic polyphosphazenes. *Pharmaceutical Research* **24**, 1944–1953 (2007).

Zhang, Y.; Jordan, J. M. Epidemiology of Osteoarthritis. *Clinics in Geriatric Medicine* **26**, 355–369 (2010).

Zhao, F. et al. Cellular Uptake, Intracellular Trafficking, and Cytotoxicity of Nanomaterials. *Small* **7**, 1322–1337 (2011).

Zhao, Q. Q. et al. Combination of poly(ethylenimine) and chitosan induces high gene transfection efficiency and low cytotoxicity. *Journal of Bioscience and Bioengineering* **105**, 65–68 (2008).

Zhao, X., Yu, S. B., Wu, F. L., Mao, Z. bin & Yu, C. L. Transfection of primary chondrocytes using chitosan-pEGFP nanoparticles. *Journal of Controlled Release* **112**, 223–228 (2006).

Zhao, Y. et al. Drug Delivery System Based on Near-Infrared Light-Responsive Molybdenum Disulfide Nanosheets Controls the High-Efficiency Release of Dexamethasone To Inhibit Inflammation and Treat Osteoarthritis. *ACS Applied Materials and Interfaces* **11**, 11587–11601 (2019).

Zheng, Y. et al. Bioinspired Hyaluronic Acid/Phosphorylcholine Polymer with Enhanced Lubrication and Anti-Inflammation. *Biomacromolecules* **20**, 4135–4142 (2019).

Zhong, G. et al. Dopamine-melanin nanoparticles scavenge reactive oxygen and nitrogen species and activate autophagy for osteoarthritis therapy. *Nanoscale* **11***(24)*, 11605–11616 (2019). https://dx.doi.org/10.1039%2Fc9nr03060c

Zhou, H. F. et al. Peptide-siRNA nanocomplexes targeting NF-κB subunit p65 suppress nascent experimental arthritis. *Journal of Clinical Investigation* **124**, 4363–4374 (2014).

Zhu, Y. et al. Light emitting diodes based photoacoustic imaging and potential clinical applications. *Scientific Reports* **8**, 1–12 (2018).

Zou, Q. Nanoparticles in Automotive Applications. In *Encyclopedia of Tribology* 2376–2381 (Springer US, 2013).

CURRICULUM VITAE